Adsorption of phenol and it's derivatives from aqueous system by modified adsorbents

Thesis
Submitted to
Babasaheb Bhimrao Ambedkar University, Lucknow
(A Central University)
Lucknow

BABASAHEB BHIMRAO AMBEDKAR UNIVERSITY
LUCKNOW
प्रज्ञा शील करूणा
ESTABLISHED 1996

for the Degree
of
Doctor of Philosophy
in
Applied Chemistry
Submitted by

Prashant Mishra
(MSc, NET-JRF & GATE)
Enrollment Number – 950/17

Under the supervision of

Prof. Kaman Singh

Department of Applied Chemistry
School for Physical Sciences
Babasaheb Bhimrao Ambedkar University (A Central University)
Lucknow, Uttar Pradesh – 226025

2022

DECLARATION

I, Prashant Mishra declare that the thesis entitled **"Adsorption of phenol and it's derivatives from aqueous system by modified adsorbents"** has been prepared by me under the supervision of **Prof. Kaman Singh**, Department of Applied Chemistry, School for Physical Sciences, Babasaheb Bhimrao Ambedkar University, Lucknow. No part of this thesis has formed the basis for the award of any degree, diploma or fellowship previously. Further, I declare that the material embodied in the present work is based on original research work and the indebtedness to others has been duly acknowledged at relevant places. I, also declare that the thesis is essentially free from all kinds of plagiarism.

Date: 02/11/2022

Prashant Mishra

Prashant Mishra
Research Scholar
Department of Applied Chemistry
Babasaheb Bhimrao Ambedkar University
Lucknow-226025, India

CERTIFICATE

This is to certify that the thesis titled **"Adsorption of phenol and it's derivatives from aqueous system by modified adsorbents"** submitted by **Mr. Prashant Mishra** is an original research work and has not been previously submitted in part or full for the award of any other degree or diploma to this or any other university.

The thesis submitted to the Babasaheb Bhimrao Ambedkar University, Lucknow satisfies all the requirements as stipulated in the ***Doctor of Philosophy (Ph.D.)*** *regulations-1999 as amended in ~~2008/2010~~/2013* and it is fit for submission and evaluation for the award of the degree of Doctor of Philosophy of the University.

Date 02/11/2022

Administrative Supervisor

Professor & Head
Department of Chemistry
School of Physical & Decision Sciences
Babasaheb Bhimrao Ambedkar University
(A Central University)
Lucknow-226025, Uttar Pradesh (INDIA)

Head of the Department

Professor & Head
Department of Chemistry
School of Physical & Decision Sciences
Babasaheb Bhimrao Ambedkar University
(A Central University)
Lucknow-226025, Uttar Pradesh (INDIA)

Acknowledgement

Milestones of life are achieved, not only by individual efforts but with the blessing, guidance and help of parents, teachers, friends, elders, and our mighty Lord. Many people have contributed directly and indirectly to my education and research. Here I will express my gratitude to all of them.

First, I would like to dedicate this thesis to my parents **Late. Akhilesh Kumar Mishra** and **Mrs. Suman Mishra**, who are the real inspiration behind my doctoral study. My parent's dedication and encouragement are invaluable and without their support, I would not be writing this note.

I express my profound gratitude to my supervisor **Prof. Kaman Singh** (Professor, Department of Applied Chemistry, BBAU, Lucknow) for their splendid guidance, imparting thoughtful suggestions at various stages of the entire work.

With profound indebtedness, I owe my sincere thanks and deep regards to **Prof. Gajanan Pandey**, (Head, Department of Applied Chemistry, BBAU, Lucknow) for his immense support and encouragement throughout the research work.

I am grateful to University Grant Commission (UGC), Delhi for financial support (UGC-JRF) during my research work. Also, I would like to thank the authors of various research articles and books whose work has been consulted, utilized and cited in this thesis.

I would like to pay my sincere thanks to **Late. Prof. D. P. Singh** (Department of Environmental Science, BBAU, Lucknow) for providing research facilities in his lab during this program.

I owe my sincere thanks to **Dr. Anjani Tiwari**, Dr. Jyoti Pandey, Dr. Shailesh Kumar, Dr. Preeti Gupta, and Dr. Jawahar Lal Jat, DAC, BBAU for their crucial contribution and ever-ready help during my research period.

I am extremely grateful to the USIC, BBAU, Lucknow for providing SEM, XRD and FT-IR facility, ACMS, IIT-Kanpur for providing XRD, SEM and Optical Profilometry facilities and SIL, Department of Chemistry, BBAU for providing BET, FT-IR and UV-Vis facilities.

Friendship is a god-given virtue and a valuable asset. I pay my heartiest thanks to my dear friends especially **Dr. Akhilesh Kumar Shukla, Santosh Mishra, Manoj Dhameja, Kijay Chauhan, Priya Singh, Deepika Singh, Hariom Kumar and Anuj Saini** without whom it was near impossible to fulfil my objective.

I also would like to thank my seniors **Dr. Ajay Kumar, Dr. Ashok Kumar** and juniors **Utkarsh, Madhu Lata, Prasenjit** and **Ayushi**, who always motivated me to tackle the day-to-day problems arising during my research work.

I am thankful to all the office staff of the Department of Applied Chemistry, especially Sarvesh Gupta, Pankaj Singh, Anuj Kumar Saini and Digvijay Singh for their cooperative behaviour.

I am particularly grateful to my mother, Mrs. Suman Mishra for the encouragement and support that she provided during the research and so to this thesis. I will remain indebted to my loving elder brother Mr. Shanshank Mishra & sister Mrs. Shilpa Mishra for their care, affection, encouragement and support. Many more have helped me in this endeavour and I would like to thank them all with an excuse of not being able to accommodate their names.

Also, I would like to thank the authors of various research articles and books whose work has been consulted, utilized and cited in my thesis.

Finally, my acknowledgement would not be complete without thanking the almighty God, for giving me the strength and determination to overcome the hardship faced in my life.

(Prashant Mishra)

CONTENTS

Preface

The industrial development of adsorbents and catalysts in the mid-twentieth century was closely associated with a renewed academic interest in adsorption science for various applications. The strong demand for fundamental research on adsorption by porous and non-porous solids attracted the attention of a number of researchers. Many applications of adsorption at the liquid-solid interface include flotation, pollution control, liquid chromatography and the refining of precious metals/mineral processing). Fundamental investigations of liquid/solid interfacial systems are therefore of great importance by analyzing the experimental data.

Phenol and its derivatives are poisonous and corrosive chemicals that are categorized as priority pollutants. Adsorption is one of the most efficient ways to get rid of phenols. In the last decade, scientists have looked at a variety of natural adsorbents for this purpose. Their adsorption capabilities range from 1 to >1000 mg/g, depending on the adsorbent's surface area, pH, temperature, phenol and surface functional group concentrations, contact time, and other parameters. Carbonaceous adsorbents, clay and natural mineral adsorbents, polymer-based adsorbents, and new adsorbents are the four classes of adsorbents evaluated for the removal of phenol and phenol compounds in this review. Polymer-based adsorbents had the highest adsorption capabilities (>1000 mg/g), whereas natural clays and new adsorbents had lesser adsorption capacities when compared to carbonaceous adsorbents. The significant potential for phenol recovery and reuse is a major advantage of phenol adsorption over other applicable methods.

The present thesis grew out of more than five years of research work. The schematic structure of the thesis comprises seven chapters. **Chapter 1** introduces the various applications and toxicity of phenolic compounds due to their exposure to the human being. It also discusses the experimental and theoretical developments in the field of surface chemistry. **Chapter 2** discusses the recent developments in the field of adsorptive removal of phenolic compounds by different classes of adsorbents. **Chapter 3** discusses the material, methodology and characterization techniques used during the research work. **Chapter 4** describes the synthesis and characterization of pea shells activated with sulfuric acid and its use to remove 4-aminophenol from aqueous medium. **Chapter 5** describes the synthesis and characterization of ultrasound-assisted sulfuric acid-treated pea shells and its use to remove phenol from aqueous medium. **Chapter 6** describes a comparative study of the synthesis and characterization of biochars-derived pea shells at different pyrolysis temperatures and its use to remove phenol from aqueous medium. **Chapter 7** describes the conclusions and future prospects of the present research work.

Chapter-1

Introduction and objectives of the present work

1.1. Phenol and its derivatives

1.1.1. Properties and application

A hydroxyl (-OH) group linked to an aromatic ring distinguishes the family of chemical substances known as phenols or phenolics. The simplest phenolic chemical, phenol is a benzene derivative. A phenyl (-C_6H_5) group is joined to a hydroxyl (-OH) group to form the molecule. It has the chemical formula C_6H_5OH. Despite having the same functional group as alcohols, where the -OH group is joined to an aliphatic carbon, phenols' chemistry is quite dissimilar to that of alcohols. Phenol (C_6H_5OH), which is the name of the first member of the family and also serves as a generic word for the entire group, is also referred to as benzenol or carbolic acid [1,2]. When pure, it is a colourless to white solid; however, the commercial product, which includes some water, is a liquid. The crystalline, hygroscopic substance phenol has a distinct unpleasant smell and a strong, burning taste. The phenol odour threshold is 0.04 ppm, and a strong, extremely sweet odour has been noted. A moderate amount of phenol can dissolve in water to form a solution because it evaporates more slowly than water. The term "derivatives of phenol and phenolic compounds" refers to the other members of the family [3].

A colourless, crystalline chemical with a distinctive smell, phenol (hydroxybenzene) is soluble in both water and organic solvents [4]. It is frequently used in the chemical, oil, coal processing, and metallurgical industries for the synthesis of alkylphenols, cresols, xylenols, phenolic resins, aniline, and other chemicals. Additionally, phenol is utilised in the manufacture of textiles, explosives, insecticides, and colours [5–7]. Additionally, it is employed in chemical analysis as a reagent and disinfectant [8,9]. On a large scale, coal tar is used to create phenol [10]. Chemically speaking, phenol

can also be made from benzene and propylene, toluene oxidation, and a reaction between chlorobenzene and sodium hydroxide [11–14].

The operations of the chemical and pharmaceutical industries, the mineral (non-metallic) products sector, the steel and metal products sector, the pulp, paper, and wood products sector, the steel and metal products sector, and the petroleum refining and products sector are to blame for the presence of phenols into the environment due to human actions [15–22]. Additionally, phenol is released into the air from car exhaust [23]. The substances enter ecosystems due to the penetration of the urban or industrial effluent to the surface water [24]. Moreover, the occurrence of phenols in the environment stems from the production and use of numerous pesticides, in particular phenoxy herbicides like 2.4-dichlorophenoxyacetic acid (2,4-D) or 4-chloro-2- methylphenoxyacetic acid (MCPA) and also phenolic biocides like pentachlorophenol (PCP), dinoseb pesticides [25]. Some phenols can be created naturally, such as when organic matter decomposes and forms phenol and p-cresol (chlorinated phenol) [26]. Phenol has a fire risk.

As a precursor to a variety of materials and practical chemicals, it is generated on a huge scale (about 7 billion kg/year) [27]. Phenol is very flammable and dissolves in several organic solvents, but only to a limited extent in water at room temperature. Above 68 ºC, it becomes completely water-soluble. Log octanol/water partition coefficient (log $K_{o/w}$) is 1.46 for this substance. At room temperature, it is only moderately volatile. It is a weak acid that is extremely susceptible to oxidation and electrophile substitution reactions in its ionised form. In addition to being present in many everyday items including antiseptics, healthcare products, resins, plastics, cosmetics, health aids, meals, and beverages, phenols and phenolic compounds are widely used in a variety of industries, including the production of polymeric resin and

the refining of oil. As a result, these substances are frequently found in surface water and industrial effluents.

1.1.2. Toxicity of phenols

Unspecified toxicity associated with a compound's hydrophobicity and the production of free radicals are the two basic mechanisms underlying phenol toxicity [28–30]. Phenol's solubility in a cell's compartments and potential for interaction with particular cell and tissue structures are both influenced by hydrophobicity [31]. For instance, the rise in chlorine atoms in chlorophenols correlates with an increase in hydrophobicity, which increases the compound's toxicity [29]. The location of the substituent plays a role on the compound's degree of toxicity. For illustration, adding a chlorine atom to a phenol molecule in the 2-position reduces its hazard, but adding one in the 3-position makes the product more poisonous [32,33]. After entering the cell, phenols actively convert, primarily with the help of oxidases found inside cytochrome P450 [34,35]. Through the creation of electrophilic metabolites which could adsorb to and harm DNA or enzymes, transformation processes can occasionally enhance the hazard of specific chemicals. Acute toxicity, histological alterations, mutagenicity, and carcinogenicity are all aspects of phenols' harmful influence.

1.1.3. Environmental concern of phenols

Among the first substances listed as a priority pollutant by the US Environmental Protection Agency was phenol (USEPA). A few phenol and phenolic compounds have been classified as major pollutants by the USEPA and the European Commission (EC) owing to significant toxicity and environmental impacts. Priority phenols are made up of a wide variety of substituted phenolic compounds, such as halogenated (such as chlorophenol), nitrated (such as 2-nitrophenol), alkylated (such as 2,4-

dimethylphenol), and ether (such as methoxyphenol) derivatives. The phenols that have been given priority status include phenol, 2-chlorophenol, 2,4-dichlorophenol, 2,4,6-trichlorophenol, pentachlorophenol, 2-nitrophenol, 4-nitrophenol, 2,4-dinitrophenol, 2-methyl-4,6-dinitrophenol, 2,4-dimethylphenol, and 4-chloro-3-methylphenol. In a number of industrial operations, priority phenols are created or used. They are frequently utilised as pulp processing aids, sanitizers, preservatives, and other intermediates in the production of insecticides. Priority phenols, sadly, are now widespread environmental contaminants detected in ambient air, soil/sediments, and drinkable water. Numerous important phenols, particularly chlorophenols, have a reputation for being hazardous, carcinogenic, and persistent in the environment.

1.2. Introduction to adsorption

In particular, the history of adsorption science and technology, as well as the industrial necessities that served as the impetus, are pertinent to current practice. This is because a lot of the processes that are currently in use, as well as many potential future developments, have their roots in earlier discoveries. Furthermore, many theoretical ideas, research findings, and terminology related to physical adsorption go back several decades. As a result, the current status of physisorption will be introduced by a summary of the key moments in the development of physical adsorption, with a focus on theory. At the solid-gas interface, physisorption will be the main topic of discussion.

The rationale for prioritising this contact is that investigations of adsorption at the solid-liquid interface, both theoretical and experimental, came before those from the gaseous phase. However, several isotherm equations for adsorption at the solid-liquid interface, especially those that deal with adsorption from dilute solutions, are derived from the theoretical description of individual gases and their mixes on solid surfaces.

1.2.1. Experimental development of adsorption

Although some adsorption-related phenomena were recognised in antiquity, the first quantitative findings were made by Scheele and Fontana [36] in 1773 and 1777, respectively, who reported several experiments on the uptake of gases by charcoal and clays. The present use of adsorption is related to Lowitz's discovery [37] that the uptake of organic contaminants by charcoal caused tartaric acid solutions to become less coloured. Since de Saussure's study was published in 1814, adsorption has been the subject of systematic studies [38]. He came to the conclusion that all gases are adsorbed by porous materials (such as sea foam, cork, charcoal, and asbestos), and that heat is also evolved during this process. As a result, he became the first to recognise the widespread nature of adsorption and revealed its exothermic nature. De Saussure also discovered that porous materials extract gases that condense easily to the maximum extent.

At a steady temperature, Chappuis tested the ammonia's adsorption onto asbestos and charcoal [39,40]. Additionally, he discovered that charcoal absorbs gases at different pressures, including air, carbon dioxide, and sulphide. In the process of wetting adsorbents with liquids, he performed the first calorimetric measurement of heat evolution. Du Bois-Reymond came up with the phrase "adsorption," although Kayser is the one who first used it in literature. The findings of adsorption experiments at a constant temperature were described throughout the following few years using the phrases "isotherm" and "isothermal curve." In addition, Kayser created certain theoretical ideas that were fundamental to the monomolecular adsorption theory [41,42].

In 1909, McBain coined the term "absorption" to describe how carbon absorbs hydrogen far more slowly than it does by adsorption [43]. He suggested using the

word "sorption" to describe both adsorption and absorption. It is sometimes difficult to tell these two phenomena apart and define them clearly. In ambiguous situations, the term "sorption" and, as a result, the phrases "sorbent," "sorbate," and "sorptive" should be used.

Adsorption methods are primarily used in practice when other substances selectively pull certain components out of mixes. Tswett discovered selective adsorption in 1903 [44]. He used silica materials to separate chlorophyll and other plant pigments by making use of this phenomenon. Due to the varying adsorption affinities of silica gel for different colours, this separation was made possible. Column solid/liquid adsorption chromatography is the name given to the Tswett method. A new analytical method, as well as a new branch of surface research, were both born out of this discovery. Few people are aware that Dewar experimentally discovered selective adsorption in 1904 [45].

Chromatography, one of the most significant analytical techniques today, is currently a distinct and well-developed body of knowledge evolved from adsorption [46]. For the industrial separation of complicated mixtures, it is frequently used. The historical history of chromatography is discussed in the book by Ettre and Zlatkis, which highlights some significant developments in its theory and use as well as the researchers who should be commended for creating this technology [47–49].

1.2.2. Theoretical development of adsorption

The most crucial features of commercial sorbents, such as specific surface area, pore size or energy distribution, and pore volume, are provided by isotherm equations that deal with the physical adsorption of gases and vapours. These extremely particular curves can be used to evaluate the adsorption mechanism, which is directly related to interactions between adsorbent and adsorbate molecules, and they allow evaluating

the effectiveness of commercial adsorbents used in purification, separation, and other utilitarian operations.

Adsorption isotherms, or mathematical adsorption equations, can be used to achieve the accurate interpretation of practical adsorption isotherms. These equations are created by closely coupling the adsorption system's physical model assumptions. In most cases, practical observation leads to the model assumptions. The outcomes of the investigation enable the development of a theory on the nature of the adsorption process. Experimental evidence can be used to verify this theory. A hypothesis becomes a theory, or an appropriate adsorption equation if it is not refuted by additional trials. So, a theory that explains the behaviour of the adsorption system under investigation is put to the test. A theory is continuously evaluated and used as a roadmap for new investigations. ***Theory and experiment have been working together to develop adsorption science.***

Before 1914, there was no idea that made it possible to interpret adsorption isotherms. Although the Freundlich equation was utilised, it was not theoretically supported [50]. According to McBain, van Bemmelen put forth the empirical equation described above in 1888 [51].

Boedecker also put forth the so-called Freundlich adsorption isotherm in 1895 as an empirical equation [52]. Because Freundlich gave it a lot of attention and made it widely used, this equation is referred to as his equation in the literature [53]. There were two definitions of adsorption phenomena postulated between 1914 and 1918. These descriptions are connected to figures like Polanyi [54,55], Eucken [56] and Langmuir [57].

The initial formulation of the Langmuir equation, which came from kinetic research, was predicated on the idea that there are a fixed number of energetically

comparable adsorption sites on the adsorbent surface, each of which can accommodate one molecule of a perfect gas. Whether chemical or physical, the bonding to the adsorption sites must be strong enough to prevent the movement of molecules that have been adsorbed along the surface. Since adsorbed molecules can travel around the surface in non-localized adsorption, it was supposed that localised adsorption was distinct from that. Lateral interactions between the adsorbate molecules were disregarded because the bulk phase is made up of a perfect gas. This results in the formation of a monolayer surface phase on the energetically homogenous surface of the adsorbent.

Langmuir provided a clear explanation of monomolecular adsorption on energetically homogenous surfaces for the first time [58,59].

The Langmuir hypothesis was used to explain chemisorption and, with certain limitations, physical adsorption. The Langmuir equation's constant parameters have a clearly defined physical meaning (in contrast to the parameters of the empirical Freundlich equation). Later, when this equation was derived by Volmer [60] inside the framework of phenomenological thermodynamics and by Fowler within statistical thermodynamics [61] as well, its significance became very evident. With one sort of adsorption active centre, the Langmuir equation reasonably accurately explains physical (or chemical) adsorption on solid surfaces.

In an effort to take into consideration the heterogeneity of solid adsorbents and the multilayer nature of adsorption, Langmuir endeavoured to expand the scope of his theoretical framework. He observed that numerous instances do not support one of his theory's essential assumptions, which relates to the homogeneity of the adsorbent surface. Because the adsorption sites are dispersed over energetically distinct levels, the surfaces of the majority of solids are energetically heterogeneous [58].

Interestingly, a broad account of the kinetics of reactions at surfaces was developed as a result of the Langmuir investigations of gas adsorption. To explain the kinetics of surface reactions in terms of his monolayer equation, Langmuir claimed that surface catalysis is typically preceded by chemisorption. He also demonstrated how one could use the adsorption isotherm to interpret the kinetics of numerous surface processes. Due to the significance of catalysis in industry, these key studies in the field of surface catalysis served as the foundation for more in-depth and extensive research that is being done today. The Nobel Prize in Chemistry was given to Langmuir in 1932 for "***his discoveries and research in the field of surface chemistry***" [62].

Later, there were some efforts made to generalise the Langmuir equation by accounting for lateral interactions between adsorbed molecules, their mobility, and the energetic surface heterogeneity of the materials. But one should think of the Langmuir equation as a useful equation that describes the so-called ideal localised monolayer. The ideal localised monolayer model holds a prominent place in surface and adsorption science despite its obvious flaws. It made it possible to launch extensive theoretical investigations, the goal of which was, and is, to find ever-more accurate and authentic descriptions of experimental adsorption systems [63,64].

The equation of multilayer isotherm developed by Brunauer *et al.* in 1938 marked another important turning point in the growth of the adsorption sciences [65]. Before the multilayer adsorption theory, Brunauer and Emmett published two influential studies in 1935 [66] and 1937 [67]. For the first time, Brunauer and Emmett also suggested calculating the monolayer adsorption quantity from the so-called point B of the experimental isotherm [66,67].

Initially, the monomolecular adsorption isotherm and the BET equation were derived from kinetic considerations similar to those put forth by Langmuir. Cassie

[68] performed the initial statistical thermodynamic derivation. Subsequently, Fowler and Guggenheim [69] and Hill [70] offered a significantly altered derivation.

The Langmuir equation being applicable to every adsorption layer is the main presumption of the BET theory. The initial adsorption layer forms on a variety of uniformly energetic surface locations, similar to the Langmuir theory. The two most important simplifying presumptions are that, starting with the second adsorbed layer, the condensation heat is equal to the evaporation heat of gas and that the ratio between the rate constant of uptake from one layer and the condensation of a lower situated layer is the same for all the layers. These presumptions were later thoroughly explored in the literature. *In a sense,* ***the Langmuir isotherm is generalised by the BET isotherm.***

The BET adsorption isotherm was first developed for a specific model of an adsorption layer[65], and then it was expanded to a limited number of layers (n) [71,72]. Frenkel, Halsey, and Hill presented a different, well-known method for multilayer adsorption that is typically referred to as the FHH slab theory [73–75]. Later, a number of BET equation modifications were put out, but they did not gain widespread acceptance for the analysis of gas and vapour adsorption processes.

In 1940, Brunauer *et al.* added to the BET theory by incorporating an extra contribution to the energy of adsorption that occurs from the forces of capillary condensation. Contrary to the BET isotherm, a wider range of relative pressures can be applied with the so-called BDDT equation. The four variables in this equation can be adjusted, but they cannot be evaluated separately, making it a pretty complicated equation [76,77].

The identification of the five primary types of adsorption isotherms for gases and vapours is another significant contribution made by Brunauer *et al.* This

identification is known as the BDDT classification, and it is suggested by IUPAC as the foundation for a more thorough categorization of adsorption isotherms [78]. Fig. 1.1 depicts the different types of adsorption isotherm.

The BET theory was the first to develp a general theory of physical adsorption despite its limitations.

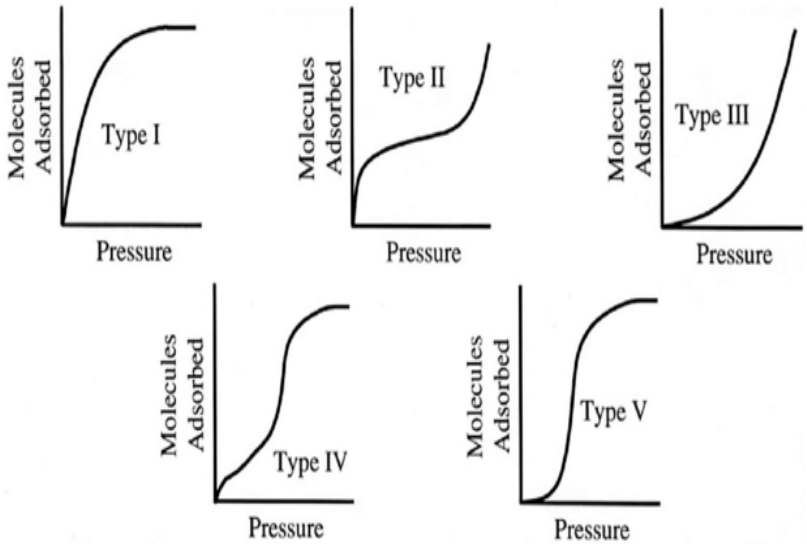

Fig. 1.1: Types of adsorption isotherms

The complete isothermal process, including capillary condensation, capillary polymerization, and monomolecular adsorption, is described. Unluckily, the last region is depicted in an inadequate manner, especially if the material has a heterogeneous porous structure with pores of different capillary lengths. The equality of the heats of adsorption and condensation, as well as the stability of the adsorption coefficient ratio between individual adsorption layers, cannot be assumed, hence this theory cannot be used to explain adsorption at temperatures above the critical temperature.

To measure the specific surface area of fine powders and porous materials, however, the so-called BET low-temperature nitrogen method is still frequently used as the accepted standard [79].

The foundation of the Langmuir and BET theories is the idea that mono- or multilayer adsorption occurs on an interface geometrical surface. Flat macroscopic adsorbents' surface area serves as the fundamental geometrical characteristic. Langmuir [80] hypothesised that adsorption must take place according to a distinct process on adsorbents with tiny pores that are proportionate to the sizes of molecules adsorbed. A high adsorption field manifests in micropores when any type of adsorption interaction results in physical adsorption across their entire surface. Because there is a shortage of micropore space, the subsequent molecules that adsorb there do not form adsorption layers; instead, they fill the micropores to capacity in accordance with the micropore filling mechanism. Therefore, ***the volume of micropores rather than their "surface" is a fundamental geometrical feature defining microporous adsorbents.***

The adsorption potential and the typical adsorption curve make up the Polanyi theory's fundamental ideas. The adsorption potential and distance from the solid surface are simply related by this characteristic curve. The characteristic adsorption equation was given to this relationship. The above indicated distance can be expressed in terms of adsorbed phase volume units. Over a broad range of temperatures, Polanyi [54,55] assumed that the adsorption potential is independent of the latter. This implies that the characteristic adsorption curve is also temperature-independent. The fact that the van der Waals forces are likewise temperature independent leads to this conclusion. This isn't necessarily true, though, for polar adsorbates.

It is desirable to find adsorption isotherms at other temperatures after calculating the curve characteristic for a specific temperature. The characteristic adsorption equation is partially replaced by the Polanyi potential theory because it does not provide a clear equation for the adsorption isotherm [81]. The Polanyi hypothesis, which bases its predictions on the van der Waals equation's description of

a three-dimensional layer adsorbed, posits that the adsorbate concentration increases at a suitable low temperature and that its condensation into a liquid occurs on the adsorbent flat surface. It is important to distinguish between capillary condensation, which occurs when the adsorbent has a porous structure, and condensation, which can only occur on a solid's flat surface. Zsigmondy [82], who looked at how silica materials absorbed water vapours, found the capillary condensation phenomenon. Zsigmondy demonstrated the possibility of physisorbed vapour condensation in small pores below the saturated standard vapour pressure. The presence of a liquid meniscus in the adsorbent capillaries is the primary prerequisite for the capillary condensation. As is well knowledge, the concave meniscus is where saturated vapour pressure decreases. This behaviour is quite well represented by the Kelvin [83] equation for cylindrical pores with pore widths between 2 and 50 nm, or for mesopores. Although its primary drawbacks are still unclear, this equation is nevertheless often employed for pore size analysis. Mono- and/or multilayer adsorption on the pore walls is invariably followed by capillary condensation. In contrast to the actual adsorption of gases by porous solids, it means that this phenomena is significant but secondary. Therefore, if the thickness of the adsorbed layer is known, the true pore width may be calculated.

Zsigmondy was the first to pay attention to capillary condensation, also known as adsorption, on the inner walls of capillaries [82]. This remarkably accurate result is consistent with current theories on how gases and vapours are absorbed by porous (i.e., industrial) adsorbents. Mono- and multilayer adsorption are typically involved in such a process, which is then followed by capillary condensation during the last step of uptake. According to the porous nature of different adsorbents, the quantitative contribution of capillary condensation to the uptake of a given vapour varies. For

adsorbents, where mesopores make up a significant portion of porosity, this mechanism predominates [84]. The 'hysteresis loop,' which can be seen on many experimental adsorption isotherms, is a crucial aspect of capillary condensation. Foster [85] assert that polymolecular adsorption and capillary condensation both contribute to the formation of the adsorption branch of a hysteresis loop, whereas the condensation phenomena alone is responsible for the desorption branch's appearance.

According to their forms, De Boer [86] categorised the capillary hysteresis loops and connected the latter to the presence of specific types of pores. He identified five different varieties of hysteresis loops using a single vertical or steep branch. The majority of adsorbents have non-homogeneous porous structures, therefore the experimental hysteresis loops of adsorption-desorption isotherms combine two or more de Boer type kinds. Fig. 1.2 depicts the types of hysteresis loops formed in the adsorption-desorption cycle.

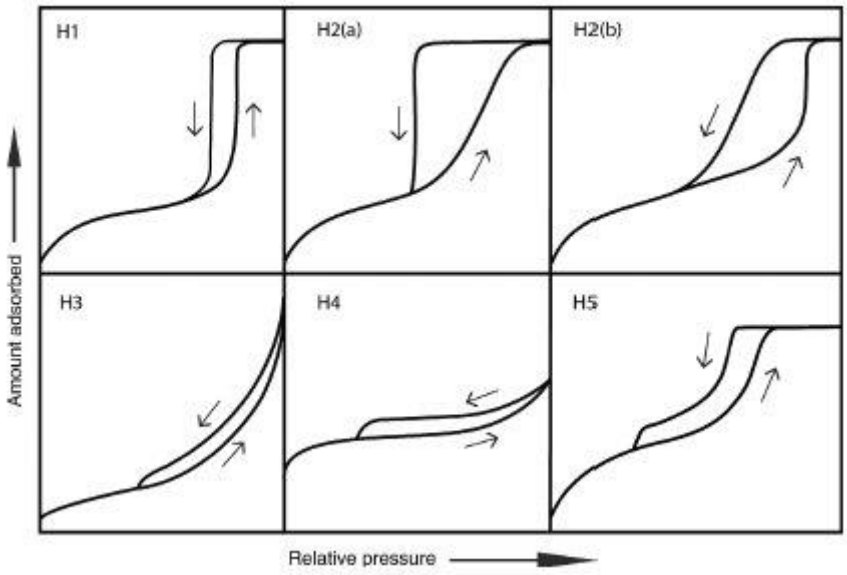

Fig. 1.2: Five types of hysteresis loops formed in adsorption-desorption cycle.

Various attempts have been made up to this point to evaluate the capillary condensation phase of adsorption isotherms in order to measure the mesopore size

distribution function. To get accurate results, these procedures should be properly followed in accordance with the IUPAC standard [84]. The Polanyi theory currently has a relatively historical significance. However, the widely acknowledged Dubinin-Radushkevich hypothesis, often known as the TVFM (Theory of Volume Filling of Micropores), which is constantly being refined, was inspired by the Polanyi theory. The majority of industrial adsorbents have a well-developed porous structure [87–89], and TVFM is important for this property [90]. The DR equation does not use a well-defined model process to represent the physisorption of gases, in contrast to the Langmuir and BET equations. It is more heavily influenced by adsorption energy considerations. The DR equation and its many variants are crucial for understanding the features of most commercial adsorbents, which have a sophisticated porous structure with pores of all sizes and shapes, but micropores are the most important component.

It is challenging to determine which of the fundamental adsorption concepts that have been offered so far are right. The Polanyi thermodynamic theory does not specify an exact adsorption isotherm equation or provide a thorough explanation of how the process works. The analytical DR equation results from the development of this theory, which describes adsorption on microporous surfaces, but it still has a semi-empirical nature. The Langmuir equation and the method of calculating solid surface area based on it can be used in systems where the adsorption process is not complicated by the development of a multilayer, by adsorption in micropores, or by capillary condensation.

The range of relative pressures between 0.05 and 0.35 is covered by the BET equation, which reduces to the Langmuir equation in the region of low relative pressures. It implies that a relatively small area is covered by the experimental data

and this equation being in agreement. The BET equation's application frequently leads to variations in which the predicted adsorption values are too modest at low pressures and too big at high pressures. The BET equation makes it possible to accurately determine the specific surface area of macroporous adsorbents and briefly porous ones with few micropores. Although under a specific range of relative pressures, the experimental data can correlate to a linear form of the BET equation, the presence of micropores that the adsorbate molecules fill leads to inaccurate results.

As a result, the BET theory can only be used in the region of medium relative pressure levels, or after the creation of a monolayer. Moreover, capillary condensation rarely occurs in the range of relative pressures under discussion. The BET equation can provide good answers in some circumstances for relative pressures up to 0.5 [83]. In the capillary condensation area, the BET theory should be used cautiously, in particular, if the adsorbent is characterised by a large spectrum of capillary sizes. In this area, the Kelvin equation is usually applied. Finally, the BET theory cannot be used to describe adsorption on microporous adsorbents where the DR isotherm is an expression considered to be correct.

Accurately describing the free energy change is the minimum requirement we place on any theory. This is due to various enthalpy and entropy effects at various levels of the adsorbent surface coverage. The BET's and Langmuir's enthalpy and entropy contributions, as well as their concordance with the experiment is, at best, semi-quantitative [76]. Entropy values are too high and predicted enthalpy values are too low. As a result, there are various questions about how well the physical picture presented by both BET and Langmuir theories may be used. The aforementioned observations show that, during the early stages of adsorption science, attempts to extend the theory of gas or vapour adsorption to encompass the entire

range of pressures were unsuccessful. To achieve even better results and a more accurate description of the real mechanism of adsorption from the gaseous phase, the next step in the studies of adsorption will be pursued.

It should be emphasised at this point that a general theory of adsorption, which would incorporate all elements impacting a specific process, may result in an isotherm equation which is so sophisticated that it could accurately represent each experimental isotherm regardless of its shape. Since none of the constants in such an equation can be established empirically, it is meaningless. ***It frequently occurs that a theory's simplicity can also be its greatest strength.***

Finally, it should be noted that we just covered the fundamental ideas and equations relating to adsorption isotherms. The equations for mobile and mobile-localized adsorption, as well as isotherms that take into account lateral interactions between molecules in the surface monolayer, were left out. These equations are easily deduced by using the simple assumption that molecules in the surface phase form the surface film, whose behaviour is defined by the so-called surface equation of state. This equation, which is a two-dimensional equivalent of the corresponding three-dimensional equation of state, deals with the surface pressure (also known as spreading pressure) of the film on the adsorption. It is possible to use the Gibbs adsorption isotherm to describe this adsorption. As a result, using the Gibbs adsorption equation, the adsorption isotherm and a surface equation of state can be interconverted. The different adsorption isotherms were generated using various assumptions for the two-dimensional adsorbed gas. There are several equations for ideal non-localized monolayers [83], including the Henry law, the Langmuir equation [80], the Volmer [60] and Hill-de Boer [91] equations for non-ideal and non-localized monolayers, and the Fowler-Guggenheim [92] equation for non-ideal but localised

monolayers. But the statistical thermodynamics formalism can be used to generate the aforementioned equations [70,93]. The study of phase transitions in the adsorbed layers made extensive use of the two-dimensional equations of state.

1.3. Objectives of the research work

The objectives of the present research work are as follows:

- **Preparation of the various modified adsorbents using Pea shells (PS) as a precursor.**
- **Characterization of prepared modified adsorbents by various techniques such as SEM-EDS, BET, XRD, FT-IR, and Optical profilometry and validation of the results obtained with experimental results of the adsorption of phenol and its derivatives onto various modified adsorbents.**
- **Adsorption of phenol and its derivatives onto modified adsorbents of the PS from aqueous medium.**
- **The effect of various parameters such as effect of adsorbate concentration, adsorbent dose, pH, ionic strength, temperature, contact time, and the urea, etc. on adsorption.**
- **Investigation of the applicability of various adsorption isotherms for the interpretation of the adsorption mechanism.**
- **Applicability of various kinetic models to check the variation of adsorption with time.**
- **Investigation of the thermodynamics of the adsorption.**

1.4. Organization of the thesis

The thesis consists of seven chapters as briefly described below:-

Chapter 1 introduces about wastewater contaminants and their types, basic information related to phenol and its derivatives. The uses and toxicity of phenol and its derivatives is briefly discussed. This chapter also discusses the adsorption phenomenon and its experimental and theoretical development with time. Further, this chapter describes the obejectives of the present research work.

Chapter 2 thoroughly discusses the recent developments in the field of adsorptive removal of phenol and its derivatives with categories of adsorbents.

Chapter 3 presents instrumental techniques used to characterize the prepared Pea shells adsorbent. It also deals with the details of methodology of adsorption applied for studied phenol and derivatives onto modified Pea shells adsorbent.

Chapter 4 deals with the preparation of an inexpensive adsorbent (pea shells activated with sulfuric acid, PSASA) from agricultural waste (pea shells), and to use it to remove hazardous 4-Aminophenol effectively (4-AP). SEM, FT-IR, and XRD studies provided substantial 4-AP adsorption onto the PSASA. The surface topography of the PSASA surface revealed its high degree of unevenness, and BET analysis verified the PSASA's macroporous characteristic. Multiple tests were conducted to determine the effects of adsorbent dosage, temperature, pH, PZC, the addition of KCl and urea, and the starting concentration of 4-AP on adsorption. As the temperature rises from 25°C to 45°C, a decrease in 4-AP adsorption uptake is seen. At an ideal pH of 7.0 and 25ºC, the maximum adsorption uptake (qm) was found to be 106.11 mg/g. The Langmuir isotherm provided the best explanation for the experimental data, with high R^2 values, out of all the examined adsorption isotherm models. The kinetics of adsorption were discovered to be well explained by the

pseudo-first-order model. The thermodynamic result supports the physical and exothermic nature of the adsorption phenomenon. Electrostatic interaction, hydrogen bonds, and the π-π exchange process were the main factors controlling the adsorption of 4-AP. As a result of the current research's useful findings, we can use the PSASA as a reasonably priced adsorbent to remove phenolics from water and wastewater stream.

Chapter 5 deals with preparation of an adsorbent derived from Pea shells (ultrasound-assisted sulphuric acid-treated pea shells, USAPS) that was employed to remove phenol. SEM-EDS, FT-IR, XRD, optical profilometry, BET, and PZC techniques were used to characterise the USAPS sample. The adsorption characteristics were greatly improved by the application of ultrasound during the chemical activation. By adjusting the pH (2–9), temperature (25–45°C), USAPS dose (0.1–0.6 g/100 ml), phenol concentration (50–500 mg/L), and addition of inorganic salts, the adsorption of phenol onto USAPS was investigated (0.1 M KCl and 0.1 M $CaCl_2$). With 0.1 g/100 ml of the USAPS dosage, the maximal phenol absorption was found to be 125.77 mg/g for 500 mg/L of phenol at pH 7 and 25°C. Temperature rise and the USAPS dose had a negative impact on adsorption, but the addition of 0.1 M KCl and 0.1 M $CaCl_2$ reduced the maximum phenol absorption from 125.77 mg/g to 103.45 mg/g and 84.11 mg/g, respectively. The equilibrium data were best explained by the Langmuir model, whereas the time-dependent phenol elimination was best explained by the pseudo-second-order kinetic model. The thermodynamic analysis showed that there was no structural change at the adsorbent-adsorbate interface, demonstrating the physical character of adsorption.

Chapter 6 presents the use of Pea (Pisum sativum) peels as a precursor for the production of biochar at three distinct temperatures (250ºC: PP250, 500ºC: PP500,

and 750ºC: PP750) utilising moderate pyrolysis for one hour in order to remove phenol from an aqueous medium effectively. SEM, XRD, and FT-IR were used to characterise the samples of biochar. Temperature and solution pH was used to track the elimination of phenol. It was discovered that 6.0 pH and 25ºC were the ideal conditions for maximum adsorption. The adsorption capacity of PP250 is primarily influenced by the presence of NaCl and urea in the solution, while PP500 and PP750's adsorption potential is only marginally influenced concluding absence of hydrogen bonding and electrostatic interactions in case of PP500 and PP750 during adsorption. The adsorption data were best explained by the Langmuir isotherm. The q_{max} was determined to be 34.63, 46.70, and 60.10 mg/g for the PP250, PP500, and PP750, respectively. The kinetic data were most successfully explained by a pseudo-second-order model. The physical and exothermic nature of adsorption was supported by thermodynamic parameters.

Chapter 7 describes the conclusion and future prospects of the present research work.

References

[1] S.H. Lin, R.S. Juang, Adsorption of phenol and its derivatives from water using synthetic resins and low-cost natural adsorbents: A review, J. Environ. Manage. 90 (2009) 1336–1349. https://doi.org/10.1016/J.JENVMAN.2008.09.003.

[2] D. Chen, A.K. Ray, Photocatalytic kinetics of phenol and its derivatives over UV irradiated TiO2, Appl. Catal. B Environ. 23 (1999) 143–157. https://doi.org/10.1016/S0926-3373(99)00068-5.

[3] Ö. Özdemir, Synthesis of new luminescent bis-azo-linkage Schiff bases containing amino-phenol and its derivative. Part I: Studying of their tautomeric, acidochromic, thermochromic, ionochromic, and photolüminesence properties, J. Photochem. Photobiol. A Chem. 380 (2019) 111868. https://doi.org/10.1016/J.JPHOTOCHEM.2019.111868.

[4] H.J. Swarts, F.J.M. Verhagen, J.A. Field, J.B.P.A. Wijnberg, Trichlorinated phenols from hypholoma elongatum, Phytochemistry. 49 (1998) 203–206. https://doi.org/10.1016/S0031-9422(97)01067-4.

[5] A. Abd Gami, M. Yunus Shukor, K. Abdul Khalil, F. Aini Dahalan, A. Khalid, S. Aqlima Ahmad, Phenol and its toxicity, J. Environ. Microbiol. Toxicol. 2 (2014) 11–23. https://doi.org/10.54987/JEMAT.V2I1.89.

[6] R.M. Bruce, J. Santodonato, M.W. Neal, Summary review of the health effects associated with phenol, Toxicol. Ind. Health. 3 (1987) 535–568. https://doi.org/10.1177/074823378700300407.

[7] V. Niedan, I. Pavasars, G. Öberg, Chloroperoxidase-mediated chlorination of aromatic groups in fulvic acid, Chemosphere. 41 (2000) 779–785. https://doi.org/10.1016/S0045-6535(99)00471-3.

[8] J. Yin, R. Chen, Y. Ji, C. Zhao, G. Zhao, H. Zhang, Adsorption of phenols by magnetic polysulfone microcapsules containing tributyl phosphate, Chem. Eng. J. 157 (2010) 466–474. https://doi.org/10.1016/J.CEJ.2009.12.008.

[9] K. Stringfellow, P. Anderson, D. Caldwell, J. Lee, J. Byrd, J. McReynolds, J. Carey, D. Nisbet, M. Farnell, Evaluation of disinfectants commonly used by the commercial poultry industry under simulated field conditions, Poult. Sci. 88 (2009) 1151–1155. https://doi.org/10.3382/PS.2008-00455.

[10] C. Karr, P.M. Brown, P.A. Estep, G.L. Humphrey, Identification and Determination of Low-Boiling Phenols in Low Temperature Coal Tar, Anal. Chem. 30 (1958) 1413–1416. https://doi.org/10.1021/ac60140a037.

[11] L. Lin, M. Yoshioka, Y. Yao, N. Shiraishi, Preparation and properties of phenolated wood/phenol/formaldehyde cocondensed resin, J. Appl. Polym. Sci. 58 (1995) 1297–1304. https://doi.org/10.1002/app.1995.070580811.

[12] K. Bujnowski, A. Adamczyk, L. Synoradzki, o-aminomethyl derivatives of phenols. Part 1. Benzylamines: Properties, structure, synthesis and purification, Org. Prep. Proced. Int. 39 (2007) 153–184. https://doi.org/10.1080/00304940709356009.

[13] M.E. Uddin, R.K. Layek, N.H. Kim, D. Hui, J.H. Lee, Preparation and properties of reduced graphene oxide/polyacrylonitrile nanocomposites using

polyvinyl phenol, Compos. Part B Eng. 80 (2015) 238–245. https://doi.org/10.1016/j.compositesb.2015.06.009.

[14] T.B. Johnson, E.F. Kohmann, The preparation and properties of some higher phenols and their ethers, J. Am. Chem. Soc. 36 (1914) 1259–1268. https://doi.org/10.1021/ja02183a016.

[15] R. Chirinos, R. Pedreschi, H. Rogez, Y. Larondelle, D. Campos, Phenolic compound contents and antioxidant activity in plants with nutritional and/or medicinal properties from the Peruvian Andean region, Ind. Crops Prod. 47 (2013) 145–152. https://doi.org/10.1016/j.indcrop.2013.02.025.

[16] W. Zheng, S.Y. Wang, Antioxidant activity and phenolic compounds in selected herbs, J. Agric. Food Chem. 49 (2001) 5165–5170. https://doi.org/10.1021/jf010697n.

[17] K. Kümmerer, Drugs in the environment: Emission of drugs, diagnostic aids and disinfectants into wastewater by hospitals in relation to other sources - A review, Chemosphere. 45 (2001) 957–969. https://doi.org/10.1016/S0045-6535(01)00144-8.

[18] J. Tremp, P. Mattrel, S. Fingler, W. Giger, Phenols and nitrophenols as tropospheric pollutants: Emissions from automobile exhausts and phase transfer in the atmosphere, Water, Air, Soil Pollut. 68 (1993) 113–123. https://doi.org/10.1007/BF00479396.

[19] M. Czaplicka, Sources and transformations of chlorophenols in the natural environment, Sci. Total Environ. 322 (2004) 21–39. https://doi.org/10.1016/j.scitotenv.2003.09.015.

[20] Y. xun ZHANG, M. SHAO, Y. hang ZHANG, L. min ZENG, L. yan HE, B. ZHU, Y. jie WEI, X. lei ZHU, Source profiles of particulate organic matters emitted from cereal straw burnings, J. Environ. Sci. 19 (2007) 167–175. https://doi.org/10.1016/S1001-0742(07)60027-8.

[21] L. Wachowski, R. Pietrzak, Phenols, Manag. Glob. Resour. Univers. Process. (2020) 275–301. https://doi.org/10.1201/9780429346132-32.

[22] C. Lu, X. Wang, S. Dong, J. Zhang, J. Li, Y. Zhao, Y. Liang, L. Xue, H. Xie, Q. Zhang, W. Wang, Emissions of fine particulate nitrated phenols from various on-road vehicles in China, Environ. Res. 179 (2019) 108709. https://doi.org/10.1016/j.envres.2019.108709.

[23] C. Lu, X. Wang, S. Dong, J. Zhang, J. Li, Y. Zhao, Y. Liang, L. Xue, H. Xie, Q. Zhang, W. Wang, Emissions of fine particulate nitrated phenols from various on-road vehicles in China, Environ. Res. 179 (2019) 108709. https://doi.org/10.1016/J.ENVRES.2019.108709.

[24] L. Ritter, K. Solomon, P. Sibley, K. Hall, P. Keen, G. Mattu, B. Linton, Sources, pathways, and relative risks of contaminants in surface water and groundwater: A perspective prepared for the Walkerton inquiry, J. Toxicol. Environ. Heal. - Part A. 65 (2002) 1–142. https://doi.org/10.1080/152873902753338572.

[25] D.M. Munnecke, L.M. Johnson, H.W. Talbot, S. Barik, Microbial Metabolism and Enzymology of Selected Pesticides, Biodegrad. Detoxif. Environ. Pollut.

(2018) 1–32. https://doi.org/10.1201/9781351070201-1.

[26] P.J. Hernes, R. Benner, Photochemical and microbial degradation of dissolved lignin phenols: Implications for the fate of terrigenous dissolved organic matter in marine environments, J. Geophys. Res. Ocean. 108 (2003) 3291. https://doi.org/10.1029/2002JC001421.

[27] V.M. Zakoshansky, The cumene process for phenol-acetone production, Pet. Chem. 2007 474. 47 (2007) 273–284. https://doi.org/10.1134/S096554410704007X.

[28] A.R. Murray, E. Kisin, V. Castranova, C. Kommineni, M.R. Gunther, A.A. Shvedova, Phenol-induced in vivo oxidative stress in skin: Evidence for enhanced free radical generation, thiol oxidation, and antioxidant depletion, Chem. Res. Toxicol. 20 (2007) 1769–1777. https://doi.org/10.1021/tx700201z.

[29] B. Bukowska, J. Michałowicz, A. Krokosz, P. Sicińska, Comparison of the effect of phenol and its derivatives on protein and free radical formation in human erythrocytes (in vitro), Blood Cells, Mol. Dis. 39 (2007) 238–244. https://doi.org/10.1016/J.BCMD.2007.06.003.

[30] C. Hansch, S.C. McKarns, C.J. Smith, D.J. Doolittle, Comparative QSAR evidence for a free-radical mechanism of phenol-induced toxicity, Chem. Biol. Interact. 127 (2000) 61–72. https://doi.org/10.1016/S0009-2797(00)00171-X.

[31] C.D. Selassie, T. V. Desoyza, M. Rosario, H. Gao, C. Hansch, Phenol toxicity in leukemia cells: a radical process?, Chem. Biol. Interact. 113 (1998) 175–190. https://doi.org/10.1016/S0009-2797(98)00027-1.

[32] L. Yang, G. Liu, M. Zheng, Y. Zhao, R. Jin, X. Wu, Y. Xu, Molecular Mechanism of Dioxin Formation from Chlorophenol based on Electron Paramagnetic Resonance Spectroscopy, Environ. Sci. Technol. 51 (2017) 4999–5007. https://doi.org/10.1021/acs.est.7b00828.

[33] T. Ge, J. Han, Y. Qi, X. Gu, L. Ma, C. Zhang, S. Naeem, D. Huang, The toxic effects of chlorophenols and associated mechanisms in fish, Aquat. Toxicol. 184 (2017) 78–93. https://doi.org/10.1016/J.AQUATOX.2017.01.005.

[34] J.R. Reed, G.F. Cawley, T.G. Ardoin, B. Dellinger, S.M. Lomnicki, F. Hasan, L.W. Kiruri, W.L. Backes, Environmentally persistent free radicals inhibit cytochrome P450 activity in rat liver microsomes, Toxicol. Appl. Pharmacol. 277 (2014) 200–209. https://doi.org/10.1016/J.TAAP.2014.03.021.

[35] G.O. Rankin, A. Sweeney, C. Racine, T. Ferguson, D. Preston, D.K. Anestis, 4-Amino-2-chlorophenol: Comparative in vitro nephrotoxicity and mechanisms of bioactivation, Chem. Biol. Interact. 222 (2014) 126–132. https://doi.org/10.1016/J.CBI.2014.10.001.

[36] E.M. Flanigen, Chapter 2 Zeolites and Molecular Sieves an Historical Perspective, Stud. Surf. Sci. Catal. 58 (1991) 13–34. https://doi.org/10.1016/S0167-2991(08)63599-5.

[37] E. Robens, Some intriguing items in the history of adsorption, Stud. Surf. Sci. Catal. 87 (1994) 109–118. https://doi.org/10.1016/S0167-2991(08)63070-0.

[38] E. Robens, S. Jayaweera, Early history of adsorption measurements, Adsorpt. Sci. Technol. 32 (2014) 425–442. https://doi.org/10.1260/0263-6174.32.6.425.

[39] H. Swenson, N.P. Stadie, Langmuir's Theory of Adsorption: A Centennial Review, Langmuir. (2019). https://doi.org/10.1021/acs.langmuir.9b00154.

[40] F.G. Keyes, The heats of adsorption of several gases and vapors on charcoal, J. Am. Chem. Soc. 49 (1927) 142–156. https://doi.org/10.1021/JA01400A020/ASSET/JA01400A020.FP.PNG_V03.

[41] H.H. Lowry, G.A. Hulett, Studies in the adsorption by charcoal. II. Relation of oxygen to charcoal, J. Am. Chem. Soc. 42 (1920) 1408–1419. https://doi.org/10.1021/ja01452a014.

[42] C.H. Giles, A.P. D'Silva, I.A. Easton, A general treatment and classification of the solute adsorption isotherm part. II. Experimental interpretation, J. Colloid Interface Sci. 47 (1974) 766–778. https://doi.org/10.1016/0021-9797(74)90253-7.

[43] J.W. McBain, XCIX. The mechanism of the adsorption ("sorption") of hydrogen by carbon , London, Edinburgh, Dublin Philos. Mag. J. Sci. 18 (1909) 916–935. https://doi.org/10.1080/14786441208636769.

[44] J. Livengood, Why was M. S. Tswett's chromatographic adsorption analysis rejected?, Stud. Hist. Philos. Sci. Part A. 40 (2009) 57–69. https://doi.org/10.1016/J.SHPSA.2008.12.003.

[45] General and physical chemistry, J. Chem. Soc. Abstr. 86 (1904) B221. https://doi.org/10.1039/ca9048605221.

[46] L.R. Snyder, Column Efficiencies In Liquid Adsorption Chromatography: Past, Present and Future, J. Chromatogr. Sci. 7 (1969) 352–360. https://doi.org/10.1093/CHROMSCI/7.6.352.

[47] J.H. Knox, J. Jurand, Determination of paracetamol and its metabolites in urine by high-performance liquid chromatography using ion-pair systems, J. Chromatogr. A. 149 (1978) 297–312. https://doi.org/10.1016/S0021-9673(00)80994-2.

[48] L.R. Snyder, J.J. Kirkland, J.L. Glajch, Practical HPLC Method Development, Pract. HPLC Method Dev. (1997). https://doi.org/10.1002/9781118592014.

[49] S.G. Shirazi, G. Guiochon, On non-linear waves in chromatography: Introduction, J. Chromatogr. A. 734 (1996) 3–5. https://doi.org/10.1016/0021-9673(96)00092-1.

[50] H. Freundlich, Second Liversidge lecture. Surface forces and chemical equilibrium, J. Chem. Soc. (1930) 164–179. https://doi.org/10.1039/JR9300000164.

[51] E.K. RIDEAL, The Sorption of Gases and Vapours by Solids, Nature. 130 (1932) 222–222. https://doi.org/10.1038/130222a0.

[52] C.H. Giles, The History and Use of the Freundlich Adsorption Isotherm, J. Soc. Dye. Colour. 89 (1973) 287–291. https://doi.org/10.1111/J.1478-4408.1973.TB03158.X.

[53] W. Clayton, Capillary and colloid chemistry. By Prof. H. Freundlich. Translated by H. Stafford Hatfield, B.Sc., Ph.D. pp. xv+883. London: Methuen and Co., Ltd., 1926. Price: 50s, J. Soc. Chem. Ind. 45 (1926) 797–798. https://doi.org/10.1002/JCTB.5000454407.

[54] M. Polanyi, The potential theory of adsorption, Science (80-.). 141 (1963) 1010–1013. https://doi.org/10.1126/science.141.3585.1010.

[55] M. Polànyi, Einiges über Adsorption und Kapillarität vom Standpunkte des II. Hauptsatzes, Zeitschrift Für Phys. Chemie. 88U (1914) 622–631. https://doi.org/10.1515/ZPCH-1914-8839.

[56] A. Eucken, On the existence of active centres in chemical adsorption and contact catalysis, Discuss. Faraday Soc. 8 (1950) 128–134. https://doi.org/10.1039/DF9500800128.

[57] M.H. Armbruster, J.B. Austin, The Adsorption of Gases on Plane Surfaces of Mica, J. Am. Chem. Soc. 60 (1938) 467–475. https://doi.org/10.1021/ja01269a066.

[58] I. Langmuir, The Evaporation, Condensation and Reflection of Molecules and the Mechanism of Adsorption, Phys. Rev. 8 (1916) 149. https://doi.org/10.1103/PhysRev.8.149.

[59] I. Langmuir, The constitution and fundamental properties of solids and liquids. Part I. Solids, J. Am. Chem. Soc. 38 (1916) 2221–2295. https://doi.org/10.1021/ja02268a002.

[60] M. Volmer, Thermodynamische Folgerungen ans der Zustandsgleichung für adsorbierte Stoffe, Zeitschrift Für Phys. Chemie. 115U (1925) 253–260. https://doi.org/10.1515/zpch-1925-11519.

[61] R.H. Fowler, A Statistical Derivation of Langmuir's Adsorption Isotherm, Math. Proc. Cambridge Philos. Soc. 31 (1935) 260–264. https://doi.org/10.1017/S0305004100013359.

[62] I. Langmuir, Vapor pressures, evaporation, condensation and adsorption, J. Am. Chem. Soc. 54 (1932) 2798–2832. https://doi.org/10.1021/ja01346a022.

[63] G.S. Rushbrooke, C.A. Coulson, The thermodynamic derivation of langmuir's isotherm, Math. Proc. Cambridge Philos. Soc. 36 (1940) 248–251. https://doi.org/10.1017/S0305004100017254.

[64] L.D. Asnin, A.A. Fedorov, Y.S. Chekryshkin, Thermodynamic parameters of adsorption described by the logarithmic Temkin isotherm, Russ. Chem. Bull. 2001 502. 50 (2001) 217–219. https://doi.org/10.1023/A:1009509813738.

[65] S. Brunauer, P.H. Emmett, E. Teller, Adsorption of Gases in Multimolecular Layers, J. Am. Chem. Soc. 60 (1938) 309–319. https://doi.org/10.1021/ja01269a023.

[66] P.H. Emmett, S. Brunauer, The Use of Low Temperature van der Waals Adsorption Isotherms in Determining the Surface Area of Iron Synthetic Ammonia Catalysts, J. Am. Chem. Soc. 59 (1937) 1553–1564. https://doi.org/10.1021/ja01287a041.

[67] S. Brunauer, P.H. Emmett, The Use of Low Temperature van der Waals Adsorption Isotherms in Determining the Surface Areas of Various Adsorbents, J. Am. Chem. Soc. 59 (1937) 2682–2689. https://doi.org/10.1021/ja01291a060.

[68] A.B.D. Cassie, Multimolecular absorption, Trans. Faraday Soc. 41 (1945) 450–458. https://doi.org/10.1039/TF9454100450.

[69] G.D. Halsey, The Role of Surface Heterogeneity in Adsorption, Adv. Catal. 4

(1952) 259–269. https://doi.org/10.1016/S0360-0564(08)60616-1.

[70] T.L. Hill, Statistical Mechanics of Multimolecular Adsorption II. Localized and Mobile Adsorption and Absorption, J. Chem. Phys. 14 (2004) 441. https://doi.org/10.1063/1.1724166.

[71] N.K. ADAM, The Adsorption of Gases and Vapours, Nature. 155 (1945) 154–155. https://doi.org/10.1038/155154a0.

[72] S. Brunauer, P.H. Emme, Chemisorptions of Gases on Iron Synthetic Ammonia Catalysts, J. Am. Chem. Soc. 62 (1940) 1732–1746. https://doi.org/10.1021/ja01864a026.

[73] F.H. MacDougall, Kinetic Theory of Liquids. By J. Frenkel., J. Phys. Colloid Chem. 51 (2002) 1032–1033. https://doi.org/10.1021/J150454A025.

[74] T.L. Hill, Theory of Physical Adsorption, Adv. Catal. 4 (1952) 211–258. https://doi.org/10.1016/S0360-0564(08)60615-X.

[75] G.D. Halsey, The role of heterogeneity in adsorption and catalysis, Discuss. Faraday Soc. 8 (1950) 54–56. https://doi.org/10.1039/DF9500800054.

[76] S.J. Gregg, J. Jacobs, An examination of the adsorption theory of Brunauer, Emmett, and Teller, and Brunauer, Deming, Deming and Teller, Trans. Faraday Soc. 44 (1948) 574–588. https://doi.org/10.1039/TF9484400574.

[77] A.S. Michaels, Chemical Analysis: Physical Adsorption of Gases. D. M. Young and A. D. Crowell. Butter-worth, Washington, D.C., 1962. xii + 426 pp. Illus. $13., Science (80-.). 141 (1963) 1268–1268. https://doi.org/10.1126/SCIENCE.141.3587.1268.A.

[78] K.S.W. Sing, D.H. Everett, R.A.W. Haul, L. Moscou, R.A. Pierotti, J. Rouquerol, T. Siemieniewska, Reporting Physisorption Data for Gas/Solid Systems with Special Reference to the Determination of Surface Area and Porosity, Pure Appl. Chem. 57 (1985) 603–619. https://doi.org/10.1351/pac198557040603.

[79] K.S.W. Sing, Physisorption of nitrogen by porous materials, J. Porous Mater. 1995 21. 2 (1995) 5–8. https://doi.org/10.1007/BF00486564.

[80] I. Langmuir, The constitution and fundamental properties of solids and liquids. II. Liquids, J. Am. Chem. Soc. 39 (1917) 1848–1906. https://doi.org/10.1021/ja02254a006.

[81] A. Titoff, Die Adsorption von Gasen durch Kohle, Zeitschrift Für Phys. Chemie. 74U (1910) 641–678. https://doi.org/10.1515/ZPCH-1910-7428.

[82] R. Zsigmondy, Über die Struktur des Gels der Kieselsäure. Theorie der Entwässerung, Zeitschrift Für Anorg. Chemie. 71 (1911) 356–377. https://doi.org/10.1002/ZAAC.19110710133.

[83] L.R. Fisher, J.N. Israelachvili, Direct experimental verification of the Kelvin equation for capillary condensation, Nat. 1979 2775697. 277 (1979) 548–549. https://doi.org/10.1038/277548a0.

[84] S. Inoue, N. Ichikuni, T. Suzuki, T. Uematsu, K. Kaneko, Capillary Condensation of N2 on Multiwall Carbon Nanotubes, J. Phys. Chem. B. 102 (1998) 4689–4692. https://doi.org/10.1021/JP973319N.

[85] A.G. Foster, The sorption of condensible vapours by porous solids. Part I. The

applicability of the capillary theory, Trans. Faraday Soc. 28 (1932) 645–657. https://doi.org/10.1039/TF9322800645.

[86] J.H. De Boer, S. Kruyer, The two-dimensional van der Waals constants of molecules adsorbed on charcoal and graphite, Trans. Faraday Soc. 54 (1958) 540–547. https://doi.org/10.1039/TF9585400540.

[87] S.M. Manocha, Porous carbons, Sadhana - Acad. Proc. Eng. Sci. 28 (2003) 335–348. https://doi.org/10.1007/BF02717142.

[88] F.A.L. Dullien, V.K. Batra, Determination of the Structure of Porous Media, Ind. Eng. Chem. 62 (1970) 25–53. https://doi.org/10.1021/ie50730a004.

[89] K.S.W. Sing, Characterization of porous materials: Past, present and future, Colloids Surfaces A Physicochem. Eng. Asp. 241 (2004) 3–7. https://doi.org/10.1016/j.colsurfa.2004.04.003.

[90] N.D. Hutson, R.T. Yang, Theoretical basis for the Dubinin-Radushkevitch (D-R) adsorption isotherm equation, Adsorpt. 1997 33. 3 (1997) 189–195. https://doi.org/10.1007/BF01650130.

[91] J.H. De Boer, Adsorption Phenomena, Adv. Catal. 8 (1956) 17–161. https://doi.org/10.1016/S0360-0564(08)60538-6.

[92] G.F. Cerofolini, Localized adsorption with lateral interactions on patchwise heterogeneous surfaces, Thin Solid Films. 26 (1975) 53–59. https://doi.org/10.1016/0040-6090(75)90166-2.

[93] T.L. Hill, Statistical Mechanics of Adsorption. V. Thermodynamics and Heat of Adsorption, J. Chem. Phys. 17 (2004) 520. https://doi.org/10.1063/1.1747314.

Chapter-2

Review of literature

2.1. Introduction

Phenol is an organic compound that is used in the production of nylon 6, synthetic fibres, polycarbonate plastics, epoxy, and resins, among other things. The Environmental Protection Agency has designated it as a priority pollutant with a permitted concentration in drinking water of 0.005 mg/L. The toxicity of phenol has been well recognised (Centers for Disease Control and Prevention, 2009); its increased presence in water has a noticeable impact on the taste and odour of the water (Water Environment Partnership in Asia 2012). Phenolic compounds, such as phenol, chlorophenol (CP), ethylphenol, isopropyl phenol, nitrophenol, and many others, are found in industrial wastewaters from coking plants, textile industries, petroleum refineries, coal gasification, resin production, dye synthesis, paper mills, pharmaceutical industries, and herbicide and fungicide manufacturing. (Hannaford and Kuek 1999). When phenol reacts with chloride ions in water, it forms CPs like 2-CP, 4-dichlorophenol (4-DCP), and 2,4,6-trichlorophenol (2,4,6-TCP), which are more poisonous and stable. Phenol concentrations in industrial wastewaters range from 1 mg/L in paint production to 7000 mg/L in coal conversion wastewaters. (Metcalf and Eddy Inc. 2003). For the removal of phenol compounds from industrial wastewater, a variety of technical procedures are available, including membrane filtering, electrochemical and chemical oxidation, and adsorption. Adsorption is a particularly appealing technique since it has cheap capital and operating costs, is easy to monitor, and provides for the reuse of adsorbents and the recovery of phenols for recycling [1]. The removal of phenol compounds from wastewater by various adsorbents is discussed in this review, which is divided into groups based on the nature/origin of the compounds. The first category is the most extensive, and it includes commercial activated carbon (CAC), a petroleum-based product with

demonstrated high adsorption capacity in a variety of applications, as well as activated carbons (ACs) derived from agricultural, food, and industrial wastes. Natural materials such as clays and minerals belong to the second group of adsorbents. The third category includes polymer-based adsorbents, while the fourth category includes unique adsorbents created using innovative materials and processes. Chemical and physical changes of the adsorbents listed are also covered in the relevant sections. The adsorption performance of each group of adsorbents is explained, and adsorption data is supplied in table format for easy comparison by researchers and industrial operators.

2.2. Carbonaceous adsorbents

AC is used in different industries for decolorization, smell removal, dechlorination, filtration, sewage treatment, wastewater treatment, drinking water conditioning, hydrogen purification, and ozone annihilation operations due to its highly amorphous structure and vast internal surface area. However, certain parameters in terms of AC's surface area, porosity, pore size distribution, and adsorption characteristics may be required for each operation. Coal and petroleum products are traditional sources of ACs, however, unconventional or so-called novel sources of ACs include a wide range of agricultural and industrial wastes that can be used to make ACs.

2.2.1. Fossil-AC adsorbents

Since 1500 B.C., charcoal, the earliest carbonaceous precursor of AC, has been utilised for drinking water filtration as the oldest adsorbent [2]. Petroleum coke and lignite are the primary sources of CAC, and the processing of these materials makes CAC an expensive adsorbent. AC is divided into two categories based on its physical characteristics: granular AC (GAC) and powdered AC (PAC). In comparison to PAC, GAC has bigger particle size but a smaller exterior surface.

GAC has a faster diffusion rate and is hence favoured for adsorption of gases, vapours, and odours, particularly in continuous mode. GAC has a greater initial cost, but a lower operational cost, owing to the lower GAC replacement cost.

PAC, on the other hand, has a tiny particle size < 50 m in diameter and a cheap initial capital cost [3]. It's commonly used in batch adsorption, and the dosage can be changed as needed. Due to the small particle size of PAC, it is difficult to recover and renew. It also causes a build-up of sludge in the treatment filters. AC was described by Dabrowski [4] as a material with optimal adsorption capacity for phenol compounds with low molecular weight. Ania *et al.* [5] found that GACs and PACs have adsorption capabilities of 303 and 226 mg/g, respectively. Ahmaruzzaman and Sharma [6] reported adsorption capacities of CAC for phenol and PNP 322.5 and 526.3 mg/g respectively. Sulaymon and Ahmed [7] achieved 380.2, 350, and 219.9 mg/g removal of ortho-chlorophenol (*o*-CP), phenol, and 4-CP/g respectively by CAC. Although ACs have excellent adsorption capacities, the expensive cost of CAC, as well as the high disposal costs related with the irreversible adsorption of phenols on PAC, limits their use in industrial wastewater treatment.

2.2.2. Industrial waste-based adsorbents

Industrial waste is another abundant source of possible adsorbents. During bauxite processing, the aluminium industry produces 1–2 tonnes of red mud leftovers for every tonne of alumina produced [8]. Tor *et al.* [9] evaluated this extremely alkaline solid waste (pH 10–12.5) and found that it had an adsorption capacity of 4.127 mg/g , which increased to 8.16 mg/g after the red mud was neutralised with hydrochloric acid. Tancredi *et al.* [10] pyrolyzed Eucalyptus grandis sawdust, a major byproduct from Uruguay's increasing wood sector, to produce PAC. The adsorbent had a surface area of 590 m^2/g and was combined with carboxymethyl cellulose as a binder and

kaolin as a reinforcement, resulting in a phenol adsorption capacity of 64 mg/g. Makrigianni *et al.* [11] achieved 51.92 mg/g adsorption capacity using acid-treated pyrolytic tyre char (PTC). The hydrogen bonding of phenol with the surface groups of PTC is thought to be based on a p-p electron donor/acceptor interaction mechanism. Tang *et al.* [12] made a porous adsorbent from raw coal slag by chemically activating sieved coal slag, then leaching silica oxides and reacting it with calcium hydroxide to make a white powder adsorbent. This adsorbent had a phenol adsorption capacity of 63.78 mg/g, which is significantly greater than that of raw coal slag. The AC was made from polyethylene propylene (PET), which absorbed 162–278 mg/g of phenol when mixed with coal-tar pitch. They were characterised for pore size distribution, and the following trends were discovered: first, a higher mesopore volume was associated with a shorter activation period; second, the boundary layer effect was lower for carbons with higher hydrophilicity; and finally, phenol is primarily adsorbed within micropores with a diameter one to two times larger than the diameter of a phenol molecule (0.75 nm) [13]. Such a substantial association suggests that the adsorbents with a mesopore content could be developed to target increased phenol adsorption. Thang *et al.* [14] used Chicken manure biochar (CBC) for the adsorption of the phenol and 4-NP. CBC was prepared in the temperature range of 200 - 600ºC under the nitrogenous environment. The q_{max} for phenol and 4-NP was found to be 106.2 and 148.1 mg/g respectively at pH and temperature 22ºC. The reason behind the increased uptake of 4-NP than phenol was the presence $–NH_2$ group resulting in the greater electrostatic interatction between CBC and 4-NP [14]. Lütke *et al.* [15] prepared AC from black wattle barke obtained from tanning industry waste. Wattle bark was activated using $ZnCl_2$ resulting in a mesoporous material with a surface area of 414.097 m^2/g. The q_{max} of phenol removal was 98.57 mg/g at 55ºC.

The adsorption capacities of the raw, untreated natural adsorbents reported thus far were not very spectacular; nevertheless, pretreatment and/or modification of these low-cost adsorbents resulted in significantly enhanced adsorption capacities, equivalent to CACs.

2.2.3. Agriculture waste-based adsorbents

Agricultural wastes have been used as precursors in the manufacture of low-cost AC to remove toxins from the environment. Although the adsorption properties of these adsorbents vary, their manufacturing costs are lower than CACs. Furthermore, a varied range of agricultural wastes is readily available in significant quantities in the area, making these adsorbents accessible to local industrial operators for wastewater treatment. Furthermore, the use of diverse wastes to manufacture carbonaceous adsorbents has a significant impact on local solid waste management.

Coconut (Cocos nucifera) is the India's one of the most important agricultural crop [16]. Tons of shells, husk, and coir pith waste are generated by vast coconut plantations. These ingredients are utilized to make coconut shell-based AC, which accounts for about 18 % of global CAC production [17]. Many studies have looked into the activation of coconut AC precursors, and others have looked into the adsorption capacity of coconut-based ACs for phenol removal. Hu and Srinivasan [18] found that coconut shell AC (CSAC) activated with potassium hydroxide (KOH) had adsorption capacities of 206, 257, and 267 mg/g for phenol, 4-nitrophenol (4-NP), and 4-CP, respectively. At the acidic condition, Namasivayam and Kavitha [19] investigated the adsorption of pentachlorophenol (PCP), 2,4-DCP, and phenol by plain coconut coir pith and found that the adsorption capacities were 3.66, 19.12, and 48.31 mg/g, respectively. At increased temperatures, Namasivayam and Kavitha [20] achieved adsorption of 2,4-DCP 92.58 mg/g onto $ZnCl_2$ activated coir pith carbon.

The adsorption of PCP and TCP by CSAC activated with KOH and CAC was investigated by Radhika and Palanivelu [21]. In the adsorption of PCP, CAC outperformed CSAC (72.769 mg/g); but, in the adsorption of TCP, CSAC outperformed CAC with adsorption of 122.336 mg/g compared to 112.35 mg/g by CAC. About 35% of the fruit is made up of coconut husk or coir pith, a fibre that covers the coconut shell. Tan *et al.* [22] removed 716.10 mg/g of 2,4,6-TCP from coconut husk AC at 30ºC. (CHAC). TCP adsorption was improved by increasing agitation, time, and acidic pH. At increased temperatures, Din *et al.* [23] found 205.8 mg/g of phenol removal onto KOH-CO_2 activated CSAC. The adsorption efficiency of CSAC treated with $Cu(NO_3)_2$ was reported to be 239.85 mg/g at pH 8 by Singh and Balomajumder [24]. Despite the fact that the adsorbent's surface area reduced from 81.82 to 30.54 m^2/g after treatment, the phenol adsorption capacity was significantly higher than that of the agricultural-based adsorbents. The results of the Fourier transform infrared spectroscopy spectrum for the original, after treatment, and after adsorption of adsorbents suggested that phenol molecules were adsorbed via a chemisorption mechanism, i.e. interaction between the solute and the functional groups on the adsorbent surface increased significantly after treatment. The results highlighted the significance of surface functional group concentrations in enhancing phenol binding to the adsorbent surface. Singh and Balomajumder [25] modified CSAC by immobilising Pseudomonas putida cells in the carbon; however, only an 18.9 mg/g phenol adsorption was reached at pH 7–8, which was attributed to phenol's harmful effect on microorganism cells, resulting in unsatisfactory performance.

In the Asian region, rice husk is another prevalent agricultural waste. After harvesting, it is frequently burned on-site in rice plantations, resulting in considerable air pollution. The husk removed during the milling process accounts for about 20 %

of paddy weight. Rice husk is high in amorphous and crystalline forms of silica, which helps to remove contaminants from wastewater. Rice husk is converted to rice husk ash (RHA) during burning, and incomplete combustion results in carbonised rice husk.

Mahvi *et al.* [26] investigated the adsorption of phenol on raw RH and RHA at pH levels ranging from 5 to 11, and found that RHA had the maximum removal of 0.866 mg/g at pH 5 and RH had the lowest removal of 0.0022 mg/g at pH 11. The effect of acidic pretreatment on raw rice husk was investigated by Daffalla *et al.* [27], who found a considerable increase in adsorption efficiency. The most significant effect was reported in RH sulfuric acid treatment, which removed 40.21 % of phenol, a two-fold increase over untreated RH. Only pretreatment with citric acid resulted in a slight increase of 3 %, whereas hydrochloric and nitric acids boosted adsorption efficiency by at least 50 %. The elimination of surface contaminants, enhanced porosity, and exposure of more hydroxyl and other functional groups on the RH surface are all linked to the effect of inorganic acids on RH adsorption capacity. Srinivas and Das [28,29] investigated the phenol adsorption onto black gram husk (BGA), green gram husk (GGH) and RH in the pH range of 5-12. These adsorbents were pretreated with H_2SO_4 in 1:1 ratio for 24 h and the pyrolysed at the temperature of 800ºC. The Redlich-Petorson model best explain the adsorption phenomena and the q_{max} for adsorption were in the order of BGA > GGA .RH i.e. 11.17 > 10.23 > 6.11 mg/g respectively, at the pH 5.1.

Adsorption of 2,4-DCP onto coconut bagasse, on the other hand, was higher at 50.53 mg/g, which was attributed to the composition of coconut and the affinity between the adsorbent and the solute [30].

Tea farms abound in South Asia, and tea leaves can be used to remove phenol. At

pH 7 and 30ºC, Gupta and Balomajumder [31] found that tea leaves biomass had an adsorption capacity of 9.487 mg phenol/g; however, as the temperature was increased to 50ºC, the adsorption capacity of phenol declined.

2.2.4. Food waste-based adsorbents

Any organic waste can theoretically be carbonized, activated, and used as an adsorbent. The carbonaceous adsorbent bagasse fly ash can be made from sugar cane bagasse, for example (BFA). Gupta *et al.* [32] employed activated BFA to remove phenol and 4-NP from wastewater, with 95 % and 99.9 % removal rates, respectively. According to Srivastava *et al.* [33], BFA has a phenol adsorption capability of 23.83 mg/g.

Corn cob is a large-scale post-production waste product of food processing. For every 100 kg of maize produced, about 18 kg of corn cob is collected [34]. El-Hendawy *et al.* [35] used phosphoric acid to activate corn cob char, resulting in a phenol adsorption capacity of 177.6 mg/g. Tseng and Tseng [36] developed KOH-activated cottony structure corn cob carbon, which absorbed 232.0, 362.8, and 333.7 mg/g of phenol, pCP (), and 2,4-DCP, respectively. The adsorption capacity of AC produced with greater KOH levels increased to 340, 485, and 451.2 mg/g, respectively.

Okeowo *et al.* [37] studied the phenol adsorption on the AC of mango seed shell modified with microwave assisted Ag-Au nanoparticles and reported the maximum phenol uptake of 47.8 mg/g at 35 ºC.

Seafood contains chitin, a natural polymer found in the protective shells of crustaceans that can be converted to chitosan through alkaline deacetylation [38]. Because of the huge number of amino and hydroxyl functional groups in its structure, chitosan possesses adsorption potential. Milhome *et al.* [39] found that

non-pretreated chitosan removed 1.26 mg/g of phenol, which was easily regenerated with high efficiency (95 %) by ethanol-water in four successive cycles.

Oliveira *et al.* [40] used chitosan to adsorb 2,4-DCP and 2,4,6-TCP in a fixed-bed adsorption column, reporting 6.0 and 27.6 mg/g adsorption capacities, respectively.

To remove CPs, Zhou *et al.* [41] combined chitosan with salicylaldehyde and β-cyclodextrin to produce the CS-SA-CD bifunctional adsorbent. The maximal removal of phenol, 2-CP, 4-CP, 2,4-DCP, and 2,4,6-TCP by CS-SA- CD was 59.74, 70.52, 96.43, 315.46, and 375.94 mg/g, suggesting that CS-SA- CD has a strong affinity for DCP and TCP. In five cycles, the adsorption effectiveness of phenol and CPs onto CS-SA-CD remained between 80 % and 91 %, and the adsorbent could be easily regenerated with ethanol.

2.3. Clay and mineral-based adsorbents

Clay, zeolite, bentonite, montmorillonite, and red mud are only a few examples of naturally occurring minerals with adsorption potential. For example, in the 1970s, zeolite, a crystalline hydrated aluminosilicate mineral (TO_4), was studied for its excellent selectivity, consistent pore size, and ease of regeneration. When compared to CAC, zeolite with a larger Si/Al ratio demonstrated phenolic compound adsorption selectivity, whereas pure siliceous zeolite with an infinite Si/Al ratio showed higher adsorption capacity [42]. Gupta *et al.* [43] investigated red mud as a phenol adsorbent and found that the positive surface charges on the red mud adsorbent attract negatively charged phenol chemicals, with removal capacities of 59.2 mg/g for phenol, 117.3 mg/g for 2-CP, 127.1 mg/g for 4-CP, and 130 mg/g for 2,4-DCP. As the amount of chlorine atoms rose, the adsorption dropped in the following order: 4-CP > 2-CP > phenol > 2,4- DCP. Cardenas *et al.* [44] investigated the phenol and CP

adsorption by porous clay heterostructures (PCH). In the elimination of phenol, 2,5-DCP, and 3,4-DCP, the adsorption capacities reached 14.5, 45.5, and 48.7 mg/g, respectively. Pillaring during the manufacture of PCH adsorbent is linked to the synthesis of hydrophobic and hydrophilic silanol and siloxane groups. Increased phenol uptake occurs when the initial phenol concentration is reduced and the contact time is reduced.

According to Zaitan *et al.* [45], hydrophobic zeolites have a higher phenol adsorption affinity. Natural zeolite, on the other hand, is hydrophilic, necessitating surface modification to make hydrophobic zeolite, which raises the cost of zeolite and makes it more susceptible to humidity. At 25ºC, Rushdi *et al.* [46] found that zeolite had a phenol adsorption capacity of 34.5 mg/g.

Bentonite, a montmorillonite clay containing highly exchangeable cations such as Sodium (I), Calcium (II), and Hydrogen, is another clay adsorbent (I). Natural clay, unlike zeolite, has a lower phenol elimination efficiency. Most clays have a lot of exchangeable ions on the surface as well as a lot of microscopic surface area, thus they can adsorb cationic, anionic, and neutral molecules. Natural clay was used by Djebbar *et al.* [47] to remove up to 60 % of phenol, with a maximum adsorption capacity of 15 mg/g at pH 5.0 and 23ºC. When compared to natural clay, processed activated clays always have better adsorption capacities. At pH 7, Varank *et al.* [48] found that clay had a 68 % adsorption effectiveness of 4-nitrophenol. Clay adsorbents have the disadvantage of forming a jelly-like sticky material in aqueous solution, resulting in excessive adsorbent use. Cheng *et al.* [49] prepared zeolite and AC-based composite (X/ AC) from elutrilithe by adding pitch powder and solid SiO_2 to adsorb phenol. The composite's surface area and porosity increased due to the presence of aluminosilicate and AC. In comparison to natural

zeolite, which has a 34.5 mg/g adsorption capacity, phenol adsorption increased from 37.92 mg/L at 25ºC to 40.31 mg/g at 40ºC and pH 6.5 [46].

Surface reactivity, chemical, physical, and structural features of adsorbents are targeted for modification. Chemical, physical, and biological modifications are the three types of changes. The most frequent way for making the surface functional groups of the adsorbent acidic, basic, or neutral chemical treatment. Acidic surface functional groups have a greater affinity for heavy metals, whereas basic surface functional groups bind organic molecules such as phenols. Thermal treatment of adsorbents is also a physical alteration. The introduction of microorganisms capable of altering the adsorbent properties as a result of their growth is referred to as biological modification. Clay, for example, has hydrophilic surface features that can be converted to hydrophobic surface properties by using a cationic surfactant, often a quaternary alkylammonium. The most commonly modified clays for wastewater treatment are bentonite and montmorillonite. Due to chain interaction and multilayer development, Yapar *et al.* [50] found that hexadecyl-trimethyl-ammonium (HDTMA) was entirely adsorbed by bentonite even when the treatment amount surpassed its cation exchange capacity. The adsorption effectiveness for phenol, on the other hand, was modest (between 5 % and 25 %), although it improved as the initial phenol content and adsorbent dosage were raised. According to Zahir and Najwa [51], the amount of phenol removed from aqueous solution increased in the following order: phenol, PCP, 2,4-DCP, with 2,4-DCP having the lowest water solubility, indicating that surface hydrophobicity is a key factor in determining the extent of phenol adsorption capacity. Kuleyin [52] evaluated the adsorption of phenol and 4-CP onto HDTMA and benzyl dimethyl tetradecyl ammonium (BDTDA) surfactant-modified zeolite, which boosted the zeolite's hydrophobicity and hence adsorption capacity up

to 80 %, particularly for 4-CP (98 %). BDTDA treatment improved the zeolite's adsorption characteristics even more. Uday *et al.* [53] used a long-chain alkylammonium cation, HDTMA bromide, and a short-chain alkylammonium cation, phenyltrimethylammonium (PTMA) bromide, to modify bentonite and kaolinite to produce four types of organo-clays: HDTMA-bentonite, HDTMA-kaolinite, PTMA-bentonite, and PTMA-kaolinite. Raw bentonite and kaolinite had adsorption capacities of 0.247 and 0.468 mg/g after 2 hours, respectively, whereas treated bentonite and kaolinite reached adsorption equilibrium in 30–50 minutes. Bentonite responded better to HDTMA modification, producing the maximum adsorption capacity of 8.435 mg/g, whereas PTMA modification yielded an adsorption capacity of 3.481 mg/g. HDTMA-modified kaolinite, on the other hand, exhibited a less apparent improvement, removing 2.351 mg/g of phenol, whereas PTMA-modified kaolinite removed 0.675 mg/g of phenol.

Senturk *et al.* [54] employed cationic surfactant CTAB to modify bentonite, resulting in the removal of 333 mg/g of phenol in at least five cycles without adsorbent renewal. Desorption efficiency was 96.6 % after regeneration with 20 % acetone. At lower pH, phenol adsorption was stronger, and at pH > 9, it significantly dropped. Furthermore, increasing the temperature to 40ºC reduced the efficiency of phenol removal. The adsorption of phenol by natural and modified clinoptilolite, a natural zeolite, was investigated by Sprynskyy *et al.* [55]. At low phenol concentrations, treatment with a 3 % w/w solution of HDTMA-Cl produced an adsorption capacity of > 90 %. The addition of NaOH, on the other hand, resulted in phenol elimination of approximately 50 %, but raw clinoptilolite adsorption was quite weak. Hulya *et al.* [56] investigated the adsorption of o-nitrophenol, m-nitrophenol, and PNPs on two types of organo-bentonite treated with HDTMA and polyethene

glycol (PEG) surfactants at different temperatures. The results showed that m-nitrophenol and PNP adsorption onto HDTMA-modified bentonite was good, with 208.33 and 133.33 mg/g, respectively. In single systems, phenol adsorption was shown to be higher than in the binary systems. Only PNP (344.83 mg/g) adsorbed well onto PEG-modified bentonite; both adsorbents had weak affinity for 2-NP.

Luo *et al.* [57] used hexamethylene bis-pyridinium dibromides (HMBPs) to make reduced charge montmorillonites (RCMs) with phenol adsorption of 41.88 mg/g at pH 6. Clay charge was shown to have an important role in the binding of phenol molecules to the HMBP-RCM surface by enlarging interlayer space and converting the surface from hydrophilicity to hydrophobicity. More importantly, it was discovered that the fundamental adsorption driving force in phenols was the -polar contact between the pyridine and benzene rings. This conclusion points in the right direction for phenol adsorption research, which should focus on adsorbents with the right functional groups. Ma *et al.* [58] used polyhydroxy-aluminum (Al13)-pillared montmorillonites with cationic (C16) and zwitterionic surfactants to modify inorganic-organic montmorillonites (Z16). The types and doses of surfactants had a significant impact on the adsorption capacity of the adsorbents, which ranged from 6.33 to 16.93 mg/g. The phenol elimination was unaffected by the presence of phosphate and cadmium ions.

2.4. Polymer-based adsorbents.

2.4.1. Polystyrene-based adsorbents

Because of their mechanical stiffness, excellent selectivity, big capacity, customizable pore size, and surface chemistry structure, polymeric adsorbents have been viewed as a potentially cost-effective alternative to widely employed AC for the removal of organic contaminants from industrial wastewater [59–62].

Furthermore, under mild conditions, organic eluting agents can be used to regenerate polymer-based adsorbents. Polymer adsorbents can be classified into two categories: those based on polystyrene (PS) and those based on polyacrylic ester (PAE).

A PS-based resin, also known as a crosslinked styrene-divinylbenzene polymer, is formed by polymerizing styrene monomer with divinylbenzene as the crosslinking agent. Pore-forming substances utilised during polymerization, such as toluene and xylene, result in adsorbents with a large porosity structure. The higher the crosslinking agent ratio, the more surface area is produced and the pore size distribution is narrowed [63]. PS resin is non-polar and hydrophobic, making it ideal for removing non-polar and aromatic chemicals from polar liquids. For phenol, PCP, and PNP, for example, SP-206, a PS matrix crosslinked with divinylbenzene polymer, had adsorption capabilities of 5.89, 196.0, and 113.37 mg/g, respectively [64]. In just a few minutes, the adsorbent may be regenerated with 0.05 N NaOH.

Meanwhile, Amberlite resin (XAD-16) removed 141.17 and 291.82 mg/g of phenol and CP at pH 6, respectively [65]. The significantly higher removal of CP by XAD-16 is attributed to its higher solubility and surface hydrophobicity. As the compound is a non-polar polymeric resin, the van der Waals force is the main driving force between the phenol and resin, which also enables resin regeneration and subsequent phenol recovery, whereas XAD-4, a non-ionic resin with macro reticular structure and large surface area, removed 30.89 mg of 4-CP/g [66]. However, the adsorption capacity of XAD-4 may vary for various phenol compounds; thus, Li *et al.* (2004) obtained adsorption capacities of 56.76, 127.22, 380.26 and 277.94 mg/g for phenol, *p*-cresol, PCP, and PNP, respectively, in acidic medium.

In the 1960s, Alexandrovich *et al.* [67] developed a novel kind of PS adsorbent

called hypercrosslinked polymer by extensively chloromethylating and post-crosslinking preformed PS adsorbent in the presence of a bifunctional crosslinking agent and a Friedel-Crafts catalyst. The first substance induced the development of crosslinking bridges that held PS chains apart and prevented the collapse of the resin pores. In comparison to macro-reticular PS adsorbent, this resin typically displays a greater porous surface area and stronger adsorbate-adsorbent affinity [61,63]. According to Azanova and Hradil [68], hypercrosslinked polymeric adsorbents may bind organic molecules three times more quickly than macroporous adsorbents. Hypercrosslinked resins do, however, have some drawbacks. First, because there is a high degree of crosslinking during polymerization, there is less adsorbate penetration into the polymer bulk, which lowers the total adsorption capacity. Second, a group of chemicals known as chloromethyl methyl ether is utilised in the post-crosslinking method to achieve further crosslinking. a human carcinogen (Environmental Protection Agency 2000). And finally, the vinyl-benzyl chloride monomer has a high cost of manufacture. Macroreticular PS and hypercrosslinked PS adsorbents were examined in a number of investigations for their adsorption capacities. Pan *et al.* [69] evaluated the adsorption capability of a hypercrosslinked adsorbent, NDA-100, and reported 207.7 mg phenol/g and 140.9 mg/g of 4-NP removalat 25ºC. Liu *et al.* [70] found that NDA-100 has a large volume of micropores and a surface area of 943 m^2/g. ZCH-101, a different hypercrosslinked polymeric adsorbent, also significantly adsorbs phenol at a rate of 384.6 mg/g [71]. Due to the presence of polar carbonyl and hydroxyl groups on their surfaces, the hypercrosslinked adsorbents demonstrated a few times better phenol adsorption capacity than XAD-4.

2.4.2. Modified polymeric adsorbents

Other functional groups, including as acetyl, amine, benzoyl, carboxyl, hydroxy-

methyl, and amino groups, can be introduced into the polymer matrix to modify polymeric adsorbents. Ming *et al.* [72] changed the non-polar Amberlite XAD-4 adsorbent (NDA-100), a macrorecticular PS adsorbent, utilising dimethylamine functional groups, and evaluated the efficacy of the new adsorbent against IRA-96C. (a weak-base adsorbent). These three adsorbents had the highest phenol adsorption capacities in the following order: NDA-103 > IRA-96C > XAD-4. In addition to hydrogen bonds and van der Waals forces, the tertiary amino groups are in charge of the enhanced attraction between phenol and NDA-103. Despite having a smaller surface area than XAD-4 and fewer amino groups than IRA-96C, NDA-103 showed a potent affinity for phenol. Similar patterns for aminated NDA-101 and NDA-103 adsorbents were validated by Zhang *et al.* [73].

Huang [74] used formaldehyde carbonyl groups to modify the chloromethylated PS-based adsorbent HJ-1. The generated contact between the formaldehyde carbonyl group and the hydrogen atoms of the phenol hydroxyl group plays a key role in phenol elimination. HJ-1 underwent chemical alteration to become more hydrophilic and polar on the surface, which enhanced its adsorption capacity to 174.2 mg/g. In order to create the HJ-M05 polymeric adsorbent, Huang *et al.* [59] also changed the HJ-55 hypercrosslinked PS resin using diethylenetriamine. HJ-M05 resin's polarity was improved by the nucleophilic substitution of chlorine by the polar diethylenetriamine groups on HJ-55's surface, although its surface area and pore volume were smaller than those of its precursor. This was due to the resin's lower chlorine content. HJ-55 and HJ-M05 have respective phenol adsorption capabilities of 178.1 and 201.7 mg/g. The HJ-M05 resin was simply regenerable by NaOH, same like the HJ-Z01 resin.

N-methylacetamide was used to modify the chloromethylated PS-based

hypercrosslinked resin HJ-Z01 in three separate Friedel-Crafts, methylamination, and acetylation reactions. The HJ-Z01 surface area and pore size reduced as a result of the alteration, while the adsorption capacity increased significantly to 170.2 mg/g of phenol. An intriguing development in the development of polymeric adsorbents with even larger capacity and reusability is the considerable impact of various polar functional groups on the adsorptive characteristics of polymer-based adsorbents. Enyoh *et al.* [75] used modification of microplastics obtained from polyethylene terpthalate (PETMP) and used it for phenol adsorption. They prepared pristine- (Pr-PETMP), modified (mod-PETMP) and Ag-PET. The q_{max} of Pr-PETMP, mod-PETMP and Ag-PETMP for phenol adsorption were found to be 0.226, 0.126 and 0.216 mg/g respectively at pH 6 and 25ºC.

2.4.3. Polyacrylic ester-based adsorbents

The manufacture of polyacrylic ester adsorbent is identical to that of PS adsorbent; however, polymerization requires a monomer. Because acrylate is more reactive during the copolymerization process than PS adsorbent, it is more stable and has higher mechanical strength. Acrylate is a monomer used to create polyacrylic ester adsorbent. Because of its polarity, hydrophilicity, and the intermolecular hydrogen bonding that occurs between the hydroxyl group of phenols and the carbonyl group of the polymeric matrix, acrylic ester polymer is an efficient adsorbent of phenols [76]. However, the competing impact of water may impair phenol's ability to adsorb in an aqueous solution. In comparison to PS-based adsorbents, polyacrylic ester resin regeneration is significantly simpler. Polyacrylic ester adsorbents are made from an acrylate monomer and are polar, hydrophilic, and adsorbents. PS adsorbents, in contrast, are non-polar, hydrophobic, and composed of the styrene monomer.

One of the commercially accessible polyacrylic ester adsorbents is called

Amberlite XAD-7, and it is made by synthesizing weakly polar crosslinked methacrylate polymers. The covalently attached ester groups to the porous polymeric matrix of XAD-7 are somewhat positively charged in acidic medium and increase the inner surface's hydrophilicity [77]. The ability of phenol to bind to XAD-7 was demonstrated in an acidic media where it was able to remove 22.8 mg/g of 4-CP in just 2 h [66], however an alkaline medium caused a dramatic decline in adsorption capacity. It was simple to use ethanol to completely regenerate the exhausted XAD-7. An acrylic ester-based crosslinked copolymer (BMS) resin with the ability to remove phenol from a highly concentrated solution was created by Qiu *et al.* [78]. The adsorption performance of BMS-resin was compared to that of AC fibre and PS resin (XAD-4), which demonstrated that BMS-resin removed more phenol in the concentration range of 100 to 1000 mg/L (pH 7.0). It was explained by the size of their surfaces, 1029.45 and 750 m^2/g, respectively. However, when tested at a concentration of 93,000 mg /L of phenol, BMS- resin showed an exceptional adsorption capacity of > 1000 mg/g, which was attributed to the copolymer's many ester linkages, which allowed a hydrogen connection to form between the ester carbonyl group and the phenol hydroxyl group. The affinity between BMS-resin and phenol was shown to be increased by increasing phenol concentration. Additionally, BMS-resin was entirely regenerated using 5 % NaOH 20 times in a row, and each time it kept its high adsorption capability.

2.5. Novel adsorbents

To increase adsorption capabilities, a number of materials and compounds that have undergone thermal and chemical alterations have recently been evaluated as adsorbents. To enrich composite hydrophilic polyurethane (HPU) for the adsorption of phenol, Massalha *et al.* [79] separately added dry biomass, clay, and PAC to it. Along

with the mechanical qualities, the tested adsorption capacities of the foams' formulations rose from 2.85 to 39.9 mg/g. However, because of the hydrophilicity of polyurethane, the resulting adsorption capacity was substantially less than that of plain PAC. Although the study showed promising potential for phenol adsorption using composite materials, their adsorption capacity still has to be increased through additional surface treatment. Multiwalled carbon nanotubes (MWCNTs), whose capacity at pH 7 reached 32.23 mg/g, were studied by Abdel-Ghani *et al.* [80] for their ability to adsorb phenol. It was discovered that significant irregularities in the nanotube preparation process caused by different specific surface areas (40–600 m^2/g) for the same batch of nanotubes may cause variations in the adsorption capacity of nanotubes. In 2015, Wang *et al.* created 3D-graphene aerogels-mesoporous silica (GAs-MS) frameworks with large surface area (1000.80 m^2/g) and a small mesopore size distribution (1.87 nm), which demonstrated a good adsorption capacity of 90 mg/g of phenol. The characteristics of the adsorbent were successfully modified by the researchers to improve phenol removal, following a general trend in the development of adsorbents that target certain contaminants. This study did show a lot of improvement over other innovative adsorbent materials described in this section. The adsorbent was also renewed using an ethanol solution while retaining a stable mesoporous structure. In their study, Strachowski and Bystrzejewski [81] compared the phenol, 2-CP, and 4-CP adsorption on AC (1187 m^2/g), MWCNTs (156 m^2/g), and carbon-encapsulated iron nanoparticles (CEINs) (36 m^2/g). Phenol was absorbed by AC the best (250–550 mg/g), MWCNTs on average (24–87 mg/g), and CEINs the least ((5–11 mg/g). According to report [81], 4-CP had the greatest affinity for the sorbent surface. Additionally, compared to AC, the adsorption rates of the three chemicals were several-fold greater for CNT and CEIN.

The adsorption of phenol and PCP onto the composite, which reached 123.45 and 120.48 mg/g, respectively, was assessed by Kakavandi *et al.* [82] after they created PAC impregnated with Fe_3O_4 magnetic nanoparticles (MNPs). Compared to the adsorption capacities of magnetite and plain PAC, these capacities were significantly higher (30.8 and 64.7 mg/g respectively). A combination of methanol, NaOH, and NaCl was used to regenerate the adsorbent efficiently in five successive cycles. In order to remove phenol from an aqueous solution, Yoon *et al.* [83] created iron oxide nanoparticles (NPs). Iron oxide nanoparticles (NPs) with and without methyl acrylic acid (MAA) coating had significantly better adsorption capabilities at pH ranges of 3–7, 950 mg/g for MAA-coated NPs and 550 mg/g for uncoated NPs. The higher negative oxygen charge that was created on the NP surface as a result of coating caused a significant increase in the adsorption capacity.

Titania NPs, graphene oxide (GO), and titania-GO each have adsorption capabilities of 0.70, 1.81, and 23.7 mg/g for the elimination of phenol, according to Fua *et al.* [84]. The evaluated adsorbents can photodegrade the adsorbed phenol as well. By dissolving the PS core in tetrahydrofuran and trapping it in the meso-channelled silica shell, Chen *et al.* [85] created hollow mesoporous carbon spheres (HMCSs) with a consistent mesopore size (4.1 nm). Comparing HMCSs' high phenol adsorption capacity (207.8 mg/g) to the capacities of AC (92.59 mg/g), carbon nanofibers (150 mg/g), carbon nanotubes (165 mg/g), and hollow micropore carbon nanospheres (137 mg/g), the latter two were found to be inferior. The increased mass transfer of phenol molecules within the mesoporous matrix was credited with this notable increase. MWCNTs and SWCNTs, two nanosized adsorbents, had adsorption capabilities of 64.60 mg/g and 50.51 mg/g, respectively, at pH 6.57 and 4.65, according to Dehghani *et al.* [86]. More phenol molecules were adsorbed on

MWCNTs than SWCNTs, mostly because of the smaller diameter of the micropores, despite the fact that the specific surface area of SWCNTs (700 m^2/g) was significantly higher than that of MWCNTs (270 m^2/g).

On the other hand, a different study on the adsorption of phenol by carbon nanotubes revealed very low capacities of 1.0977 and 2.7778 mg/g at pH 6 for CNTs and CNT-Al_2O_3, with surface areas of 155.5 and 227.5 m^2/g, respectively, [87]. For CNTs (1.2887 mg/g) and CNT-Al_2O_3 (2.7778 mg/g), the adsorption of 4-CP on the same adsorbents was remarkably similar. The findings highlighted the negligible phenol adsorption ability of nanotubes, which encouraged the use of other adsorbents, especially in light of the high cost of producing and disposing of nanotubes and their potential for environmental pollution. With a surface area of 45.9 m^2/g and a large pore volume, GO was grafted with poly (N-isopropylacrylamide) (PNIPAM) by Gong *et al.* [88]. The presence of different hydrogen bonds in the synthesised adsorbent led to its selectivity for phenol adsorption. The amount of phenol that was adsorbed by GO was 3.9556 mg/g, whereas GO-PNIPAM saw an increase to 12.7425 mg/g. Additionally, the adsorbent was recyclable due to its thermosensitivity and self-flocculation qualities, which significantly improved its effectiveness and ability to be used with grafted GO for the phenol treatment of contaminated wastewater. The adsorption capacities of the previously described new adsorbents ranged from 1.09 to 207.8 mg/g, which is less than the efficiency of CACs but closer to the capacities displayed by waste-based adsorbents.

$NiFe_2O_4$ NPs were created and employed by Changmai and Purkait [89] to modify the surface of PAC. This new adsorbent's maximum adsorption capability was 93.25 mg/g. Once the initial phenol concentration was increased from 20 to 100 mg/L, the phenol adsorption efficiency increased up to 100 %.

2.6. Conclusion

Polymer adsorbents exhibit exceptional powers to bind phenols, according to a comparison of the adsorption capacities of different adsorbents to remove phenol and phenol derivatives. Most carbonaceous adsorbents, waste-based ACs, and CACs outperformed natural clays and minerals in terms of performance. However, the modified clays dramatically increased the amount of phenol removed, whereas novel adsorbents showed a very low and widely variable adsorption capacity up to this point. Overall, the high reusability potential of adsorbents and the high recovery potential of phenol-two crucial elements for sustainable practice—are the common and major advantages of all stated adsorbents.

References

[1] A.O. Dada, J.O. Ojediran, A.P. Olalekan, Sorption of Pb 2+ from Aqueous Solution unto Modified Rice Husk: Isotherms Studies, Adv. Phys. Chem. 2013 (2013). https://doi.org/10.1155/2013/842425.

[2] D. Mohan, C.U. Pittman, Arsenic removal from water/wastewater using adsorbents—A critical review, J. Hazard. Mater. 142 (2007) 1–53. https://doi.org/10.1016/J.JHAZMAT.2007.01.006.

[3] E. Saputra, S. Muhammad, H. Sun, S. Wang, Activated carbons as green and effective catalysts for generation of reactive radicals in degradation of aqueous phenol, RSC Adv. 3 (2013) 21905–21910. https://doi.org/10.1039/c3ra42455c.

[4] A. Dąbrowski, Adsorption — from theory to practice, Adv. Colloid Interface Sci. 93 (2001) 135–224. https://doi.org/10.1016/S0001-8686(00)00082-8.

[5] C.O. Ania, J.B. Parra, J.J. Pis, Effect of texture and surface chemistry on adsorptive capacities of activated carbons for phenolic compounds removal, Fuel Process. Technol. 77–78 (2002) 337–343. https://doi.org/10.1016/S0378-3820(02)00072-3.

[6] M. Ahmaruzzaman, D.K. Sharma, Adsorption of phenols from wastewater, J. Colloid Interface Sci. 287 (2005) 14–24. https://doi.org/10.1016/J.JCIS.2005.01.075.

[7] A.H. Sulaymon, K.W. Ahmed, Competitive Adsorption of Furfural and Phenolic Compounds onto Activated Carbon in Fixed Bed Column, Environ. Sci. Technol. 42 (2007) 392–397. https://doi.org/10.1021/ES070516J.

[8] M. Shirzad-Siboni, S.J. Jafari, M. Farrokhi, J.K. Yang, Removal of Phenol from Aqueous Solutions by Activated Red Mud: Equilibrium and Kinetics Studies, Environ. Eng. Res. 18 (2013) 247–252. https://doi.org/10.4491/EER.2013.18.4.247.

[9] A. Tor, Y. Cengeloglu, M.E. Aydin, M. Ersoz, Removal of phenol from aqueous phase by using neutralized red mud, J. Colloid Interface Sci. 300 (2006) 498–503. https://doi.org/10.1016/J.JCIS.2006.04.054.

[10] N. Tancredi, N. Medero, F. Möller, J. Píriz, C. Plada, T. Cordero, Phenol adsorption onto powdered and granular activated carbon, prepared from Eucalyptus wood, J. Colloid Interface Sci. 279 (2004) 357–363. https://doi.org/10.1016/J.JCIS.2004.06.067.

[11] V. Makrigianni, A. Giannakas, Y. Deligiannakis, I. Konstantinou, Adsorption of phenol and methylene blue from aqueous solutions by pyrolytic tire char: Equilibrium and kinetic studies, J. Environ. Chem. Eng. 3 (2015) 574–582. https://doi.org/10.1016/J.JECE.2015.01.006.

[12] W. Tang, H. Huang, Y. Gao, X. Liu, X. Yang, H. Ni, J. Zhang, Preparation of a novel porous adsorption material from coal slag and its adsorption properties of phenol from aqueous solution, Mater. Des. 88 (2015) 1191–1200. https://doi.org/10.1016/J.MATDES.2015.09.079.

[13] E. Lorenc-Grabowska, M.A. Diez, G. Gryglewicz, Influence of pore size distribution on the adsorption of phenol on PET-based activated carbons, J.

Colloid Interface Sci. 469 (2016) 205–212. https://doi.org/10.1016/J.JCIS.2016.02.007.

[14] P.Q. Thang, K. Jitae, B.L. Giang, N.M. Viet, P.T. Huong, Potential application of chicken manure biochar towards toxic phenol and 2,4-dinitrophenol in wastewaters, J. Environ. Manage. 251 (2019) 109556. https://doi.org/10.1016/J.JENVMAN.2019.109556.

[15] S.F. Lütke, A. V. Igansi, L. Pegoraro, G.L. Dotto, L.A.A. Pinto, T.R.S. Cadaval, Preparation of activated carbon from black wattle bark waste and its application for phenol adsorption, J. Environ. Chem. Eng. 7 (2019) 103396. https://doi.org/10.1016/J.JECE.2019.103396.

[16] L.J. Pham, Coconut (Cocos nucifera), Ind. Oil Crop. (2016) 231–242. https://doi.org/10.1016/B978-1-893997-98-1.00009-9.

[17] N. Arena, J. Lee, R. Clift, Life Cycle Assessment of activated carbon production from coconut shells, J. Clean. Prod. 125 (2016) 68–77. https://doi.org/10.1016/J.JCLEPRO.2016.03.073.

[18] Z. Hu, M.P. Srinivasan, Preparation of high-surface-area activated carbons from coconut shell, Microporous Mesoporous Mater. 27 (1999) 11–18. https://doi.org/10.1016/S1387-1811(98)00183-8.

[19] C. Namasivayam, D. Kavitha, Adsorptive removal of 2-chlorophenol by low-cost coir pith carbon, J. Hazard. Mater. 98 (2003) 257–274. https://doi.org/10.1016/S0304-3894(03)00006-2.

[20] C. Namasivayam, D. Kavitha, Adsorptive Removal of 2,4-Dichlorophenol from Aqueous Solution by Low-Cost Carbon from an Agricultural Solid Waste: Coconut Coir Pith, Sep. Sci. Technol. 39 (2004) 1407–1425. https://doi.org/10.1081/SS-120030490.

[21] M. Radhika, K. Palanivelu, Adsorptive removal of chlorophenols from aqueous solution by low cost adsorbent—Kinetics and isotherm analysis, J. Hazard. Mater. 138 (2006) 116–124. https://doi.org/10.1016/J.JHAZMAT.2006.05.045.

[22] I.A.W. Tan, A.L. Ahmad, B.H. Hameed, Preparation of activated carbon from coconut husk: Optimization study on removal of 2,4,6-trichlorophenol using response surface methodology, J. Hazard. Mater. 153 (2008) 709–717. https://doi.org/10.1016/J.JHAZMAT.2007.09.014.

[23] A.T. Mohd Din, B.H. Hameed, A.L. Ahmad, Batch adsorption of phenol onto physiochemical-activated coconut shell, J. Hazard. Mater. 161 (2009) 1522–1529. https://doi.org/10.1016/J.JHAZMAT.2008.05.009.

[24] N. Singh, C. Balomajumder, Simultaneous removal of phenol and cyanide from aqueous solution by adsorption onto surface modified activated carbon prepared from coconut shell, J. Water Process Eng. 9 (2016) 233–245. https://doi.org/10.1016/J.JWPE.2016.01.008.

[25] N. Singh, C. Balomajumder, Simultaneous biosorption and bioaccumulation of phenol and cyanide using coconut shell activated carbon immobilized Pseudomonas putida (MTCC 1194), J. Environ. Chem. Eng. 4 (2016) 1604–1614. https://doi.org/10.1016/J.JECE.2016.02.011.

[26] M. Ahmaruzzaman, V.K. Gupta, Rice Husk and Its Ash as Low-Cost

Adsorbents in Water and Wastewater Treatment, Ind. Eng. Chem. Res. 50 (2011) 13589–13613. https://doi.org/10.1021/IE201477C.

[27] S.B. Daffalla, H. Mukhtar, M.S. Shaharun, Effect of organic and inorganic acid pretreatment on structural properties of rice husk and adsorption mechanism of phenol, Int. J. Chem. Environ. Eng. 3 (2012) 192–200.

[28] V. Srihari, A. Das, The kinetic and thermodynamic studies of phenol-sorption onto three agro-based carbons, Desalination. 225 (2008) 220–234. https://doi.org/10.1016/J.DESAL.2007.07.008.

[29] V. Srihari, A. Das, Comparative studies on adsorptive removal of phenol by three agro-based carbons: Equilibrium and isotherm studies, Ecotoxicol. Environ. Saf. 71 (2008) 274–283. https://doi.org/10.1016/J.ECOENV.2007.08.008.

[30] K.P. Singh, A. Malik, S. Sinha, P. Ojha, Liquid-phase adsorption of phenols using activated carbons derived from agricultural waste material, J. Hazard. Mater. 150 (2008) 626–641. https://doi.org/10.1016/j.jhazmat.2007.05.017.

[31] A. Gupta, C. Balomajumder, Simultaneous adsorption of Cr(VI) and phenol onto tea waste biomass from binary mixture: Multicomponent adsorption, thermodynamic and kinetic study, J. Environ. Chem. Eng. 3 (2015) 785–796. https://doi.org/10.1016/j.jece.2015.03.003.

[32] V.K. Gupta, S. Sharma, I.S. Yadav, D. Mohan, Utilization of Bagasse Fly Ash Generated in the Sugar Industry for the Removal and Recovery of Phenol and p-Nitrophenol from Wastewater, 180È186 J. Chem. T Echnol. Biotechnol. 71 (1998) 180–186. https://doi.org/10.1002/(SICI)1097-4660(199802)71:2.

[33] V.C. Srivastava, M.M. Swamy, I.D. Mall, B. Prasad, I.M. Mishra, Adsorptive removal of phenol by bagasse fly ash and activated carbon: Equilibrium, kinetics and thermodynamics, Colloids Surfaces A Physicochem. Eng. Asp. 272 (2006) 89–104. https://doi.org/10.1016/J.COLSURFA.2005.07.016.

[34] J. Kaåomierczak, P. Nowicki, R. Pietrzak, Sorption properties of activated carbons obtained from corn cobs by chemical and physical activation, Adsorption. 19 (2013) 273–281. https://doi.org/10.1007/s10450-012-9450-y.

[35] A.N.A. El-Hendawy, S.E. Samra, B.S. Girgis, Adsorption characteristics of activated carbons obtained from corncobs, Colloids Surfaces A Physicochem. Eng. Asp. 180 (2001) 209–221. https://doi.org/10.1016/S0927-7757(00)00682-8.

[36] R.L. Tseng, S.K. Tseng, Pore structure and adsorption performance of the KOH-activated carbons prepared from corncob, J. Colloid Interface Sci. 287 (2005) 428–437. https://doi.org/10.1016/J.JCIS.2005.02.033.

[37] I.O. Okeowo, E.O. Balogun, A.J. Ademola, A.O. Alade, T.J. Afolabi, E.O. Dada, A.G. Farombi, Adsorption of Phenol from Wastewater Using Microwave-Assisted Ag–Au Nanoparticle-Modified Mango Seed Shell-Activated Carbon, Int. J. Environ. Res. 2020 142. 14 (2020) 215–233. https://doi.org/10.1007/S41742-020-00244-7.

[38] G.L. Rorrer, T.Y. Hsien, J.D. Way, Synthesis of Porous-Magnetic Chitosan Beads for Removal of Cadmium Ions from Waste Water, Ind. Eng. Chem. Res.

32 (1993) 2170–2178. https://doi.org/10.1021/ie00021a042.

[39] M.A.L. Milhome, D. De Keukeleire, J.P. Ribeiro, R.F. Nascimento, T.V. Carvalho, D.C. Queiroz, Removal of phenol and conventional pollutants from aqueous effluent by chitosan and chitin, Quim. Nova. 32 (2009) 2122–2127. https://doi.org/10.1590/S0100-40422009000800025.

[40] A. Moreira De Oliveira, M. Aparecida, L. Milhome, T. Vieira Carvalho, R.M. Cavalcante, R. Ferreira Do Nascimento, H. Monte, Use of Low-cost Adsorbents to Chlorophenols and Organic Matter Removal of Petrochemical Wastewater, Orbital Electron. J. Chem. . 5 (2013) 171–178. https://doi.org/10.17807/orbital.v5i3.477.

[41] L.C. Zhou, X.G. Meng, J.W. Fu, Y.C. Yang, P. Yang, C. Mi, Highly efficient adsorption of chlorophenols onto chemically modified chitosan, Appl. Surf. Sci. 292 (2014) 735–741. https://doi.org/10.1016/J.APSUSC.2013.12.041.

[42] M. Khalid, G. Joly, A. Renaud, P. Magnoux, Removal of Phenol from Water by Adsorption Using Zeolites, Ind. Eng. Chem. Res. 43 (2004) 5275–5280. https://doi.org/10.1021/IE0400447.

[43] V.K. Gupta, I. Ali, V.K. Saini, Removal of Chlorophenols from Wastewater Using Red Mud: An Aluminum Industry Waste, Environ. Sci. Technol. 38 (2004) 4012–4018. https://doi.org/10.1021/ES049539D.

[44] S. Arellano-Cárdenas, T. Gallardo-Velázquez, G. Osorio-Revilla, M. del S. López-Cortez, Preparation of a Porous Clay Heterostructure and Study of its Adsorption Capacity of Phenol and Chlorinated Phenols from Aqueous Solutions, Water Environ. Res. 80 (2008) 60–67. https://doi.org/10.2175/106143007x220653.

[45] H. Zaitan, D. Bianchi, O. Achak, T. Chafik, A comparative study of the adsorption and desorption of o-xylene onto bentonite clay and alumina, J. Hazard. Mater. 153 (2008) 852–859. https://doi.org/10.1016/J.JHAZMAT.2007.09.070.

[46] R.I. Yousef, B. El-Eswed, A.H. Al-Muhtaseb, Adsorption characteristics of natural zeolites as solid adsorbents for phenol removal from aqueous solutions: Kinetics, mechanism, and thermodynamics studies, Chem. Eng. J. 171 (2011) 1143–1149. https://doi.org/10.1016/J.CEJ.2011.05.012.

[47] M. Djebbar, • F Djafri, • M Bouchekara, • A Djafri, Adsorption of phenol on natural clay, Appl. Water Sci. 2012 22. 2 (2012) 77–86. https://doi.org/10.1007/S13201-012-0031-8.

[48] G. Varank, A. Demir, K. Yetilmezsoy, S. Top, E. Sekman, M.S. Bilgili, Removal of 4-nitrophenol from aqueous solution by natural low-cost adsorbents, Indian J. Chem. Technol. 19 (2012) 7–25.

[49] W.P. Cheng, W. Gao, X. Cui, J.H. Ma, R.F. Li, Phenol adsorption equilibrium and kinetics on zeolite X/activated carbon composite, J. Taiwan Inst. Chem. Eng. 62 (2016) 192–198. https://doi.org/10.1016/J.JTICE.2016.02.004.

[50] S. Yapar, V. Özbudak, A. Dias, A. Lopes, Effect of adsorbent concentration to the adsorption of phenol on hexadecyl trimethyl ammonium-bentonite, J. Hazard. Mater. 121 (2005) 135–139.

https://doi.org/10.1016/J.JHAZMAT.2005.01.021.

[51] Z. Rawajfih, N. Nsour, Characteristics of phenol and chlorinated phenols sorption onto surfactant-modified bentonite, J. Colloid Interface Sci. 298 (2006) 39–49. https://doi.org/10.1016/J.JCIS.2005.11.063.

[52] A. Kuleyin, Removal of phenol and 4-chlorophenol by surfactant-modified natural zeolite, J. Hazard. Mater. 144 (2007) 307–315. https://doi.org/10.1016/J.JHAZMAT.2006.10.036.

[53] U.F. Alkaram, A.A. Mukhlis, A.H. Al-Dujaili, The removal of phenol from aqueous solutions by adsorption using surfactant-modified bentonite and kaolinite, J. Hazard. Mater. 169 (2009) 324–332. https://doi.org/10.1016/J.JHAZMAT.2009.03.153.

[54] H.B. Senturk, D. Ozdes, A. Gundogdu, C. Duran, M. Soylak, Removal of phenol from aqueous solutions by adsorption onto organomodified Tirebolu bentonite: Equilibrium, kinetic and thermodynamic study, J. Hazard. Mater. 172 (2009) 353–362. https://doi.org/10.1016/J.JHAZMAT.2009.07.019.

[55] M. Sprynskyy, T. Ligor, M. Lebedynets, B. Buszewski, Kinetic and equilibrium studies of phenol adsorption by natural and modified forms of the clinoptilolite, J. Hazard. Mater. 169 (2009) 847–854. https://doi.org/10.1016/J.JHAZMAT.2009.04.019.

[56] H. Koyuncu, N. Yildiz, U. Salgin, F. Köroğlu, A. Çalimli, Adsorption of o-, m- and p-nitrophenols onto organically modified bentonites, J. Hazard. Mater. 185 (2011) 1332–1339. https://doi.org/10.1016/J.JHAZMAT.2010.10.050.

[57] Z. Luo, M. Gao, S. Yang, Q. Yang, Adsorption of phenols on reduced-charge montmorillonites modified by bispyridinium dibromides: Mechanism, kinetics and thermodynamics studies, Colloids Surfaces A Physicochem. Eng. Asp. 482 (2015) 222–230. https://doi.org/10.1016/J.COLSURFA.2015.05.014.

[58] L. Ma, J. Zhu, Y. Xi, R. Zhu, H. He, X. Liang, G.A. Ayoko, Adsorption of phenol, phosphate and Cd(II) by inorganic–organic montmorillonites: A comparative study of single and multiple solute, Colloids Surfaces A Physicochem. Eng. Asp. 497 (2016) 63–71. https://doi.org/10.1016/J.COLSURFA.2016.02.032.

[59] J. Huang, X. Jin, S. Deng, Phenol adsorption on an N-methylacetamide-modified hypercrosslinked resin from aqueous solutions, Chem. Eng. J. 192 (2012) 192–200. https://doi.org/10.1016/J.CEJ.2012.03.078.

[60] B. Pan, X. Chen, B. Pan, W. Zhang, X. Zhang, Q. Zhang, Preparation of an aminated macroreticular resin adsorbent and its adsorption of p-nitrophenol from water, J. Hazard. Mater. 137 (2006) 1236–1240. https://doi.org/10.1016/J.JHAZMAT.2006.04.016.

[61] X. Zeng, T. Yu, P. Wang, R. Yuan, Q. Wen, Y. Fan, C. Wang, R. Shi, Preparation and characterization of polar polymeric adsorbents with high surface area for the removal of phenol from water, J. Hazard. Mater. 177 (2010) 773–780. https://doi.org/10.1016/J.JHAZMAT.2009.12.100.

[62] J. Huang, H. Zha, X. Jin, S. Deng, Efficient adsorptive removal of phenol by a diethylenetriamine-modified hypercrosslinked styrene–divinylbenzene (PS)

resin from aqueous solution, Chem. Eng. J. 195–196 (2012) 40–48. https://doi.org/10.1016/J.CEJ.2012.04.098.

[63] B. Pan, B. Pan, W. Zhang, L. Lv, Q. Zhang, S. Zheng, Development of polymeric and polymer-based hybrid adsorbents for pollutants removal from waters, Chem. Eng. J. 151 (2009) 19–29. https://doi.org/10.1016/J.CEJ.2009.02.036.

[64] H. Moon, S.K. Kook, H.C. Park, Adsorption of phenols onto a polymeric sorbent, Korean J. Chem. Eng. 1991 83. 8 (1991) 168–176. https://doi.org/10.1007/BF02706679.

[65] K. Abburi, Adsorption of phenol and p-chlorophenol from their single and bisolute aqueous solutions on Amberlite XAD-16 resin, J. Hazard. Mater. 105 (2003) 143–156. https://doi.org/10.1016/J.JHAZMAT.2003.08.004.

[66] M.S. Bilgili, Adsorption of 4-chlorophenol from aqueous solutions by xad-4 resin: Isotherm, kinetic, and thermodynamic analysis, J. Hazard. Mater. 137 (2006) 157–164. https://doi.org/10.1016/J.JHAZMAT.2006.01.005.

[67] V. Alexandrovich, V. Davankov, V. Rogozhin, M. Tsjurupa, US 3,729,457 Macronet polystyrene structures for ionites and method of producing same, (1973) 771.

[68] V. V. Azanova, J. Hradil, Sorption properties of macroporous and hypercrosslinked copolymers, React. Funct. Polym. 41 (1999) 163–175. https://doi.org/10.1016/S1381-5148(99)00029-2.

[69] B.C. Pan, F.W. Meng, X.Q. Chen, B.J. Pan, X.T. Li, W.M. Zhang, X. Zhang, J.L. Chen, Q.X. Zhang, Y. Sun, Application of an effective method in predicting breakthrough curves of fixed-bed adsorption onto resin adsorbent, J. Hazard. Mater. 124 (2005) 74–80. https://doi.org/10.1016/J.JHAZMAT.2005.03.052.

[70] F.Q. Liu, M.F. Xia, S.L. Yao, A.M. Li, H.S. Wu, J.L. Chen, Adsorption equilibria and kinetics for phenol and cresol onto polymeric adsorbents: Effects of adsorbents/adsorbates structure and interface, J. Hazard. Mater. 152 (2008) 715–720. https://doi.org/10.1016/J.JHAZMAT.2007.07.071.

[71] X. Zhang, A. Li, Z. Jiang, Q. Zhang, Adsorption of dyes and phenol from water on resin adsorbents: Effect of adsorbate size and pore size distribution, J. Hazard. Mater. 137 (2006) 1115–1122. https://doi.org/10.1016/J.JHAZMAT.2006.03.061.

[72] Z.W. Ming, C.J. Long, P.B. Cai, Z.Q. Xing, B. Zhang, Synergistic adsorption of phenol from aqueous solution onto polymeric adsorbents, J. Hazard. Mater. 128 (2006) 123–129. https://doi.org/10.1016/J.JHAZMAT.2005.03.036.

[73] W. Zhang, Q. Du, B. Pan, L. Lv, C. Hong, Z. Jiang, D. Kong, Adsorption equilibrium and heat of phenol onto aminated polymeric resins from aqueous solution, Colloids Surfaces A Physicochem. Eng. Asp. 346 (2009) 34–38. https://doi.org/10.1016/J.COLSURFA.2009.05.022.

[74] J. Huang, Treatment of phenol and p-cresol in aqueous solution by adsorption using a carbonylated hypercrosslinked polymeric adsorbent, J. Hazard. Mater. 168 (2009) 1028–1034. https://doi.org/10.1016/J.JHAZMAT.2009.02.141.

[75] C.E. Enyoh, Q. Wang, P.E. Ovuoraye, Response Surface Methodology for modeling the Adsorptive uptake of Phenol from Aqueous solution Using Adsorbent Polyethylene Terephthalate Microplastics, Chem. Eng. J. Adv. (2022) 100370. https://doi.org/10.1016/J.CEJA.2022.100370.

[76] A.W. Trochimczuk, M. Streat, B.N. Kolarz, Highly polar polymeric sorbents: Characterization and sorptive properties towards phenol and its derivatives, React. Funct. Polym. 46 (2001) 259–271. https://doi.org/10.1016/S1381-5148(00)00056-0.

[77] B. Pan, B. Pan, W. Zhang, Q. Zhang, Q. Zhang, S. Zheng, Adsorptive removal of phenol from aqueous phase by using a porous acrylic ester polymer, J. Hazard. Mater. 157 (2008) 293–299. https://doi.org/10.1016/J.JHAZMAT.2007.12.102.

[78] X. Qiu, N. Li, X. Ma, S. Yang, Q. Xu, H. Li, J. Lu, Facile preparation of acrylic ester-based crosslinked resin and its adsorption of phenol at high concentration, J. Environ. Chem. Eng. 2 (2014) 745–751. https://doi.org/10.1016/J.JECE.2013.11.016.

[79] N. Massalha, A. Brenner, C. Sheindorf, Y. Haimov, I. Sabbah, Enriching composite hydrophilic polyurethane foams with PAC to enhance adsorption of phenol from aqueous solutions, Chem. Eng. J. 280 (2015) 283–292. https://doi.org/10.1016/J.CEJ.2015.06.015.

[80] N.T. Abdel-Ghani, G.A. El-Chaghaby, F.S. Helal, Individual and competitive adsorption of phenol and nickel onto multiwalled carbon nanotubes, J. Adv. Res. 6 (2015) 405–415. https://doi.org/10.1016/J.JARE.2014.06.001.

[81] P. Strachowski, M. Bystrzejewski, Comparative studies of sorption of phenolic compounds onto carbon-encapsulated iron nanoparticles, carbon nanotubes and activated carbon, Colloids Surfaces A Physicochem. Eng. Asp. 467 (2015) 113–123. https://doi.org/10.1016/J.COLSURFA.2014.11.044.

[82] B. Kakavandi, M. Jahangiri-Rad, M. Rafiee, A.R. Esfahani, A.A. Babaei, Development of response surface methodology for optimization of phenol and p-chlorophenol adsorption on magnetic recoverable carbon, Microporous Mesoporous Mater. 231 (2016) 192–206. https://doi.org/10.1016/J.MICROMESO.2016.05.033.

[83] S.U. Yoon, B. Mahanty, H.M. Ha, C.G. Kim, Phenol adsorption on surface-functionalized iron oxide nanoparticles: modeling of the kinetics, isotherm, and mechanism, J. Nanoparticle Res. 18 (2016) 1–10. https://doi.org/10.1007/s11051-016-3478-y.

[84] C.C. Fu, R.S. Juang, M.M. Huq, C. Te Hsieh, Enhanced adsorption and photodegradation of phenol in aqueous suspensions of titania/graphene oxide composite catalysts, J. Taiwan Inst. Chem. Eng. 67 (2016) 338–345. https://doi.org/10.1016/J.JTICE.2016.07.043.

[85] A. Chen, Y. Li, Y. Yu, Y. Li, K. Xia, Y. Wang, S. Li, L. Zhang, Synthesis of hollow mesoporous carbon spheres via "dissolution-capture" method for effective phenol adsorption, Carbon N. Y. 103 (2016) 157–162. https://doi.org/10.1016/J.CARBON.2016.02.091.

[86] M.H. Dehghani, M. Mostofi, M. Alimohammadi, G. McKay, K. Yetilmezsoy, A.B. Albadarin, B. Heibati, M. AlGhouti, N.M. Mubarak, J.N. Sahu, High-performance removal of toxic phenol by single-walled and multi-walled carbon nanotubes: Kinetics, adsorption, mechanism and optimization studies, J. Ind. Eng. Chem. 35 (2016) 63–74. https://doi.org/10.1016/J.JIEC.2015.12.010.

[87] Ihsanullah, H.A. Asmaly, T.A. Saleh, T. Laoui, V.K. Gupta, M.A. Atieh, Enhanced adsorption of phenols from liquids by aluminum oxide/carbon nanotubes: Comprehensive study from synthesis to surface properties, J. Mol. Liq. 206 (2015) 176–182. https://doi.org/10.1016/J.MOLLIQ.2015.02.028.

[88] Z. Gong, S. Li, W. Han, J. Wang, J. Ma, X. Zhang, Recyclable graphene oxide grafted with poly(N-isopropylacrylamide) and its enhanced selective adsorption for phenols, Appl. Surf. Sci. 362 (2016) 459–468. https://doi.org/10.1016/J.APSUSC.2015.11.251.

[89] M. Changmai, M.K. Purkait, Kinetics, equilibrium and thermodynamic study of phenol adsorption using NiFe2O4 nanoparticles aggregated on PAC, J. Water Process Eng. 16 (2017) 90–97. https://doi.org/10.1016/J.JWPE.2016.12.011.

Chapter-3

Materials, methods and characterization techniques

3.1. Introduction

All the basic materials employed during the experiments were of analytical grade, purchased from the Sigma Aldrich, Fisher Scientific and Merck India chemical supplier, and were used without further chemical purification. The details of methods and characterization techniques used during the adsorption process are described in the present chapter.

3.2. Materials used

All the reagents used for synthesis and experimental studies were of analytical and laboratory grade. The Pea shells (PS) were collected from a local market, Lucknow, India. Phenol (99.5 %), 4-aminophenol (99.5 %), sodium hydroxide (98%), hydrochloric acid (35.5%), potassium chloride (99.5%), methanol and isopropyl alcohol (99.9%), sodium sulphate (99.9%), sulfuric acid (98%), cetrimide (96%), Calcium Chloride (99 %) and Urea (99%) High-purity grade of nitrogen gas (99.99%) and helium gas (99.99%) were used for physiochemical characterization of the sample supplied by Krishna Gas Agencies (Lucknow, India). The double distilled water (DDW) was prepared using a double distillation unit (GLDD15AQ, Glassco Laboratory Equipment Pvt. Ltd, Ambala Cantt., India) and used for the preparation of modified adsorbent, batch adsorption experiments and other required purposes throughout this study.

3.3. Adsorption study

Different batch adsorption experiments were performed using a temperature-controlled magnetic stirrer to examine the effects of time and the rate of adsorption. Adsorbate solutions were poured into 100 ml conical flasks for every batch, each with a separate and precise beginning concentration. Beginning with 100 to 700 mg/L, the adsorbate concentration was varied. A pH adjustment was made after

adding 0.1 g of PS adsorbent to each conical flask. At various constant temperatures, these flasks with various starting concentrations were set up on a magnetic stirrer. To determine how time affected the removal of adsorbate, samples were taken out of the stirrer at various time intervals. Even though a few samples were left in a magnetic stirrer for 12 hours, equilibrium was reached in only 4-5 of those hours. After the samples had been filtered and centrifuged, the concentration of adsorbate in the solution was determined using a UV-visible spectrophotometer (Carry 100).

Eq. 1 can be used to calculate the equilibrium adsorbed quantity of the adsorbate, which is denoted by q_e:

$$q_e = \frac{(C_0 - C_e)V_s}{m} \quad (1)$$

In the sample, Vs (in L) is the sample's volume, m (in g) is the PS adsorbent's mass, and Co and Ce are the adsorbate solution's initial and equilibrium concentrations, respectively (both expressed in mg/L). Eq. 2 determines the adsorption capacity (qt) at any given time:

$$q_t = \frac{(C_0 - C_t)V_s}{m} \quad (2)$$

Where C_t is the concentration of adsorbate solution at any time t.

3.4. Characterization of modified adsorbent

3.4.1. UV-Vis spectroscopy

An essential physical instrument that uses light from the electromagnetic spectrum's ultraviolet, visible, and near-infrared regions is ultraviolet (UV) spectroscopy. The amount of absorbing species in the solution, route length, and absorbance are all linearly related by the Beer-Lambert law. As a result, for a fixed path length, UV-Vis spectroscopy can be used to determine the concentration of the absorbing species. This method is incredibly straightforward, adaptable, quick, precise, and economical. The UV-Vis-NIR Spectrophotometer is the tool used for ultraviolet-visible (or UV-

Vis) spectroscopy. By utilising radiative radiation from the ultraviolet (UV), visible (Vis), and near-infrared (NIR) spectra, this can be used to evaluate liquids, gases, and solids. Predetermined wavelengths in these zones have been established as UV: 300–400 nm, Vis: 400–765 nm, and NIR: 765–3200 nm.

Principle: When a light beam passes through an object and reaches a detector, its wavelength is determined. Crucial facts regarding the chemical structure and molecular count are revealed by the measured wavelength [1]. This makes it possible to collect data that is both quantitative and qualitative. Radiation with a wavelength between 160 and 3500 nm can be used to collect information by its transmittance, absorbance, or reflectance. Electrons are moved into excited states or anti-bonding orbitals as a result of incident energy being absorbed. The photon energy needs to be equal to or greater than the electron's required energy in order for this transfer to take place. The core idea behind how absorption spectroscopy works is this procedure.

The sample absorbs some of the energy of the incident wave when the light of a particular wavelength and energy is focused onto it. The absorbance of the sample is recorded by a photodetector, which also analyzes the energy of the transmitted light from the specimen. It is generated by plotting the light's wavelength against the sample's absorption or transmission spectra [2]. The core tenet of quantitative analysis is the Lambert-Beer rule, often known as the Bouguer-Beer law, which states that a solution's absorbance increases proportionally with the concentration of analytes (Fig. 2). For a given wavelength, the absorbance (unit less) A is represented as the molar absorptivity of the absorbing species (M^{-1} cm^{-1}), b is the path length of the specimen holder (typically 1 cm), and c is the concentration of the solution (M).

$$A = a.b.c \quad (3)$$

UV−Vis spectrometer can monitor absorbance or transmittance in UV – visible wavelength range. The relation between incident light of intensity 'I_o' and transmitted light of intensity 'I' is described as follows.

Transmittance (T) is given by I/Io and $(I/I_o)*100$ gives the transmittance rate (T%). Absorbance (abs) is the inverse of transmittance and given by:

$$\log\left(\frac{1}{T}\right) = log\left(\frac{I_o}{I}\right) \quad (4)$$

$$T = \frac{I}{I_o} = 10^{-kcl} \quad (5)$$

$$Abs = \log\left(\frac{1}{T}\right) = \log\left(\frac{I_o}{I}\right) = -kcl \quad (6)$$

The proportionality constant is shown here by the letter k. In contrast to absorbance, which exhibits a relationship between sample concentration and optical path (Beer's law and Bouguer's law), the transmittance is independent of sample concentration. In addition, k is written as 'ε' and explained as the molar absorption coefficient when the optical path is 1 cm and the concentration of the target substance is 1 mol/l. The material's molar absorption coefficient is typical under particular circumstances. The Bouguer-Beer rule takes the exclusion of all stray, produced, scattered, and reflected light [3].

Instrumentation: An ultraviolet and visible light source, a monochromator (wavelength selector), a sample stage, and a detector make up a spectrometer's main parts. Typically, light sources consist of tungsten filaments. Most often, a photodiode or CCD is used as the detector. To filter light of a specific wavelength before feeding it to the detector, photodiodes work with monochromators. It is necessary to turn off the visible lamp while keeping an eye on the UV spectrum absorbance, and the opposite is also true. **Fig. 3.1 and 3.2** depict UV−Vis Spectrometer used in the experiments and instrumentation respectively.

Fig. 3.1: UV (Carry 100). Source: SIL, DOC, BBAU, Lucknow

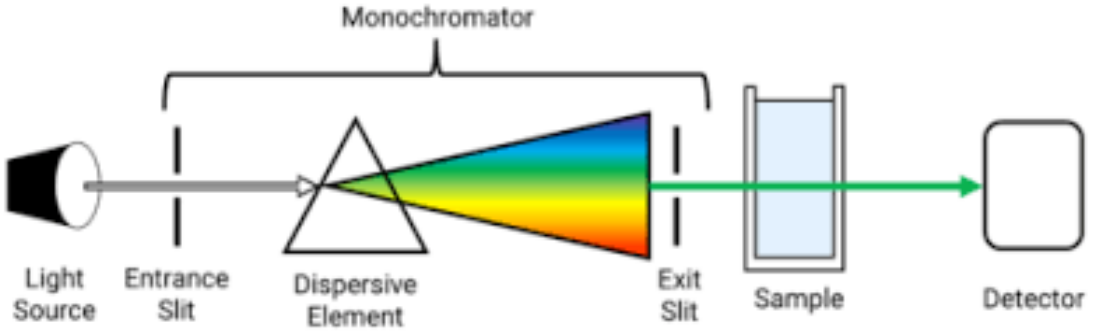

Fig. 3.2: Instrumentation of UV-Vis Spectrometer

UV Source: In its working wavelength range, the power of the radiating source shouldn't change. By electrically stimulating deuterium or hydrogen at low pressures, the continuous UV spectrum is created. The process of producing an excited molecular species, which then splits into two atomic species and a UV photon, is the mechanism for producing UV light. Both deuterium and hydrogen lamps have emission wavelengths in the 160 to 375 nm range. The cuvettes' material must be chosen so as not to absorb the light falling upon them because doing so will cause mistakes in the absorption spectrum that is ultimately produced. Thus, quartz is usually used.

Cuvettes: Light is generated from a monochromator source and split into two pieces by a half-mirror splitter before it reaches the sample. One component (or sample beam) moves through the cuvette containing the material to be analysed in a solution

in a clear solvent. The second beam, often known as the reference beam, moves through a cuvette that contains only solvent. Containers for reference and sample solutions must be clear to the passing beam.

Detectors: The detector measures the amount of light that the cuvettes are emitting, and it sends this information to a metre so that it can record and show the values. The intensities of light beams are calculated and compared by electronic detectors. A number of UV-Vis spectrophotometers feature two detectors, a phototube and a photomultiplier tube, and simultaneously monitor the reference and sample beams. In UV-Vis equipment, the photomultiplier tube is the detector that is most frequently utilised. It consists of an anode, many dynos, and a photoemissive cathode that emits electrons when photons touch it. Dynods also emit several electrons when a single electron strikes them. After entering the tube, the incident photon strikes the cathode. Multiple electrons are then released from the cathode and driven toward the first dynode (whose potential is 90V more positive than the cathode). For every electron that strikes the initial dynode, numerous more electrons are released. These electrons are subsequently accelerated in the direction of the second dynode, creating additional electrons that are accelerated in the direction of the third dynode and so on. At the anode, all of the electrons are eventually gathered. Each initial photon has now generated 10^6–10^7 electrons. Amplification and measurement are done on the generated current. Photomultipliers have quick response times and are extremely delicate to UV and visible light.

3.4.2. Fourier Transform Infrared (FT-IR) spectroscopy

Infrared spectroscopy's preferred technique is known as FT-IR, or Fourier Transform InfraRed. An object is subjected to IR radiation during infrared spectroscopy. The sample absorbs a portion of the infrared light, while passing through it unaffected

(transmitted). The resulting spectrum gives the sample a molecular fingerprint by displaying the molecule absorption and transmission. Over 70 years have passed since infrared spectroscopy became a mainstay method for materials analysis in labs [4]. With absorption peaks that match the frequency of vibrations between the bonds of the atoms making up the material, an infrared spectrum acts as a fingerprint of a sample. No two compounds have the same infrared spectrum since every substance is made up of a particular combination of atoms. As a result, every single type of substance may be identified (qualitatively analysed) using infrared spectroscopy. Additionally, the size of the spectral peaks provides a clear picture of the amount of material present. Infrared is a fantastic tool for quantitative analysis when combined with modern software techniques. The shortcomings of dispersive devices were addressed by the development of Fourier Transform Infrared (FT-IR) spectroscopy. The lengthy scanning procedure was the biggest challenge. It was necessary to develop a technique for sensing all infrared wavelengths simultaneously as opposed to separately. An interferometer, a very basic optical tool, was used to create a solution. All of the infrared frequencies are "encoded" into a special kind of signal that the interferometer generates. The measurement time for the signal is typically on the order of one second or less. As a result, the time component per sample is decreased from several minutes to a few seconds. This implies that all frequencies are measured concurrently when the interferogram is being measured. As a result, measurements made with the interferometer are completed quite quickly [5]. The observed interferogram signal cannot be easily evaluated since the analyst needs a frequency spectrum (a depiction of the strength at each frequency) to make an identification. It is necessary to have a method for "decoding" the various frequencies. The Fourier transformation, a well-known mathematical method, can be used to do this. The

computer handles this transformation and then provides the user with the desired spectral data for analysis [6]. Fig. 3.3 and 3.4 depict FT-IR Spectrometer used in the experiments and instrumentation respectively.

Fig. 3.3: FTIR (Nicole 6700) Source. USIC, BBAU, Lucknow

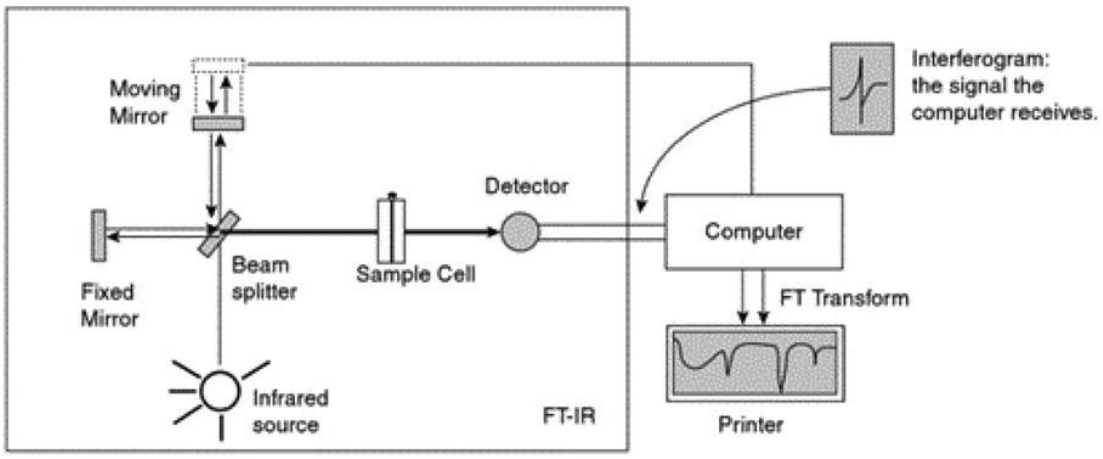

Fig. 3.4: Instrumentation of FT-IR Spectrometer

Instrumentation

The source: A bright black-body source emits infrared light. This beam goes through a hole that regulates the energy delivered to the sample (and, ultimately, to the detector).

The interferometer: The interferometer is where "spectral encoding" happens once the beam enters. The interferometer then releases the interferogram signal as a result.

The sample: Depending on the sort of analysis being done, the beam enters the

sample compartment where it either passes through or is reflected off the sample's surface. Here, particular energy frequencies that are distinctively typical of the sample are absorbed.

The detector: The detector receives the beam at the end for the last measurement. The detectors employed were created specifically to measure the unique interferogram signal.

The computer: The measured signal is converted to digital form and transferred to the computer, where it undergoes the Fourier transformation. The user is then shown the finished infrared spectrum for interpretation and any additional editing.

A background spectrum must be assessed in order to provide a relative scale for the absorption intensity. Typically, there is no sample in the beam for this measurement. To determine the "percent transmittance," this measurement can be compared to the one made with the sample inside the beam. The spectrum produced by this method is devoid of all instrumental features. Therefore, the sample alone is solely responsible for all observed spectrum characteristics. Because this spectrum is unique to the device, multiple sample measurements can be made from a single background measurement.

3.4.3. Powder X-ray Diffraction (XRD)

Crystalline materials make up about 95% of all solid substances. Diffraction patterns result from X-ray interactions with crystalline materials (Phase). A New Method of Chemical Analysis was the title of a 1919 presentation by A.W.Hull [7]. In this passage, he observed that "... every crystalline substance gives a pattern; the same substance always gives the same pattern, and in a mixture of substances each produces its pattern independently of the others." Therefore, the X-ray diffraction pattern of a pure substance is similar to the substance's fingerprint [7]. As a result, the

powder diffraction approach is perfect for characterising and identifying polycrystalline phases. On magnetic or optical media, about 50,000 inorganic and 25,000 organic single components, crystalline phases, and diffraction patterns have been gathered and maintained as standards. Powder diffraction is mostly used in search/match procedures to identify sample components. The amount of each phase in the sample is also indicated by the areas under the peak [8].

Fig. 3.5: X-ray diffraction (Panalytical) Source. ACMS, IIT, Kanpur

Fig. 3.6: X-ray Diffraction (Bruker ECOD8 ADVANCE), Source. USIC, BBAU, Lucknow

Principle: An atom's electrons coherently scatter light. Every atom can be thought of as a coherent point scatterer. The quantity of electrons surrounding an atom determines how strongly it scatters light. Because they are arranged in a periodic grid, the atoms in a crystal can diffract light. X-rays have a wavelength that is comparable to the separation between atoms. A diffraction pattern is created by the scattering of X-rays from atoms, and it contains details on the arrangement of the atoms within the crystal. Glass and other amorphous materials don't form diffraction patterns because they lack a periodic array with long-range order. Bragg's equation serves as the foundation for how X-ray diffraction operates [9].

$$2dSin\theta = n\lambda \quad (7)$$

Where n is an integer number, is the X-ray wavelength, d is the distance between atomic planes, and is the angle at which X-rays and atomic planes are diffracted. This rule illustrates the link between the lattice distance, diffraction angle, and incident X-ray wavelength in a crystalline material. Fig. 3.5 and 3.6 depict the X-ray diffractometer used in the experiments and Fig. 3.7 depicts the XRD instrumentation.

Instrumentation

Sample: It is crucial to have a material with an auniform, level surface when doing powder or polycrystalline diffraction. We typically crush the material down to particles with a cross-section of between 0.002 mm and 0.005 mm, if possible. The ideal sample is uniform and has randomly scattered crystallites (we will later point out problems which will occur if the specimen deviates from this ideal state). To achieve a nice, flat surface, the material is pushed into a sample holder.

Goniometer: A goniometer is a device utilized that includes a sample holder, detector arm, and related gears. Below is a diagram illustrating how a Bragg-Brentano reflection goniometer operates. If the sample were curved on the focusing circle, a

focusing mechanism would be present. The distance between the sample and the detector is equal to the distance between the X-ray focus spot and the sample. The reflected (diffracted) beam will remain focused on the circle with a constant radius if we drive the sample holder and detector in a 1:2 connection. On this circle, the detector moves. The X-ray tube is stationary in the THETA: 2θ goniometer, while the sample moves by the angle and the detector simultaneously moves by the angle 2θ. Small or loosely packed samples may be prone to falling off the sample holder when the value of 2θ is high.

Diffractometer slit system: We often use the line focus or line source of the tube for powder diffraction. The line source produces radiation in all directions, however limiting divergence in the direction of the line focus is required to improve focusing. This is accomplished by directing the incident beam via a Soller slit that has a number of narrow gaps that are positioned closely together.

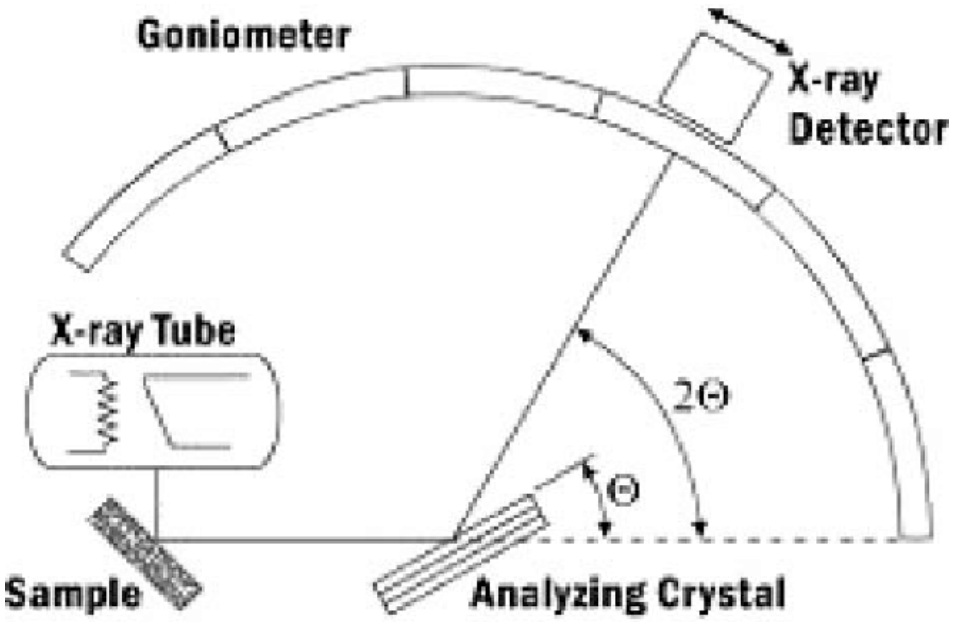

Fig. 3.7: Instrumentation of X-ray Diffractometer

3.4.4. Scanning Electron Microscopy (SEM)

The scanning electron microscope is a piece of apparatus used in scanning electron microscopy to examine material topographies at extremely high magnifications [10]. Although SEM magnifications can reach more than 300,000 X, the majority of applications in the production of semiconductors only need for magnifications of less than 3,000 X. To analyse die/package cracks and fracture surfaces, bond failures, and physical flaws on the die or package surface, SEM inspection is frequently utilised.

Fig. 3.8: Scanning Electron Microscope with EDS (JEOL, Japan; model JSM-6490LV)

Source USIC BBAU

Working and instrumentation: An electron beam is focused on a spot volume of the sample during SEM analysis, transferring energy to the spot as a result. These initial electrons, also known as primary electrons, knock electrons loose from the material itself [11]. A positively biased grid or detector attracts and collects the dislodged electrons, sometimes referred to as secondary electrons, which are then converted into a signal. The region being inspected is covered by the electron beam as it creates numerous such signals to create the SEM image. These signals are further amplified, processed, and translated into images of the desired topography. Finally, a CRT displays the image. The number of secondary electrons gathered during inspection

depends on the energy of the source electrons. As the energy of the primary electron beam rises, the specimen emits more secondary electrons until a particular threshold is achieved. Beyond this point, the number of secondary electrons gathered decreases as the primary beam's energy rises since the primary beam is already causing electrons deep within the specimen to become activated. Before emitting at the surface, electrons from such depths typically combine again.

The primary electron beam causes the emission of backscattered (or reflected) electrons from the specimen in addition to secondary electrons. Backscattered electrons have a clear path and higher energy than secondary electrons. As a result, unless the detector is immediately in their direction of passage, they cannot be caught by a secondary electron detector. Backscattered electrons are referred to as all emissions above 50 eV.

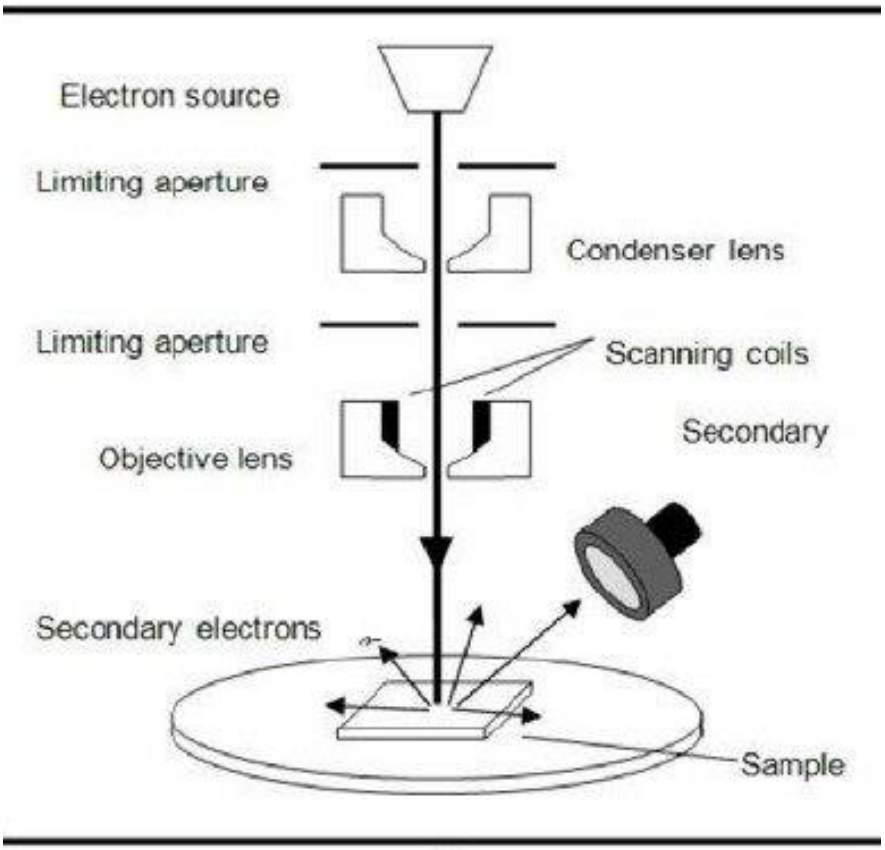

Fig. 3.9: Schematic diagram of SEM

Since the yield of the collected backscattered electrons grows monotonically with the atomic number of the object, backscattered electron imaging is effective for differentiating between different materials. Backscatter imaging can distinguish between elements with at least a 3-atomic number difference; materials with this difference would emerge with strong contrast on the image. Backscatter imaging, for instance, would make it simpler to analyse the remaining Au on an Al bond pad after the Au ball bond has lifted off since the Au would shine out against the Al background. To analyse specimen composition, an SEM may be fitted with an EDX analysis system [12]. The identification of substances and pollutants, as well as determining the relative quantities of each on the specimen's surface, can be done with the help of EDX analysis.

3.4.5. Brunauer Emmett Taylor (BET) surface analysis

This method is applied to recognize the physical adsorption of gas molecules on the surface of nanostructure materials and assists as a fundamental technique for estimation of surface area analysis of nanoparticles expressed in m^2/g per unit volume [13]. The BET method is applied to multilayer adsorption of materials and is commonly used those gases which do not react to the surface on nanoparticle materials act as adsorbates for the measurement of specific surface area. Nitrogen gas is specially used as adsorbate for the surface inquiry by the BET method [14]. The tenet of BET surface area examination is an augmentation of Langmuir theory based on the adsorption theory of monolayer to multilayer adsorption with some hypotheses such as gas molecules adsorb on materials with infinite layers and adsorb gas molecules can interact with adjacent layers only [15]. The BET equation can be represented as:

$$\frac{P}{(P^o - P)v} = \frac{1}{v_m C} + \frac{(C-1)}{v_m}\frac{P}{P^o} \quad (8)$$

Where P is the equilibrium pressure, P^o is the saturation pressure of nitrogen gas as adsorbate at a temperature of adsorption, v is the total quantity of gas adsorbed, v_m is the quantity of gas adsorbed on monolayer and C is the BET constant, which can be expressed as:

$$C = exp\frac{(E_1 - E_2)}{RT} \quad (9)$$

Where E_1 represents the adsorption of heat on the first layer and E_2 is for the second and higher. So from an equation of adsorption isotherm graph is plotted between $\frac{P}{(P^o - P)v}$ and $\frac{P}{P^o}$. This plot is known as BET plot. To obtain a linear graph, the value of P/P^o is $0.05 < P/P^o < 0.35$.

Fig. 3.10: BET instrument (BELSORP-max, Japan), DoC, BBAU

From this, the value of slope (S) and intercept (I) measure the gas quantity (v_m) of adsorbed monolayer gas and BET constant, C used following equation:

$$v_m = \frac{1}{S+1} \quad (10)$$

The total area (S_{total}) and specific surface area (S_{BET}) is measured with the help of the following equation:

$$S_{total} = \frac{v_m N s}{V} \tag{11}$$

$$S_{BET} = \frac{S_{total}}{a} \tag{12}$$

Where v_m is the volume unit, N is the Avogadro's number, s is the cross-section surface area of adsorbed gas, V is the molar volume of adsorbate gas and a is the amount of adsorbent.

3.4.6. Optical profilometry

An instrument called a 3D surface profilometer is used to assess the surface of different precision devices and materials at the sub-nanometer scale [16]. In order to perform non-contact scanning on the surface of the device and create a 3D image of the surface, it is based on the theory of white light interference technology, paired with a precision Z-scanning module and a 3D modelling algorithm. The system software processes and analyses data on the 3D image of the device's surface, resulting in the 2D and 3D parameters that indicate the device's surface's quality [17]. In order to create a 3D optical detecting equipment for device surface topography. A measurement head, a loading platform, a tilt knob, a computer, a vibration isolation base, and a workbench make up the majority of a 3D surface profiler. The measuring head, which primarily comprises of a motion motor, scanning module, and optical system, is the essential component of a 3D surface profilometer. A dual-channel air floating vibration isolation system is also included with the 3D surface profiler. This system can be connected to a reliable air supply or a typical silent air compressor and can operate steadily without an external air source [18].

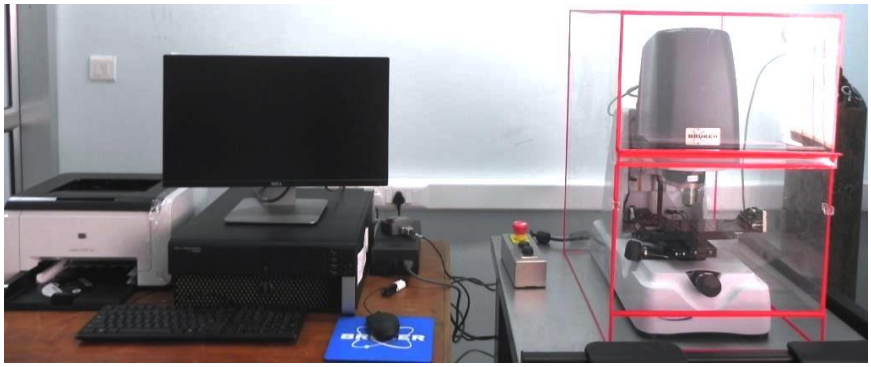

Fig. 3.11: Optical profilometer (Bruker, USA), ACMS, IIT- Kanpur

Principle and working: The 3D surface profilometer uses white light scanning interferometry, a non-contact measurement technique that uses interference fringe to evaluate deviations between the sample test surface and project reference surface. Scanning with white light interferometry is a great tool for measuring uneven and discontinuous surfaces [19]. The results are based on the absolute physical height since the test results of white light scanning are individually examined based on the light intensity signal at each pixel. When measuring imperfect samples, single wavelength laser interference methods lack this benefit. When processing the data of each pixel, the phase shift method combines the phase results of nearby pixels, and the original result is based on phase rather than physical distance. Because it can detect rough or step-jump pattern surfaces, white light interferometric scanning has a significant advantage in coarse sample surface data measurement [20]. The monochromatic phase shift approach has the benefit of fast speed while analysing the smooth sample surface. To begin measuring, the sample was positioned beneath the loading platform's lens, the motor connection was checked, listened for outside noise, and verified the instrument's condition. The interference fringes on the sample surface was found by moving the Z-axis with the joystick. The measurement started when scanning settings and naming were finished. The data processing module was entered and selected the default levelling for the plane sample [21].

References

[1] Y. Guo, C. Liu, R. Ye, Q. Duan, Advances on Water Quality Detection by UV-Vis Spectroscopy, Appl. Sci. 2020, Vol. 10, Page 6874. 10 (2020) 6874. https://doi.org/10.3390/APP10196874.

[2] J.E. Birdwell, A.S. Engel, Characterization of dissolved organic matter in cave and spring waters using UV–Vis absorbance and fluorescence spectroscopy, Org. Geochem. 41 (2010) 270–280. https://doi.org/10.1016/J.ORGGEOCHEM.2009.11.002.

[3] M.S.H. Akash, K. Rehman, Ultraviolet-Visible (UV-VIS) Spectroscopy, Essentials Pharm. Anal. (2020) 29–56. https://doi.org/10.1007/978-981-15-1547-7_3.

[4] J.S. Gaffney, N.A. Marley, D.E. Jones, Fourier Transform Infrared (FTIR) Spectroscopy, Charact. Mater. (2012) 1–33. https://doi.org/10.1002/0471266965.COM107.PUB2.

[5] A.A. Ismail, F.R. van de Voort, J. Sedman, Chapter 4 Fourier transform infrared spectroscopy: Principles and applications, Tech. Instrum. Anal. Chem. 18 (1997) 93–139. https://doi.org/10.1016/S0167-9244(97)80013-3.

[6] Z. Bacsik, J. Mink, G. Keresztury, FTIR spectroscopy of the atmosphere. I. Principles and methods, Appl. Spectrosc. Rev. 39 (2004) 295–363. https://doi.org/10.1081/ASR-200030192.

[7] A. Chauhan, Powder XRD Technique and its Applications in Science and Technology, J. Anal. Bioanal. Tech. 5 (2014) 5. https://doi.org/10.4172/2155-9872.1000212.

[8] H.S.C. O'Neill, W.A. Dollase, C.R. Ross, Temperature dependence of the cation distribution in nickel aluminate (NiAl2O4) spinel: a powder XRD study, Phys. Chem. Miner. 1991 185. 18 (1991) 302–319. https://doi.org/10.1007/BF00200188.

[9] C.G. Pope, X-Ray Diffraction and the Bragg Equation, J. Chem. Educ. 74 (1997) 129–131. https://doi.org/10.1021/ED074P129.

[10] M. Henini, Scanning electron microscopy: An introduction, III-Vs Rev. 13 (2000) 40–44. https://doi.org/10.1016/S0961-1290(00)80006-X.

[11] S.H. Aharinejad, A. Lametschwandtner, Fundamentals of Scanning Electron Microscopy, Microvasc. Corros. Cast. Scanning Electron Microsc. (1992) 44–51. https://doi.org/10.1007/978-3-7091-9230-6_3.

[12] W. Zhou, R. Apkarian, Z.L. Wang, D. Joy, Fundamentals of scanning electron microscopy (SEM), Scanning Microsc. Nanotechnol. Tech. Appl. (2007) 1–40. https://doi.org/10.1007/978-0-387-39620-0_1.

[13] W.G. McMILLAN, E. TELLER, The assumptions of the B.E.T. theory., J. Phys. Colloid Chem. 55 (1951) 17–20. https://doi.org/10.1021/j150484a003.

[14] T. Adschiri, T. Furusawa, Relation between CO2-reactivity of coal char and BET surface area, Fuel. 65 (1986) 927–931. https://doi.org/10.1016/0016-2361(86)90200-0.

[15] S. Lowell, J.E. Shields, M.A. Thomas, M. Thommes, Surface Area Analysis

from the Langmuir and BET Theories, (2004) 58–81. https://doi.org/10.1007/978-1-4020-2303-3_5.

[16] W. Du, J. Li, C. Hu, F. Lv, D. Cai, H. Ouyang, Application of 3D surface profilometer in single cut sample inspection, J. Phys. Conf. Ser. 2220 (2022) 012014. https://doi.org/10.1088/1742-6596/2220/1/012014.

[17] W. Kapłonek, T. Mikolajczyk, D.Y. Pimenov, M.K. Gupta, M. Mia, S. Sharma, K. Patra, M. Sutowska, High-accuracy 3D optical profilometry for analysis of surface condition of modern circulated coins, Materials (Basel). 13 (2020) 1–19. https://doi.org/10.3390/ma13235371.

[18] S. Van der Jeught, J.J.J. Dirckx, Real-time structured light profilometry: a review, Opt. Lasers Eng. 87 (2016) 18–31. https://doi.org/10.1016/J.OPTLASENG.2016.01.011.

[19] P. Vangla, G.M. Latha, Surface topographical analysis of geomembranes and sands using a 3D optical profilometer, Geosynth. Int. 24 (2017) 151–166. https://doi.org/10.1680/jgein.16.00023.

[20] M. Zahidi, M. Assoul, J. Mignot, B. Bellaton, A fast 2D/3D optical profilometer for wide range topographical measurement, Wear. 165 (1993) 197–203. https://doi.org/10.1016/0043-1648(93)90335-J.

[21] J.M. Rodriguez, R. V. Curtis, D.W. Bartlett, Surface roughness of impression materials and dental stones scanned by non-contacting laser profilometry, Dent. Mater. 25 (2009) 500–505. https://doi.org/10.1016/J.DENTAL.2008.10.003.

Chapter-4

Effective removal of 4-aminophenol from aqueous environment by pea (Pisum sativum) shells activated with sulfuric acid

4.1. Introduction

Water pollution is steadily increasing. The range of harmful compounds in the aquatic environment is growing due to unchecked anthropogenic processes and industrial effluents [1]. Various industries discharge water that contains harmful chemicals such azo dyes, pesticides, PAHs, and phenol, among others [2]. Due to its widespread release from several industries, including tanning, plastic, medicines, coke manufacturing, and dying, exposure of phenolic compounds in the aquatic system is given more attention out of these [3–6]. Phenols are prioritised pollutants because even in low concentrations, they may have a negative impact on living' life [7].

Through manufacturing sectors and chemical processes, the organic phenolic 4-Aminophenol (4-AP) is known to escape into the aquatic system [8]. Long-term excessive use of 4-AP has been linked to persistent kidney infection, hemolytic adequacy, and increased strong lipofuscin testimony in tissues [9]. According to toxicology studies, 4-AP is present in the effluents of commercial colouring industries. This substance is toxic to the kidneys, liver, and nervous system as well as having nephrotoxic effects, methemoglobinemia, serious sensitivities, dermatitis, rash, shaking, cerebral pains, seizures, unconsciousness, bronchial asthma, and lung aggravation [10–14]. According to a recent study by De Souza *et al.*, the oxidation of 4-AP in the process of colouring hair results in the production of a number of hazardous compounds, including quinoneimine, semi-quinoneimine radical, dimmers to tetramers, etc [15]. Diverse physical, chemical, and synthetic procedures have been tried and failed to address the organic contaminants found in wastewater. A shift to a sustainable, cost-effective replacement for 4-AP is therefore of the greatest priority. Utilizing adsorbents made of natural materials could be a safeguard in this regard.

One of the most important methods for removing phenolic and other harmful chemicals is adsorption [16]. This phenomenon serves as the foundation for several crucial utilitarian processes. A lot of catalytic reactions begin with the substrate being absorbed [17]. Variations in component concentrations at the interface are becoming more crucial to the performance of separation procedures in both laboratory and industrial settings. Additionally, important subjects like soil filtration, air filtration, water filtration, and sewage filtration are discussed in this context [18]. This is partially due to the fact that the study of interfaces requires extremely rigorous testing in order to obtain relevant and reliable results, which makes having a fundamental understanding of scientific concepts a long way behind the times. However, there has been a noticeable increase in the amount of work being done in recent years to bridge the gap between the theory and practice. In addition, kinds of solid adsorbents, including carbonaceous and inorganic materials, have been studied in the past few decades [19]. Due to their significant usage in science and industry as well as their unique sorption, catalytic, magnetic, optical, and thermal properties, a wide variety of nanostructured solids have recently attracted a lot of attention [20]. Despite the fact that adsorption's development was somewhat zigzagging up until the 1918s, it is now generally accepted that this area of surface science has become a clearly defined branch of physical science, representing an inherently interdisciplinary field that crosses the fields of chemistry, physics, biology, and engineering.

An expensive adsorbent that is frequently employed for wastewater treatment is activated carbon [21]. Therefore, scientists are concentrating on creating adsorbents that are affordable, sustainable, and readily available. In this context, using industrial, domestic, and agricultural waste as an adsorbent could be a beneficial strategy. As a result, the field of adsorbent preparation for pollutant removal has undergone

systematic development. Rice husk, groundnut shell, and coconut shell have all recently been used to create various agro waste-based biochars using the physical activation method [22]. There have also been numerous biochar-based catalysts and composites created [23,24]. Some chemical modifications, such as sucrose-spherical carbon activated with KOH and caffeic acid functionalized corn starch, have also been made to increase the adsorption capacity [25,26]. Several naturally occurring, modified inorganic adsorbents, including zeolite, clay minerals, and layered double hydroxides [27]. A comparison table of the present study of 4-AP removal with previously studied adsorbents [28–31] is shown in Table 4.1.

Table 4.1: Comparison of q_{max} of different studies for 4-AP removal

Adsorbents	Conditions		q_{max} (mg/g)	References
	pH	Temp (°C)		
3D-graphene oxide-maize amylopectin composites	5	25	116.4	[28]
8% Calcined Layered Double Hydroxide into Alginate Hydrogel Beads	NA	45	36.46	[29]
6% Calcined Layered Double Hydroxide into Alginate Hydrogel Beads	NA	45	98.23	[29]
Antimony ferrocyanides	7	30	190.00	[30]
Cadmium ferrocyanides	7	30	250.00	[30]
Zirconium ferrocyanides	7	30	125.00	[30]
Poly(aryl ether ketone) Containing Pendant Carboxyl Groups	2	20	0.30	[31]
PSASA	7	25	106.11	Present study

Keeping this in mind, we chose modified Pea shells (PS) as an adsorbent and investigated it in this analysis for the removal of 4-AP. The removal of 4-AP from the aqueous stream appears to be a possibility with the PS disposal. Furthermore, PS is an

excellent adsorbent for the elimination of harmful compounds from an aqueous system due to its abundant and free availability throughout the world.

The preparation of an adsorbent activated with H_2SO_4 and used for the removal of 4-AP is the scientific contribution of the current study. PS was used as a precursor. To examine its physicochemical properties, the PSASA underwent thorough characterisation utilising a variety of techniques, including BET, XRD, FT-IR spectroscopy, optical profilometry, SEM-EDS, and point of zero charge (PZC). The tests were planned to gather data on the ideal conditions under which PSASA operates most effectively. Additionally, research in isotherm, kinetics, and thermodynamics were carried out to assess the nature and method of 4-AP removal from PSASA. The current work attempts to propose a economically viable alternative for the removal of such harmful compounds from aquatic habitats, taking into account the limited knowledge that is currently accessible and the rash use of 4-AP.

4.2. Materials and methods

4.2.1. Preparation of the adsorbent (PSASA)

Green peas (Pisum sativum) were procured at Lucknow's neighbourhood market in Purania (Naveen Galla Mandi; 26.8930° N, 80.9356° E). The PS was cleaned with deionized water to remove grime, and then it was allowed to dry for 48 hours in full sun. PS was dried, ground in an acoustic grinder to a particle size of 75 microns or less, and stored in a desiccator. Pouring PS into 50 % H_2SO_4 (v/v) for 24 h allowed for chemical adaption. The PS was placed in a furnace and heated to 800ºC. Over the course of 30 min, the furnace temperature was raised at a rate of 10°C per minute until it reached the desired level [32]. The PSASA was cleaned for 10 minutes with distilled water after cooling, and then it was dried at 105ºC. The dried adsorbent was sieved to a size within the range of 75 ~ 300 µm and then stored safely.

4.2.2. Characterization of adsorbent

4.2.2.1. Point of zero charge (PZC)

Using the salt addition method, surface charge analysis (PZC) of the PSASA was carried out using 0.1 N KCl and 0.002 M cetrimide solution as salt. Six distinct stoppered flasks of 100 ml each were filled with 20 ml of KCl and 20 ml of cetrimide solution. The pH of each flask was kept at 2, 4, 6, 8, 10, and 12, respectively, using 0.1 N HCl and 0.1 N NaOH, and then 50 ml of volume was kept using 0.1 N KCl and 0.002 M cetrimide [33]. Each stoppered flask contained 0.2 g of the PSASA sample for the PZC estimation, and it was vigorously agitated for 6 h until equilibrium was reached. After stirring, the solutions were timed shaken for 36 h. The pH of each solution was then measured after 36 h. The intersection value of a plot between pH change and initial pH yielded PZC.

4.2.2.2. Brunnaur- Emmet- Teller (BET) analysis

A BET surface area analyser (BELSORP-max, Japan) was used to look at the PSASA sample's mean pore diameter, specific surface area, and total pore volume. The PSASA (0.2 g) was heated for 5–6 h at 120°C in a vacuum. The adsorbent was put into a glass sample tube that was stored in liquid nitrogen for N_2 adsorption and desorption after 6 h. Using the conventional Brunauer-Emmett-Teller (Wager) condition, the surface area and pore measurement were calculated, and the Barrett-Joyner-Halenda (BJH) method was used to calculate the pore size.

4.2.2.3. Scanning Electron Microscopy (SEM) with Energy Dispersive X-ray Spectrometry (EDS) analysis

The PSASA and PSASA after adsorption were fixed in 2.5 % glutaraldehyde at 4ºC for a period of 4 h followed by phosphate buffer washing and dehydration using C_2H_5OH (10 %, 30 %, 50 %, 70 %, and 9 5%) for 5 min separately [34]. The final

dehydration was done with absolute alcohol for 30 min. After dehydration, samples were further mounted on platinum stub by using carbon tape. SEM coupled with EDS was done for the SEM image and analysis of composition and elemental distribution (JEOL, Japan; model JSM-6490LV).

4.2.2.4. Optical profilometry

A 3-D optical profilometer (Bruker, USA) was used to examine optical profilometry data from the PSASA, including surface shape, surface roughness, and step height.

4.2.2.5. FT-IR analysis

The PSASA and PSASA after adsorption were ground with KBr (1:10 ratio) and pelleted for the FT-IR spectra investigation. For functional group analysis, the pellet was additionally fitted to the FT-IR socket of a Thermo- Scientific Nicole 6700 (USA). The IR spectrum (4000–400 cm^{-1}) was obtained using 32 scan numbers for each spectra and a resolution of 5-7 cm^{-1}.

4.2.2.6. X-ray Diffraction analysis

Using a powder X-ray diffractometer (XRD) (RigakuMiniflex II desktop), the PSASA's crystallographic behaviour was studied, as well as PSASA's behaviour following adsorption. Copper Kα radiation (λ = 1.5405 Aº) was used to scan the samples at a rate of 2º/min at an angle range of 20º to 70º. Software programmes Match3 and Origin pro2016 were used to evaluate the raw data.

4.2.3. Batch adsorption studies

A temperature-controlled magnetic stirrer was used to study the effects of time and the rate of adsorption using a number of experimental batch adsorption schemes. Each batch of 4-AP solutions had 100 ml conical flasks filled with solutions at varied and distinct starting concentrations. The initial 4-AP concentration ranged from 100 to 700 mg/L. The pH was adjusted after adding 0.1 g of PSASA to each conical flask.

These flasks were set up on a magnetic stirrer at various constant temperatures with variable starting concentrations. To determine how the elimination of 4-AP was effected by time, samples were taken out of the stirrer at various time intervals. The equilibrium was reached in 4-5 h despite certain samples being stirred in a magnetic device for 12 h. Following the first filtering and centrifuging of the samples, the concentration of 4-AP in solution was determined using a UV-visible spectrophotometer (Carry 100).

Eq. 1 can be used to determine the equilibrium adsorbed amount of 4-AP represented by q_e:

$$q_e = \frac{(C_0 - C_e)V_s}{m} \quad (1)$$

In the sample, Vs (in L) represents the sample's volume, m (in g) represents the PSASA's mass, and Co and Ce (in mg/L) represent the 4-AP solution's initial and equilibrium concentrations, respectively.

The adsorption capacity of 4-AP at any time (q_t) is calculated by Eq. 2:

$$q_t = \frac{(C_0 - C_t)V_s}{m} \quad (2)$$

Where C_t is the concentration of 4-AP solution at any time t.

4.2.4. Effect of the PSASA dose

In this work, the impact of the PSASA dose on the adsorption of 4-AP was examined. In six different conical flasks holding 100 mg/L solutions of the 4-AP, it was done by adding 0.1, 0.2, 0.3, 0.4, 0.5, and 0.6 g of the PSASA while maintaining the pH and temperature at 7.0 and 25ºC, respectively.

4.2.5. Effect of pH

Numerous studies have demonstrated that the adsorption process is impacted by pH changes. Therefore, since the pH of a solution affects 4-AP's chemistry and [H^+] and

[OH^-] concentrations have a direct impact on the adsorption process, research into the effect of pH on 4-AP adsorption is necessary [35].

In the present analysis, 0.1 N HCl and 0.1 N NaOH were used to set the pH of the 4-AP solution at a specific value. The pH of the 4-AP solution was set to a range of 5 to 11. The initial 4-AP concentration and temperature were set at 100 mg/L and 25ºC, respectively, with a change in pH values.

4.2.6. Effect of temperature

To understand the nature of adsorption, the adsorption of 4-AP to the PSASA was examined at various temperatures. Depending on their physical, chemical, and bonding features, the temperature has a variety of effects on adsorbents and adsorbates. The adsorbent's adsorption capacity reached its peak at an ideal temperature in many adsorption investigations. [36].

The potential of the PSASA for removing 4-AP under varying temperatures was explored in this research. Experiments were performed at different temperatures (25-45ºC) and concentrations of 4-AP (100-700 mg/L) at pH 7.0.

4.2.7. Effect of KCl and urea addition

The ionic strength of the solution affects the adsorption process in both favourable and unfavourable ways, as has been demonstrated in several studies. Since urea largely breaks hydrogen bonds, its presence in the solution has an impact on how much adsorption occurs [36,37].

A specific quantity of KCl and urea with different molarities were added to a solution containing 4-AP in order to study their effects on adsorption. At pH 7.0 and 25°C, 100 mg/L solutions of 4-AP with 0.1 g of the PSASA were added, along with 0.1-0.6 mol/L concentrations of salts and urea.

4.2.8. Adsorption isotherm

Adsorption isotherms are curves that show how much adsorbate, per unit mass of adsorbent, is absorbed at a given temperature. The Freundlich, Temkin, and Langmuir isotherm are the adsorption isotherms that are most frequently employed to understand adsorption behaviour.

Freundlich isotherm

The Freundlich adsorption isotherm, in which the development of monolayers is not constrained, is typically used to describe heterogeneous surface adsorption. The basis for this model's operation is the exponential distribution of active adsorption sites at the heterogeneous surface of adsorbent [38]. The non-linear form of the Freundlich equation is as follows:

$$q_e = K_F {C_e}^{1/n} \quad (3)$$

Where, K_F: Freundlich constant ($mg^{1-(1/n)}.L^{1/n}.g^{-1}$) and 1/n: Intensity of adsorption. The linear form of the equation is written as:

$$lnq_e = lnK_F + \frac{1}{n} lnC_e \quad (4)$$

The max adsorption capacity was calculated using the Halsey equation. [39]:

$$K_F = {q_m/C_o}^{1/n} \quad (5)$$

Where C_o is the initial concentration.

Temkin isotherm

Adsorbent-adsorbate interaction causes all molecules in the layer to exhibit a drop in heat of adsorption as surface coverage increases. This is the main characteristic of the Temkin isotherm [40]. The non-linear Temkin isotherm form may be written as follows:

$$q_e = \frac{RT}{b} \ln K_T C_e \quad (6)$$

Where, K_T and b are Temkin constant (L/g) and heat of adsorption constant (J/mol). The equation can be stated in linear form as:

$$q_e = \frac{RT}{b} lnK_T + \frac{RT}{b} lnC_e \quad (7)$$

Langmuir isotherm

The Langmuir model was based on the idea that during adsorption, an adsorbate monolayer forms at the adsorbent surface and prevents the creation of a multilayer. The interaction between the active sites of the adsorbent is likewise denied by this approach [41]. The Langmuir equation can be written as follows:

$$q_e = \frac{q_m K_L C_e}{1+K_L C_e} \quad (8)$$

Where, K_L (L/mg): Langmuir constant; C_e (mg/L): equilibrium concentration of 4-AP: q_e (mg/g): the amount of 4-AP adsorbed at equilibrium and q_m (mg/g): maximum adsorption. The linear form of the equation is written as:

$$\frac{C_e}{q_e} = \frac{1}{q_m K_L} + \frac{C_e}{q_m} \quad (9)$$

4.2.9. Kinetic study

To analyse the reaction kinetics, the amount of adsorption has been measured at various time points. The experimental data can be described using one of the different kinetic models that produces a straight line and has the highest values of the correlation coefficient (r) and coefficient of determination (R^2). Investigating the experimental data involved using the following kinetic models [42]:

Pseudo-first-order model:

$$\ln(q_e - q_t) = lnq_e - k_1 t \quad (10)$$

Pseudo-second-order model:

$$\frac{t}{q_t} = \frac{1}{k_2 {q_e}^2} + \frac{t}{q_e} \quad (11)$$

Where k_1 and k_2 are pseudo-first and pseudo-second-order rate constant respectively.

Intra particle diffusion model

$$q_t = k_p t^{0.5} + C \quad (12)$$

For kp, which is the particle-related rate constant in units of g/mg.min0.5, and C, which is a constant in units of mg/g.

4.3. Results and discussion

4.3.1. Characterization of adsorbent

4.3.1.1. PZC

PZC (Fig. 4.1a) describes the surface charge of the PSASA [43]. PZC value is the pH at which surface charge is zero; surfaces that have a pH below it are positively charged, and surfaces that have a pH above it are negatively charged. The PSASA's PZC value in the current investigation was 10.15, indicating that the surface was neutral at this pH. The PSASA surface tended to be positively charged at pH values below PZC, which may have an advantage in attracting electronegative oxygen or nitrogen of 4-AP by hydrogen bonding.

4.3.1.2. BET analysis

Using Brunauer-Emmett-Teller (BET) analysis, the physicochemical properties of the PSASA, including its specific surface area, surface nature, total pore volume, and particle size distribution, were examined (Fig 4.1b-d). The Barrett-Joyner-Halenda (BJH) model was used to determine the pore size distribution of the PSASA [44]. Results showed that the adsorbent's specific surface area (S_{BET}), mean pore diameter, and total pore volume (p/p^o) were, respectively, 5.15 m^2/g, 71.309 nm, and 0.990, confirming the PSASA's macroporous nature. Hysteresis loop (H-3 type) in the

adsorption-desorption curve in the current investigation showed decreased desorption of some N_2 molecules in the adsorbent's capillaries, which was a blatant sign of the PSASA's porous nature. In addition, the macroporous nature of adsorbent was confirmed by Dabrowski (microporous, < 2 nm; mesoporous, 2–50 nm; macroporous, > 50 nm) and IUPAC nomenclature [17] through evaluating pore size and adsorption-desorption curve. Similar hysteresis loops have been earlier reported by Singh *et al.* and Li *et al.* [37,45].

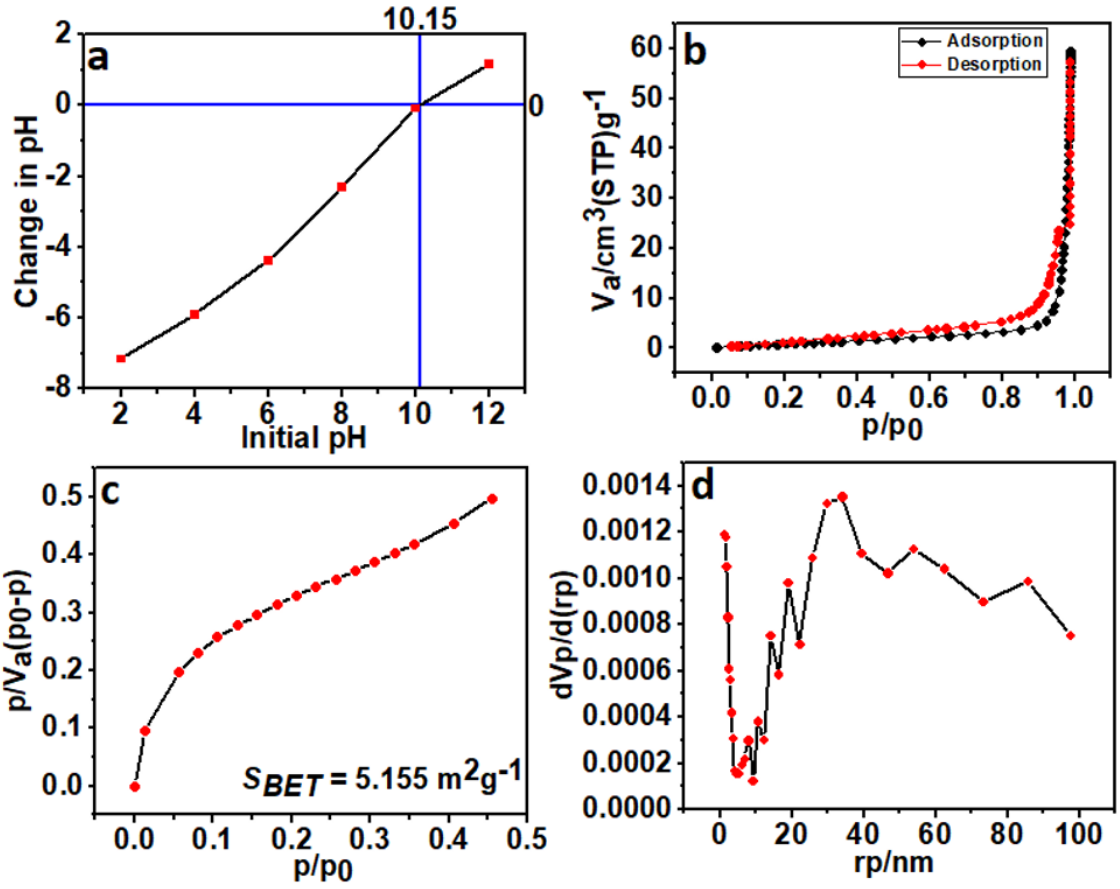

Fig. 4.1: PZC (a), N_2 adsorption-desorption (b), BET (c) and BJH (d) graphs of the PSASA.

4.3.1.3. SEM coupled EDS study

Using SEM, the structural morphology of PSASA and the PSASA after-adsorption were studied. The SEM picture shows morphological changes in terms of size and

appearance (Fig. 4.2a-b). The PSASA SEM image showed a variety of shell morphologies, including round protuberances and porous appearances that highlighted the surface roughness. Because the adsorption site and surface area are larger, increasing the surface roughness of the PSASA denotes a high adsorption potential [46]. The SEM picture of the PSASA surface after adsorption revealed significant ordered 4-AP adsorption. Different elements found in the PSASA were explained by SEM coupled EDS data. The elemental abundance in terms of percent atomic weight was determined using EDS. The maximal elemental composition of the PSASA was found to be in the following order: O>S>K> Ca> C. The after-adsorption PSASA's EDS data showed an increased percentage of C and O, which is indicative of the adsorption of 4-AP. Singh *et al.* [47] also noted a significant amount of C in the adsorbed surface.

4.3.1.4 Optical profilometry

Using an optical profilometer (Bruker, USA) in veridical scanning interferometry (VSI) mode, the surface waviness and surface roughness of the PSASA sample have been determined (Fig. 4.2c-d). A 3D optical profilometry (OP) image gave the surface's areal parameter, whereas a 2D-OP image gives topographical characteristics. Surface topography parameters such as Roughness average (Ra), Maximum profile peak height (Rp), Root mean square (RMS) roughness (Rq), Maximum height of the profile (Rt), and Maximum profile valley depth (Rv) in the PSASA were 12.093 µm, 84.721 µm, 15.698 µm, 155.735 µm, and -71.014 µm, respectively. The results of the current investigation demonstrated that there was a substantial difference between Ra and Rt values, clearly indicating that the PSASA surface had more irregularities as a result of the powerful oxidising agent H_2SO_4 and high temperature. Capillaries are

formed inside the PSASA surface, which is a hallmark quality of porous materials, as indicated by a very high negative value of Rv.

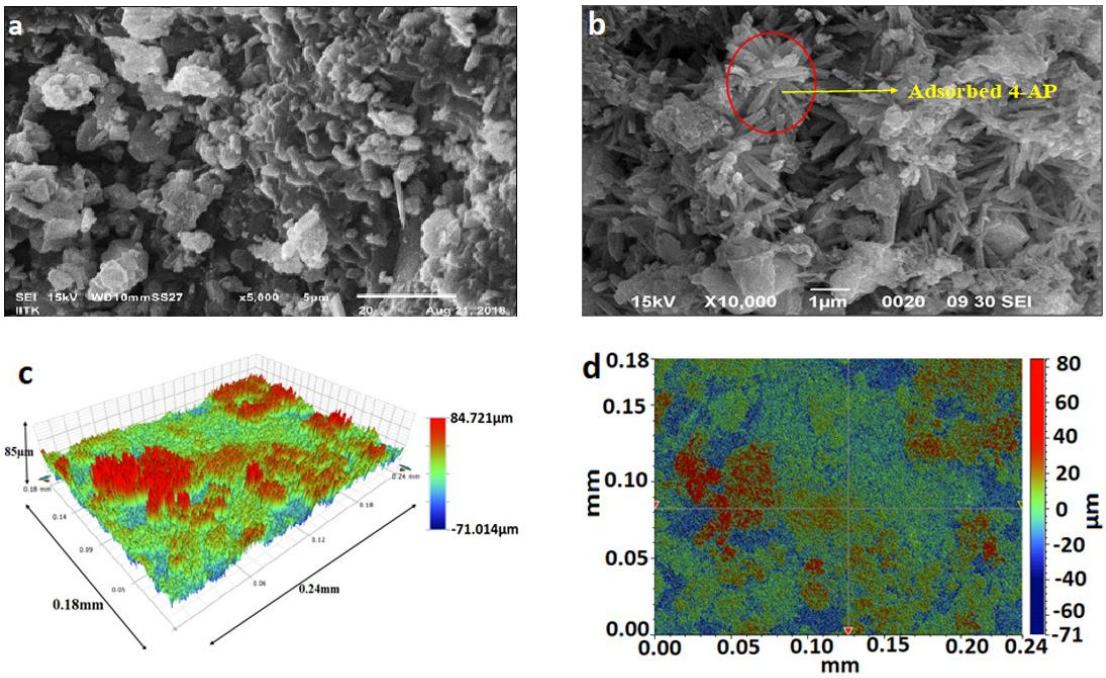

Fig 4.2: SEM images of the PSASA (a) and after adsorption PSASA (b), 3D (c) and 2D (d) optical profilometry image of the PSASA.

4.3.1.5. FT-IR analysis

Fig. 4.3a-b shows the FT-IR spectra of the PSASA and the PSASA after adsorption. The PSASA's FT-IR spectrum is made up of a number of bands with different functional groups. The presence of the band at 3430 cm^{-1} may be caused by secondary alcohol's O-H stretching. [48]. Alkane -C-H stretching is predicted by the weak band at 2923.5 cm^{-1}. The band at 1621 cm^{-1} is due to the conjugated alkene stretching in C=C form [49]. The secondary alcohol's O-H bending and C-O stretching are represented by the bands that are present at 1429 and 1108 cm^{-1}, respectively [48].

The modifications seen in the after-adsorption PSASA's FT-IR spectrum validated the adsorption of 4-AP onto the PSASA surface and gave us an insight as to how it worked. The after adsorption PSASA's FT-IR spectra showed three important

differences. The O-H stretching of the hydrogen-bonded alcohol was first detected in a band at 3390.9 cm^{-1}, suggesting the importance of hydrogen bonding between the PSASA surface and 4-AP during the adsorption process. Second, a band corresponding to the C=C stretching of the aromatic ring was found at 1506.7 cm^{-1}. This band suggests that the PSASA surface and 4-AP exchanged π-electrons, weakening the C=C bond strength of the aromatic ring. This is because the C=C stretching of the pure aromatic ring of 4-AP is typically seen at a relatively higher wavenumber. Third, a band was observed at 1239.1 cm^{-1} corresponds to the C-N stretching of the aromatic amines.

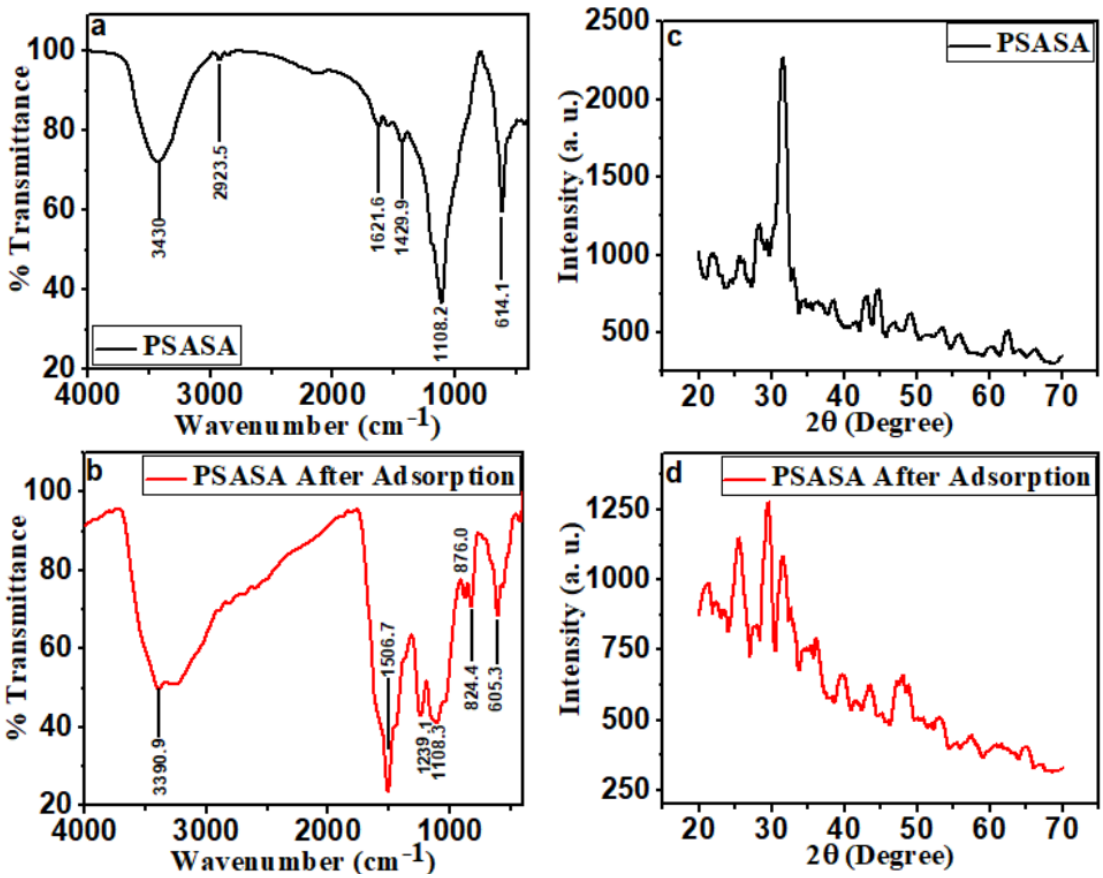

Fig 4.3: FTIR spectra of the PSASA (a) and after adsorption PSASA (b) and XRD plot of the PSASA (c) and after adsorption PSASA (d).

4.3.1.6. X-ray diffraction analysis

The PSASA's XRD graph is shown in Fig. 4.3c. The PSASA XRD spectrum only shows one distinct peak at a 2θ of 33°, which supports the activated carbon's characteristic [50,51] and points to an ordered graphitic crystalline structure [52], Other peaks, which were broad and tiny in size, might have been caused by the presence of molecules containing K, S, or Ca. According to the degree of crystallinity analysis, the PSASA had an overall amorphous nature with 19.55 % of its crystalline content and 80.45 % of its amorphous content. This fact has been further supported by XRD data, which show that a substantial quantity of 4-AP adsorption has occurred because the after-adsorption PSASA's crystalline content has decreased to 13.21 % and its amorphous content has increased to 86.79 %. Fig. 4.3d displays the XRD plot of the after adsorption PSASA.

4.3.2. Effect of PSASA dose

Fig. 4.4a depicts the impact of the PSASA dose on the adsorption of 4-AP. From 0.1 to 0.6 g/100 ml of PSASA was used. When the PSASA dose was increased from 0.1 g to 0.2 g, the adsorption uptake fell from 40.87 to 26.83 mg/g. With an increase in PSASA dose, the adsorption uptake reduced continuously but more slowly. This decrease in 4-AP uptake per unit mass of PSASA was caused by the addition of more adsorption sites as PSASA dose was increased. As initial concentration is the most efficient driving force to overcome the resistance of mass transfer from the adsorbate to the adsorbent, the slower rate of adsorption was likely caused by a decrease in contact between 4-AP and the PSASA [53]. Maximum removal per unit mass of the PSASA was observed at 0.1 g.

4.3.3. Effect of pH

Fig. 4.4b depicts the impact of solution pH on the asdorption of 4-AP onto PSASA. It is clear from Fig. 4.4b that there were two steps to the uptake of 4-AP. 4-AP adsorption increased in the first stage from pH 4.0 to 7.0, and it fell in the second stage from pH 8.0 to 11.0. At pH 7.0 and 100 mg/L 4-AP concentration, the maximum adsorption uptake of 40.87 mg/g was seen. Similar results were seen when the tests were performed at a 200-400 mg/L concentration. Based on the acidity of 4-AP and the PZC of the PSASA, it is possible to evaluate the experiment's results. The PSASA's PZC was 10.15, as previously discussed, meaning that the surface was positively charged at pH levels below this number. The 4-AP's acidic characteristics caused an increase in adsorption uptake from pH 4–7. Since the 4-AP has a pKa value of 5.48, it was in protonated form at pH levels below 5.48, which reduced its electrostatic contact with the PSASA surface. When pH was raised to 7.0, 4-AP's deprotonated form displayed the strongest electrostatic interaction with the PSASA surface [54]. Because the negatively charged [OH^-] was vying for the positively charged PSASA surface with the deprotonated 4-AP, the 4-AP uptake steadily decreased in the basic range up to pH 9.0. At pH 10.0, the PSASA surface was neutral, which caused a considerable drop in the uptake of 4-AP and suggests that the adsorption occurred via other pathways. The negatively charged PSASA surface and the deprotonated form of 4-AP resulted in enhanced electrostatic repulsion, which further decreased 4-AP uptake at pH 11.0.

4.3.4. Effect of temperature

The effects of temperature on the adsorption system are shown in Fig. 4.4c at 25°C, 35°C, and 45°C. At various concentrations of 4-AP (100-700 mg/L), the impact of these temperatures on 4-AP adsorption was assessed. The largest reduction in

adsorption uptake with temperature increase was observed at the lowest 4-AP concentration (100 mg/L). When the temperature was increased by 20ºC and the initial concentration of 4-AP was 100 mg/L, the 4-AP adsorption uptake decreased from 40.87 mg/g to 21.19 mg/g, which is roughly 50 % of the initial uptake value. For the higher 4-AP concentrations, comparable trends were seen, but the rate of adsorption uptake declined more slowly as the temperature rose. Adsorption uptake decreased with a rise in temperature at starting concentrations of 600 mg/L and 700 mg/L by about 26 % and 25 %, respectively. This indicates that temperature has a larger influence on lower concentrations of 4-AP and a lesser influence on higher concentrations of 4-AP. The results mentioned above support the idea that adsorption is exothermic.

4.3.5. Effect of KCl and urea addition

The outcome of the addition of KCl and urea at various concentrations is shown in Fig. 4.4d. The addition of KCl and urea had a detrimental effect on adsorption, as can be seen in Fig. 4.4d. Adsorption uptake decreased from 40.87 mg/g to 17.63 mg/g in the presence of 0.1 M KCl in the 4-AP solution. In addition, the adsorption uptake was very little impacted by rising KCl concentration. The PSASA surface becomes more positive with the dissociation of KCl in water, which causes a competition of negatively charged species for surface sites of the PSASA, which is likely what causes the decrease in 4-AP uptake following KCl addition [55].

Urea addition studies were carried out to determine the function of hydrogen bonding in the adsorption process. Given that urea is a hydrogen bond breaker, it is clear from the experimental data that adding urea in various concentrations to the 4-AP solution significantly reduced the amount of adsorption. The role of hydrogen

bonds in the adsorption process of the investigated system was therefore confirmed by experimental results.

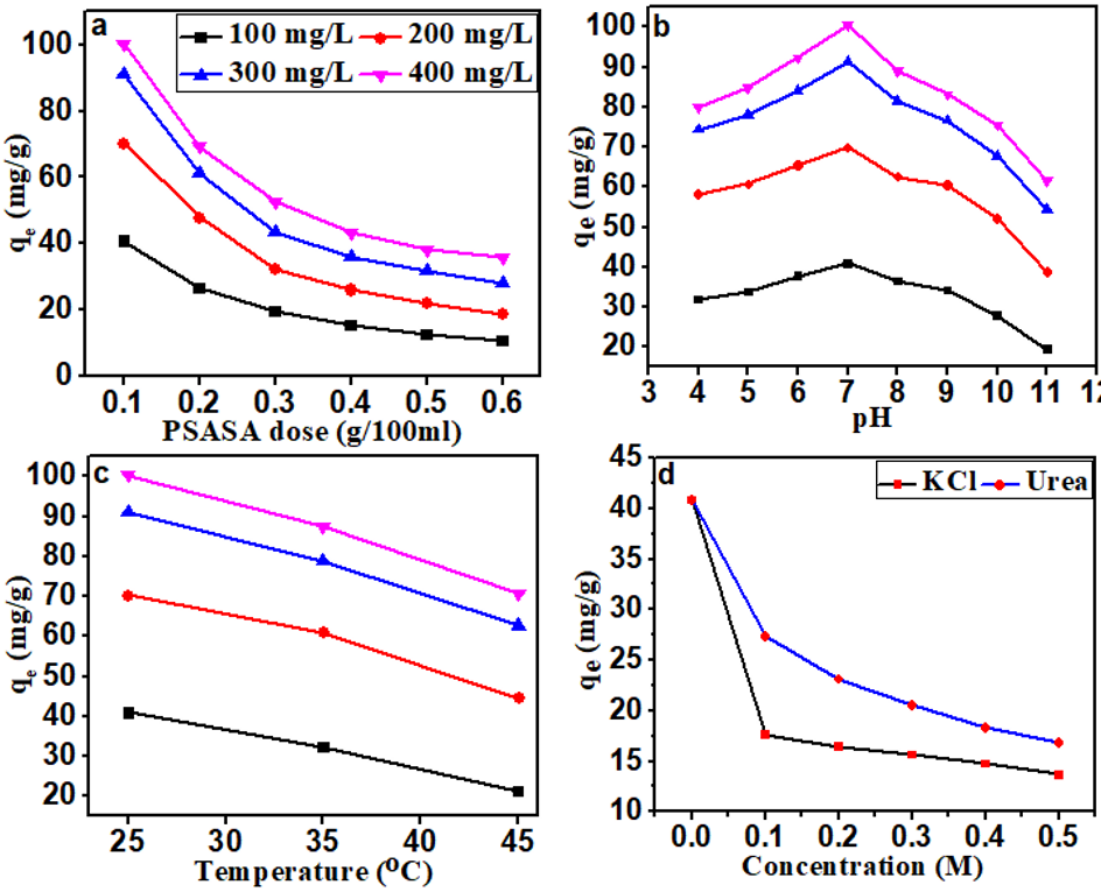

Fig 4.4: Effect of adsorbent dose at pH 7.0 & 25ºC (a), effect of pH at 25ºC & 0.1g of the PSASA (b) effect of temperature at pH 7.0 & 0.1g the PSASA (c), and effect of KCl & urea addition on 100 mg/L concentration at pH 7.0 & 25ºC (d) on uptake of 4-AP.

4.3.6. Adsorption isotherms

Adsorption isotherm shape provides understanding of adsorption behaviour. Giles categorised the patterns of adsorption isotherms into four groups: S, L, H, and C. These isotherms are then further categorized into subgroups based on how porous the adsorbent is [56]. The amount adsorbed versus equilibrium concentration graphs at various temperatures showed an L type of adsorption isotherm, indicating that 4-AP molecules and solvent molecules did not compete for PSASA surface sites (Fig. 4.5a).

Adsorption uptake decreased by 20–25 % between 25 and 45°C, demonstrating the exothermic and reversible character of the adsorption phenomenon. The following three regularly used adsorption isotherms were evaluated and questioned for their usefulness.

Freundlich isotherm

By graphing lnqe vs lnCe, the linearized Freundlich isotherm was used to analyse experimental data under various conditions. The Freundlich plot is depicted in Fig. 4.5b, and Table 4.2 reports the values for K_F, n, q_{max}, r, and R^2. At 25°C, 35°C, and 45°C temperatures, the intensity of adsorption (n) was found to be 2.48, 2.01, and 1.60, respectively. This indicated that the favorability of adsorption steadily decreases with increasing temperature. According to the literature, a value of n between 2 and 10 indicates good adsorption, 1-2 indicates moderate adsorption, and less than 1 indicates poor adsorption [57]. The R^2 values vary from 0.89 to 0.91. The Freundlich equation's parameters provided a good account of the adsorption tests. Nevertheless, at higher equilibrium concentrations and temperatures, Freundlich isotherm revealed a minor divergence from the adsorption results. As a result, the Freundlich isotherm cannot adequately explain the experimental results.

Temkin isotherm

Linear regression was used to calculate the Temkin isotherm equation's parameters. The Temkin isotherm was shown (Fig. 4.5c) between q_e and lnCe, and Table 4.2 contains a list of the Temkin equation's parameters. Adsorption equilibrium data provide an acceptable linear fit to the Temkin model, supporting the premise that binding energy is distributed uniformly. The linear fit value (R^2) was between 0.94 and 0.97. The Temkin assumption that heat adsorption would decrease linearly with an increase in surface coverage due to an interaction between the adsorbent and

adsorbate was confirmed by the R^2 value, but it diverges at higher equilibrium concentrations of 4-AP.

Table 4.2: Parameters obtained from different adsorption isotherm models for 4-AP adsorption onto the PSASA

Parameters	**Temperature**		
	25ºC	**35ºC**	**45ºC**
Langmuir			
K_L (L/mg)	9.9×10^{-3}	6.00×10^{-3}	3.43×10^{-3}
q_{max} (mg/g)	127.55	125.15	123.15
R_L	0.502	0.625	0.744
r	0.996	0.993	0.964
R^2	0.992	0.986	0.93
Freundlich			
K_F ($mg^{1-(1/n)} L^{1/n} g^{-1}$)	9.12	4.66	1.69
n	2.48	2.01	1.60
q_{max} (mg/g)	58.41	46.07	29.90
r	0.947	0.954	0.947
R^2	0.896	0.911	0.897
Temkin			
K_T (L/g)	8.5×10^{-2}	4.88×10^{-2}	3.04×10^{-2}
b (J/mol)	85.65	82.55	91.47
r	0.971	0.985	0.982
R^2	0.944	0.971	0.964

Langmuir isotherm

Regression analysis was used to linearize and examine the Langmuir isotherm model. The K_L, q_{max}, r, and R^2 parameters that were determined are shown in Table 4.2 along with the Langmuir graph that was plotted at different temperatures and shows Ce/qe against Ce (Fig. 4.5d).

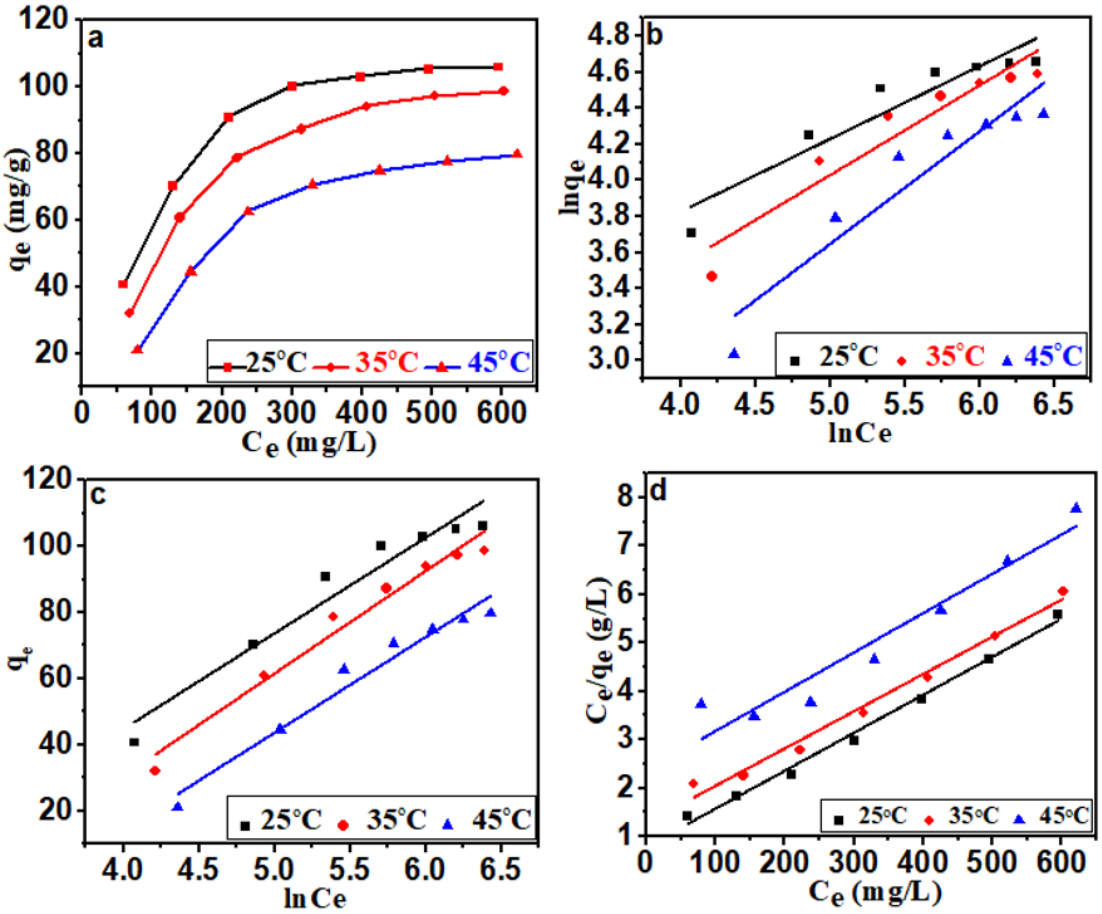

Fig 4.5: Variation of 4-AP adsorption with equilibrium concentration at pH 7.0 & 0.1g of the PSASA (a) and plots of Freundlich isotherm (b), Temkin isotherm (c), and Langmuir isotherm (d).

A dimensionless constant can serve as a representation of the degree of adsorption favorability, R_L [58]: $R_L = 1/(1+ K_L C_o)$, where C_o is the initial concentration of 4-AP and K_L is Langmuir constant. The values of $R_L = 1$ denote linear adsorption, $R_L > 1$ unfavourable adsorption, $R_L = 0$ irreversible adsorption, and $0 < R_L > 1$ favourable adsorption. The range of favourable and reversible adsorption was represented by the R_L values (Table 4.2) at various temperatures. The best linear fit of the adsorption equilibrium data is provided by the R^2 values, which range from 0.93 to 0.99. The values of the q_{max} determined using the Langmuir equation were more than two times higher than those determined by the Freundlich equation. The Langmuir isotherm

provides the most accurate explanation of the equilibrium data, as can be shown from the discussion above. A comparable finding was made by Mishra *et al.* [59].

4.3.7. Kinetics of adsorption

The adsorption of 4-AP at various time points is shown in Fig. 4.6a. The graph shows the absorption of 4-AP with time at 25ºC at varied starting concentrations (100–400 mg/L). It was shown from the graph that the 4-AP uptake increased with passing time, regardless of the 4-AP's starting concentration. The trials lasted for 5 h, and it was found that the graph of 4-AP uptake ascended quickly in the first 60 min, progressively slowed down in the following hours, and then flattened out in the last hours of the experiment. For each concentration of 4-AP, comparable trends were seen. It was deduced from the plot that the rate of adsorption uptake increased rapidly as the initial concentration of 4-AP increased; this likely happened because a higher initial concentration increases the gradient between the concentration of 4-AP at the PSASA surface and the concentration of 4-AP in the bulk of the solution. Adsorption uptake at 100 mg/L concentration was 25.54 mg/g for the first 60 min of the experiment, rose to 40.34 mg/g at 200 mg/L concentration, and increased to around 1.5 times (57.36 mg/g) at 400 mg/L initial concentration [60].

The kinetic data were assessed using the linearized forms of the rate laws shown in equations 10, 11, and 12. Regression analysis was used to determine the values of various parameters for the pseudo-first-order, pseudo-second-order, and intra-particle models, and the results are shown in Table 4.3. For concentrations between 100 and 400 mg/L, the rate laws were plotted and displayed in Fig. 4.6a. The graph between $\ln(q_e - q_t)$ versus t was plotted for the pseudo-first-order kinetics, and this best explained the kinetic outcomes. All of the concentrations had R^2 values that were higher than 0.99, indicating that the solvent had no influence on the adsorption

phenomenon [61]. The graph and calculated rate constant values make it clear that the initial concentration of 100 mg/L was the concentration at which adsorption of 4-AP occurred the quickest. This gradual increase in 4-AP adsorption uptake over time is most likely the result of the PSASA's pores becoming saturated with 4-AP molecules.

The pseudo-second-order and intra-particle model plot's r and R^2 values were less than 0.99, and experimental data did not match the predicted parameters. Fig. 4.6b–d displays the plots for the three kinetic models.

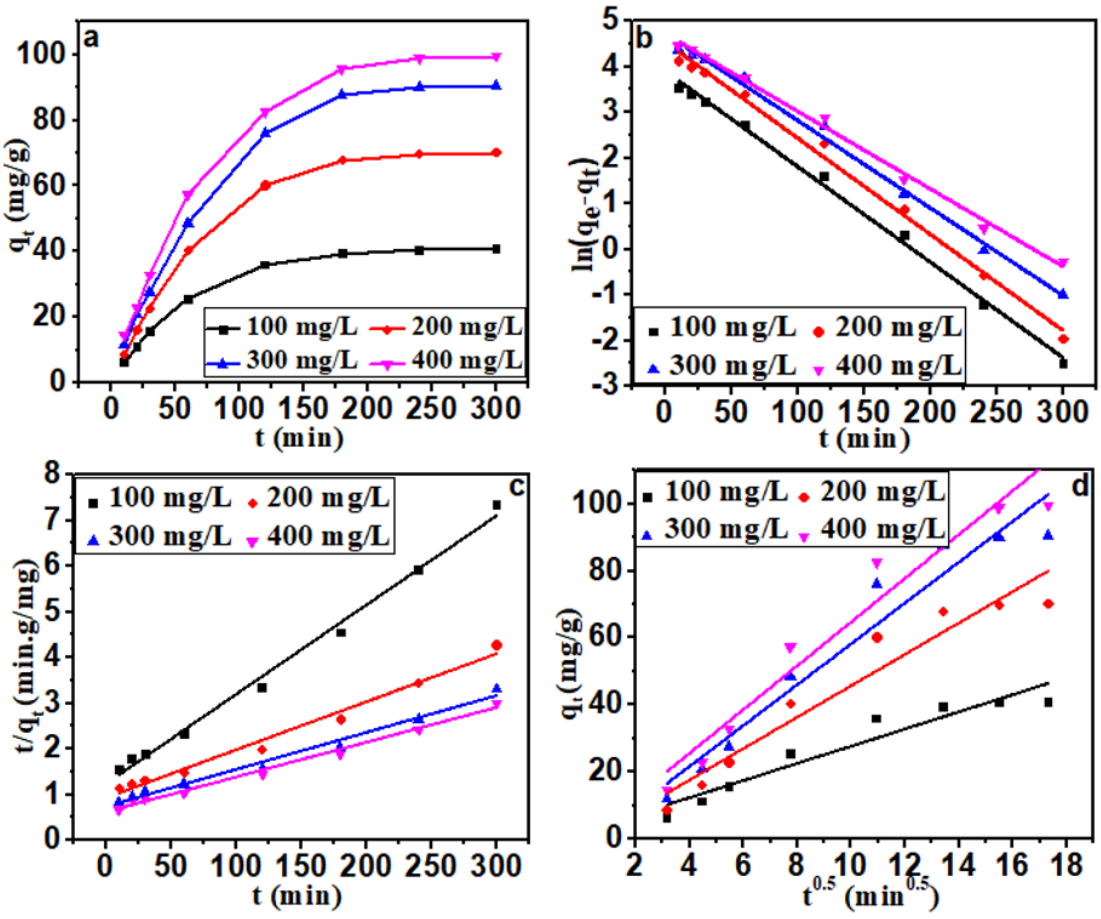

Fig. 4.6: Variation of 4-AP uptake with time at pH 7.0 & 25°C (a), pseudo-first-order (b), pseudo-second-order (c) and intra-particle kinetic plot (d).

Table 4.3: Parameters obtained from different kinetic models for 4-AP adsorption onto the PSASA

Parameters	**Concentration**			
	100 mg/L	**200 mg/L**	**300 mg/L**	**400 mg/L**
Pseudo-first-order				
k_1 (min^{-1})	2.09×10^{-2}	2.1×10^{-2}	1.91×10^{-2}	1.69×10^{-2}
q_e (mg/g)	48.97	92.64	112.94	111.06
r	-0.998	-0.997	-0.997	-0.997
R^2	0.996	0.994	0.994	0.995
Pseudo-second-order	3.07×10^{-4}	1.19×10^{-4}	8.82×10^{-5}	9.29×10^{-5}
k_2 (g/mg.min)	51.15	95.14	123.76	131.57
q_e (mg/g)	0.996	0.992	0.993	0.995
r	0.993	0.985	0.986	0.990
R^2				
Intra-particle				
k_p (g/mg. $min^{0.5}$)	2.55	4.67	6.08	6.51
C (mg/g)	2.04	-1.07	-2.69	-0.51
r	0.960	0.966	0.972	0.971
R^2	0.922	0.934	0.944	0.943

4.3.8. Activation energy and thermodynamics of 4-AP adsorption onto PSASA

The temperature of a reaction directly affects both the rate of the reaction and its rate constant, which is a well-known fact. The least amount of energy necessary to complete the adsorption reaction is referred to as the activation energy of adsorption. The relation between the rate constant and reaction temperature is used to calculate the adsorption activation energy using the Arrhenius equation. The Arrhenius equation is given by the following equation:-

$$lnk_1 = lnA - \frac{E_a}{RT} \quad (13)$$

Where, k_1 = pseudo-first-order rate constant (min^{-1}), A = frequency factor (min^{-1}) and E_a = activation energy (kJ/mol).

The activation energy of adsorption was calculated using temperature-based kinetics (Fig. 4.7a) and a pseudo-first-order kinetic model (Fig. 4.7b), with Table 4.4 containing the k_1 values at various temperatures. As it was previously discussed, pseudo-first-order kinetics provides the best-fit explanation to the kinetic data. Table 4.4 lists the values of Ea and A, which were calculated from the slope and intercept of a graph between lnk_1 and 1/T (Fig. 4.7c). The activation energy in the current study was 7.898 kJ/mol, indicating the physical character of adsorption as this energy is between 5 and 40 kJ/mol [62].

The standard state thermodynamic parameters such as change in Gibbs free energy (ΔG^o), change in entropy (ΔS^o), and change in enthalpy (ΔH^o) were calculated with the following Eq. :

$$\Delta G^o = \Delta H^o - T\Delta S^o \quad (14)$$

$$lnK_L{}^o = \frac{\Delta S^o}{R} - \frac{\Delta H^o}{RT} \quad (15)$$

Where $K_L{}^o$ is Langmuir constant in standard state; R is universal gas constant (J/mol.K); and T is absolute temperature (K), respectively.

Following formula was used to determine $K_L{}^o$,

$$\boldsymbol{K_L{}^o = K_L \times molecular\ weight\ of\ 4-AP \times 1000} \quad (16)$$

Numerous instances of ΔG^o being derived from the Langmuir constant (L/mg) without making it unitless are documented, which demonstrates a methodological flaw in the derivation of thermodynamic data [63]. In this work, the Langmuir constant was first transformed into the standard state, and other parameters were subsequently determined with the aid of Eq. 16 [64].

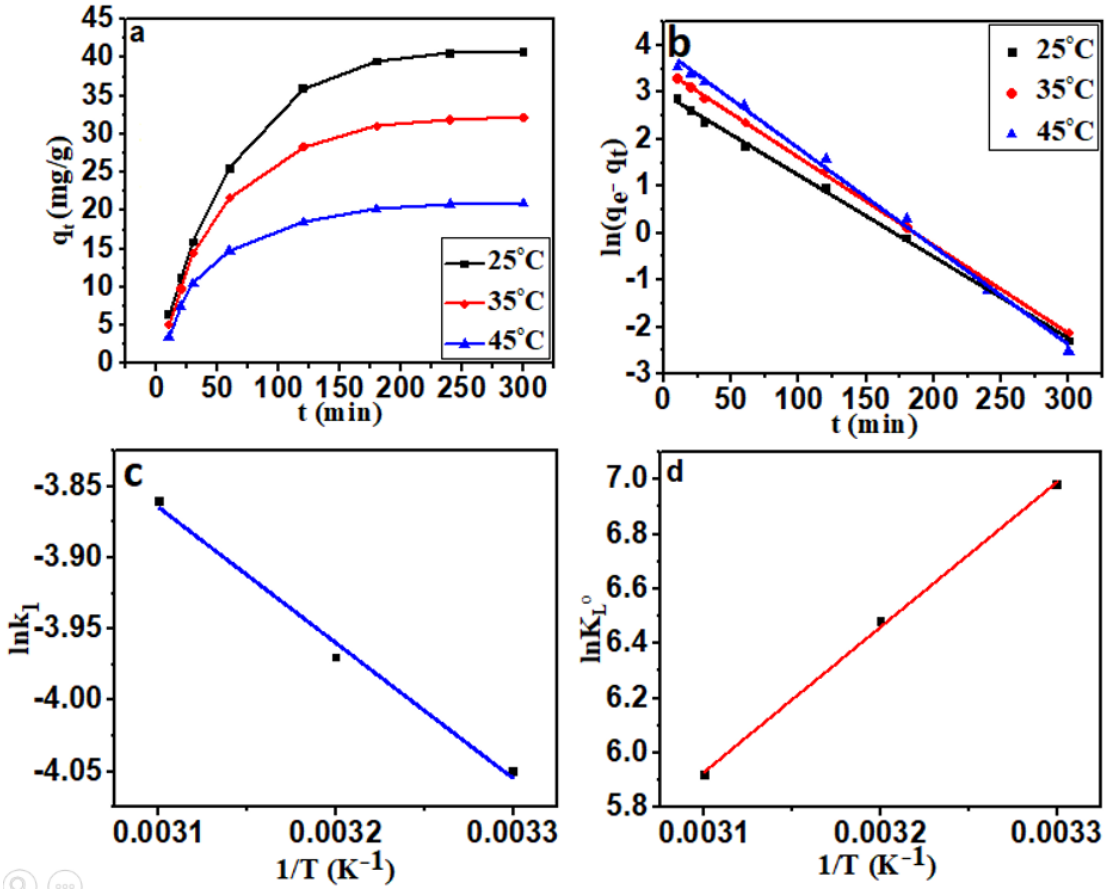

Fig. 4.7: Temperature-based variation of 4-AP uptake with time for 100 mg/L concentration (a), the temperature-based pseudo-first-order kinetic plot for 100 mg/L concentration (b), Arrhenius plot between $\ln k_1$ *versus* 1/T (c), and thermodynamic plot between $\ln K_L^{\circ}$ versus 1/T (d).

In Fig. 4.7d, a graph illustrating how $lnK_L{}^o$ changes with 1/T is depicted. Table 4.4 lists the results. A reduction in the system's randomness caused the value of ΔS^o to be negative, indicating that adsorption was favorable. By having a negative value for ΔH^o, the exothermic behaviour of adsorption was demonstrated. The ΔG^o computed at various temperatures were in the range of -40 - 0 kJ/mol, indicating that adsorption is occurring by a physisorption mechanism. Negative values support the spontaneous nature of adsorption.

Table 4.4: Thermodynamic parameters of adsorption

	25ºC	**35ºC**	**45ºC**	
k_1 (min^{-1})	1.73 x 10^{-2}	1.87 x 10^{-2}	2.09 x 10^{-2}	
E_a (kJ/mol)				7.89
A (min^{-1})				0.398
ΔG^o(kJ/mol)	-18.04	-17.17	-16.30	
$K_L{}^o$	9.31 x 10^2	5.64 x 10^2	3.22 x 10^2	
ΔH^o (kJ/mol)				-44.06
ΔS^o (J/K.mol)				-87.29

4.4. Conclusion

In the current investigation, the PSASA's ability to remove harmful 4-AP from an aqueous medium was evaluated. Compared to previously reported adsorbents, the PSASA showed better adsorption capability. Temperature, pH, adsorbent dosage, and salt addition were used to adjust the adsorption of 4-AP onto the PSASA. The pseudo-first-order and Langmuir models best explained the kinetic and adsorption isotherm, which pointed to monolayer adsorption at the PSASA surface. Thermodynamic study confirmed the exothermic and physical nature of adsorption. Given PSASA's significant adsorption potential, its availability in nature, and the inexpensive cost of chemical activation, it may therefore be inferred that adsorption occurs spontaneously. Applying this kind of adsorbent has positive effects on the environment because it doesn't need to be regenerated because it is freely available.

References

[1] P. Singh, A. Borthakur, A review on biodegradation and photocatalytic degradation of organic pollutants: A bibliometric and comparative analysis, J. Clean. Prod. 196 (2018) 1669–1680. https://doi.org/10.1016/J.JCLEPRO.2018.05.289.

[2] S. Zhang, B. Li, X. Wang, G. Zhao, B. Hu, Z. Lu, T. Wen, J. Chen, X. Wang, Recent developments of two-dimensional graphene-based composites in visible-light photocatalysis for eliminating persistent organic pollutants from wastewater, Chem. Eng. J. 390 (2020) 124642. https://doi.org/10.1016/J.CEJ.2020.124642.

[3] W. Raza, J. Lee, N. Raza, Y. Luo, K.H. Kim, J. Yang, Removal of phenolic compounds from industrial waste water based on membrane-based technologies, J. Ind. Eng. Chem. 71 (2019) 1–18. https://doi.org/10.1016/J.JIEC.2018.11.024.

[4] B. Wang, B. Huang, W. Jin, S. Zhao, F. Li, P. Hu, X. Pan, Occurrence, distribution, and sources of six phenolic endocrine disrupting chemicals in the 22 river estuaries around Dianchi Lake in China, Environ. Sci. Pollut. Res. 2012 205. 20 (2012) 3185–3194. https://doi.org/10.1007/S11356-012-1236-Y.

[5] H.N. Catherine, M.H. Ou, B. Manu, Y. hsin Shih, Adsorption mechanism of emerging and conventional phenolic compounds on graphene oxide nanoflakes in water, Sci. Total Environ. 635 (2018) 629–638. https://doi.org/10.1016/J.SCITOTENV.2018.03.389.

[6] J.S. Park, M.T. Brown, T. Han, Phenol toxicity to the aquatic macrophyte Lemna paucicostata, Aquat. Toxicol. 106–107 (2012) 182–188. https://doi.org/10.1016/J.AQUATOX.2011.10.004.

[7] A. Markiewicz, K. Björklund, E. Eriksson, Y. Kalmykova, A.M. Strömvall, A. Siopi, Emissions of organic pollutants from traffic and roads: Priority pollutants selection and substance flow analysis, Sci. Total Environ. 580 (2017) 1162–1174. https://doi.org/10.1016/J.SCITOTENV.2016.12.074.

[8] A. Tolosana-Moranchel, D. Ovejero, B. Barco, A. Bahamonde, E. Díaz, M. Faraldos, An approach on the comparative behavior of chloro / nitro substituted phenols photocatalytic degradation in water, J. Environ. Chem. Eng. 7 (2019) 103051. https://doi.org/10.1016/J.JECE.2019.103051.

[9] Z.L. Hegedus, U. Nayak, Para-aminophenol and structurally related compounds as intermediates in lipofuscin formation and in renal and other tissue toxicities, Arch. Physiol. Biochem. 99 (1991) 99–105. https://doi.org/10.3109/13813459109145911.

[10] P.D. Josephy, T. Eling, R.P. Mason, The horseradish peroxidase-catalyzed oxidation of 3,5,3',5'-tetramethylbenzidine. Free radical and charge-transfer complex intermediates., J. Biol. Chem. 257 (1982) 3669–3675. https://doi.org/10.1016/S0021-9258(18)34832-4.

[11] C. Klos, M. Koob, C. Kramer, W. Dekant, p-Aminophenol nephrotoxicity:

Biosynthesis of toxic glutathione conjugates, Toxicol. Appl. Pharmacol. 115 (1992) 98–106. https://doi.org/10.1016/0041-008X(92)90372-Y.

[12] G.J. Nohynek, D. Duche, A. Garrigues, P.A. Meunier, H. Toutain, J. Leclaire, Under the skin: Biotransformation of para-aminophenol and para-phenylenediamine in reconstructed human epidermis and human hepatocytes, Toxicol. Lett. 158 (2005) 196–212. https://doi.org/10.1016/J.TOXLET.2005.03.014.

[13] J.C. de Souza, B.F. da Silva, D.A. Morales, G. de A. Umbuzeiro, M.V.B. Zanoni, Assessment of the autoxidation mechanism of p-toluenediamine by air and hydrogen peroxide and determination of mutagenic environmental contaminant in beauty salon effluent, Sci. Total Environ. 685 (2019) 911–922. https://doi.org/10.1016/J.SCITOTENV.2019.06.252.

[14] J.C. de Souza, M.V.B. Zanoni, A.M. Oliveira-Brett, Genotoxic permanent hair dye precursors p-aminophenol and p-toluenediamine electrochemical oxidation mechanisms and evaluation in biological fluids, J. Electroanal. Chem. 857 (2020) 113509. https://doi.org/10.1016/J.JELECHEM.2019.113509.

[15] J.C. de Souza, B.F. da Silva, D.A. Morales, G. de A. Umbuzeiro, M.V.B. Zanoni, Assessment of p-aminophenol oxidation by simulating the process of hair dyeing and occurrence in hair salon wastewater and drinking water from treatment plant, J. Hazard. Mater. 387 (2020) 122000. https://doi.org/10.1016/J.JHAZMAT.2019.122000.

[16] Y. Park, G.A. Ayoko, R. Kurdi, E. Horváth, J. Kristóf, R.L. Frost, Adsorption of phenolic compounds by organoclays: Implications for the removal of organic pollutants from aqueous media, J. Colloid Interface Sci. 406 (2013) 196–208. https://doi.org/10.1016/J.JCIS.2013.05.027.

[17] A. Dąbrowski, Adsorption — from theory to practice, Adv. Colloid Interface Sci. 93 (2001) 135–224. https://doi.org/10.1016/S0001-8686(00)00082-8.

[18] J.T. Trimmer, D.C. Miller, J.S. Guest, Resource recovery from sanitation to enhance ecosystem services, Nat. Sustain. 2019 28. 2 (2019) 681–690. https://doi.org/10.1038/s41893-019-0313-3.

[19] M. Darder, P. Aranda, C. Ruiz-García, F.M. Fernandes, E. Ruiz-Hitzky, The Meeting Point of Carbonaceous Materials and Clays: Toward a New Generation of Functional Composites, Adv. Funct. Mater. 28 (2018) 1704323. https://doi.org/10.1002/ADFM.201704323.

[20] T.A. Saleh, P. Parthasarathy, M. Irfan, Advanced functional polymer nanocomposites and their use in water ultra-purification, Trends Environ. Anal. Chem. 24 (2019) e00067. https://doi.org/10.1016/J.TEAC.2019.E00067.

[21] S.J.T. Pollard, G.D. Fowler, C.J. Sollars, R. Perry, Low-cost adsorbents for waste and wastewater treatment: a review, Sci. Total Environ. 116 (1992) 31–52. https://doi.org/10.1016/0048-9697(92)90363-W.

[22] S. Praveen, R. Gokulan, T.B. Pushpa, J. Jegan, Techno-economic feasibility of biochar as biosorbent for basic dye sequestration, J. Indian Chem. Soc. 98 (2021) 100107. https://doi.org/10.1016/J.JICS.2021.100107.

[23] M. Qiu, B. Hu, Z. Chen, H. Yang, L. Zhuang, X. Wang, Challenges of organic pollutant photocatalysis by biochar-based catalysts, Biochar 2021 32. 3 (2021) 117–123. https://doi.org/10.1007/S42773-021-00098-Y.

[24] L. Liang, F. Xi, W. Tan, X. Meng, B. Hu, X. Wang, Review of organic and inorganic pollutants removal by biochar and biochar-based composites, Biochar 2021 33. 3 (2021) 255–281. https://doi.org/10.1007/S42773-021-00101-6.

[25] F. Liu, S. Hua, C. Wang, M. Qiu, L. Jin, B. Hu, Adsorption and reduction of Cr(VI) from aqueous solution using cost-effective caffeic acid functionalized corn starch, Chemosphere. 279 (2021) 130539. https://doi.org/10.1016/J.CHEMOSPHERE.2021.130539.

[26] K.C. Bedin, A.C. Martins, A.L. Cazetta, O. Pezoti, V.C. Almeida, KOH-activated carbon prepared from sucrose spherical carbon: Adsorption equilibrium, kinetic and thermodynamic studies for Methylene Blue removal, Chem. Eng. J. 286 (2016) 476–484. https://doi.org/10.1016/J.CEJ.2015.10.099.

[27] J.Q. Jiang, S.M. Ashekuzzaman, Development of novel inorganic adsorbent for water treatment, Curr. Opin. Chem. Eng. 1 (2012) 191–199. https://doi.org/10.1016/J.COCHE.2012.03.008.

[28] X.R. Zhao, X. Xu, J. Teng, N. Zhou, Z. Zhou, X.Y. Jiang, F.P. Jiao, J.G. Yu, Three-dimensional porous graphene oxide-maize amylopectin composites with controllable pore-sizes and good adsorption-desorption properties: Facile fabrication and reutilization, and the adsorption mechanism, Ecotoxicol. Environ. Saf. 176 (2019) 11–19. https://doi.org/10.1016/J.ECOENV.2019.03.069.

[29] R. Shan, Y. He, T. Zi, G. Wang, X. Liu, Z. Han, T. Zhang, Y. Zhu, Immobilization of Calcined Layered Double Hydroxide into Alginate Hydrogel Beads for PNP and PAP Removal: Kinetics, Isotherms, Thermodynamics, and Mechanism, Water. Air. Soil Pollut. 229 (2018) 1–18. https://doi.org/10.1007/S11270-018-3976-X/FIGURES/11.

[30] B.B. Tewari, M. Boodhoo, Removal of p-aminophenol and p-nitrophenol from aqueous solution through adsorption on antimony, cadmium, and zirconium ferrocyanides, J. Colloid Interface Sci. 289 (2005) 328–332. https://doi.org/10.1016/J.JCIS.2005.04.032.

[31] X. Li, X. Zhou, J. Mu, L. Lu, D. Han, C. Lu, M. Wang, Thermodynamics and kinetics of p -aminophenol adsorption on poly(aryl ether ketone) containing pendant carboxyl groups, J. Chem. Eng. Data. 56 (2011) 4274–4277. https://doi.org/10.1021/JE2009297.

[32] R. Dod, G. Banerjee, S. Saini, Adsorption of Methylene Blue Using Green Pea Peels (Pisum sativum): A Cost-effective Option for Dye-based Wastewater Treatment, Biotechnol. Bioprocess Eng. 17 (2012) 862–874. https://doi.org/10.1007/s12257-011-0614-5.

[33] K. Singh, A. Kumar, S.K. Pandey, S. Awasthi, S.P. Gupta, P. Mishra, Interpretation of Adsorption Behavior of Carboxymethyl Cellulose onto

Functionalized Accurel Polymeric Surface, Ind. Eng. Chem. Res. 59 (2020) 19102–19116. https://doi.org/10.1021/ACS.IECR.0C03894.

[34] D. Prakash, N.N. Nawani, A rapid and improved technique for scanning electron microscopy of actinomycetes, J. Microbiol. Methods. 99 (2014) 54–57. https://doi.org/10.1016/J.MIMET.2014.02.005.

[35] A. Abdelhay, A. Al Bsoul, A. Al-Othman, N.M. Al-Ananzeh, I. Jum'h, A.A. Al-Taani, Kinetic and thermodynamic study of phosphate removal from water by adsorption onto (Arundo donax) reeds, Adsorpt. Sci. Technol. 36 (2018) 46–61. https://doi.org/10.1177/0263617416684347.

[36] A. Al Bsoul, M. Hailat, A. Abdelhay, M. Tawalbeh, A. Al-Othman, I.N. Al-kharabsheh, A.A. Al-Taani, Efficient removal of phenol compounds from water environment using Ziziphus leaves adsorbent, Sci. Total Environ. 761 (2021) 143229. https://doi.org/10.1016/J.SCITOTENV.2020.143229.

[37] K. Singh, A. Kumar, S. Awasthi, S.K. Pandey, P. Mishra, Adsorption mechanism of carboxymethyl cellulose onto mesoporous mustard carbon: Experimental and theoretical aspects, Colloids Surfaces A Physicochem. Eng. Asp. 581 (2019) 123786. https://doi.org/10.1016/J.COLSURFA.2019.123786.

[38] C. Ng, J.N. Losso, W.E. Marshall, R.M. Rao, Freundlich adsorption isotherms of agricultural by-product-based powdered activated carbons in a geosmin–water system, Bioresour. Technol. 85 (2002) 131–135. https://doi.org/10.1016/S0960-8524(02)00093-7.

[39] G.D. Halsey, The Role of Surface Heterogeneity in Adsorption, Adv. Catal. 4 (1952) 259–269. https://doi.org/10.1016/S0360-0564(08)60616-1.

[40] S. Fan, Y. Wang, Z. Wang, J. Tang, J. Tang, X. Li, Removal of methylene blue from aqueous solution by sewage sludge-derived biochar: Adsorption kinetics, equilibrium, thermodynamics and mechanism, J. Environ. Chem. Eng. 5 (2017) 601–611. https://doi.org/10.1016/J.JECE.2016.12.019.

[41] I. Langmuir, The constitution and fundamental properties of solids and liquids. Part I. Solids, J. Am. Chem. Soc. 38 (1916) 2221–2295. https://doi.org/10.1021/ja02268a002.

[42] X. Guo, J. Wang, A general kinetic model for adsorption: Theoretical analysis and modeling, J. Mol. Liq. 288 (2019). https://doi.org/10.1016/J.MOLLIQ.2019.111100.

[43] M. Wolthers, L. Charlet, P. Van Cappellen, The surface chemistry of divalent metal carbonate minerals; a critical assessment of surface charge and potential data using the charge distribution multi-site ion complexation model, Am. J. Sci. 308 (2008) 905–941. https://doi.org/10.2475/08.2008.02.

[44] E.P. Barrett, L.G. Joyner, P.P. Halenda, The Determination of Pore Volume and Area Distributions in Porous Substances. I. Computations from Nitrogen Isotherms, J. Am. Chem. Soc. 73 (2002) 373–380. https://doi.org/10.1021/JA01145A126.

[45] Z. Li, D. Liu, Y. Cai, Y. Wang, J. Teng, Adsorption pore structure and its fractal characteristics of coals by N2 adsorption/desorption and FESEM image

analyses, Fuel. 257 (2019) 116031. https://doi.org/10.1016/J.FUEL.2019.116031.

[46] H. Zhu, Y. Ju, C. Huang, F. Chen, B. Chen, K. Yu, Microcosmic gas adsorption mechanism on clay-organic nanocomposites in a marine shale, Energy. 197 (2020) 117256. https://doi.org/10.1016/J.ENERGY.2020.117256.

[47] K. Singh, A. Kumar, P. Mishra, S.P. Gupta, Binding aspects of carboxymethyl cellulose onto polymeric surface from its aqueous solutions, J. Dispers. Sci. Technol. (2020) 1–14. https://doi.org/10.1080/01932691.2020.1786396.

[48] J.H. van der Maas, E.T.G. Lutz, Structural information from OH stretching frequencies monohydric saturated alcohols, Spectrochim. Acta Part A Mol. Spectrosc. 30 (1974) 2005–2019. https://doi.org/10.1016/0584-8539(74)80047-4.

[49] A.S. Wexler, Infrared determination of structural units in organic compounds by integrated intensity measurements: Alkanes, alkenes and monosubstituted alkyl benzenes, Spectrochim. Acta. 21 (1965) 1725–1742. https://doi.org/10.1016/0371-1951(65)80085-6.

[50] E. Altintig, M. Onaran, A. Sarı, H. Altundag, M. Tuzen, Preparation, characterization and evaluation of bio-based magnetic activated carbon for effective adsorption of malachite green from aqueous solution, Mater. Chem. Phys. 220 (2018) 313–321. https://doi.org/10.1016/J.MATCHEMPHYS.2018.05.077.

[51] S.B. Lima, S.M.S. Borges, M. do C. Rangel, S.G. Marchetti, Effect of iron content on the catalytic properties of activated carbon-supported magnetite derived from biomass, J. Braz. Chem. Soc. 24 (2013) 344–354. https://doi.org/10.5935/0103-5053.20130044.

[52] G. Feiqiang, L. Xiaolei, J. Xiaochen, Z. Xingmin, G. Chenglong, R. Zhonghao, Characteristics and toxic dye adsorption of magnetic activated carbon prepared from biomass waste by modified one-step synthesis, Colloids Surfaces A Physicochem. Eng. Asp. 555 (2018) 43–54. https://doi.org/10.1016/J.COLSURFA.2018.06.061.

[53] A. Mandal, N. Bar, S.K. Das, Phenol removal from wastewater using low-cost natural bioadsorbent neem (Azadirachta indica) leaves: Adsorption study and MLR modeling, Sustain. Chem. Pharm. 17 (2020) 100308. https://doi.org/10.1016/J.SCP.2020.100308.

[54] A. Mandal, S.K. Das, Phenol adsorption from wastewater using clarified sludge from basic oxygen furnace, J. Environ. Chem. Eng. 7 (2019) 103259. https://doi.org/10.1016/J.JECE.2019.103259.

[55] Y. Li, X. Hu, X. Liu, Y. Zhang, Q. Zhao, P. Ning, S. Tian, Adsorption behavior of phenol by reversible surfactant-modified montmorillonite: Mechanism, thermodynamics, and regeneration, Chem. Eng. J. 334 (2018) 1214–1221. https://doi.org/10.1016/J.CEJ.2017.09.140.

[56] C.H. Giles, D. Smith, A. Huitson, A general treatment and classification of the solute adsorption isotherm. I. Theoretical, J. Colloid Interface Sci. 47 (1974)

755–765. https://doi.org/10.1016/0021-9797(74)90252-5.

[57] O. Hamdaoui, E. Naffrechoux, Modeling of adsorption isotherms of phenol and chlorophenols onto granular activated carbon: Part I. Two-parameter models and equations allowing determination of thermodynamic parameters, J. Hazard. Mater. 147 (2007) 381–394. https://doi.org/10.1016/J.JHAZMAT.2007.01.021.

[58] K.R. Hall, L.C. Eagleton, A. Acrivos, T. Vermeulen, Pore- and Solid-Diffusion Kinetics in Fixed-Bed Adsorption under Constant-Pattern Conditions, Ind. Eng. Chem. Fundam. 5 (2002) 212–223. https://doi.org/10.1021/I160018A011.

[59] P. Mishra, K. Singh, U. Dixit, Adsorption, kinetics and thermodynamics of phenol removal by ultrasound-assisted sulfuric acid-treated pea (Pisum sativum) shells, Sustain. Chem. Pharm. 22 (2021) 100491. https://doi.org/10.1016/J.SCP.2021.100491.

[60] E.C. Lima, F. Sher, A. Guleria, M.R. Saeb, I. Anastopoulos, H.N. Tran, A. Hosseini-Bandegharaei, Is one performing the treatment data of adsorption kinetics correctly?, J. Environ. Chem. Eng. 9 (2021) 104813. https://doi.org/10.1016/J.JECE.2020.104813.

[61] D.C.S. Alves, B.B. Coseglio, L.A.A. Pinto, T.R.S. Cadaval, Development of Spirulina/chitosan foam adsorbent for phenol adsorption, J. Mol. Liq. 309 (2020) 113256. https://doi.org/10.1016/J.MOLLIQ.2020.113256.

[62] M. Zulfiqar, S. Sufian, N.E. Rabat, N. Mansor, Photocatalytic degradation and adsorption of phenol by solvent-controlled TiO2 nanosheets assisted with H2O2 and FeCl3: Kinetic, isotherm and thermodynamic analysis, J. Mol. Liq. 308 (2020) 112941. https://doi.org/10.1016/J.MOLLIQ.2020.112941.

[63] E.C. Lima, F. Sher, M.R. Saeb, M. Abatal, M.K. Seliem, Comments on "Reasonable calculation of the thermodynamic parameters from adsorption equilibrium constant, Journal of Molecular Liquids 322 (2021) 114980.," J. Mol. Liq. 334 (2021) 116542. https://doi.org/10.1016/J.MOLLIQ.2021.116542.

[64] E.C. Lima, A. Hosseini-Bandegharaei, J.C. Moreno-Piraján, I. Anastopoulos, A critical review of the estimation of the thermodynamic parameters on adsorption equilibria. Wrong use of equilibrium constant in the Van't Hoof equation for calculation of thermodynamic parameters of adsorption, J. Mol. Liq. 273 (2019) 425–434. https://doi.org/10.1016/J.MOLLIQ.2018.10.048.

Chapter-5

Adsorption, kinetics and thermodynamics of phenol removal by ultrasound-assisted sulfuric acid-treated pea (Pisum sativum) shells

5.1. Introduction

The need for energy and fresh water for everyday necessities regularly increases as a result of the continued rise of the world's population. As industrial activity grows in response to rising demand from the public, harmful effluent is released into the environment's aquatic systems [1]. People are gradually getting concerned about the effects of the aforementioned behaviours due to their responsibility for rising greenhouse gas emissions and climate change [2,3]. The wastewater from a variety of businesses, including those in the pharmaceutical, steel, plastic, petroleum, rubber, and coal tar industries, contains phenol and its derivatives, which are regarded as significant pollutants for the aquatic environment [4,5]. Environmental Protection Agencies in the United States and the European Union have listed phenols as a priority contaminant [6] and these organisations set the maximum allowable phenol content at 1 ppm [7] however the WHO set the maximum threshold for clean, drinking water at 0.001 ppm [8]. The Indian Government accepts the same approach [9]. Numerous health issues, including nausea, unconsciousness, dermatitis, bronchial asthma, headaches, and infections of the liver and kidneys, are brought on by phenolic chemical toxicity. [5,10].

Scientists and environmentalists are interested in removing phenol from wastewater effluents because of its negative effects on both humans and the environment. Numerous methods have been used to reduce the concentration to the allowable level of phenolic compounds because they are produced both naturally and by human activity. These methods include photo-Fenton, electrocoagulation, adsorption, membrane processes, ultrasound, biodegradation, steam plasma jet treatment, and catalytic air oxidation [11–15]. Adsorption is the most widely used method for the removal of organic and inorganic contaminants, and activated carbon

is the most efficient and widely used adsorbent. However, despite its great adsorption capacity, activated carbon is costly to run since its high regeneration expense limits its continued use [5,16,17]. Thus, to replace activated carbon and making the adsorption process practical and affordable, adsorbents made from diverse agricultural wastes have been created [18].

Different natural agricultural wastes, including rice husk, eucalyptus leaves, date seeds, banana peels, tea remnants, sawdust remnants, and ziziphus leaves, have been used as adsorbents with positive results, according to several researcher [19–25]. According to research by Nadavala *et al*., pine bark has the highest adsorption capacity of 143 mg/g under ideal conditions for the removal of phenolic chemicals [26]. Additionally, several changes have been made to the standard activated carbon. For example, a composite material made from activated carbon modified with chitosan in a 1:1 ratio demonstrated nearly 95 % phenol elimination at concentrations lower than 50 ppm [27]. Ashanendu and Sudip [28] reported phenol removal from wastewater using clarified sludge from a basic oxygen furnace, which gave 63 % of phenol removal at the best conditions, Mishra *et al.* [29] reported phenol removal using magnetised activated carbon made from corn husks. Thue *et al.* [30] synthesised microwave-assisted activated carbon from wood chips for phenol removal. Toona Sinensis leaves that are treated with NaOH were reported by Kong *et al.* to remove phenol [31]. According to Park et al. [32], activated carbon coated with nanoparticles of iron oxide was used to remove bisphenol, and Singh *et al.* [33] employed affordable adsorbent from agricultural waste (mustard cake) to remove phenol effectively. Singh *et al.* [34] investigated the modified polypropylene's ability to adsorb phenolics.

Pisum sativum, a cold-season plant, is used to cultivate peas, which are harvested from early summer through winter in many regions of the world. In India, peas are widely farmed in the winter, and the waste from these crops, called pea shells (PS), is easily accessible in markets and households.

In the current work, a novel PS adsorbent that has undergone chemical modification is described for efficient phenol removal. Its distinctive qualities make it a successful adsorbent for phenol elimination. SEM-EDS, FT-IR, pXRD, BET-surface area analysis, optical profilometry, and PZC are used to analyse the adsorbent. Several experiments that examine the effects of pH, adsorbent concentration, temperature, surface charge analysis, and the addition of inorganic salts (KCl and $CaCl_2$) are used to study the mechanism of phenol removal. The applicability of several kinetic and adsorption isotherm models was also checked in order to understand the adsorption mechanism.

5.2. Experimental section

5.2.1. Preparation of ultrasound-assisted sulfuric acid-treated pea shells (USAPS)

To get rid of both water-soluble and insoluble contaminants, waste pea shells were gathered from local households and repeatedly cleaned with distilled water. The PS was subsequently dried in the sun for a few days, pulverised using a mechanical grinder, and sieved to remove any particles larger than 75 µm. For chemical activation, the PS was added in a 2:1 ratio to 50% v/v H_2SO_4 and allowed to sit for 24 h. This paste was heated to 750°C in the muffle furnace for 30 minutes after 24 h. After being thoroughly cleaned, the carbonised PS were placed in the Sonics Vibra-Cell VCX750 ultrasonicator and subjected to a power of 25 kHz ultrasound for1 h.

The sample was then removed from the sonicator, cleaned, dried, and stored in a desiccator for further use.

5.2.2. Characterization of USAPS

Scanning electron microscopy (SEM) analysis was used to examine the USAPS's surface morphology, and energy-dispersive X-ray spectroscopy was used to assess the USAPS sample's elemental composition (EDS). JEOL, Japan's JSM-6490LV model was used for both analyses. The USAPS sample's functional group analysis was carried out using an FT-IR spectrophotometer (Thermo- Scientific Nicole 6700, USA). With 32 scans and a resolution of 5-7 cm^{-1}, the spectra was captured between 4000-400 cm^{-1}. Powder x-ray diffractometer (RigakuMiniflex II desktop) was used to analyse the USAPS's phase. Copper Kα radiation (= 1.5405 Aº) was used to scan the USAPS at a rate of 2º/min throughout a range of 20º to 70º. Using the software programmes Origin and Match3, raw data were processed. An optical profilometer (Bruker, USA) was used to determine the topographical characteristics and aerial image of the USAPS surface. The N_2 adsorption-desorption curve, BET analysis, and Barret-Joyner-Halenda (BJH) method were each used to calculate the USAPS's mean pore size, surface area, and degree of porosity, respectively. A BET surface area analyzer (BELSORP-max, Japan) was used to do the surface area analysis. The Singh *et al.* [35] method was used to measure the PZC.

5.2.3. Batch adsorption experiments

To investigate the impact of various experimental conditions on the removal of phenol by the USAPS, several batch adsorption studies were conducted. In each experiment, 0.1 g of the USAPS dose was fixed, and 100 ml of phenol solution was added to a 100 ml conical flask at various temperatures and pH levels. Phenol's initial concentration was between 50 and 500 mg/L. The equilibrium was reached after 3 h, although some

samples were kept for 6 and 12 h and still produced the same results. Samples were examined using a Systronic double beam spectrophotometer at a wavelength of 270 nm at specific time intervals to determine the time dependency of phenol elimination.

The following equation expresses and calculates the amount of phenol adsorbed at equilibrium:-

$$q_e = \frac{(C_0 - C_e)V_s}{m} \quad (1)$$

Where, q_e: the amount of phenol adsorbed at equilibrium, C_o: initial phenol concentration, C_e: phenol concentration at equilibrium, V_s: volume of solution (in L), m: mass of the USAPS added (in g)

Equation (below) expresses and calculates the amount of phenol adsorbed at any time:

$$q_t = \frac{(C_0 - C_t)V_s}{m} \quad (2)$$

Where, q_t: the amount of phenol adsorbed at time t (in mg/g), C_t: concentration of phenol at time t (in mg/L).

5.2.4. Adsorption isotherm

Freundlich, Temkin, and Langmuir's adsorption isotherm models were modelled to explain the equilibrium data. The linear form of these isotherms is represented by the following equations:

Freundlich isotherm

$$lnq_e = lnK_F + \frac{1}{n} lnC_e \quad (3)$$

Maximum adsorption capacity (q_{max}) is calculated by using the equation given by Halsey [36]:

$$K_F = {q_m/C_o}^{1/n} \quad (4)$$

Where, K_F: Freundlich constant ($mg^{1-(1/n)}$ $L^{1/n}$ /g); 1/n: intensity of adsorption; C_o: initial concentration.

Temkin isotherm

$$q_e = \frac{RT}{b} lnK_T + \frac{RT}{b} lnC_e \quad (5)$$

Where, K_T: Temkin constant (L/g) and b: the heat of adsorption constant (J/mol).

Langmuir isotherm

$$\frac{C_e}{q_e} = \frac{1}{q_m K_L} + \frac{C_e}{q_m} \quad (6)$$

Where, K_L: Langmuir constant (L/mg) and q_{max} (mg/g): maximum adsorption.

5.2.5. Kinetic study

The pseudo-first-order, pseudo-second-order, and intra-particle diffusion models were used to examine kinetic data. The following equations serve as a representation for these models:

Pseudo-first-order model

$$\ln(q_e - q_t) = lnq_e - k_1 t \quad (7)$$

Pseudo-second-order model

$$\frac{t}{q_t} = \frac{1}{k_2 {q_e}^2} + \frac{t}{q_e} \quad (8)$$

Where, k_1: pseudo-first-order (min^{-1}) and k_2: pseudo-second-order rate constant (g/mg. min), respectively.

Intra-particle diffusion model

$$q_t = k_p t^{0.5} + C \quad (9)$$

Where, k_p: particle related rate constant ($g/mg.min^{0.5}$), and C: constant (mg/g).

5.3. Results and discussion

5.3.1. Characterization of the USAPS

Through SEM study, the surface morphology of the USAPS was discovered. Fig. 5.1 displays the USAPS's SEM picture. The SEM image clearly shows that the surface

morphology of the USAPS is quite uneven. Randomly positioned cages and voids can be found throughout the USAPS surface.

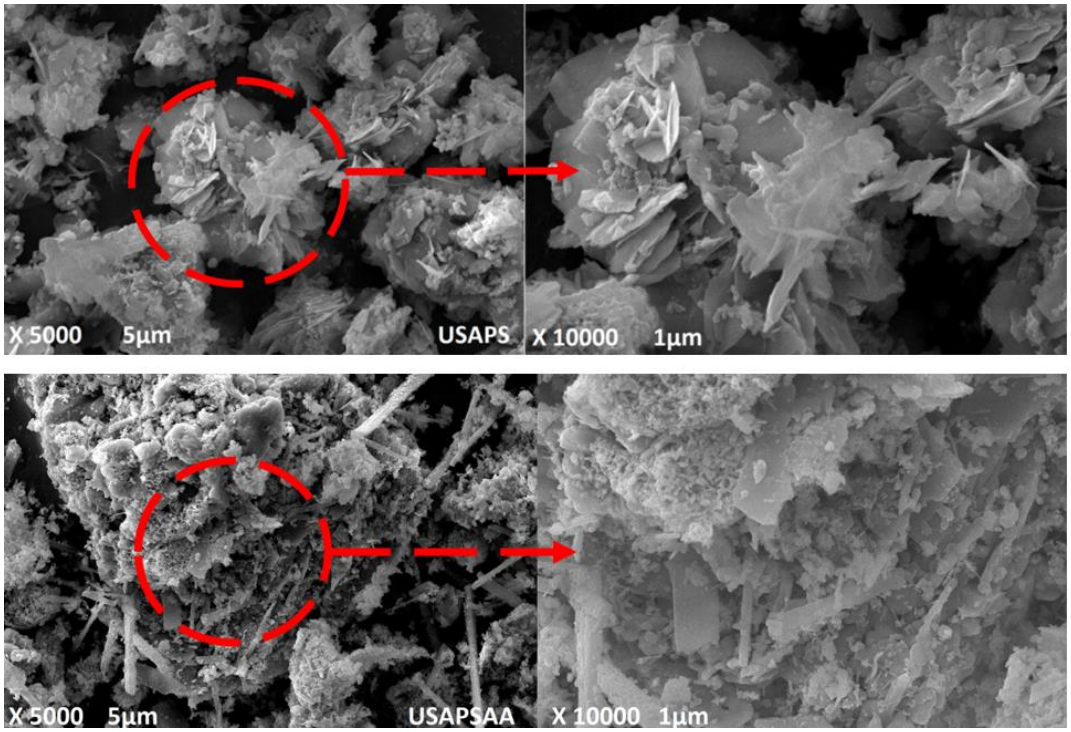

Fig. 5.1: SEM image of the USAPS and The USAPSAA.

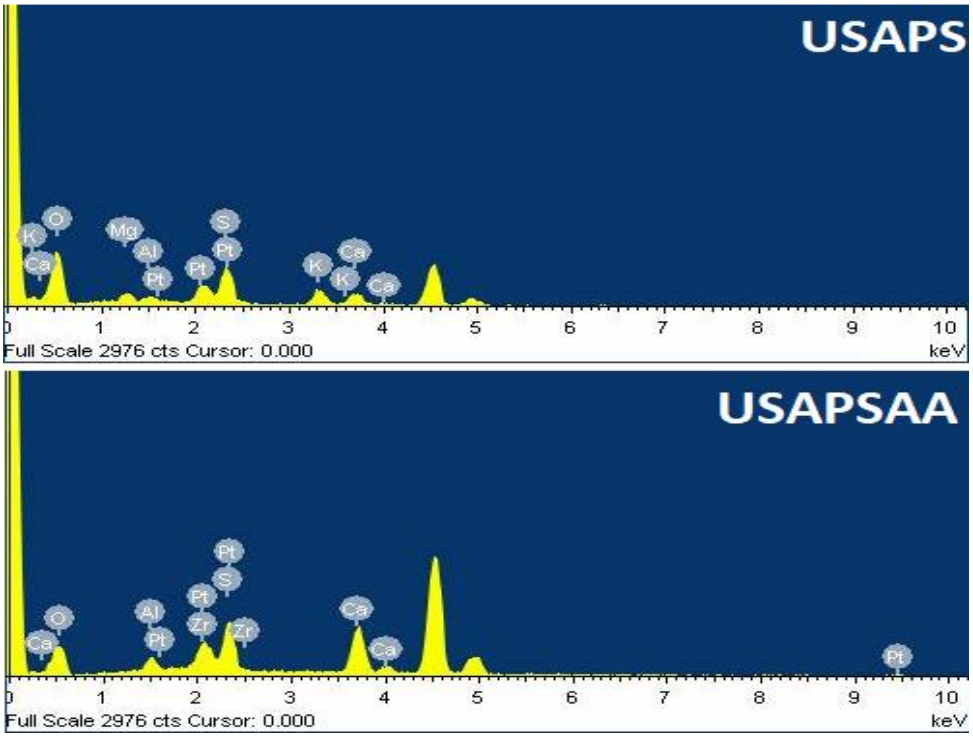

Fig. 5.2: EDS spectrum of the USAPS and the USAPSAA.

The sulfuric acid and extremely high temperature treatment of the PS resulted in the formation of these cages/voids. These cages offer improved conditions for trapping phenol molecules inside them [37–40].

According to Fig. 5.2, which depicts the EDS spectrum of the USAPS, the principal elements present in the USAPS are C, O, S, and Ca. C, O, S, and Ca all have weight percentages of 27.74 %, 57.82 %, 9.44 %, and 5.00 %, respectively. Fig. 5.1 depicts the SEM picture of the ultrasound-assisted sulphuric acid-treated pea shells after adsorption (USAPSAA). It is evident from Fig. 5.1 that phenol crystals have been deposited all over the USAPS surface.

By using FT-IR spectroscopy, the functional group analysis of the USAPS and the USAPSAA was carried out, and the spectrum is displayed in Fig. 5.3. Three small peaks at 3606.1 cm^{-1}, 3549.3 cm^{-1}, and 3407.7 cm^{-1} were discovered in the intense band; these peaks may be attributed to stretching vibrations of the O-H group of pure, hydrogen-bonded alcohol, water, or carboxylic acid [41]. Alkynes' -C≡C- triple bonds may be responsible for a weak band at 2224.7 cm^{-1} [42]. At 1624.8 cm^{-1}, a sharp band was noticed that might be the result of C=C stretching. The band at 1146.4 cm^{-1} was most likely caused by a tertiary alcohol's C-O stretching. C-S, S-O, and C-O bending vibrations may be the cause of the bands below 700 cm^{-1} being detected. Two key changes were noticed in the USAPSAA's FT-IR spectra. Two bands with poor intensities were seen at 1655.1 cm^{-1} and 1611.8 cm^{-1}, as well as a minor band with weak intensity at 3728. 5 cm^{-1}. The O-H stretching vibration of water molecules was assigned to the band at 3728.5 cm^{-1}, indicating the solvent impact during the adsorption process [43]. The bands at 1655.1 cm^{-1} and 1611.8 cm^{-1} came about as a result of a shift in the strength of the C=C bond, confirming an electron exchange between the USAPS surface and the phenol aromatic ring. [44,45].

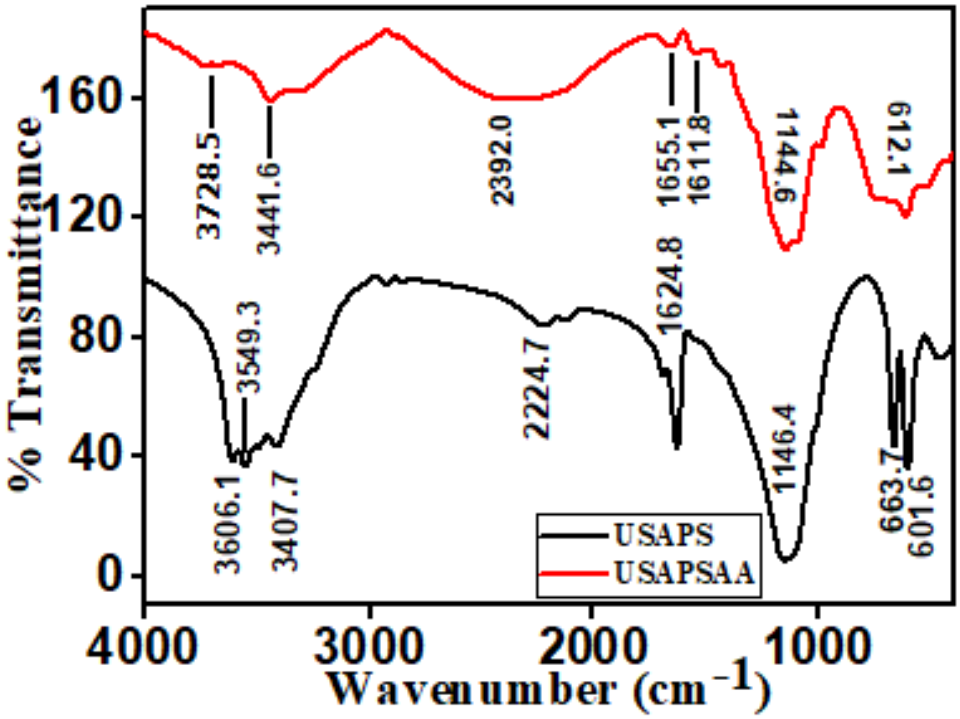

Fig. 5.3: FT-IR spetra of the USAPS and the USAPSAA.

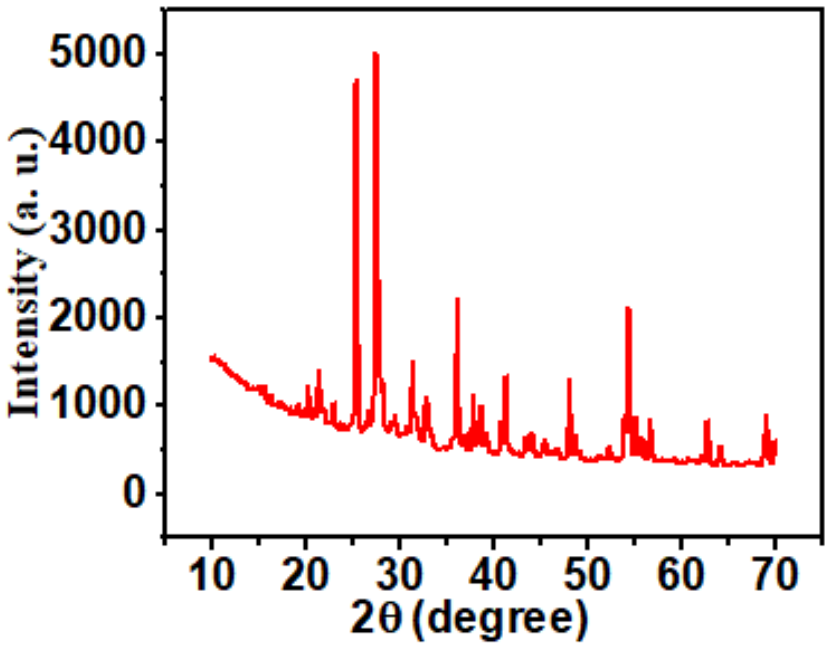

Fig. 5.4: XRD spectrum of the USAPS**.**

Fig. 5.4 displays the USAPS's XRD spectrum. The defining feature of activated carbon is shown by two prominent peaks in the XRD spectrum, which range from 20º to 30º [46]. Additionally, other minor peaks between 40° and 70° were seen, which

were likely caused by substances containing calcium. The USAPS's amorphous nature was validated by the degree of crystallinity analysis, which found that it contains 77.76 % amorphous material and 24.24 % crystalline material.

An optical profilometer operating in veridical scanning interferometry (VSI) mode was used to measure the surface topography and topographical characteristics of the USAPS. Fig. 5.5a's topographical representation of the USAPS demonstrates the high degree of surface unevenness, as indicated by the high values of the roughness average (Ra = 14.403 µm) and root mean square roughness (Rq = 18.732 µm),. The greater population of valleys under the USAPS surface, which verifies the porous nature of the USAPS and suggests that capillary action may also occur during the adsorption-desorption cycle, can be seen in the profilometry image. The presence of a sufficient number of adsorption sites over the USAPS surface is confirmed by the larger difference between Maximum profile height (Rt = 163.76 µm) and Maximum profile valley depth (Rv = -112.276 µm). The average roughness of the synthesised adsorbent rose from 11.208 µm to 14.403 µm, according to the comparison between the assessments with and without ultrasonic treatment.

To determine the specific surface area, mean pore diameter, and total pore volume of the USAPS surface, BET surface area analysis was used. In Fig. 5.5b, the N_2 adsorption-desorption curve onto the USAPS surface is depicted. The adsorption-desorption curve showed a hysteresis loop of the H_3 type, confirming that N_2 desorbs more slowly than other molecules. When some of the N_2 molecules are adsorbed in the capillaries found on the USAPS surface, there is a decreased desorption of N_2. The USAPS surface's porousness is further supported by the hysteresis loop in the adsorption-desorption curve. Singh *et al.* [47] described an analogous adsorption-desorption curve. The specific surface area (S_{BET}) and mean pore diameter of the

USAPS were calculated using the BET method (Fig. 5.5c) and were found to be, respectively, 7.0735 m^2/g and 63.712 nm. Using the IUPAC nomenclature of porous materials (microporous: < 2 nm; mesoporous: 2–50 nm; and macroporous: > 50 nm), the mean pore diameter value demonstrated that the USAPS is macroporous [48]. The total pore volume of the USAPS surface was calculated using the BJH model (Fig. 5.5d) and was found to be 0.1139 cm^3/g.

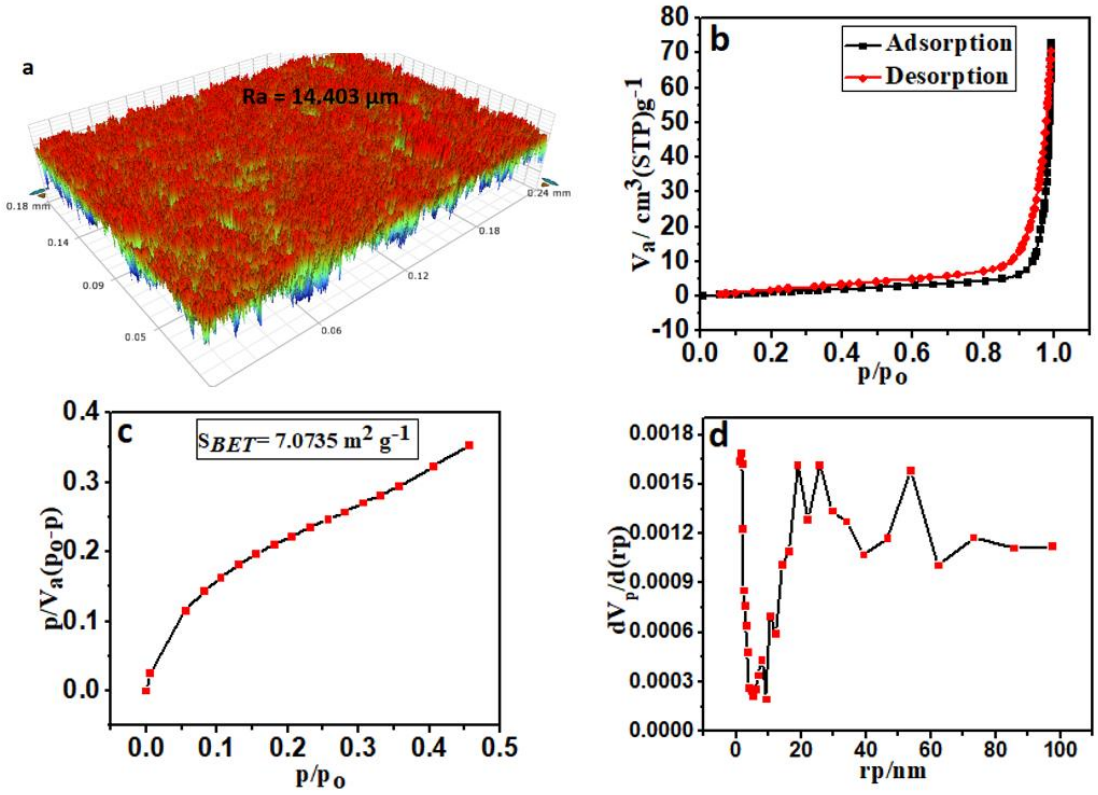

Fig. 5.5: 3D optical profilometry image (a), N_2 adsorption-desorption (b), BET (c) and BJH (d) graphs of the USAPS.

5.3.2. Point of zero charge (PZC) of the USAPS

The pH level at which a material's surface charge is zero is indicated by the PZC value. When the pH is lower than PZC, the surface's total charge will be positive, and when the pH is greater than PZC, the surface's overall charge will be negative. The

PZC value for the USAPS, which is in the basic range, was discovered to be 8.38, meaning that at pH 8.38, the USAPS surface was neutral, but at pH values below and above 8.38, the net surface charge of the USAPS was positive and negative, respectively.The graph of PZC is depicted in Fig. 5.6.

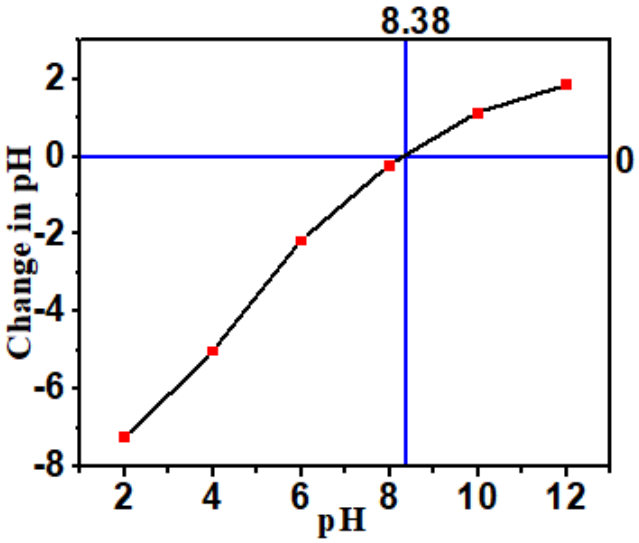

Fig. 5.6: PZC graph of the USAPS.

5.3.3. Effect of pH

Fig. 5.7a displays the change in phenol uptake with pH. The pH of the solution was maintained between 2 and 9 throughout the experiment, while other variables like the phenol concentration (50 mg/L), the USAPS dose (0.1g/100ml), contact time (180 min), and temperature (25ºC) were constant. For phenol concentrations (100-200 mg/L), experiments were repeated. Since the PZC of the USAPS was observed to be 8.38, the effectiveness of adsorption above the initial pH 9 was not examined. According to Fig. 5.7a, the adsorption of phenol progressively increases from pH 2 to an ideal value of pH 7, and then it sharply declines. At pH 7, the most phenol was adsorbed. Based on the USAPS's surface charge and phenol's acidic behaviour, these results can be explained. Despite the USAPS' net positive surface charge, there was less phenol adsorption between pH 2 and 6, which was caused by the [H^+] ions' ability

to obstruct phenol molecules from adhering to the USAPS' adsorption sites. Due to the absence of any foreign species that could have interfered with the adsorption process, electrostatic contact between phenol and the USAPS sites at pH 7 was quite high. Because the USAPS surface was positively charged at pH 8, reduced adsorption was seen, however phenol and [OH^-] both compete for adsorption sites. At pH 9, phenol and the USAPS surface are more electrostatically attracted to one another, which further reduces adsorption as the USAPS surface becomes negatively charged. Similar outcomes have already been published [24].

5.3.4. Effect of reaction temperature

The change of phenol adsorption with temperature is depicted in (Fig. 5.7b). The temperature was held between 25 and 45ºC throughout the experiment, while other variables like the phenol concentration (100 mg/L), the USAPS dose (0.1 g/100 ml), the contact period (180 min), and the pH (7) were constant. Additional concentrations (200-500 mg/L) were tested in the same experiments. The exothermic nature of adsorption was supported by the observation in Fig. 5.7b that phenol adsorption decreased as temperature increased. At 25ºC, adsorption was at its highest, whereas at 45ºC, it was at its lowest. For a concentration of 100 mg/L, the uptake of phenol dropped from 54.37 mg/g to 36.41 mg/g. For higer concentrations, the same patterns were also seen. Phenol molecules have a larger kinetic energy at higher temperatures, which reduces the likelihood that they will interact with the USAPS surface.

5.3.5. Effect of the USAPS dose

Fig. 5.7c depicts the variation in phenol adsorption with the USAPS dose. The USAPS dose ranged between 0.1 and 0.6 g/100 ml while maintaining a constant concentration of 50 mg/L, a pH of 7, a contact period of 180 minutes, and a temperature of 25ºC. For the higher concentrations (100, 150, and 200 mg/L),

experiments were repeated. On doubling the USAPS dose (0.1 to 0.2 g/100 ml), the phenol absorption decreased from 29.39 to 21.83 mg/g, as seen in Fig. 5.7c. Additionally, once the USAPS dose was increased, phenol uptake continued to fall albeit at a slower rate. Since initial concentration acts as a driving force for the mass transfer between the solid and liquid phase, the decrease in phenol uptake with an increase in the USAPS dose is likely caused by the formation of a low concentration gradient between the liquid phenol concentration and the solid phenol concentration [8].

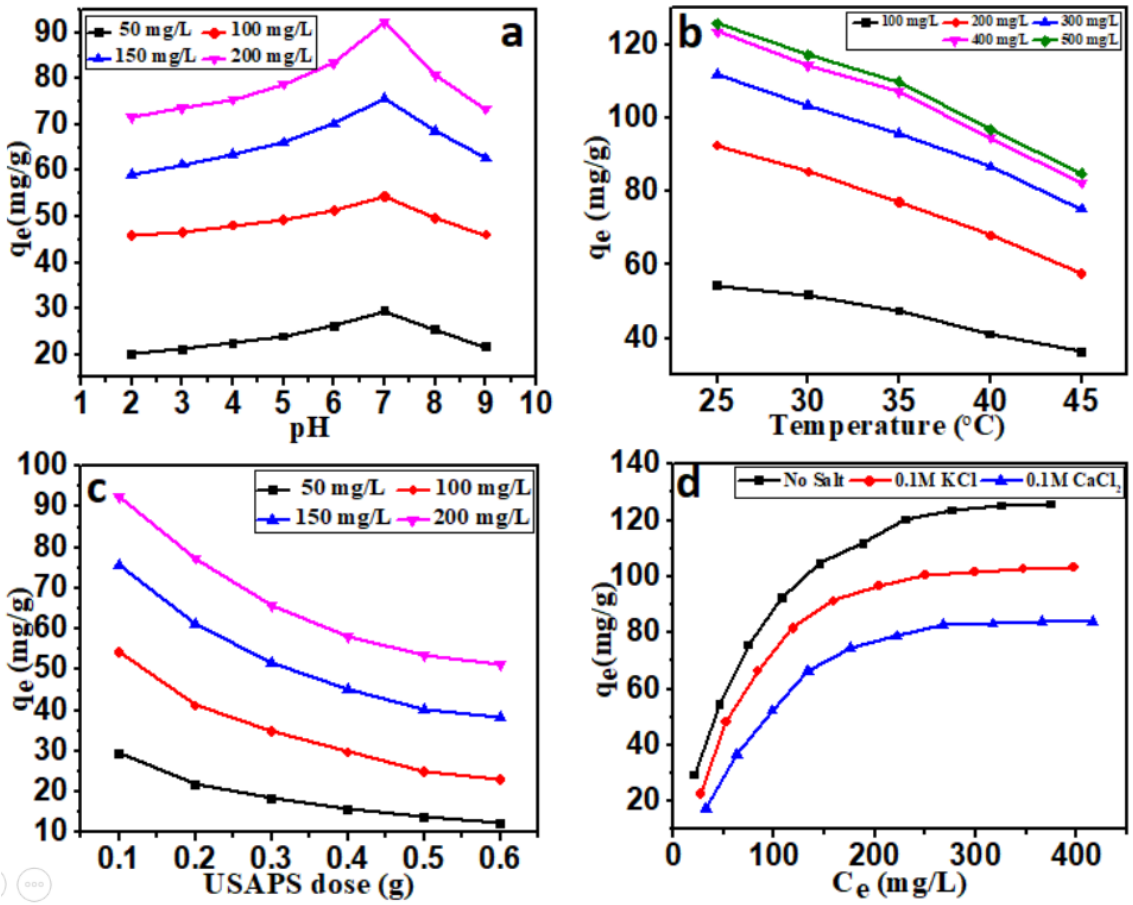

Fig. 5.7: Effect of pH at 25ºC & 0.1 g of the USAPS (a), effect of temperature at pH 7.0 & 0.1 g of the USAPS (b), Effect of the USAPS dose at pH 7.0 & 25ºC (c) and effect of salt (KCl & $CaCl_2$) addition at pH 7.0 & 25ºC on phenol uptake.

5.3.6. Effect of inorganic salt addition

Fig. 5.7d depicts the outcome of the addition of inorganic salt. Different amounts of phenol (50-500 mg/L) were mixed with 0.1 M KCl and 0.1 M $CaCl_2$ independently, while maintaining pH (7), the USAPS dose (0.1 g/100ml), temperature (25ºC), and contact duration (180 min). It is clear from Fig. 5.7d that the amount of adsorption in equilibrium reduced with the addition of 0.1 M KCl and 0.1 M $CaCl_2$, going from 125.77 mg/g to 103.45 and 84.11 mg/g, respectively. The reduction in phenol uptake was probably caused by inorganic ions blocking the adsorption sites, preventing phenol molecules from reaching the USAPS surface. Additionally, it was found that cations with a large hydration sphere, high valency, and low ionic radius have the greatest effects on phenol absorption. Li *et al.* [49] reported similar outcomes.

5.3.7. Adsorption isotherm

We can explain the adsorption behaviour by looking at the shape of the adsorption isotherm. Adsorption isotherms have been divided into four groups by Giles based on the various adsorption behaviours, that are S, H, L, and C [50].

Fig. 5.8a's depiction of the USAPS's phenol adsorption isotherm demonstrates that it follows the L type of isotherm. There is no competition between solvent and solute molecules for the adsorption sites of the adsorbate in the L type of adsorption isotherms [50]. The adsorption equilibrium data were analysed using Freundlich, Temkin, and Langmuir isotherms, and their validity was confirmed by calculating various adsorption parameters, coefficient of determination (R^2), and correlation coefficient (r) using regression analysis.

Fig. 5.8b shows the curve of the Freundlich isotherm, which was plotted between lnCe and lnq_e. Adsorption parameters were estimated using intercept and slope values, and the results are shown in Table 5.1. The n values range from 1.71 to 2.04, which

indicates moderate adsorption at various temperatures. Less than half of the q_{max} values found using experimental data were found using Hasley's equation. The R^2 value is in the 0.93 to 0.96 range, demonstrating its inability to explain the adsorption phenomenon. As a result, the adsorption of phenol onto the USAPS was not assumed to occur over a heterogeneous surface.

Table 5.1. Adsorption isotherm parameters of phenol adsorption onto the USAPS

Parameters	**Temperature**		
	25 ºC	**35 ºC**	**45 ºC**
Langmuir			
K_L (L/mg)	1.26×10^{-2}	8.44×10^{-3}	6.19×10^{-3}
q_{max} (mg/g)	156.98	149.03	121.95
r	0.998	0.993	0.996
R^2	0.996	0.98	0.993
Freundlich			
K_F ($mg^{1-(1/n)}L^{1/n}/g$)	8.17	4.60	2.87
n	2.04	1.78	1.71
q_{max} (mg/g)	55.17	41.17	28.33
r	0.967	0.969	0.982
R^2	0.935	0.939	0.965
Temkin			
K_T (L/g)	1.15×10^{-1}	7.52×10^{-2}	4.68×10^{-2}
b (J/mol)	69.90	74.29	103.36
r	0.992	0.991	0.996
R^2	0.984	0983	0.992

Fig. 5.8c depicts the curve of the Temkin isotherm plotted between q_e and $\ln C_e$ at various temperatures. Table 5.1 is a summary of the isotherm parameters. The R^2 values were in the 0.984–0.992 range, suggesting the potential of a uniform distribution of binding energy across the USAPS surface. Because the Temkin

isotherm exhibits a minor divergence at higher phenol concentrations, as seen in Fig. 5.8c, this model was unable to account for the adsorption phenomenon.

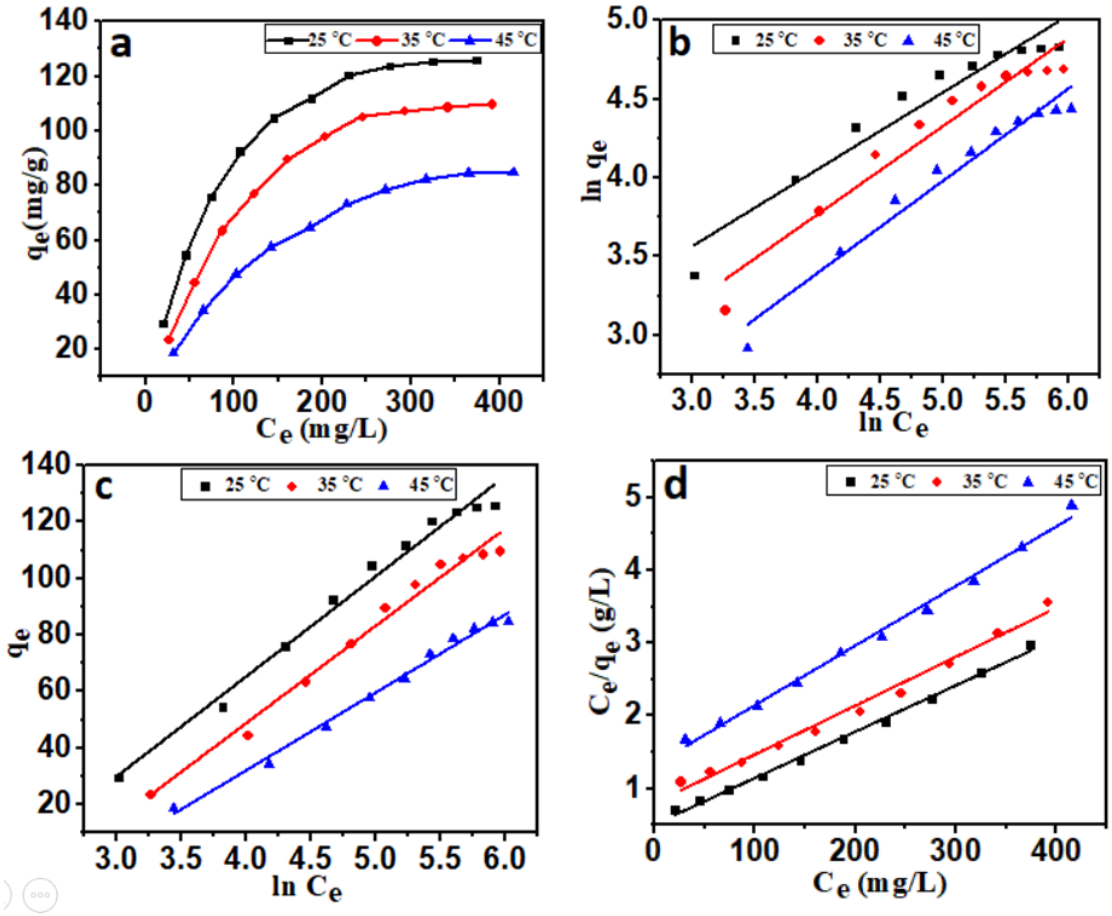

Fig. 5.8: Amount of phenol adsorbed versus equilibrium concentration at pH 7.0 & 0.1 g of the USAPS (a) and isotherm plots of Freundlich (b) Temkin (c) and Langmuir (d).

In Fig. 5.8d, the Langmuir isotherm graph between C_e/q_e and C_e is displayed. Table 5.1 lists the adsorption parameters that were derived from intercept and slope. The results were consistent with adsorption trials and the values of r and R^2 were more than 0.99. Since monolayer adsorption was thought to be possible, Langmuir isotherm was supposed to offer the best linear fit explanation for adsorption experiments. Similar studies for phenol elimination have already been described [51,52].

5.3.8. Adsorption kinetics

Fig. 5.9a depicts the change in phenol uptake (q_t) along time. According to Fig. 5.9a, there were three processes involved in the adsorption of phenol onto the USAPS. Rapid phenol removal was seen in the first stage (0–45 min), moderate phenol pickup was shown in the second stage (45–90 min), and insignificant phenol uptake was seen in the third stage (90–180 min).

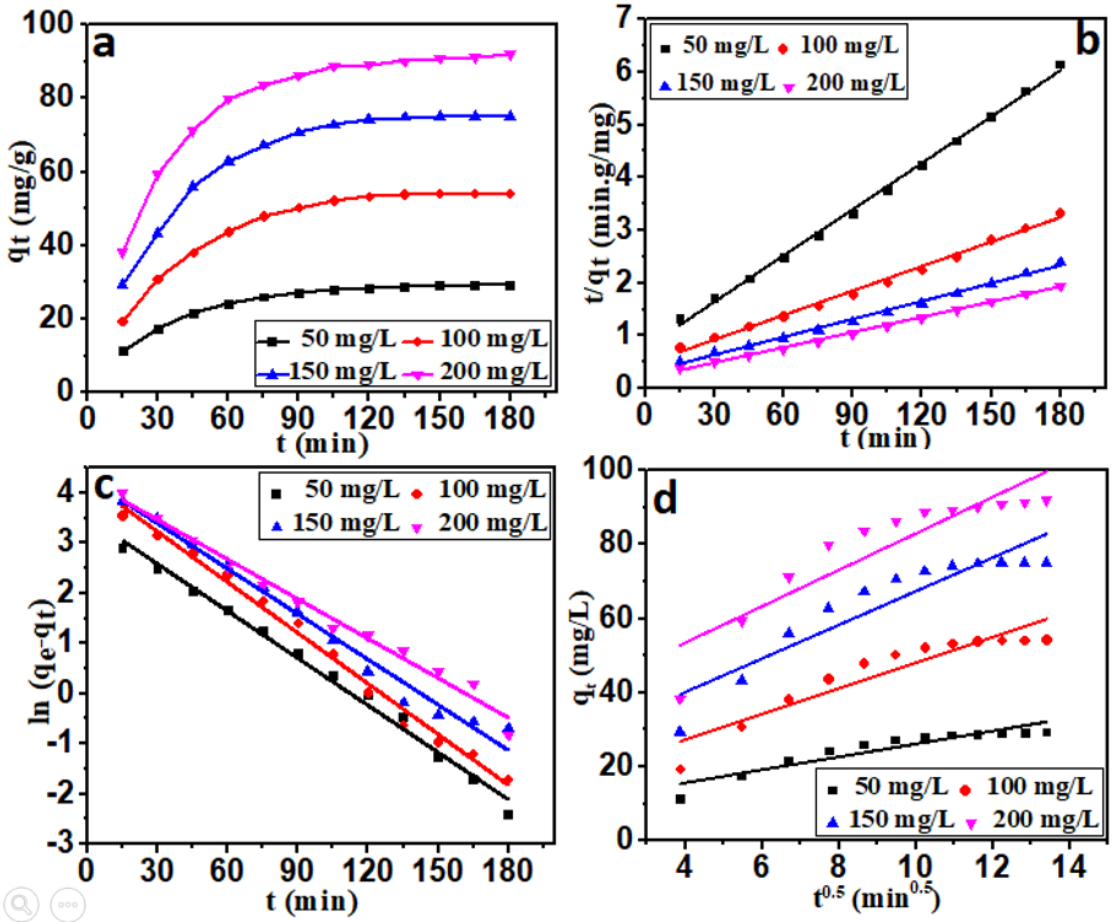

Fig. 5.9: Variation of adsorption uptake of phenol with time at pH 7.0 & 25ºC (a), pseudo-second-order kinetics plot (b), pseudo-first-order kinetics plot (c) and intra-particle model (d).

Based on the first stage's accessibility of a larger number of surface sites, these adsorption processes can be explained. As the adsorption rate approaches equilibrium in the second and third steps, it slows down. To determine whether the results of the adsorption experiment were appropriate, various kinetic models, including pseudo-

second-order, pseudo-first-order, and intra-particle models, were fitted. The graphs for these models are shown in Fig. 5.9b-d, and Table 5.2 lists the model-derived parameters.

Table 5.2: Kinetic parameters of different models at various concentrations

Parameters	**Concentration**			
	50 mg/L	**100 mg/L**	**150 mg/L**	**200 mg/L**
Pseudo-first-order				
k_1 (min^{-1})	3.12×10^{-2}	3.36×10^{-2}	3.01×10^{-2}	2.62×10^{-2}
q_e (mg/g)	33.60	68.76	72.80	67.63
r	-0.995	-0.995	-0.991	-0.992
R^2	0.991	0.991	0.983	0.985
Pseudo-second-order				
k_2 (g/mg. min)	1.10×10^{-3}	5.18×10^{-4}	4.32×10^{-4}	4.65×10^{-4}
q_e (mg/g)	34.24	64.80	88.57	104.16
r	0.998	0.997	0.997	0.998
R^2	0.997	0.995	0.995	0.997
Intra-particle				
k_p ($g/mg.min^{0.5}$)	1.74	3.46	4.54	4.91
C (mg/g)	8.53	13.33	21.84	33.69
r	0.931	0.934	0.925	0.909
R^2	0.868	0.873	0.857	0.82

Pseudo-second-order kinetics provides the best-fit explanation for kinetic data, as shown by the values estimated from this model, which are well aligned with values of experimental data (Fig. 5.9b-d). Additionally, R^2 values better than 0.99 supported the model's applicability. The outcomes agreed with the earlier published study [51,52]. The R^2 values for the pseudo-first-order and intra-particle models were in the range of

0.98-0.99 and 0.82-0.87, respectively, demonstrating their unimportance for the adsorption phenomenon.

5.3.9. Adsorption thermodynamics

The temperature-based Langmuir constant (K_L) was initially made unitless for the thermodynamic analysis [53]. Standard state thermodynamic parameters like Gibbs free energy change (ΔG^o), Entropy change (ΔS^o), change in Enthalpy (ΔH^o) were calculated using the following Eq. :

$$lnK^o = \frac{\Delta S^o}{R} - \frac{\Delta H^o}{RT} \quad (10)$$

K^o was calculated using the following formula:

$$\boldsymbol{K^o = K_L \times molecular\ weight\ of\ phenol \times 1000} \quad (11)$$

$$\Delta G^o = \Delta H^o - T\Delta S^o \quad (12)$$

Where K^o is Standard state Langmuir equilibrium constants; R: universal gas constant (J/mol.K) and T: absolute temperature (K).

Table 5.3: Thermodynamic parameters of adsorption

	25ºC	**35ºC**	**45ºC**	
ΔG^o(kJ/mol)	-17.969	-17.581	-17.193	
K^o	1185.786	7942.88	582.540	
ΔH^o (kJ/mol)				-29.51
ΔS^o (J/K.mol)				-38.74

In Fig. 5.10, the graph between lnK^o and 1/T is displayed. The results of the calculations made using the aforementioned equations are shown in Table 5.3 for all the thermodynamic parameters. The exothermic nature of the adsorption process was confirmed by a negative value for ΔH^o, and the feasibility of adsorption was established by a negative value for ΔG^o. The fact that adsorption becomes less

practicable as temperature rises was proven by the increase in ΔG^o value. The phenol-USAPS interface underwent adsorption without undergoing any structural change, according to a slightly negative value of ΔS^o.

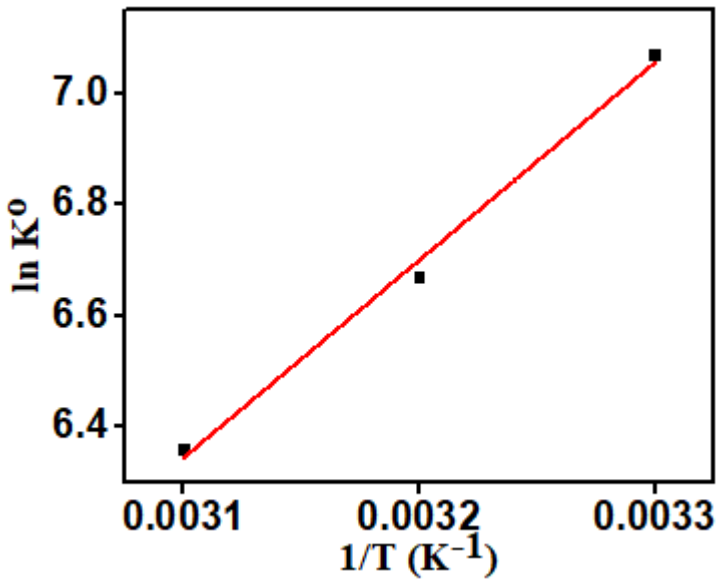

Fig. 5.10: Thermodynamic plot of $\ln K^o$ *versus* 1/T.

Conclusion

The current investigation came to the conclusion that the newly synthesised USAPS was macroporous, amorphous, had a very rough surface, and had high topographical characteristics. Temperature rise, USAPS dosage, and salt (KCl and $CaCl_2$) addition all had a negative impact on adsorption. High determination coefficient values and the Langmuir isotherm provided the best explanation for the adsorption data. The thermodynamic study confirmed that adsorption was exothermic and spontaneous with no structural change at the USAPS-phenol interface. So, it can be concluded that the USAPS has a high adsorption potential for the adsorption of phenolic compounds and can be used as an alternative to activated carbon as PS is freely available with low activation cost while regeneration is not needed due to its low cost and abundance.

References

[1] N.M. Pham, T.L.D. Huynh, M.A. Nasir, Environmental consequences of population, affluence and technological progress for European countries: A Malthusian view, J. Environ. Manage. 260 (2020) 110143. https://doi.org/10.1016/J.JENVMAN.2020.110143.

[2] A.H. Alami, A. Abu Hawili, M. Tawalbeh, R. Hasan, L. Al Mahmoud, S. Chibib, A. Mahmood, K. Aokal, P. Rattanapanya, Materials and logistics for carbon dioxide capture, storage and utilization, Sci. Total Environ. 717 (2020) 137221. https://doi.org/10.1016/J.SCITOTENV.2020.137221.

[3] M. Tawalbeh, F.H. Tezel, M. Al-Ismaily, B. Kruczek, Highly permeable tubular silicalite-1 membranes for CO2 capture, Sci. Total Environ. 676 (2019) 305–320. https://doi.org/10.1016/J.SCITOTENV.2019.04.290.

[4] N.D. Mu'azu, M. Zubair, N. Jarrah, O. Alagha, M.A. Al-harthi, M.H. Essa, Sewage Sludge ZnCl2-Activated Carbon Intercalated MgFe–LDH Nanocomposites: Insight of the Sorption Mechanism of Improved Removal of Phenol from Water, Int. J. Mol. Sci. 2020, Vol. 21, Page 1563. 21 (2020) 1563. https://doi.org/10.3390/IJMS21051563.

[5] R. Mukherjee, S. De, Adsorptive removal of phenolic compounds using cellulose acetate phthalate–alumina nanoparticle mixed matrix membrane, J. Hazard. Mater. 265 (2014) 8–19. https://doi.org/10.1016/J.JHAZMAT.2013.11.012.

[6] P. Chakraborty, S. Sampath, M. Mukhopadhyay, S. Selvaraj, G.K. Bharat, L. Nizzetto, Baseline investigation on plasticizers, bisphenol A, polycyclic aromatic hydrocarbons and heavy metals in the surface soil of the informal electronic waste recycling workshops and nearby open dumpsites in Indian metropolitan cities, Environ. Pollut. 248 (2019) 1036–1045. https://doi.org/10.1016/J.ENVPOL.2018.11.010.

[7] M.H. El-Naas, S. Al-Zuhair, M.A. Alhaija, Removal of phenol from petroleum refinery wastewater through adsorption on date-pit activated carbon, Chem. Eng. J. 162 (2010) 997–1005. https://doi.org/10.1016/J.CEJ.2010.07.007.

[8] A. Mandal, P. Mukhopadhyay, S.K. Das, Adsorptive removal of phenol from wastewater using guava tree bark, Environ. Sci. Pollut. Res. 2020 2719. 27 (2020) 23937–23949. https://doi.org/10.1007/S11356-020-08777-2.

[9] N.N. Dutta, S. Borthakur, G.S. Patil, Phase Transfer Catalyzed Extraction of Phenolic Substances from Aqueous Alkaline Stream, Http://Dx.Doi.Org/10.1080/01496399208019435. 27 (2006) 1435–1448. https://doi.org/10.1080/01496399208019435.

[10] S. Mohammadi, A. Kargari, H. Sanaeepur, K. Abbassian, A. Najafi, E. Mofarrah, Phenol removal from industrial wastewaters: a short review, New Pub Balaban. 53 (2015) 2215–2234. https://doi.org/10.1080/19443994.2014.883327.

[11] F. Al Momani, O. Gonzalez, C. Sans, S. Esplugas, Combining photo-Fenton

process with biological sequencing batch reactor for 2,4-dichlorophenol degradation, Water Sci. Technol. 49 (2004) 293–298. https://doi.org/10.2166/WST.2004.0288.

[12] T. Karami, S. Elyasi, T. Amani, Modeling and optimizing of electrocoagulation process in treating phenolic wastewater by response surface methodology: precise evaluation of significant variables, Int. J. Environ. Sci. Technol. 2018 1511. 15 (2018) 2389–2398. https://doi.org/10.1007/S13762-017-1539-0.

[13] A. Bódalo, J.L. Gómez, M. Gómez, G. León, A.M. Hidalgo, M.A. Ruíz, Phenol removal from water by hybrid processes: study of the membrane process step, Desalination. 223 (2008) 323–329. https://doi.org/10.1016/J.DESAL.2007.01.219.

[14] G. Ni, G. Zhao, Y. Jiang, J. Li, Y. Meng, X. Wang, Steam Plasma Jet Treatment of Phenol in Aqueous Solution at Atmospheric Pressure, Plasma Process. Polym. 10 (2013) 353–363. https://doi.org/10.1002/PPAP.201200155.

[15] C. Sun, T. Chen, Q. Huang, M. Zhan, X. Li, J. Yan, Activation of persulfate by CO2-activated biochar for improved phenolic pollutant degradation: Performance and mechanism, Chem. Eng. J. 380 (2020) 122519. https://doi.org/10.1016/J.CEJ.2019.122519.

[16] V.S. Tran, H.H. Ngo, W. Guo, J. Zhang, S. Liang, C. Ton-That, X. Zhang, Typical low cost biosorbents for adsorptive removal of specific organic pollutants from water, Bioresour. Technol. 182 (2015) 353–363. https://doi.org/10.1016/J.BIORTECH.2015.02.003.

[17] S.H. Lin, R.S. Juang, Adsorption of phenol and its derivatives from water using synthetic resins and low-cost natural adsorbents: A review, J. Environ. Manage. 90 (2009) 1336–1349. https://doi.org/10.1016/J.JENVMAN.2008.09.003.

[18] R. Shokoohi, H. Movahedian, A. Dargahi, A.J. Jafari, A. Parvaresh, Survey on efficiency of BF/AS integrated biological system in phenol removal of wastewater, Desalin. Water Treat. 82 (2017) 315–321. https://doi.org/10.5004/DWT.2017.20957.

[19] M.A.M. Abdallah, The potential of different bio adsorbents for removing phenol from its aqueous solution, Environ. Monit. Assess. 185 (2013) 6495–6503. https://doi.org/10.1007/s10661-012-3041-y.

[20] A. Al Bsoul, The use of eucalyptus leaves as adsorbent for copper ion removal, New Pub Balaban. 52 (2014) 7838–7844. https://doi.org/10.1080/19443994.2013.832637.

[21] S. Babel, T.A. Kurniawan, Low-cost adsorbents for heavy metals uptake from contaminated water: a review, J. Hazard. Mater. 97 (2003) 219–243. https://doi.org/10.1016/S0304-3894(02)00263-7.

[22] S. Rengaraj, S.H. Moon, R. Sivabalan, B. Arabindoo, V. Murugesan, Agricultural solid waste for the removal of organics: adsorption of phenol from water and wastewater by palm seed coat activated carbon, Waste Manag. 22 (2002) 543–548. https://doi.org/10.1016/S0956-053X(01)00016-2.

[23] S.M. Mane, A.K. Vanjara, M.R. Sawant, Removal of Phenol from Wastewater

Using Date Seed Carbon, J. Chinese Chem. Soc. 52 (2005) 1117–1122. https://doi.org/10.1002/JCCS.200500160.

[24] A. Al Bsoul, M. Hailat, A. Abdelhay, M. Tawalbeh, A. Al-Othman, I.N. Al-kharabsheh, A.A. Al-Taani, Efficient removal of phenol compounds from water environment using Ziziphus leaves adsorbent, Sci. Total Environ. 761 (2021) 143229. https://doi.org/10.1016/J.SCITOTENV.2020.143229.

[25] D.N. Jadhav, A.K. Vanjara, Removal of phenol from wastewater using sawdust, polymerized sawdust and sawdust carbon, IJCT Vol.11(1) [January 2004]. 11 (2004) 35–41.

[26] S.K. Nadavala, H. Che Man, H.-S. Woo, Biosorption of Phenolic Compounds from Aqueous Solutions using Pine (Pinus densiflora Sieb) Bark Powder, BioResources. 9 (2014) 5155–5174. https://doi.org/10.15376/biores.9.3.5155-5174.

[27] A.M. Carvajal-Bernal, F. Gómez, L. Giraldo, J.C. Moreno-Piraján, Chemical modification of activated carbons and its effect on the adsorption of phenolic compounds, Ing. Y Compet. 17 (2015) 109–119.

[28] A. Mandal, S.K. Das, Phenol adsorption from wastewater using clarified sludge from basic oxygen furnace, J. Environ. Chem. Eng. 7 (2019) 103259. https://doi.org/10.1016/J.JECE.2019.103259.

[29] S. Mishra, S.S. Yadav, S. Rawat, J. Singh, J.R. Koduru, Corn husk derived magnetized activated carbon for the removal of phenol and para-nitrophenol from aqueous solution: Interaction mechanism, insights on adsorbent characteristics, and isothermal, kinetic and thermodynamic properties, J. Environ. Manage. 246 (2019) 362–373. https://doi.org/10.1016/J.JENVMAN.2019.06.013.

[30] P.S. Thue, M.A. Adebayo, E.C. Lima, J.M. Sieliechi, F.M. Machado, G.L. Dotto, J.C.P. Vaghetti, S.L.P. Dias, Preparation, characterization and application of microwave-assisted activated carbons from wood chips for removal of phenol from aqueous solution, J. Mol. Liq. 223 (2016) 1067–1080. https://doi.org/10.1016/J.MOLLIQ.2016.09.032.

[31] X. Kong, H. Gao, X. Song, Y. Deng, Y. Zhang, Adsorption of phenol on porous carbon from Toona sinensis leaves and its mechanism, Chem. Phys. Lett. 739 (2020) 137046. https://doi.org/10.1016/J.CPLETT.2019.137046.

[32] H.S. Park, J.R. Koduru, K.H. Choo, B. Lee, Activated carbons impregnated with iron oxide nanoparticles for enhanced removal of bisphenol A and natural organic matter, J. Hazard. Mater. 286 (2015) 315–324. https://doi.org/10.1016/J.JHAZMAT.2014.11.012.

[33] K. Singh, B. Chandra, M. Gautam, Development of inexpensive adsorbent from agro-waste for phenol adsorption, J. Sci. Ind. Res. (India). 75 (2016) 444–451.

[34] K. Singh, V.K. Singh, S.K. Verma, R. Bharose, A. Suman, Characterization of modified polypropylene powder (Accurel) and its use for adsorption of phenolics from aqueous solution, Indian J. Chem. Technol. 20 (2013) 385–391.

[35] K. Singh, A. Kumar, S.K. Pandey, S. Awasthi, S.P. Gupta, P. Mishra, Interpretation of Adsorption Behavior of Carboxymethyl Cellulose onto Functionalized Accurel Polymeric Surface, Ind. Eng. Chem. Res. 59 (2020) 19102–19116. https://doi.org/10.1021/ACS.IECR.0C03894.

[36] G.D. Halsey, The Role of Surface Heterogeneity in Adsorption, Adv. Catal. 4 (1952) 259–269. https://doi.org/10.1016/S0360-0564(08)60616-1.

[37] T.J. Bandosz, C.O. Ania, Origin and Perspectives of the Photochemical Activity of Nanoporous Carbons, Adv. Sci. 5 (2018) 1800293. https://doi.org/10.1002/ADVS.201800293.

[38] D.A. Giannakoudakis, M. Barczak, M. Florent, T.J. Bandosz, Analysis of interactions of mustard gas surrogate vapors with porous carbon textiles, Chem. Eng. J. 362 (2019) 758–766. https://doi.org/10.1016/J.CEJ.2019.01.064.

[39] G.Z. Kyzas, E.A. Deliyanni, K.A. Matis, Graphene oxide and its application as an adsorbent for wastewater treatment, J. Chem. Technol. Biotechnol. 89 (2014) 196–205. https://doi.org/10.1002/JCTB.4220.

[40] Z. Christina Kampouraki, D. A. Giannakoudakis, K. S. Triantafyllidis, E. A. Deliyanni, Catalytic oxidative desulfurization of a 4,6-DMDBT containing model fuel by metal-free activated carbons: the key role of surface chemistry, Green Chem. 21 (2019) 6685–6698. https://doi.org/10.1039/C9GC03234G.

[41] N.E. Cooke, O.M. Fuller, R.P. Gaikwad, FT-i.r. spectroscopic analysis of coals and coal extracts, Fuel. 65 (1986) 1254–1260. https://doi.org/10.1016/0016-2361(86)90238-3.

[42] N.E. Cooke, O.M. Fuller, R.P. Gaikwad, FT-i.r. spectroscopic analysis of coals and coal extracts, Fuel. 65 (1986) 1254–1260. https://doi.org/10.1016/0016-2361(86)90238-3.

[43] Q.S. Liu, T. Zheng, P. Wang, J.P. Jiang, N. Li, Adsorption isotherm, kinetic and mechanism studies of some substituted phenols on activated carbon fibers, Chem. Eng. J. 157 (2010) 348–356. https://doi.org/10.1016/J.CEJ.2009.11.013.

[44] T. Zeng, E.R. Rene, S. Zhang, P.N.L. Lens, Removal of selenate and cadmium by anaerobic granular sludge: EPS characterization and microbial community analysis, Process Saf. Environ. Prot. 126 (2019) 150–159. https://doi.org/10.1016/J.PSEP.2019.03.039.

[45] S. Kang, G. Kim, J.K. Choe, Y. Choi, Effect of using powdered biochar and surfactant on desorption and biodegradability of phenanthrene sorbed to biochar, J. Hazard. Mater. 371 (2019) 253–260. https://doi.org/10.1016/J.JHAZMAT.2019.02.104.

[46] S.B. Lima, S.M.S. Borges, M. do C. Rangel, S.G. Marchetti, Effect of iron content on the catalytic properties of activated carbon-supported magnetite derived from biomass, J. Braz. Chem. Soc. 24 (2013) 344–354. https://doi.org/10.5935/0103-5053.20130044.

[47] K. Singh, A. Kumar, S. Awasthi, S.K. Pandey, P. Mishra, Adsorption mechanism of carboxymethyl cellulose onto mesoporous mustard carbon: Experimental and theoretical aspects, Colloids Surfaces A Physicochem. Eng.

Asp. 581 (2019) 123786. https://doi.org/10.1016/J.COLSURFA.2019.123786.

[48] A. Dąbrowski, Adsorption — from theory to practice, Adv. Colloid Interface Sci. 93 (2001) 135–224. https://doi.org/10.1016/S0001-8686(00)00082-8.

[49] Y. Li, X. Hu, X. Liu, Y. Zhang, Q. Zhao, P. Ning, S. Tian, Adsorption behavior of phenol by reversible surfactant-modified montmorillonite: Mechanism, thermodynamics, and regeneration, Chem. Eng. J. 334 (2018) 1214–1221. https://doi.org/10.1016/J.CEJ.2017.09.140.

[50] C.H. Giles, D. Smith, A. Huitson, A general treatment and classification of the solute adsorption isotherm. I. Theoretical, J. Colloid Interface Sci. 47 (1974) 755–765. https://doi.org/10.1016/0021-9797(74)90252-5.

[51] M. Abatal, I. Anastopoulos, D.A. Giannakoudakis, M.T. Olguin, Carbonaceous material obtained from bark biomass as adsorbent of phenolic compounds from aqueous solutions, J. Environ. Chem. Eng. 8 (2020) 103784. https://doi.org/10.1016/J.JECE.2020.103784.

[52] P.Q. Thang, K. Jitae, B.L. Giang, N.M. Viet, P.T. Huong, Potential application of chicken manure biochar towards toxic phenol and 2,4-dinitrophenol in wastewaters, J. Environ. Manage. 251 (2019) 109556. https://doi.org/10.1016/j.jenvman.2019.109556.

[53] E.C. Lima, A. Hosseini-Bandegharaei, J.C. Moreno-Piraján, I. Anastopoulos, A critical review of the estimation of the thermodynamic parameters on adsorption equilibria. Wrong use of equilibrium constant in the Van't Hoof equation for calculation of thermodynamic parameters of adsorption, J. Mol. Liq. 273 (2019) 425–434. https://doi.org/10.1016/J.MOLLIQ.2018.10.048.

Chapter-6

Adsorption of phenol onto pea peels biochar derived at three different pyrolysis temperatures: A comparative study

6.1. Introduction

Phenol is used in a wide range of industries and environments. Because it is water-soluble, it is easily incorporated into wastewater as a result of a variety of industrial activities [1]. The presence of phenolic compounds in water is caused by both natural and human-induced processes [2]. The decomposition of dead plants and animals are natural sources of phenolic chemicals in water pollution (organic debris) which makes it difficult to classify this material as it is extremely detrimental to the environment [3]. They are also produced by microbes and plants in watery environments. Industrial, household, agricultural, and municipal activity are all examples of human-caused phenolic chemical contamination in water [4] resulting in exposure of these compound to human being and disturbs their health due to their toxicity [5].

Because of their toxicity to humans and aquatic life, phenolic compounds have low permitted limits (0.5–1.0 mg/l) and must be removed from wastewaters in environmentally sound ways [6]. Despite the existence of numerous physicochemical and biological treatment strategies (solvent extraction, resin ion exchange, chemical oxidation by ozone, aerobic or anaerobic biodegradation, and so on) [7–9], the most successful and extensively used approach for phenol elimination is adsorption on activated carbon [10].

Recent studies are focusing on the exploitation of agricultural wastes for the preparation of activated carbon [11]. Because of its abundant raw ingredients, cheap cost, large surface area, and efficient pore structure, biochar has shown tremendous promise in removing water pollutants [12]. The present study is essentially an extension of our earlier study [13]. Biochar has been employed for a variety of purposes due to its porosity and unique surface functional groups, including pollutant adsorption, catalytic support, soil remediation, and energy storage [14].

Many scientists are working to understand how biochar removes phenol from water. To remove phenol, Mohammed *et al.* [15] utilised biochar of pine fruit shell produced at various temperatures. The maximal adsorption uptake varied from 10.373 to 26.738 mg/g, with a 67–99 % removal rate. Thang *et al.* [16] synthesised biochar for removing phenol from an aqueous solution using chicken manure; phenol was entirely removed in 90 minutes. For phenol, biochar's highest adsorption capacity was 106.20 mg/g [16].

To remove phenol, Lawal *et al.* [17] employed biochar obtained from oil palm leaves by steam pyrolysis; the adsorption capacity for phenol was 62.89 mg/g. Nitrogen-doped bamboo biochar prepared by pyrolysis for phenol removal and adsorption capacity was observed to be 169.0 mg/g [18]. A biochar composite of pomelo peel was used for phenol removal with q_{max} of 39.32 mg/g [19]. Table 6.1 represents a comparison of q_{max} of different biochars with present study.

Pisum sativum is a plant that is grown from winter to early summer in many regions of the world. Peas are widely farmed in India throughout the winter, and its waste, pea peels (PP), is widely available in the market and households.

The use of PP biochars for effective phenol removal is described in this paper. Its properties make it an effective adsorbent for the elimination of phenol. SEM-EDS, FT-IR, XRD, and pHzpc are used to characterize the derived biochars. The mechanism of phenol elimination is investigated using a variety of assays, including pH effect, biochar dosage, temperature, and the addition of NaCl and urea. In addition, numerous kinetic and adsorption isotherm models were tested for their relevance in determining the adsorption mechanism.

Table 6.1: Comparison table of q_{max} of various biochars.

Biochar	Pyrolysis temperature (ºC)	Phenol concentration range	Conditions		q_{max} (mg/g)	Reference
			pH	T(ºC)		
Pine fruit shell (BC350)	350	20-100	6.5	25	10.37	[15]
Pine fruit shell (BC450)	450	20-100	6.5	25	15.97	[15]
Pine fruit shell (BC550)	550	20-100	6.5	25	26.73	[15]
Chicken manure	600	10-200	7.0	22	106.20	[16]
Oil palm frond	500	20-200	6.5	45	62.89	[17]
Nitrogen doped bamboo biochar	700	100-1000	7.0	25	169.00	[18]
Pomelo peel magnetic biochar	600	20-200	5.0	30	39.32	[19]
Food waste	700	10-50	3.0	35	13.49	[35]
Magnetic palm kernel	500	10-70	8.0	30	10.84	[40]
Cow dung	800	20-500	6.0	25	518.89	[41]
Wood apple shell	700	100-400	6.0	30	102.71	[42]
Hizika fusiformis	550	10-100	6.0	25	10.39	[43]
PP250	250	30-300	6.0	25	34.63	Present work
PP500	500	30-300	6.0	25	46.70	Present work
PP750	750	30-300	6.0	25	60.10	Present work

6.2. Experimental section

6.2.1. Biochar preparation

The PP was collected from local households and rigorously washed to remove dirt. The dried PP was sun-dried for 48 h and ground with an acoustic grinder to the

particle size of 75-300 µm. The ground PP was then placed into the covered crucibles and slowly pyrolysed for 1 h in oxygen-controlled conditions at different temperatures (250, 500 and 750ºC). The pyrolysed PP was then labelled as PP250, PP500, and PP750, respectively. The biochars were then stored in airtight tubes until they could be used again.

6.2.2. Characterization of biochars

Scanning electron microscopy (SEM) analysis was used to examine the surface morphology of the biochars, while EDS was used to evaluate the elemental composition of the biochars. Both analyses were performed using a JEOL JSM-6490LV model from Japan. FT-IR spectrophotometer was used to analyse the functional groups of the biochar sample (Thermo- Scientific Nicole 6700, USA). With 32 scans and a resolution of 5-7 cm^{-1}, the spectra were captured in the range of 4000-400 cm^{-1}. The phase of the biochars was determined using a powder XRD (RigakuMiniflex II desktop). Copper Kα radiation (= 1.5405 Ao) was used to scan the biochars in a range of 2^o to 70^o at a scanning rate of 2^o/min. Using Origin, raw data was processed. El-hanandeh *et al.* [20] developed a method for determining characteristics such as pH-zero-point charge, moisture content, ash content, and yield percent (Muffle furnace (UTS AF-777) and weighing balance (WENSAR-62157)). The phenol concentration was checked employing a UV-Vis Spectrophotometer (Carry 100) at 270 nm wavelength.

6.2.3. Biosorption experiments

Biochars were tested for maximum phenol uptake under a variety of adsorption conditions. Every experiment was carried out by placing 100 ml of phenol solution into a conical flask at a different pH and temperature and adding 0.2 g of biochar to the flask. An initial concentration of phenol in the sample ranged between 30-300

mg/L. The equilibrium was reached in 3 h, however, some samples were left for 5 to 8 h with identical results. The test NaCl and urea addition was performed to check the effect of external species on phenol uptake by PP biochars. For this, 0.1-0.5 mol/L of NaCl and urea was separately added to the 30 mg/L phenol solution containing 2 g/L biochar dose at pH 6 and 25ºC. Samples were analysed at fixed time gaps to determine the time dependence of phenol removal.

Equation (1) calculates how much phenol is adsorbed at equilibrium:

$$q_e = \frac{(C_0 - C_e)V_s}{m} \quad (1)$$

There are five factors, the adsorbed amount at equilibrium (q_e) (mg/g), initial concentration (C_o) (mg/L), equilibrium concentration (C_e) (mg/L), solution volume (V) (in L), and mass of biochar added (m) (in g).

Following equation calculates phenol removal at any time 't':

$$q_t = \frac{(C_0 - C_t)V_s}{m} \quad (2)$$

At time t, q_t is amount adsorbed (in mg/g) and C_t is concentration (in mg/L).

6.2.4. Isotherm and kinetic analysis

Adsorption isotherm modelling is the best method used to describe the adsorption equilibrium data and provide the actual picture of the adsorption mechanism. The most common isotherm model were modelled to explore the phenol adsorption onto PP biochars are given as follows:

Langmuir model

$$q_e = \frac{q_m K_L C_e}{1 + K_L C_e} \quad (3)$$

Freundlich Model

$$q_e = K_F {C_e}^{1/n} \quad (4)$$

Temkin Model

$$q_e = \frac{RT}{b} \ln K_T C_e \quad (5)$$

Where, q_m; maximum phenol uptake (mg/g), K_L; Langmuir constant (L/mg), K_F; Freundlich constant ($mg^{1-(1/n)}$ $L^{1/n}$ /g), 1/n; intensity of adsorption, K_T; Temkin constant (L/g) and b; heat of adsorption (J/mol).

Pseudo-first-order (PFO)

$$q_t = q_e(1 - e^{-k_1 t}) \quad (6)$$

Pseudo-second-order (PSO)

$$q_t = \frac{k_2 q_e^2 t}{1 + k_2 q_e t} \quad (7)$$

Intra-particle diffusion (IPD)

$$q_t = k_i t^{0.5} + C \quad (8)$$

Where, k_1; PFO (min^{-1}) and k_2; PSO rate constant (g/mg. min), k_i; IPD rate constant ($g/mg.min^{0.5}$), and C: constant (mg/g).

6.3. Results and discussion

6.3.1. Characterization of biochars

The physicochemical characteristics of biochar PP250, PP500 and PP750 such as biochar yield, ash content, moisture content and pH_{zpc} are tabulated in Table 6.2.

Table 6.2: Physicochemical properties of PP biochars[#]

Biochar	Yield, % (w/w)	Moisture, % (w/w)	Ash, % (w/w)	pH_{zpc}
PP250	70.24 ± 0.3	1.47 ± 0.04	2.18 ± 0.02	5.1
PP500	55.87 ± 0.2	0.98 ± 0.03	3.85 ± 0.04	6.2
PP750	49.34 ± 0.2	0.46 ± 0.01	4.79 ± 0.01	6.4

[#] Yield, moisture and ash content analysis results are given as mean ± standard deviation for duplicate measurements.

Ash content increased (2.18 - 4.79) and biochar yield decreased (70.24 - 49.34) as the pyrolysis temperature rose from 250 to 750ºC. The decrease in biochar yield with increase in pyrolysis temperature is due to the thermal degradation of lignin and cellulose resulting in the dehydration of hydroxyl groups [21,22]. The rise in ash content is an outcome of increase in mineral content and volatilization of ligno-cellulosic matters [23,24]. The decrease in moisture content (1.47 – 0.46) with pyrolysis temperature is consistent with the results of the biochar yield and ash content. Similar findings were reported by the other investigators [25–27].

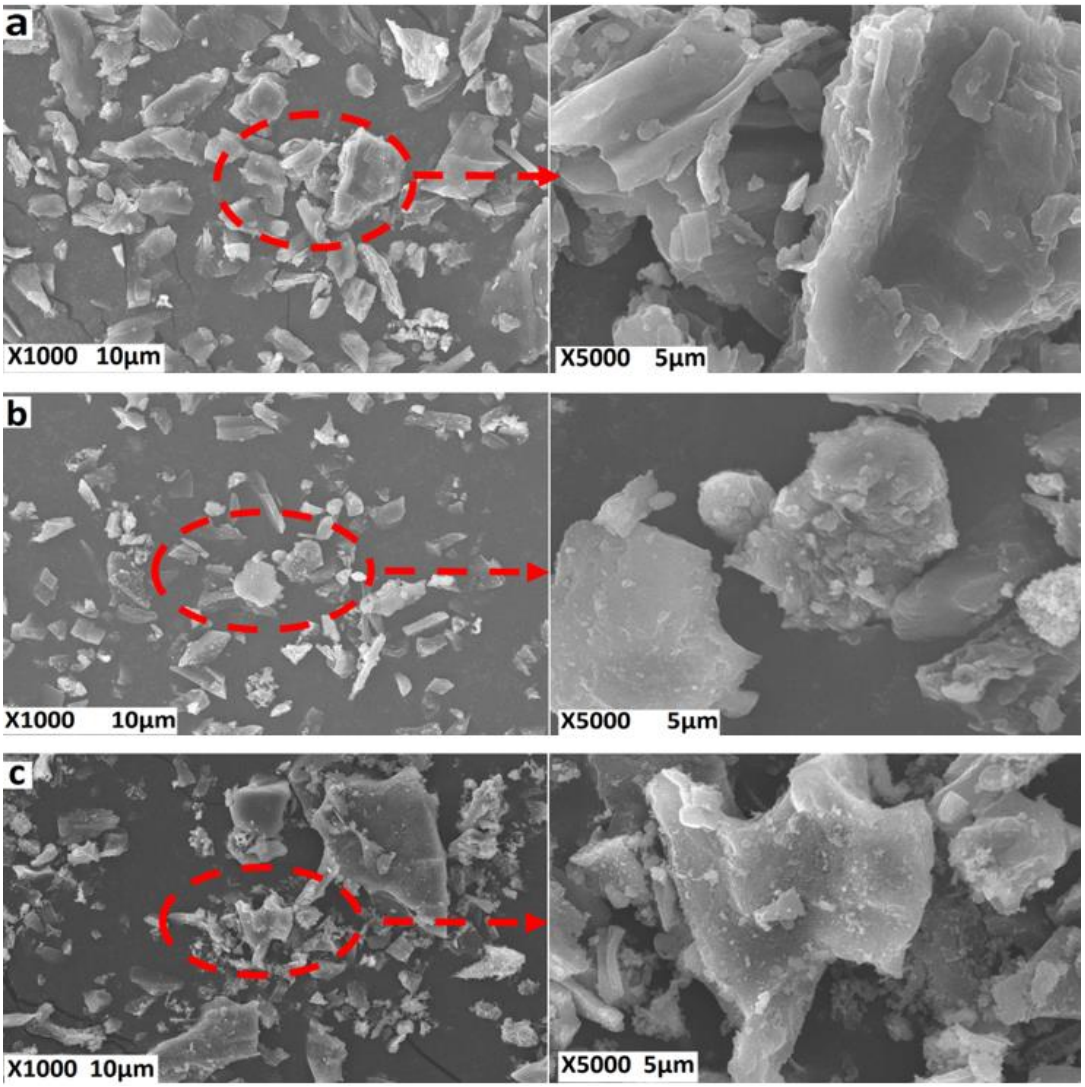

Fig. 6.1: SEM images of PP250 (a), PP500 (b) and PP750 (c) at different resolutions.

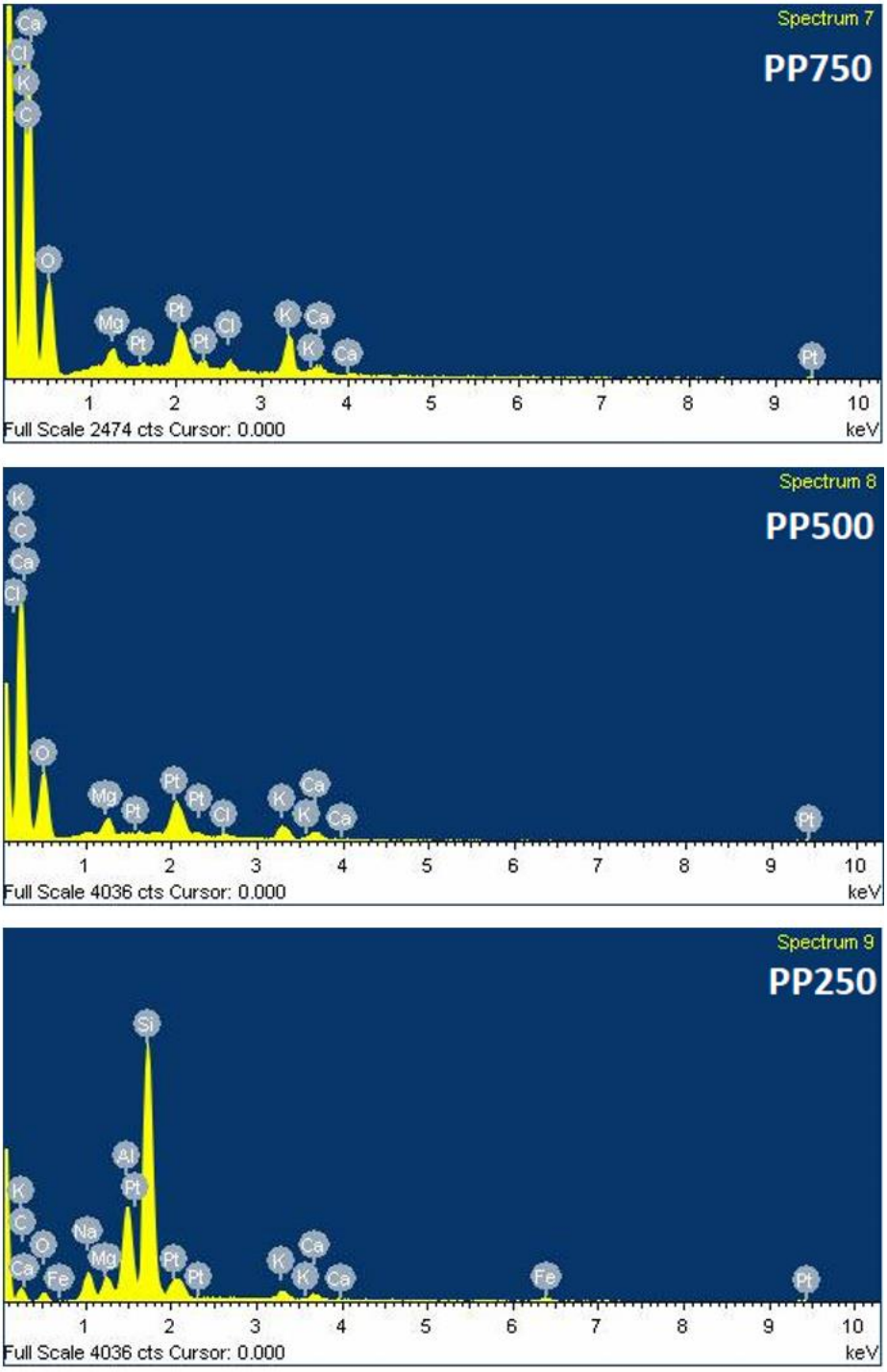

Fig. 6.2: EDS spectra of PP250, PP500 and PP750.

The SEM micrograph images of biochar PP250, PP500 and PP750 are shown in Fig. 6.1. From Fig. 6.1, it is apparent that with the increase in a pyrolysis temperature the roughness of the biochar surface increases which increased the porosity and irregularity of the biochar [28]. The increase in pyrolysis temperature results in the

dehydration of hydroxyl groups which increases the carbon content of the biochars (Fig. 6.2) with the rise in temperature indicating a high degree of carbonization resulting in greater aromaticity of biochars. Similar behaviour was observed in previous studies [15–19].

The FT-IR spectra of the PP biochars prepared at different temperatures and phenol loaded biochars (at 25ºC, pH 6.0, biochar dose 2 g/L and 30 mg/L of phenol concentration) are explicated in Fig. 6.3. The changes observed in the functional groups of PP biochar with the increase in pyrolysis temperature are in agreement with the other results of the present study [29] e.g. the polar functional groups (O-H, N-H) are not observed in the FT-IR spectra of PP500 and PP750 indicating increase in carbon content in PP500 and PP750. With the increase in temperature, the polarity of biochar decreases and the degree of aromatization increases resulting in the change in the mechanism of phenol adsorption onto PP biochar [30]. The same has been confirmed by the results of FT-IR. Fig. 6.3, revealed that PP250 consists of a large number of absorption bands in comparison to PP500 and PP750. The PP250 mainly consists of absorption bands at 3336.97 cm^{-1} (O-H stretching of alcohol), 2922.73 cm^{-1} (C-H stretching of alkanes), 1720 cm^{-1} (C=O stretching of aliphatic ketone), 1632.47 cm^{-1} (C=C stretching of substituted alkene), 1374.48 cm^{-1} (C-H bending of alkane), 1159 and 1059 cm^{-1} (C-O stretching of primary and tertiary alcohols). The PP500 consists of fewer bands than PP250, it mainly had a band at 2910 cm^{-1} (C-H stretching of alkane), 1570 cm^{-1} (C=C stretching alkene), 1415 cm^{-1} (C-H bending of alkene). The PP750 consists of bands similar to the PP500. It mainly consists of a band near 2900 cm^{-1} (C-H stretching of alkene), a shoulder near 1550 cm^{-1} (C=C stretching of alkene) and a peak at 1440 cm^{-1} (due to C-H bending of alkene). The changes perused

in the FT-IR spectra of phenol loaded biochars provided a clear picture of the adsorption.

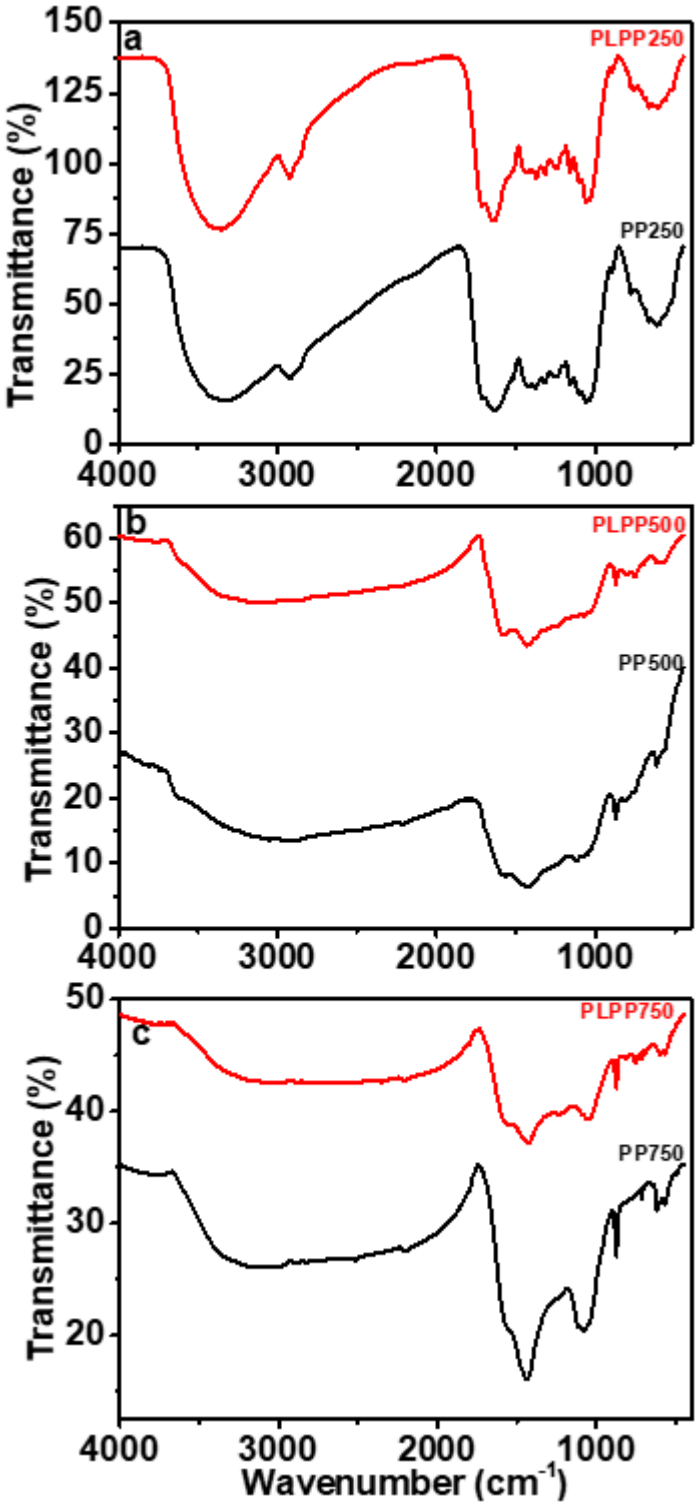

Fig. 6.3: FT-IR spectra of PP250 and PLPP250 (a), PP500 and PLPP500 (b) and PP750 and PLPP750.

In the FT-IR spectrum of Phenol Loaded PP250 (PLPP250), a shift in band position from 3336 cm^{-1} to 3349 cm^{-1} indicates the H-bonding between PP250 and phenol. In PLPP250, A 10-15 cm^{-1} shift in C=O and C=C band was observed indicating the interaction of these functional groups with phenol [31]. In FT-IR spectra of Phenol Loaded PP500 and Phenol Loaded PP750, major changes were observed in the bands of C=C stretching and C-H bending confirming phenol adsorption only through π-π interaction [15].

The XRD graph of PP250, PP500 and PP750 is mentioned in Fig. 6.4. From Fig. 6.4, it is observed that all the three biochars consist of peaks in the range of 20-30º indicating the presence of systematic graphitic structure [32]. However, peak intensities of PP500 and PP750 indicate that there was no significant change occurred in the degree of graphitization. The peak intensities of biochars between 35-40º have mounted up with rise in pyrolysis temperature resulting in the merger of the small pores into the larger ones [33].

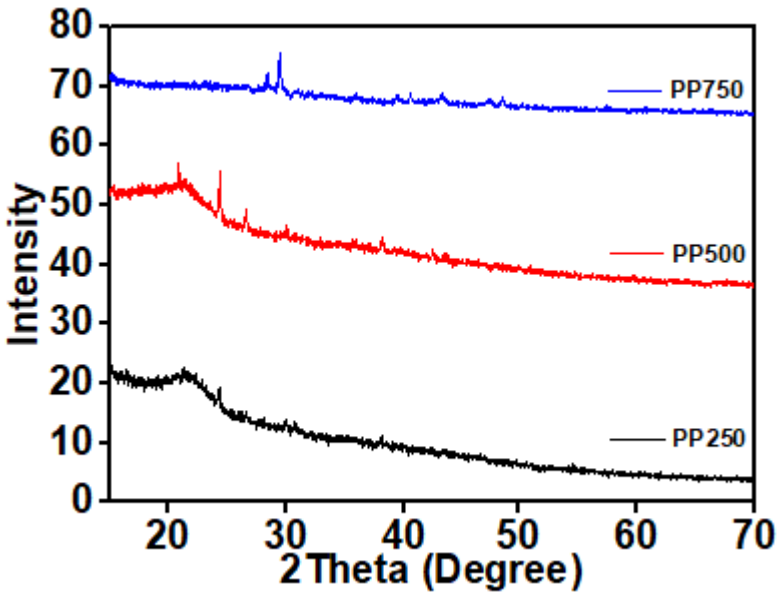

Fig. 6.4: XRD spectra of PP250, PP500 and PP750.

6.3.2. Factors affecting adsorption

6.3.2.1. Effect of biochar dose

A plot of phenol uptake against biochar dose is shown Fig. 6.5. 30 mg/L concentration of phenol was taken and the biochar dose was varied between 2-10 g/L. From Fig. 6.5, it was observed that phenol uptake decreases with an increase in biochar dose and after a certain value biochar dose, phenol uptake slightly changes with further increase in biochar dose [34,35]. This experiment was repeated for higher phenol concentration (60 and 90 mg/L) and the same pattern was observed. The decrease in phenol uptake with increasing biochar dose is due to the presence of a larger number of adsorption sites and aggregation of biochar resulting in the reduction of adsorption potential of biochar [36]. The maximum phenol uptake for PP250, PP500 and PP750 were 9.1, 11.3 and 13.5 mg/g for the biochar dose of 0.2 g/100 ml (2 g/L).

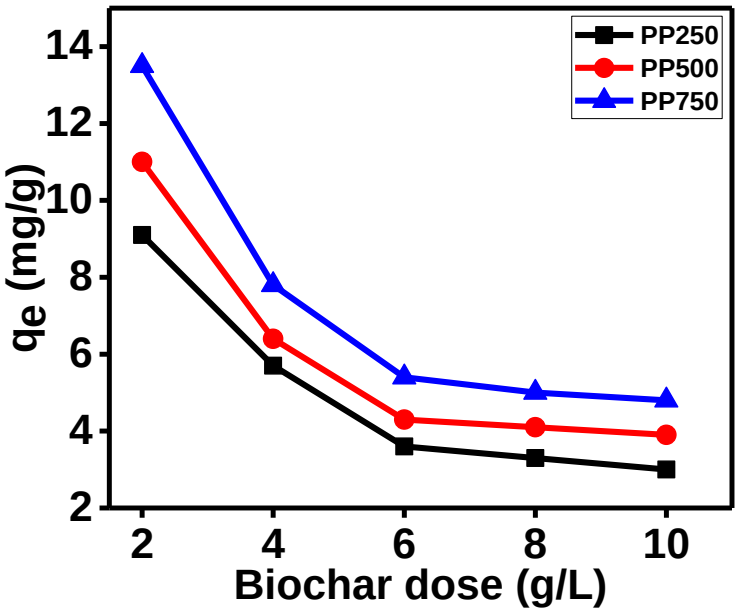

Fig. 6.5: Effect of biochar dose on phenol adsorption at 25ºC, pH 6.0, and 30 mg/L of phenol concentration.

6.3.2.2. Effect of pH

The effect of solution pH on phenol uptake by PP250, PP500 and PP750 is depicted in Fig. 6.6. This can be explained based on the fact that the chemistry of phenol is governed by its pH and pH_{zpc} of the adsorbent. The pKa of phenol is 9.92, so when the pH of the solution is below 9.92 phenol exists in the protonated form. From pH 2-5, the phenol uptake for the three biochars increases as the surface of the biochars remains positive. At pH 6, the surface of biochars becomes slightly positive resulting in the interactions between positive and negative poles of the biochar and phenol. So maximum adsorption was observed at pH 6. Above pH 6, the surface becomes negatively charged which leads to the repulsion between the phenol and biochar surface [13]. At pH 10, the biochar surfaces become more negative and phenol exists in deprotonated form resulting in repulsion among phenol molecules and with biochar surface and so phenol uptake decreases at higher pH value.

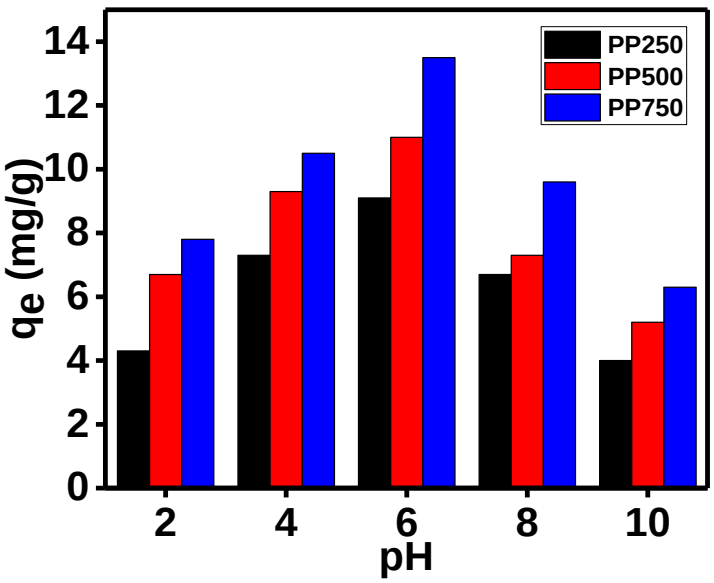

Fig. 6.6: Effect of solution pH on adsorption capacity of PP250, PP500 and PP750 at 25ºC, biochar dose 2 g/L and 30 mg/L of phenol concentration.

6.3.2.3. Effect of NaCl and urea addition

The impact of NaCl and urea addition on phenol uptake by PP250, PP500 and PP750 is depicted in Fig. 6.7. From Fig. 6.7, it is evident that the phenol uptake by PP250 is affected by the NaCl addition but the phenol uptake by PP500 and PP750 is unaffected by the NaCl addition. This is due to the reason that for PP250, electrostatic interactions plays important role in adsorption but in the case of PP500 and PP750 adsorption is due to H-bonding and π-π interaction and so is unaffected by the NaCl addition.

The urea addition negatively affects the phenol uptake by PP250, PP500 and PP750 and is exhibited in Fig. 6.8. It is well known that urea functions as H-bond breaking agent and so confirms the role of H-bonding in occurance of adsorption in the present case [37].

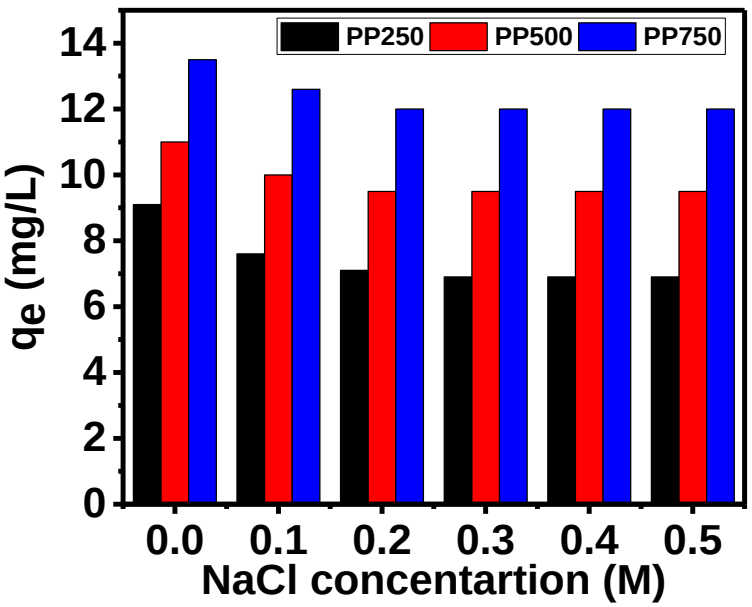

Fig. 6.7: Effect of NaCl addition on phenol adsorption onto PP250, PP500 and PP750 at 25ºC, pH 6.0, biochar dose 2 g/L and 30 mg/L of phenol concentration.

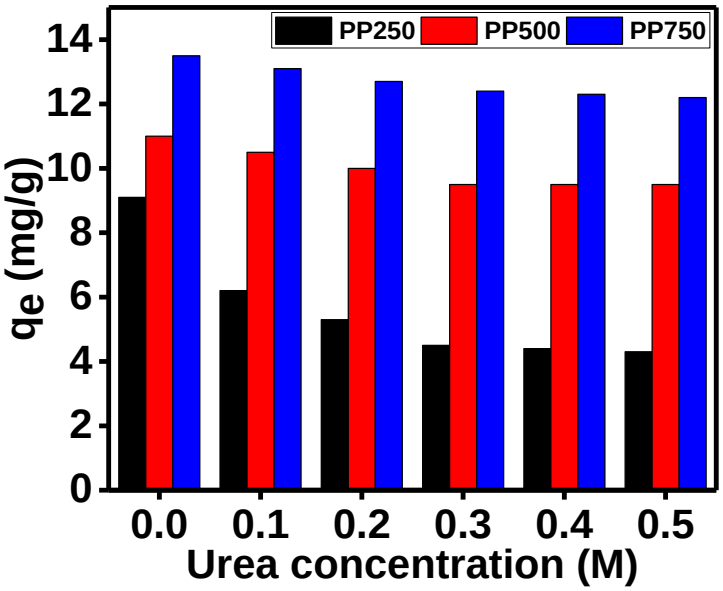

Fig. 6.8: Effect of urea addition on phenol adsorption onto PP250, PP500 and PP750 at 25ºC, pH 6.0, biochar dose 2 g/L and 30 mg/L of phenol concentration.

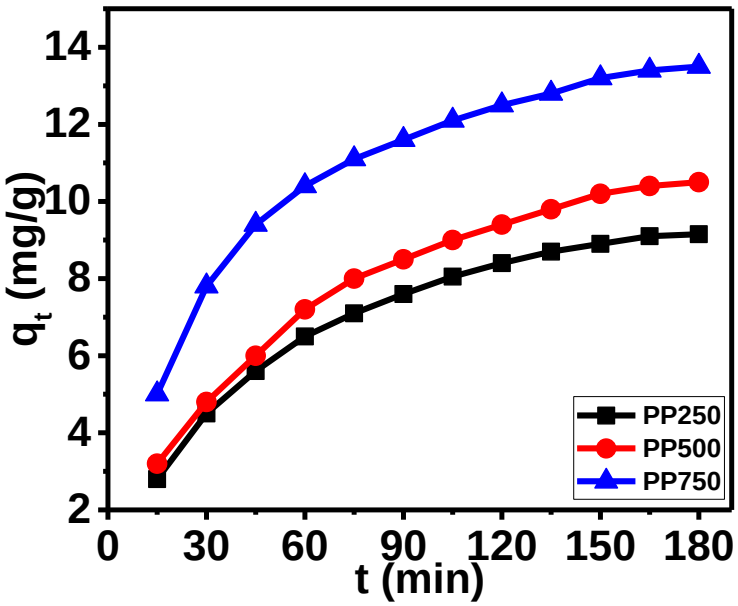

Fig. 6.9: Effect of contact time on phenol adsorption by PP250, PP500 and PP750 at 25ºC, pH 6.0, biochar dose 2 g/L and 30 mg/L of phenol concentration.

6.3.2.4. Effect of contact time

A plot of phenol uptake against time is depicted in Fig. 6.9. From Fig. 6.9, it is clear that phenol removal by PP250, PP500 and PP750 is a three-step process. In the first step, fast removal of phenol by three biochars takes place (0-45 min), In the second step, moderate removal of phenol by three biochars takes place (45-90 min). In the third step, slow removal of phenol by three biochars takes place (90-150 min), which later on becomes constant and no phenol removal is observed [17,38].

6.3.3. Adsorption isotherms

Adsorption isotherm curve illustrates the mechanism of the migration of a substance from liquid to the solid surface [39]. Tests were conducted on the three commonly used adsorption isotherms using equilibrium data of phenol adsorption onto PP250, PP500, and PP750 as depicted in Fig. 6.10. The adsorption parameters obtained from these models at three different temperatures were tabulated in Table 6.3.

According to Langmuir isotherm, there is no interaction between adsorption sites during monolayer adsorption and constant energy of adsorption for each site. The q_{max} of phenol adsorption onto PP250, PP500, and PP750 was 34.63, 46.70, and 60.10 mg/g respectively. Thus, the phenol adsorption increases with a rise in pyrolysis temperature of PP biochar. The R^2 and χ^2 values were in the range of 0.996-0.997 and 0.137-0.935 respectively confirming the Langmuir model's applicability to the adsorption data.

The Temkin isotherm assumes that as the interactions between adsorbents and adsorbates increase, so does the heat of adsorption of the layer under consideration. The adsorption data is consistent with the assumptions of the Temkin model. The heat of adsorption (b) increases with a rise in temperature resulting in a decrease in adsorbate-adsorbent interactions. The R^2 value increases and the χ^2 value decreases

with a rise in temperature indicating the suitability of this model at higher temperatures.

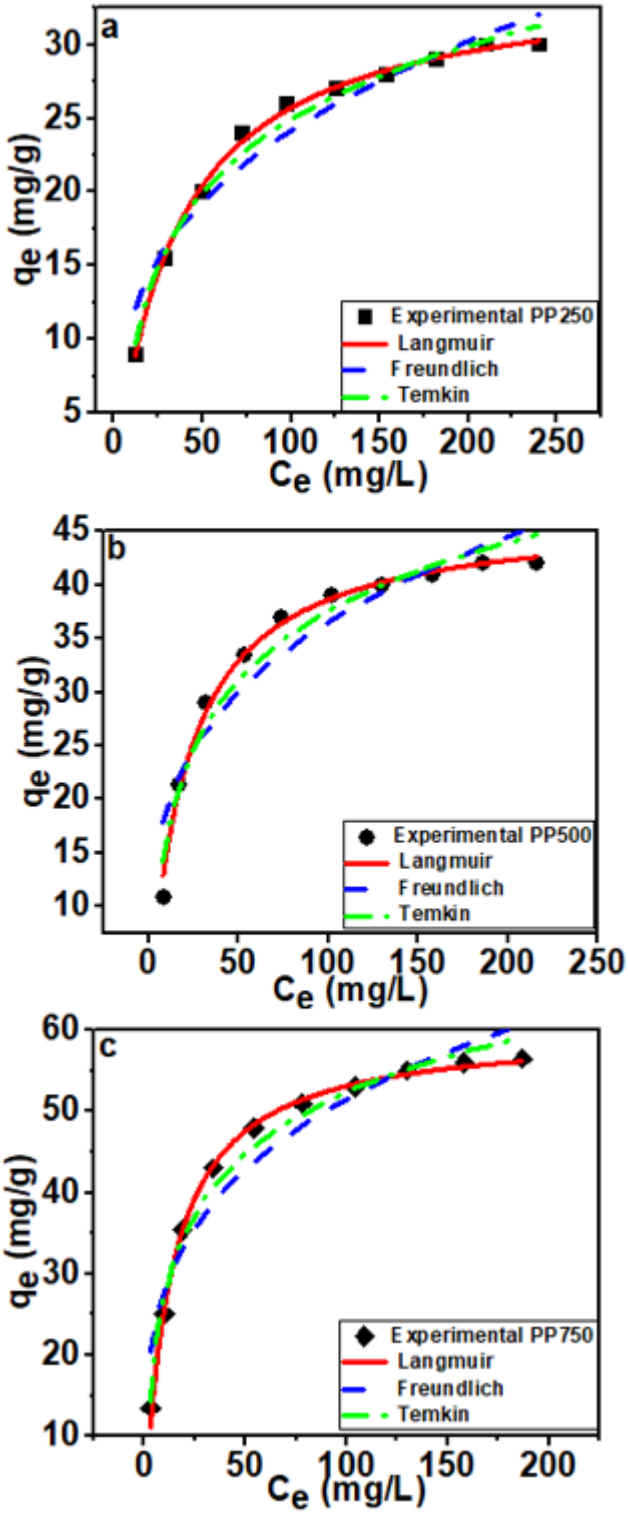

Fig. 6.10: Non-linear fit of Langmuir, Freundlich and Temkin isotherm for phenol adsorption onto PP250 (a), PP500 (b) and PP750 (c).

Table 6.3: Adsorption isotherm parameters of phenol adsorption onto PP250, PP500 and PP750 (at pH 6.0, biochar dose 2 g/L and 30-300 mg/L range of phenol concentration.)

Adsorbent	PP250			PP500			PP750		
	25 ºC	35 ºC	45 ºC	25 ºC	35 ºC	45 ºC	25 ºC	35 ºC	45 ºC
Langmuir									
q_{max} (mg/g)	34.63	33.36	31.32	46.70	37.37	31.98	60.10	49.00	40.67
K_L (L/mg)	2.87×10^{-2}	2.0×10^{-2}	1.28×10^{-2}	4.77×10^{-2}	3.28×10^{-2}	2.26×10^{-2}	7.60×10^{-2}	4.12×10^{-2}	2.79×10^{-2}
R^2 (COD)	0.997	0.996	0.995	0.994	0.996	0.998	0.996	0.998	0.995
χ^2	0.137	0.157	0.183	0.6788	0.248	0.080	0.935	0.217	0.379

Table 6.3: Continued.

Freundlich									
n	3.09	2.68	2.26	3.53	3.22	2.83	3.77	3.29	2.92
K_F ($mg^{1-(1/n)} L^{1/n} g^{-1}$	5.45	3.75	2.17	9.91	6.44	4.097	15.19	9.21	5.83
R^2 (COD)	0.940	0.940	0.955	0.900	0.923	0.948	0.932	0.925	0.941
χ^2	3.253	2.975	1.803	11.861	5.140	2.315	16.175	9.931	4.800
Temkin									
b (J/mol)	343.05	344.73	370.44	267.69	330.67	380.92	228.60	259.44	302.33
K_T (L/g)	0.316	0.186	0.116	0.57	0.360	0.225	1.252	0.489	0.279
R^2 (COD)	0.986	0.988	0.990	0.964	0.978	0.991	0.984	0.981	0.988
χ^2	0.757	0.574	0.379	4.196	1.454	0.387	3.651	2.499	0.903

Freundlich isotherm describes adsorption based on heterogeneous surfaces. Freundlich model does not hold good in the present investigation as the R^2 values are not high (0.90-0.95). Previous studies reported that the high-temperature biochar has a good adsorption potential than the low-temperature biochar indicating the significance of the present study [15,16,40–43]. Table 6.1 compares the q_{max} of phenol removal using other biochars to the q_{max} of phenol removal using PP biochars, demonstrating that PP biochars have great adsorption potential for the elimination of phenol.

6.3.4. Adsorption kinetics

The time-dependent phenol removal was tested with PFO, PSO and IPD kinetic models (Fig. 6.11) and the parameters of these models are mentioned in Table 6.4. 30 mg/L initial phenol concentration was taken.

Table 6.4: Kinetics parameters

Biochar	PP250	PP500	PP750
PFO			
$q_{e,cal}$ (mg/g)	9.24	10.97	13.15
k_1 (min^{-1})	2.06×10^{-2}	1.77×10^{-2}	2.76×10^{-2}
R^2 (COD)	0.992	0.984	0.980
χ^2	0.031	0.099	0.141
PSO			
$q_{e,cal}$ (mg/g)	11.74	14.30	15.87
k_2 (mg/g.min)	1.75×10^{-3}	1.17×10^{-3}	1.98×10^{-3}
R^2 (COD)	0.999	0.995	0.998
χ^2	0.002	0.026	0.007
IPD			
k_i	0.652	0.795	0.822
C	1.04	0.63	3.29
R^2 (COD)	0.959	0.983	0.932
χ^2	0.179	0.103	0.490

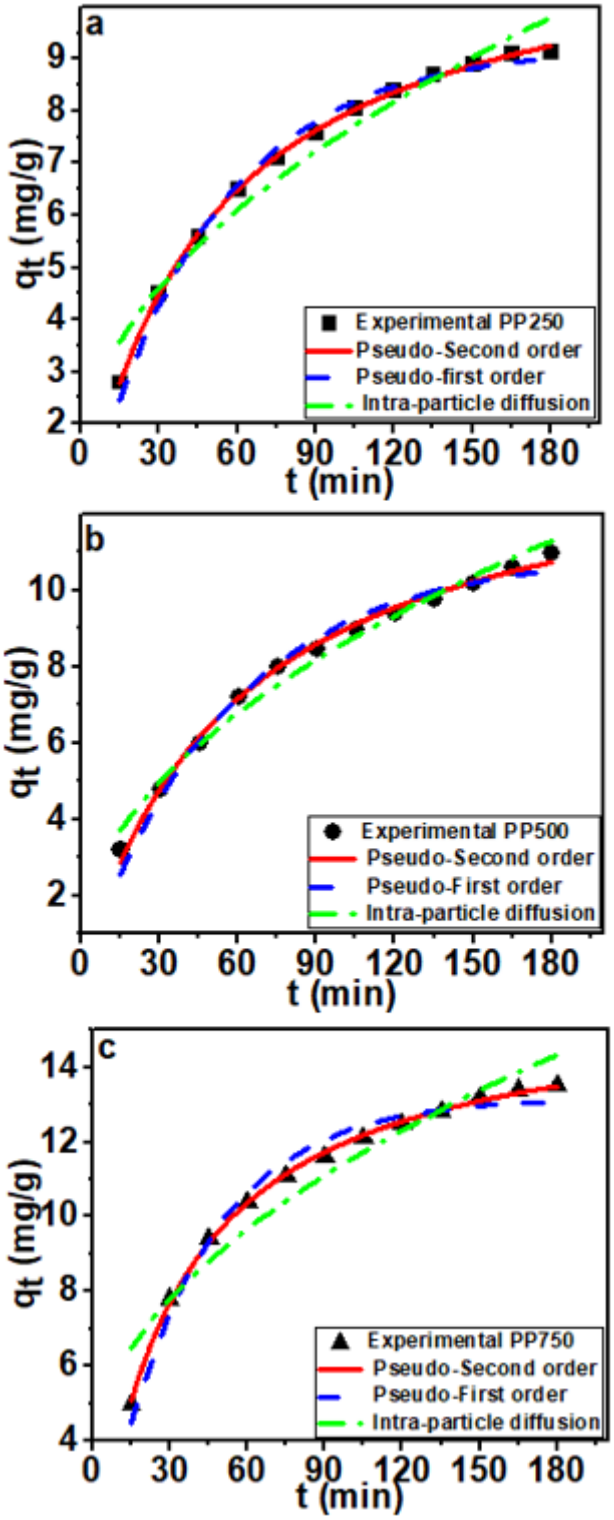

Fig. 6.11: Non-linear fit of PSO, PFO and IPD model for phenol adsorption onto PP250 (a), PP500 (b) and PP750.

From Fig. 6.11, it is clear that the PSO model provides a better explanation than the PFO model. The R^2 and χ^2 values confirmed the suitability of the PSO model for adsorption of phenol onto PP500 and PP750 but for PP250 the PFO and PSO models compete for the best fit. It can be explained based on the fact that for phenol adsorption onto PP250 there is the possibility of electrostatic interactions as well as with H-bonding and π-π interaction between PP250 and phenol but in the case of phenol adsorption onto PP500 and PP750, the possibility of electrostatic interactions was ruled out due to increase in aromatization of biochar and adsorption mainly occurred due to π-π interaction and to some extent with H-bonding [44]. The IPD model does not fit the non-linear regression analysis as its R^2 and χ^2 values did not align with the findings of the kinetic data.

6.3.5. Thermodynamics of adsorption

From the effect of the temperature experiment, it was observed that phenol uptake by PP250, PP500 and PP750 decreased with an increase in temperature (Fig. 6.12). This observation has been concreted by the results of the thermodynamic study. The thermodynamic parameters have been calculated by the following equations and tabulated in Table 6.5.

$$lnK_L^\circ = \frac{\Delta S^\circ}{R} - \frac{\Delta H^\circ}{RT} \quad (9)$$

$$\Delta G^\circ = \Delta H^\circ - T\Delta S^\circ \quad (10)$$

Where K_L° is the unitless Langmuir Constant calculated by the method given by Lima *et al.* [45]. ΔG°, ΔH°, and ΔS° are the standard state free energy change, enthalpy change and entropy change respectively.

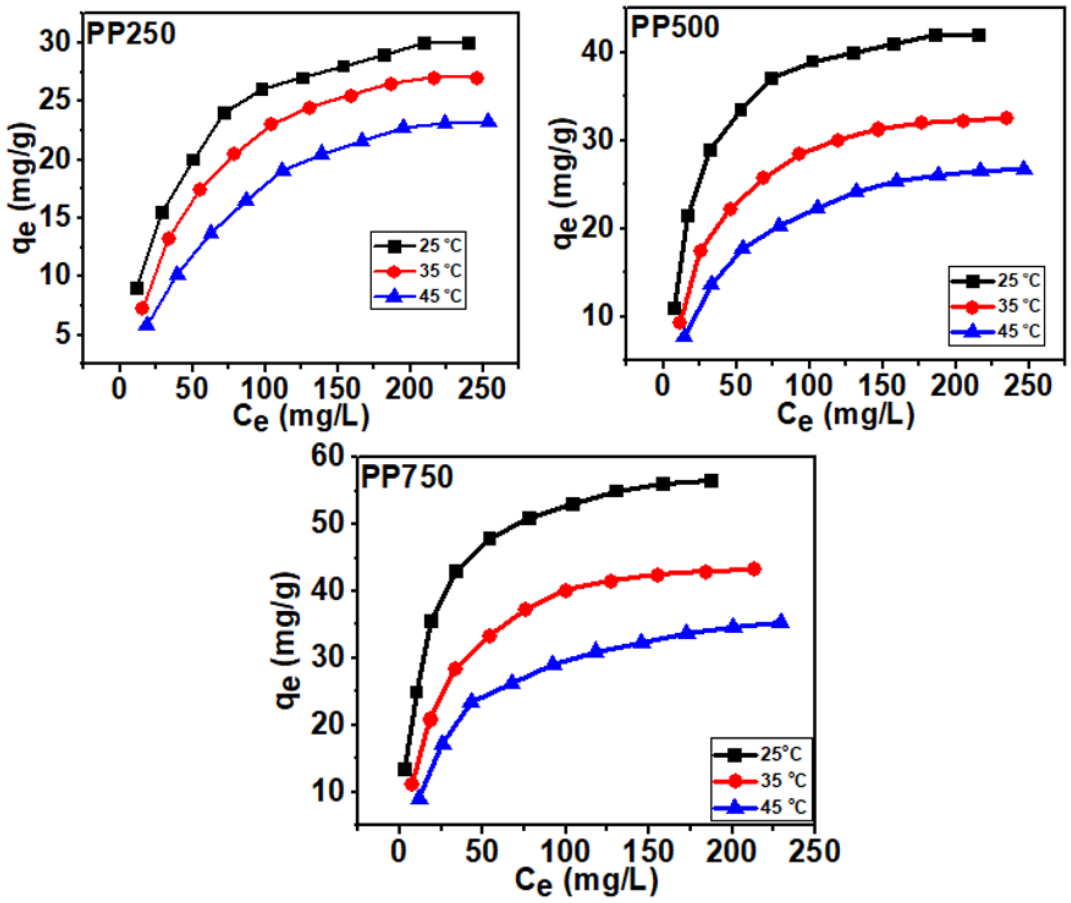

Fig. 6.12: Effect of reaction temperature on phenol adsorption by PP250, PP500 and PP750 at pH 6.0, biochar dose 2 g/L and 30-300 mg/L range of phenol concentration.

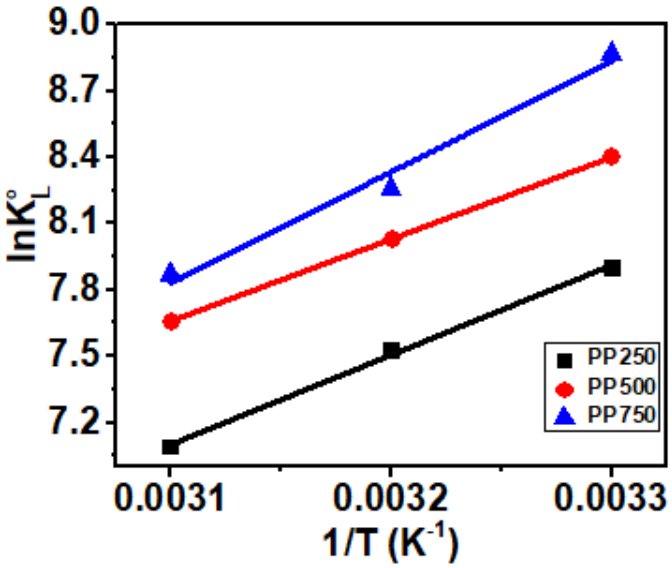

Fig. 6.13: Plot of lnK_L° *vs* 1/T for PP250, PP500 and PP750.

Table 6.5; Phenol adsorption on PP250, PP500, and PP750: Thermodynamic parameters

Biochar	25ºC	35ºC	45ºC	
PP250				
K_L°	2.70 x 10^3	1.88 x 10^3	1.20 x 10^3	
ΔG° (kJmol^{-1})	-20.16	-19.71	-19.25	
ΔH° (kJ/mol)				-33.67
ΔS° (J/K.mol)				-45.33
PP500				
K_L°	4.48 x 10^3	3.09 x 10^3	2.12 x 10^3	
ΔG° (kJmol^{-1})	-21.32	-21.00	-20.69	
ΔH° (kJ/mol)				-30.76
ΔS° (J/K.mol)				-31.67
PP750				
K_L°	7.144 x 10^3	3.879 x 10^3	2.622 x 10^3	
ΔG° (kJmol^{-1})	-22.57	-21.99	-21.35	
ΔH° (kJ/mol)				-41.57
ΔS° (J/K.mol)				-63.74

The plot of lnK_L° *vs* 1/T for PP250, PP500, and PP750 is depicted in Fig. 6.13. Input values for the ΔH°, and ΔS° values were calculated from the slope and intercept, respectively. Free energy change indicates phenol adsorption onto PP250, PP500 and PP750 is feasible based on its negative value. From 25ºC to 45ºC, there is a decrease in the negative value of free energy change, which speaks to the less use of phenol adsorption onto PP250, PP500 and PP750 at higher temperatures. The highest negative value of free energy change was insinuated by PP750 indicating it to be a suitable adsorbent for phenol removal. The free energy change for PP250, PP500 and PP750 is less than 40 kJ/mol confirming the adsorption mechanism to be governed by the physical adsorption mode [46]. A negative enthalpy change confirms that phenol

adsorption onto PP250, PP500, and PP750 is exothermic. The negative value of entropy change confirmed the reduction in the randomness at the liquid-solid interface [47].

6.4. Conclusions

The present study deals with the preparation of biochar from agriculture waste of PP at three different temperatures (250, 500 and 750ºC) using slow pyrolysis. These biochars were employed for the phenol removal from an aqueous medium. The adsorption was controlled by the change in pH, ionic strength and biochar dose. The optimum phenol uptake was observed at pH 6.0, biochar dose 2 g/L and 25ºC. The presence of NaCl in solution decreased the phenol uptake of PP250 but slightly decrease the uptake of PP500 and PP750 indicating the role of electrostatic interactions during adsorption for PP250. The maximum biosorption capacity for the PP250, PP500 and PP750 were found to be 34.63, 46.70, and 60.10 mg/g respectively. The PSO model provided the best explanation of the phenol removal by PP biochars. The Langmuir model gave the best-fit explanation and confirmed the monolayer type of adsorption. The mechanism of adsorption was governed by hydrogen bonding, electrostatic interactions and π-π interations for PP250 and for PP500 and PP750, it is governed primarily by π-π interations with some extent of hydrogen bonding. Adsorption is confirmed to be both physically and exothermically induced. Based on above results, it is clear that the PP750 exhibited excellent adsorption potential in comparison to PP500 and PP250 biochars. Hence, PP750 can preferably be used for removing contaminants from water/wastewater streams.

References

[1] B.R. Albuquerque, S.A. 8. Heleno, M.B.P.P. Oliveira, L. Barros, I.C.F.R. Ferreira, Phenolic compounds: Current industrial applications, limitations and future challenges, Food Funct. 12 (2021) 14–29. https://doi.org/10.1039/d0fo02324h.

[2] X. Qi, X. Tong, W. Pan, Q. Zeng, S. You, J. Shen, Recent advances in polysaccharide-based adsorbents for wastewater treatment, J. Clean. Prod. 315 (2021) 128221. https://doi.org/10.1016/J.JCLEPRO.2021.128221.

[3] Y.Z. Ren, Z.L. Wu, M. Franke, P. Braeutigam, B. Ondruschka, D.J. Comeskey, P.M. King, Sonoelectrochemical degradation of phenol in aqueous solutions, Ultrason. Sonochem. 20 (2013) 715–721. https://doi.org/10.1016/J.ULTSONCH.2012.09.004.

[4] W. Raza, J. Lee, N. Raza, Y. Luo, K.H. Kim, J. Yang, Removal of phenolic compounds from industrial waste water based on membrane-based technologies, J. Ind. Eng. Chem. 71 (2019) 1–18. https://doi.org/10.1016/j.jiec.2018.11.024.

[5] N. Arumugam, S. Chelliapan, H. Kamyab, S. Thirugnana, N. Othman, N.S. Nasri, Treatment of wastewater using seaweed: A review, Int. J. Environ. Res. Public Health. 15 (2018) 2851. https://doi.org/10.3390/ijerph15122851.

[6] W. Duan, F. Meng, H. Cui, Y. Lin, G. Wang, J. Wu, Ecotoxicity of phenol and cresols to aquatic organisms: A review, Ecotoxicol. Environ. Saf. 157 (2018) 441–456. https://doi.org/10.1016/J.ECOENV.2018.03.089.

[7] J. Ali, M. Tuzen, T.G. Kazi, Green and innovative technique develop for the determination of vanadium in different types of water and food samples by eutectic solvent extraction method, Food Chem. 306 (2020) 125638. https://doi.org/10.1016/J.FOODCHEM.2019.125638.

[8] E.H. Ramos, R. Nomen, J. Sempere, Recovery of Anacardic Acids from Cashew Nut Shell Liquid with Ion-Exchange Resins, Ind. Eng. Chem. Res. 57 (2018) 16903–16908. https://doi.org/10.1021/acs.iecr.8b04192.

[9] K.A. Mohamad Said, A.F. Ismail, Z. Abdul Karim, M.S. Abdullah, A. Hafeez, A review of technologies for the phenolic compounds recovery and phenol removal from wastewater, Process Saf. Environ. Prot. 151 (2021) 257–289. https://doi.org/10.1016/J.PSEP.2021.05.015.

[10] L.Y. Jun, L.S. Yon, N.M. Mubarak, C.H. Bing, S. Pan, M.K. Danquah, E.C. Abdullah, M. Khalid, An overview of immobilized enzyme technologies for dye and phenolic removal from wastewater, J. Environ. Chem. Eng. 7 (2019) 102961. https://doi.org/10.1016/J.JECE.2019.102961.

[11] K.S. Ukanwa, K. Patchigolla, R. Sakrabani, E. Anthony, S. Mandavgane, A review of chemicals to produce activated carbon from agricultural waste biomass, Sustain. 11 (2019) 6204. https://doi.org/10.3390/su11226204.

[12] L. Liang, F. Xi, W. Tan, X. Meng, B. Hu, X. Wang, Review of organic and inorganic pollutants removal by biochar and biochar-based composites,

Biochar. 3 (2021) 255–281. https://doi.org/10.1007/s42773-021-00101-6.

[13] P. Mishra, K. Singh, U. Dixit, Adsorption, kinetics and thermodynamics of phenol removal by ultrasound-assisted sulfuric acid-treated pea (Pisum sativum) shells, Sustain. Chem. Pharm. 22 (2021) 100491. https://doi.org/10.1016/J.SCP.2021.100491.

[14] J. Wang, S. Wang, Preparation, modification and environmental application of biochar: A review, J. Clean. Prod. 227 (2019) 1002–1022. https://doi.org/10.1016/J.JCLEPRO.2019.04.282.

[15] N.A.S. Mohammed, R.A. Abu-Zurayk, I. Hamadneh, A.H. Al-Dujaili, Phenol adsorption on biochar prepared from the pine fruit shells: Equilibrium, kinetic and thermodynamics studies, J. Environ. Manage. 226 (2018) 377–385. https://doi.org/10.1016/J.JENVMAN.2018.08.033.

[16] P.Q. Thang, K. Jitae, B.L. Giang, N.M. Viet, P.T. Huong, Potential application of chicken manure biochar towards toxic phenol and 2,4-dinitrophenol in wastewaters, J. Environ. Manage. 251 (2019) 109556. https://doi.org/10.1016/j.jenvman.2019.109556.

[17] A.A. Lawal, M.A. Hassan, M.A. Ahmad Farid, T.A. Tengku Yasim-Anuar, M.H. Samsudin, M.Z. Mohd Yusoff, M.R. Zakaria, M.N. Mokhtar, Y. Shirai, Adsorption mechanism and effectiveness of phenol and tannic acid removal by biochar produced from oil palm frond using steam pyrolysis, Environ. Pollut. 269 (2021) 116197. https://doi.org/10.1016/j.envpol.2020.116197.

[18] Z. Li, B. Xing, Y. Ding, Y. Li, S. Wang, A high-performance biochar produced from bamboo pyrolysis with in-situ nitrogen doping and activation for adsorption of phenol and methylene blue, Chinese J. Chem. Eng. 28 (2020) 2872–2880. https://doi.org/10.1016/j.cjche.2020.03.031.

[19] F.X. Dong, L. Yan, X.H. Zhou, S.T. Huang, J.Y. Liang, W.X. Zhang, Z.W. Guo, P.R. Guo, W. Qian, L.J. Kong, W. Chu, Z.H. Diao, Simultaneous adsorption of Cr(VI) and phenol by biochar-based iron oxide composites in water: Performance, kinetics and mechanism, J. Hazard. Mater. 416 (2021) 125930. https://doi.org/10.1016/j.jhazmat.2021.125930.

[20] A. El Hanandeh, R.A. Abu-Zurayk, I. Hamadneh, A.H. Al-Dujaili, Characterization of biochar prepared from slow pyrolysis of Jordanian olive oil processing solid waste and adsorption efficiency of Hg2+ ions in aqueous solutions, Water Sci. Technol. 74 (2016) 1899–1910. https://doi.org/10.2166/WST.2016.378.

[21] J. Zhang, J. Liu, R. Liu, Effects of pyrolysis temperature and heating time on biochar obtained from the pyrolysis of straw and lignosulfonate, Bioresour. Technol. 176 (2015) 288–291. https://doi.org/10.1016/j.biortech.2014.11.011.

[22] J. Treviño, C. Centeno, R. Caballero, The chemical composition of pea plant parts as related to harvesting time, Anim. Feed Sci. Technol. 16 (1987) 305–309. https://doi.org/10.1016/0377-8401(87)90019-8.

[23] W.T. Tsai, S.C. Liu, H.R. Chen, Y.M. Chang, Y.L. Tsai, Textural and chemical properties of swine-manure-derived biochar pertinent to its potential use as a

soil amendment, Chemosphere. 89 (2012) 198–203. https://doi.org/10.1016/j.chemosphere.2012.05.085.

[24] X. Cao, W. Harris, Properties of dairy-manure-derived biochar pertinent to its potential use in remediation, Bioresour. Technol. 101 (2010) 5222–5228. https://doi.org/10.1016/j.biortech.2010.02.052.

[25] L. Liu, G. Deng, X. Shi, Adsorption characteristics and mechanism of p-nitrophenol by pine sawdust biochar samples produced at different pyrolysis temperatures, Sci. Rep. 10 (2020) 1–11. https://doi.org/10.1038/s41598-020-62059-y.

[26] S.M. Yakout, Physicochemical Characteristics of Biochar Produced from Rice Straw at Different Pyrolysis Temperature for Soil Amendment and Removal of Organics, Proc. Natl. Acad. Sci. India Sect. A - Phys. Sci. 87 (2017) 207–214. https://doi.org/10.1007/s40010-017-0343-z.

[27] X. Dong, L.Q. Ma, Y. Zhu, Y. Li, B. Gu, Mechanistic investigation of mercury sorption by Brazilian pepper biochars of different pyrolytic temperatures based on x-ray photoelectron spectroscopy and flow calorimetry, Environ. Sci. Technol. 47 (2013) 12156–12164. https://doi.org/10.1021/es4017816.

[28] Q. Zhang, D. Zhang, W. Lu, M.U. Khan, H. Xu, W. Yi, H. Lei, E. Huo, M. Qian, Y. Zhao, R. Zou, Production of high-density polyethylene biocomposites from rice husk biochar: Effects of varying pyrolysis temperature, Sci. Total Environ. 738 (2020) 139910. https://doi.org/10.1016/J.SCITOTENV.2020.139910.

[29] G. Zhang, Q. Zhang, K. Sun, X. Liu, W. Zheng, Y. Zhao, Sorption of simazine to corn straw biochars prepared at different pyrolytic temperatures, Environ. Pollut. 159 (2011) 2594–2601. https://doi.org/10.1016/J.ENVPOL.2011.06.012.

[30] M. Zolfi Bavariani, A. Ronaghi, R. Ghasemi, Influence of Pyrolysis Temperatures on FTIR Analysis, Nutrient Bioavailability, and Agricultural use of Poultry Manure Biochars, Commun. Soil Sci. Plant Anal. 50 (2019) 402–411. https://doi.org/10.1080/00103624.2018.1563101.

[31] P. Zhang, Y. Li, Y. Cao, L. Han, Characteristics of tetracycline adsorption by cow manure biochar prepared at different pyrolysis temperatures, Bioresour. Technol. 285 (2019) 121348. https://doi.org/10.1016/J.BIORTECH.2019.121348.

[32] P. Pariyar, K. Kumari, M.K. Jain, P.S. Jadhao, Evaluation of change in biochar properties derived from different feedstock and pyrolysis temperature for environmental and agricultural application, Sci. Total Environ. 713 (2020) 136433. https://doi.org/10.1016/J.SCITOTENV.2019.136433.

[33] R. Azargohar, S. Nanda, J.A. Kozinski, A.K. Dalai, R. Sutarto, Effects of temperature on the physicochemical characteristics of fast pyrolysis bio-chars derived from Canadian waste biomass, Fuel. 125 (2014) 90–100. https://doi.org/10.1016/J.FUEL.2014.01.083.

[34] P. Mishra, K. Singh, U. Dixit, A. Agarwal, R. Ahmad Bhat, Effective removal

of 4-Aminophenol from aqueous environment by pea (Pisum sativum) shells activated with sulfuric acid: Characterization, isotherm, kinetics and thermodynamics, J. Indian Chem. Soc. 99 (2022) 100528. https://doi.org/10.1016/J.JICS.2022.100528.

[35] C.G. Lee, S.H. Hong, S.G. Hong, J.W. Choi, S.J. Park, Production of Biochar from Food Waste and its Application for Phenol Removal from Aqueous Solution, Water. Air. Soil Pollut. 230 (2019) 1–13. https://doi.org/10.1007/S11270-019-4125-X/TABLES/4.

[36] K. Singh, A. Kumar, S. Awasthi, S.K. Pandey, P. Mishra, Adsorption mechanism of carboxymethyl cellulose onto mesoporous mustard carbon: Experimental and theoretical aspects, Colloids Surfaces A Physicochem. Eng. Asp. 581 (2019) 123786. https://doi.org/10.1016/J.COLSURFA.2019.123786.

[37] K. Singh, A. Kumar, S.K. Pandey, S. Awasthi, S.P. Gupta, P. Mishra, Interpretation of Adsorption Behavior of Carboxymethyl Cellulose onto Functionalized Accurel Polymeric Surface, Ind. Eng. Chem. Res. 59 (2020) 19102–19116. https://doi.org/10.1021/acs.iecr.0c03894.

[38] T. Sarchami, N. Batta, L. Rehmann, F. Berruti, Removal of phenolics from aqueous pyrolysis condensate by activated biochar, Can. J. Chem. Eng. 99 (2021) 2368–2385. https://doi.org/10.1002/CJCE.24102.

[39] J. Wang, X. Guo, Adsorption isotherm models: Classification, physical meaning, application and solving method, Chemosphere. 258 (2020) 127279. https://doi.org/10.1016/J.CHEMOSPHERE.2020.127279.

[40] M.N. Hairuddin, N.M. Mubarak, M. Khalid, E.C. Abdullah, R. Walvekar, R.R. Karri, Magnetic palm kernel biochar potential route for phenol removal from wastewater, Environ. Sci. Pollut. Res. 26 (2019) 35183–35197. https://doi.org/10.1007/S11356-019-06524-W/TABLES/9.

[41] M. Jain, S.A. Khan, A. Sahoo, P. Dubey, K.K. Pant, Z.M. Ziora, M.A.T. Blaskovich, Statistical evaluation of cow-dung derived activated biochar for phenol adsorption: Adsorption isotherms, kinetics, and thermodynamic studies, Bioresour. Technol. 352 (2022) 127030. https://doi.org/10.1016/j.biortech.2022.127030.

[42] N.S. Kumar, H.M. Shaikh, M. Asif, E.H. Al-Ghurabi, Engineered biochar from wood apple shell waste for high-efficient removal of toxic phenolic compounds in wastewater, Sci. Rep. 11 (2021) 1–17. https://doi.org/10.1038/s41598-021-82277-2.

[43] W. seok Shin, Adsorption characteristics of phenol and heavy metals on biochar from Hizikia fusiformis, Environ. Earth Sci. 76 (2017) 1–9. https://doi.org/10.1007/s12665-017-7125-4.

[44] A.M. Awad, S.M.R. Shaikh, R. Jalab, M.H. Gulied, M.S. Nasser, A. Benamor, S. Adham, Adsorption of organic pollutants by natural and modified clays: A comprehensive review, Sep. Purif. Technol. 228 (2019) 115719. https://doi.org/10.1016/J.SEPPUR.2019.115719.

[45] E.C. Lima, A. Hosseini-Bandegharaei, J.C. Moreno-Piraján, I. Anastopoulos, A

critical review of the estimation of the thermodynamic parameters on adsorption equilibria. Wrong use of equilibrium constant in the Van't Hoof equation for calculation of thermodynamic parameters of adsorption, J. Mol. Liq. 273 (2019) 425–434. https://doi.org/10.1016/J.MOLLIQ.2018.10.048.

[46] A. Mandal, N. Bar, S.K. Das, Phenol removal from wastewater using low-cost natural bioadsorbent neem (Azadirachta indica) leaves: Adsorption study and MLR modeling, Sustain. Chem. Pharm. 17 (2020) 100308. https://doi.org/10.1016/J.SCP.2020.100308.

[47] X. Kong, H. Gao, X. Song, Y. Deng, Y. Zhang, Adsorption of phenol on porous carbon from Toona sinensis leaves and its mechanism, Chem. Phys. Lett. 739 (2020) 137046. https://doi.org/10.1016/J.CPLETT.2019.137046.

Chapter-7

Conclusion and future prospects

7.1. Conclusion

The objectives of this research were to evaluate the adsorption of phenol and 4-aminophenol (4-AP) in aqueous conditions onto low-cost modified adsorbents such as ultrasound-assisted sulfuric acid-treated pea shells (USAPS), PS biochars (PP250, PP500 and PP750) and Pea shell activated with sulfuric acid (PSASA) by batch adsorption study. The modelling of the experimental data in various kinetic and thermodynamic models is also probed. Based on batch kinetic data, the adsorption isotherm model was applied for the assessment and prediction of adsorption results. The physical and chemical properties of the adsorbents were determined to enable hypotheses to be made regarding the mechanisms of adsorption. The following conclusions are drawn from the basis of different experimental and kinetic data as derived during the research investigation. The graphical representation of the carried out research work is shown in Fig. 7.1, Fig. 7.2, and Fig. 7.3.

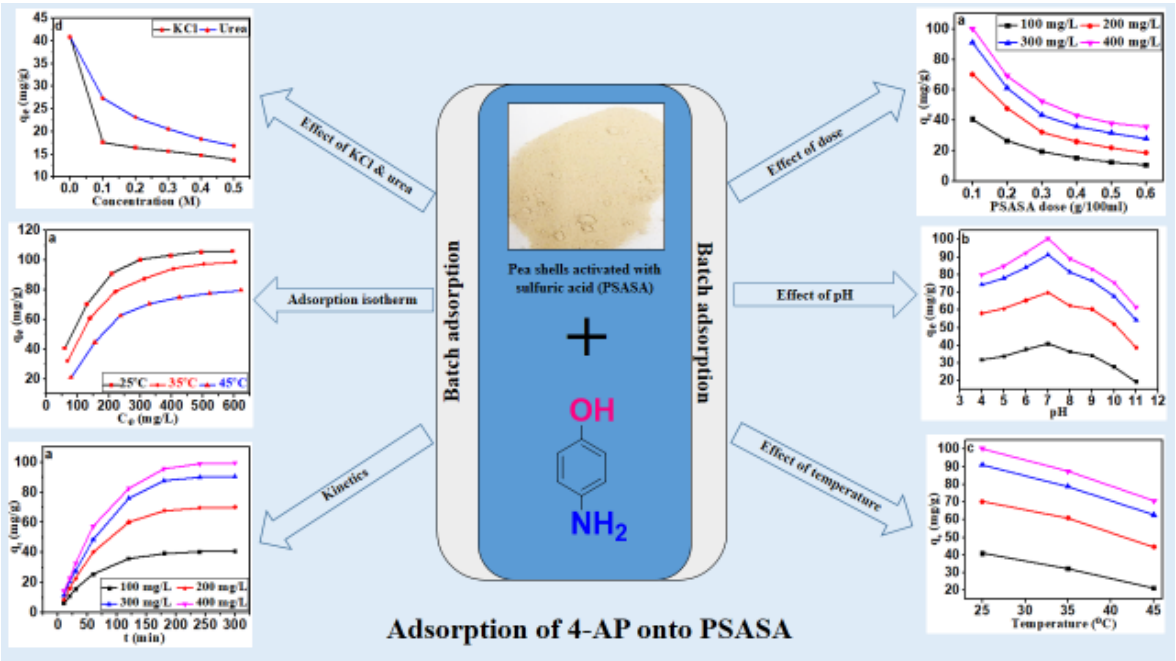

Fig. 7.1: Graphical representation of the 4-AP Adsorption onto PSASA

- The PSASA, USAPS and PS biochars (PP250, PP500 and PP750) were characterized by various techniques such as SEM-EDS, FT-IR, pXRD, BET, and optical profilometry. The results obtained from these techniques validated the use of the aforementioned adsorbents for the effective removal of the phenol and 4-AP.
- The removal of phenol by USAPS and PS biochars (PP250, PP500 and PP750) and 4-AP by PSASA from an aqueous solution is highly dependent on the pH of the solution which affects the surface charge of the adsorbent and the degree of ionization of the adsorbate. The adsorbed amount of phenol and 4-AP decreases when the pH value is greater than 7. It seems that the phenol and 4-AP removal capabilities with USAPS and PSASA were increased at pH value 7, respectively, whereas, for PS biochars (PP250, PP500 and PP750), phenol removal capabilities increased at pH 6 under the given test conditions.

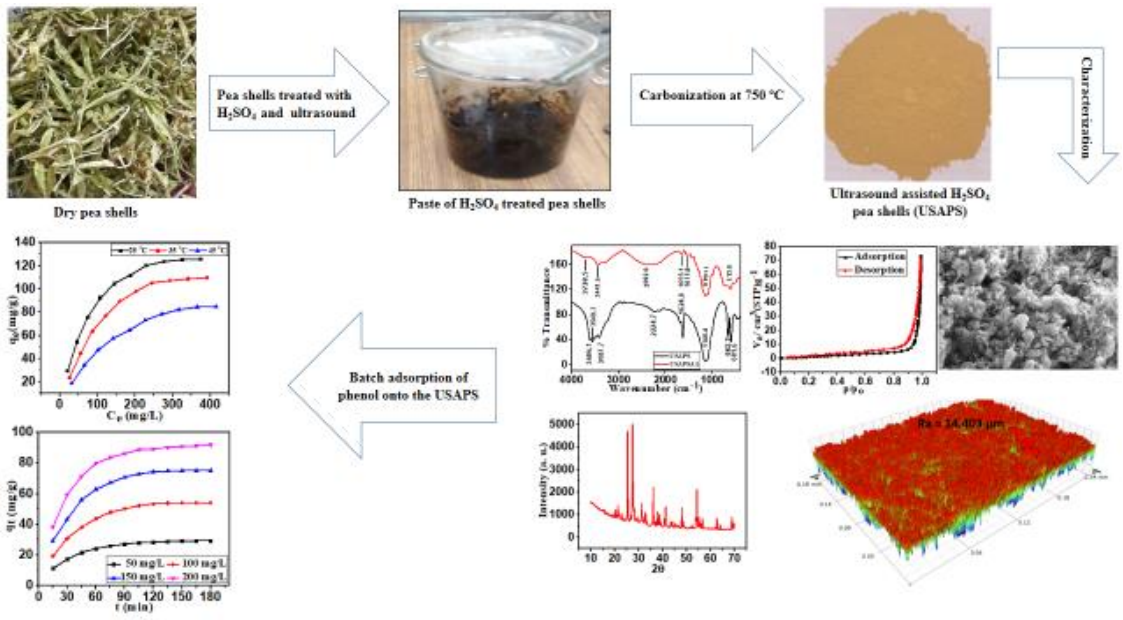

Fig. 7.2: Graphical representation of the phenol adsorption onto USAPS

- The adsorption equilibrium of phenol by USAPS and PS biochars (PP250, PP500 and PP750) and 4-AP by PSASA are described by the Freundlich, Langmuir and Temkin adsorption isotherm. Out of these isotherm models Langmuir adsorption isotherm successfully explained the adsorption of phenol and 4-AP onto PS modified adsorbents used in the experiments. It concludes the applicability of Lagmuir theory i.e. the formation of monolayer during the adsorption. The maximum phenol uptake by USAPS, PP250, PP500 and PP750 were found to be 125.77, 34.63, 46.70, and 60.10 mg/g respectively, whereas maximum 4-AP uptake by PSASA was found to be 106.11 mg/g.
- The kinetics of phenol adsorption by USAPS and PS biochars (PP250, PP500 and PP750) and 4-AP by PSASA were studied by the Pseudo-first-order, Pseudo-second-order and intra-particle diffusion model. The kinetics of phenol adsorption by USAPS and PS biochars (PP250, PP500 and PP750) was best explained by the pseudo-second-order model whereas the kinetics of the 4-AP adsorption was best explained by the Pseudo-first-order model. The intra-particle diffusion model does not hold good for the adsorption of phenol and 4-AP as it deviates with an increase in reaction time or with a decrease in adsorption.
- The thermodynamic study revealed that the adsorption of phenol by USAPS and PS biochars (PP250, PP500 and PP750) and 4-AP by PSASA were physical and exothermic in nature with no alterations at the adsorbent-adsorbate interface.
- The removal of phenol by USAPS and 4-AP by PSASA took place through electrostatic interactions, hydrogen bonding and π-π interactions among adsorbent and adsorbate interfaces. The removal of phenol by PP250 took place through electrostatic interactions, hydrogen bonding and π-π interaction, whereas by

PP500 through π-π interactions with some extent of hydrogen bonding and by PP750 through π-π interactions only.

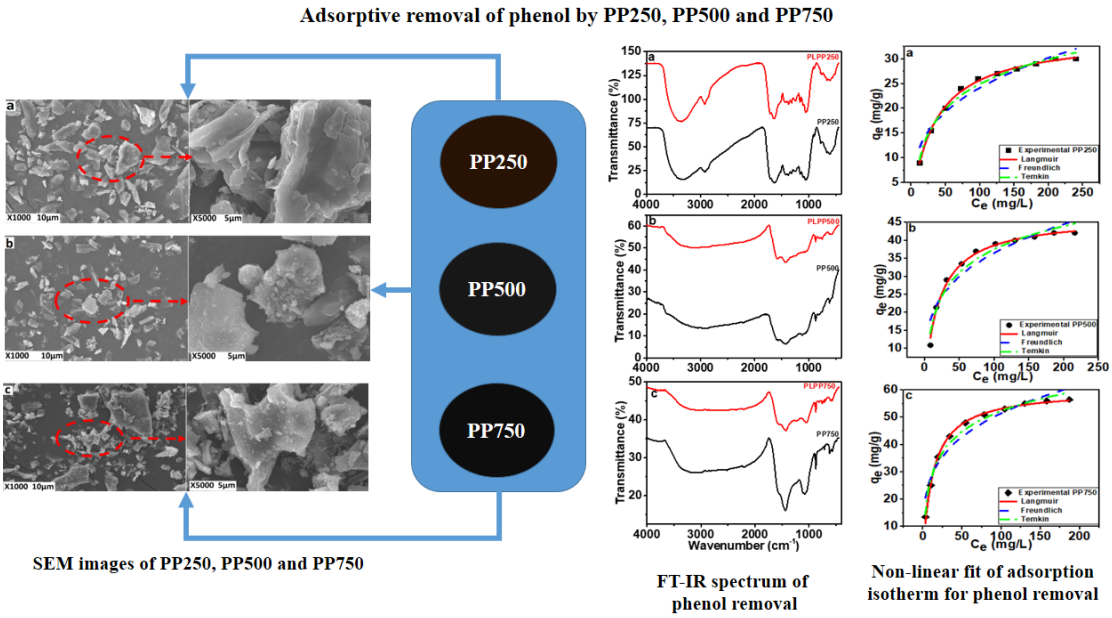

Fig. 7.3: graphical representation of the phenol removal by PP250, PP500 and PP750

7.2. Prospects of the study

The research embodied in this thesis is focusing on the following study:-

- Adsorptive removal of 4-AP by Pea shell treated with sulfuric acid from an aqueous medium has been studied.
- Removal of phenol by ultrasound-assisted sulfuric acid treated pea shells from the aqueous system has been investigated.
- A comparative study of phenol removal by pea shells biochar derived at different temperatures from the aqueous system has been performed.
- In depth characterization of the prepared pea shells adsorbents has been performed.
- Adsorption isotherm, kinetic and thermodynamic studies have been performed to interpret the adsorption mechanism of removal phenols by pea shells adsorbents.

It is anticipated that the findings of these investigations can be extended to systems of significant importance including water and wastewater treatment.

7.3. Future Prospects

The usage of low-cost adsorbents has introduced a new area of research for water/wastewater treatment, and it also brings more opportunities in producing a better way of management. The future perspectives of low-cost adsorbents can be determined by exploring the use of sustainable products in removing hazardous material from wastewater. Following are some important areas and scopes for future research:

- To explore the possibilities, functionalization/modifications/pre-treatment of agro-waste-based materials to improve their adsorption potential.
- More batches of these adsorbents should be analysed for their physical and chemical parameters and surface properties so that the results can be correlated to their utilization as a cheaper adsorbent for the treatment of effluents from different industries.

List of publications

1. **Prashant Mishra**, Kaman Singh, Utkarsh Dixit, Adsorption, kinetics and thermodynamics of phenol removal by ultrasound-assisted sulfuric acid-treated pea (Pisum sativum) shells; *Sustainable Chemistry and Pharmacy, Elsevier;* 22 (2021) 100491. (**I.F. 5.464**)
2. **Prashant Mishra**, Kaman Singh, Utkarsh Dixit, Ankita Agarwal, Rayees Ahmad Bhat; Effective removal of 4-Aminophenol from aqueous environment by pea (Pisum sativum) shells activated with sulfuric acid: Characterization, isotherm, kinetics and thermodynamics; *Journal of the Indian Chemical Society, Elsevier;* 99 (2022) 100528. (**I. F. 0.243**)
3. **Prashant Mishra**, Kaman Singh, Gajanan Pandey; A comparative study of phenol removal by Pisum-sativum peels biochars derived at different pyrolysis temperatures: Isotherm, kinetic and thermodynamic modelling; 2022, *ChemistrySelect; 7 (2022)* e202202856. doi.org/10.1002/SLCT.202202856. (**I.F. 2.3**)
4. Rayees A. Bhat, Kaman Singh, D. Kumar, Ashok Kumar, **Prashant Mishra**; Antimicrobial studies of the Zn(II) complex of S-benzyl-β-(N-2-methyl-3-phenylallylidene)dithiocarbazate; *Journal of Coordination Chemistry, Taylor & Francis;* (**I.F. 1.869**) *doi.org/10.1080/00958972.2022.2083962*
5. Kaman Singh, K.K. Sharma, R.K. Singh, **Prashant Mishra**, Ankita Agarwal, Anita Suman, Pankaj Singh; Sugar solutions colour measurement : Problems and Prospects; *Asian Sugar Journal*, Vol. 1, No. 1, Jan-Apr, 2021 : 32-67. (**I.F. NA**)
6. Kaman Singh, **Prashant Mishra**; The influence of different qualities of mops reagent on the measured sugar colour in solution; e - *Proceed. Sug. Tech. Assoc. India*, 79, 361-364, 2021. (**I.F. NA**)
7. Kaman Singh, **Prashant Mishra**, Ashok Kumar; Selection of pH for measurement of sugar solution colour; *Proceed. Sug. Tech. Assoc. India*, 77, 461-480, 2019. (**I.F. NA**)
8. **Prashant Mishra**; Alternative uses of sugarcane to mitigate green house gases generation; *Proceeding of GCGHGSPCT*, 62-63, 44, 2019; ISBN: 978-93-88237-65-9 (**I.F. NA**)

List of Conferences, Seminars, Webinars and Workshop

A. International conferences

1. ***Poster Presentation***: Lucknow Climate Change Conference on Control of Green House Gases at the Source by Physical and Chemical Technology (LCCCCGGSPCT_2k22), organized by Department of Chemistry, Babasaheb Bhimrao Ambedkar University (A Central University) Lucknow, Uttar Pradesh (India), 22-24 April 2022
2. ***Oral Presentation***: International E-Conference on Sustainable and Futuristic Materials (SFM-2021) organized by International Research Center and Department of Chemistry, Kalasalingam Academy of Research and Education, Krishnankoil, Department of Chemistry, J. M. Patel Arts, Commerce & Science College, Bhandara, and Department of Chemistry, Kamla Nehru Mahavidyalaya, Nagpur, 29-30 November 2021.
3. ***Oral Presentation***: Global Conference on the Control of Green House Gases at the Source by Physical and Chemical Technology (GCCGHGSPCT2k19), organized by Department of Chemistry, Babasaheb Bhimrao Ambedkar University (A Central University) Lucknow, Uttar Pradesh (India), 22-24 April 2019.
4. ***Poster Presentation***: International Symposium on Advances in Functional & Biological Materials organized by Humboldt Academy Lucknow & Department of Physics, University of Lucknow, 28 February 2019.
5. ***Poster Presentation***: International Conference on "Chemical Sciences: National and Global Perspective" organized by Department of Chemistry, Lucknow Christian College, Lucknow, 29-31 October 2018.
6. Participated in Virtual International Conference on Multifunctional Advanced Materials (VICMAM-2021)' organized by the Department of Chemistry, JVM's Degree College in collaboration with Association of Chemistry Teachers (ACT), 9-10 August 2021.
7. Participated in the Rayat-Bahra Connect Webinar Series 2020 on Chemistry as a Profession: Career Prospective by Dr. Avnesh Kumari- Senior Technical Officer-II, CSIR-IHBT Palampur Dr. Rajni Garg- Prof. & HOD, Dept. of Chemistry, Rayat Bahra University, 29 May 2020.

8. Participated in the International Webinar on Chemistry Education (IWCE-2021) organized by Department of Chemistry, Kamla Nehru Mahavidyalaya, Nagpur, Govt. Madhav Science P G College, Ujjain, and Association of Chemistry Teachers (ACT), Mumbai, 4-5 February 2022.

B. National Conferences

1. ***Oral Presentation***: National Conference on " Science & Technology: Rural Development" organized by The Indian Science Congress Association: Haridwar Chapter at Department of Chemistry, Gurukul Kangri Vishwavidyalaya, Haidwar, 15-16 February 2020
2. ***Oral Presentation***: 77th Annual Convention & International Sugar Expo 2019 held at Kolkata, West Bengal & organized by The Sugar Technologist' Association of India, New Delhi, 17-19 July 2019.
3. ***Poster Presentation***: 9th Conference of Indian Science Congress Association: (Haridwar Chapter) on "Future India: Science & Technology" organized by Department of Biological Sciences, CBS&H, G. B. Pant University of Agriculture and Technology, Pantnagar, 13-14 October 2018.
4. Participated in the National Webinar on "Green Chemistry For Sustainable Future" organized by Department of Chemistry, J. M. Patel Arts, Commerce & Science College, Bhandara, 21-22 January 2022.
5. Participated in 79th Annual Convention & International Sugar Expo 2021 held at NSI Kanpur & organized by The Sugar Technologist' Association of India, New Delhi, 4-5 October 2021.
6. Participated in the National Webinar on " Recent Advances in Chemistry" organized by the Department of Chemistry & IQAC, Govt. G. N. A. P G College, Bhatapara (C.G), 26 July 2021.
7. Participated in Young Scientist Conference of India International Science Festival (IISF-2018) held at Lucknow, 5-8 October 2018.
8. Participated in 1st North Indian Science Congress held at Babasaheb Bhimrao Ambedkar University (A Central University) Lucknow, Uttar Pradesh (India), 10-11 January 2018.

C. Workshops

1. Participated in Workshop on Integrating Scopus in Research Workflow at Babasaheb Bhimrao Ambedkar University/Elsevier, 19 May 2021.
2. Participated in National Workshop cum Training on Cheminformatic in Drug Discovery and Research organized by Babasaheb Bhimrao Ambedkar University (A Central University) Lucknow, in collaboration with Wetlab Championship E-Cell (IIT Bombay Event), 26-27 February 2020.
3. Participated in Workshop on Introduction to MATLAB: Programming & Applications organized by Ebrains Techno Solutions Pvt. Ltd. at Department of Physics, University of Lucknow, 28 & 31 March 2018.

Publications

Journal of the Indian Chemical Society 99 (2022) 100528

Contents lists available at ScienceDirect

Journal of the Indian Chemical Society

journal homepage: www.journals.elsevier.com/journal-of-the-indian-chemical-society

Effective removal of 4-Aminophenol from aqueous environment by pea (Pisum sativum) shells activated with sulfuric acid: Characterization, isotherm, kinetics and thermodynamics

Prashant Mishra [a], Kaman Singh [a,*], Utkarsh Dixit [a], Ankita Agarwal [b], Rayees Ahmad Bhat [a]

[a] Advance Center of Surface Science, Department of Chemistry, Babasaheb Bhimrao Ambedkar University (A Central University), Lucknow, 226025, India
[b] Department of Chemistry, Faculty of Science, University of Lucknow, Lucknow, 2206007, India

ARTICLE INFO

Keywords:
4-Aminophenol
Pea shells
Adsorption isotherm
Activation energy
Pseudo-first-order

ABSTRACT

The threat of phenol contamination in aquatic ecosystems is significant for the health of the earth's water systems as well as all humans on it. The present study was conducted to synthesize a cost-effective adsorbent (pea shells activated with sulfuric acid, PSASA) from agriculture waste (pea shells) and its use for effective removal of toxic 4-Aminophenol (4-AP). Newly designed PSASA exhibited significant adsorption of 4-AP which was confirmed by SEM, FT-IR, and XRD analysis. Surface topography confirmed high unevenness of the PSASA surface and the macroporous feature of the PSASA was confirmed by BET analysis. . Multiple testing was done to see how various factors affected adsorption such as adsorbent dose, temperature, pH, PZC, the effect of KCl and urea addition and the effect of the initial concentration of 4-AP. A drop in adsorption uptake of 4-AP was observed as the temperature increases from 25 °C to 45 °C. Maximum adsorption uptake (q_m) was found to be 106.11 mg/g at an optimum pH of 7.0 and 25 °C. Among various adsorption isotherm models tested, Langmuir Isotherm gave the best explanation with high R^2 values of experimental data. The pseudo-first-order model was found to explain the kinetics of adsorption well. The thermodynamic finding confirms the adsorption process was physical and exothermic. The adsorption of 4-AP was primarily governed by electrostatic interaction, hydrogen-bonding and π-π exchange mechanism. Because of the positive outcomes of the present research, we can use the PSASA as a cost-effective adsorbent for removing phenolic compounds.

1. Introduction

The contamination of water is continuously rising. The unabated anthropogenic processes and industrial effluents increase the variety of toxic substances in the aquatic environment [1]. Water exposed to toxic contaminants such as azo dyes, insecticides, PAH, and phenol, and so on, flows out of various industries [2]. Out of these, contamination of phenolic compounds in the aquatic environment receives greater attention owing to its wider release from several industries including tanning, plastic, pharmaceuticals, coke fabricating, dying [3–6]. Phenols are considered priority pollutants since their low concentration may cause a severe impact on the lives of organisms [7].

4-Aminophenol (4-AP) is an organic phenolic and is known to release in the aquatic environment through various industries and chemical processing [8]. The long haul over-the-top utilization of 4-AP has been related to interminable renal infection, hemolytic frailty, and expanded strong lipofuscin testimony in tissues [9]. Toxicological tests have indicated the presence of 4-AP in the effluents of commercial colouring industries which may cause nephrotoxic impacts, methemoglobinemia, serious sensitivities, dermatitis, rash, shaking, cerebral pains, seizures, unconsciousness, bronchial asthma, and lung aggravation, just as harmful to the kidneys, liver, and nervous system [10–14]. A recent study by De Souza et al. reported that oxidation of 4-AP in the process of hair dying produces various toxic substances including quinoneimine, semi-quinoneimine radical, dimmers to tetramers, etc. [15]. To treat the organic pollutants, present in wastewater various physical, chemical, and synthetic techniques have been utilized yet could not get the desired result. Therefore, a transition towards a cost-effective sustainable alternative for the removal of 4-AP is of utmost priority. In this regard, utilization of naturally derived adsorbents could be a protective measure.

Adsorption is one of the most significant techniques used for the

* Corresponding author.
E-mail address: singh.kaman@bbau.ac.in (K. Singh).

https://doi.org/10.1016/j.jics.2022.100528
Received 3 September 2021; Received in revised form 16 January 2022; Accepted 10 May 2022
Available online 13 May 2022

evacuation of phenolic and other toxic compounds [16]. Several critical utilitarian processes are based on this phenomenon. Adsorption of the substrate is the starting point for many catalytic processes [17]. When it comes to separation techniques in the laboratory and industrial settings, variations in component concentrations at the interface are becoming more important to success. Furthermore, such crucial topics as water filtration, sewage filtration, air filtration, and soil filtration are addressed in this context as well [18]. Having a basic understanding of scientific ideas is a long way behind the times; this is partly because the study of interfaces requires very rigorous testing to get relevant and accurate results. Recent years, however, have seen a significant increase in the amount of effort being put in to close the gap between theory and practice. Aside from that, new classes of solid adsorbents have been developed over the last few decades, including both carbonaceous and inorganic materials [19]. A broad range of nanostructured solids are extensively used in science and industry, and they have gotten a lot of interest recently because of their sorption, catalytic, magnetic, optical, and thermal properties [20]. However, although the development of adsorption has been rather zigzagging up until the 1918s, this arm of surface science is now generally considered to have developed into a well-defined branch of physical science representing an intrinsically interdisciplinary area that spans the disciplines of chemistry, physics, biology, and engineering. Activated carbon is a widely used adsorbent for wastewater treatment which is costly [21]. So, researchers are focusing on the preparation of cost-effective, sustainable, easily available adsorbents. In this regard, utilization of agricultural, household, and industrial waste as an adsorbent may be a win-win approach. Therefore we have seen a systematic development in the field of adsorbent preparation for contaminant removal. Recently, different agriculture waste-based biochars from rice husk, groundnut shell and coconut shell have been prepared through physical activation method [22]. Various biochar-based catalysts [23] and biochar-based composites [24] have also been developed. To enhance the adsorption capacity, some chemical modification has also been done such as caffeic acid functionalised corn starch, KOH- activated carbon from sucrose spherical carbon etc. [25,26]. Some modified natural inorganic adsorbents such as clay minerals, zeolite and layered double hydroxides [27]. A comparison table of the present study of 4-AP removal with previously studied adsorbents [28–31] is shown in Table 1.

Keeping this point in mind, we have selected modified Pea shells (PS) as an adsorbent and tested in this study for the 4-AP removal. The disposition of the PS seems to have the potential of 4-Ap removal from the aqueous stream. Further, the exuberant and free worldwide availability of PS makes it a suitable adsorbent for the removal of toxic substances from an aqueous system.

Table 1
Comparison of q_m of different studies for 4-AP removal.

Adsorbents	Conditions		q_{max} (mg/g)	References
	pH	Temp (°C)		
3D-graphene oxide-maize amylopectin composites	5	25	116.4	[24]
8% Calcined Layered Double Hydroxide into Alginate Hydrogel Beads	NA	45	36.46	[25]
6% Calcined Layered Double Hydroxide into Alginate Hydrogel Beads	NA	45	98.23	[25]
Antimony ferrocyanides	7	30	190.00	[26]
Cadmium ferrocyanides	7	30	250.00	[26]
Zirconium ferrocyanides	7	30	125.00	[26]
Poly(aryl ether ketone) Containing Pendant Carboxyl Groups	2	20	0.30	[27]
PSASA	7	25	106.11	This study

NA= Not affected.

The scientific contribution of the present research is to prepare an adsorbent activated with H_2SO_4, using PS as a precursor followed by its application for the 4-AP removal. In-depth characterization of the PSASA using different techniques such as BET, XRD, FT-IR spectroscopy, optical profilometry, SEM-EDS, point of zero charge (PZC), etc was done to explore its physicochemical properties. The experiments were designed to extract the information of the optimized conditions at which the PSASA works at its maximum efficiency. In addition to this, isotherm, kinetics and thermodynamic studies were conducted to interpret the mechanism and nature of 4-AP removal onto the PSASA. Taking limited available data of information and headlong utilization of 4-AP into account, the present study aims to provide a cost-effective alternative for the removal of such toxic substances from aquatic environments.

2. Materials and methods

2.1. Preparation of the adsorbent (PSASA)

Green pea (*Pisum sativum*) were collected from the local market of Lucknow (Naveen Galla Mandi, Purania; 26.8930° N, 80.9356° E). After the PS was washed with deionized water to eliminate dirt, it was let to dry in direct sunlight for 48 h. PS dried and ground to a particle size of 75 μm or less in an acoustic grinder and kept in a desiccator. Chemical adaptation was accomplished by pouring PS into 50% H_2SO_4 (v/v) for 24 h. The chemically-treated PS were kept in a furnace at 800 °C. The furnace temperature was gradually increased to the set point, with a rate of 10 °C per minute, over a period of 30 min [32]. After cooling, the PSASA was cleaned with deionized water for 10 min, then dried at 105 °C. The dried adsorbent was sieved to get a size within the limit of 75–300 μm and stored.

2.2. Characterization of adsorbent

2.2.1. Point of zero charge (PZC)

Surface charge analysis (PZC) of the PSASA was done using the salt addition method [33], in which 0.1 N KCl and 0.002 M Cetrimide solution were used as salt. 20 ml KCl and 20 ml Cetrimide solution were kept in six different stoppered flasks (100 ml) and pH of each flask were maintained to pH 2, 4, 6, 8, 10 and 12, respectively using 0.1 N HCl and 0.1 N NaOH and then after maintaining 50 ml volume using 0.1 N KCl and 0.002 M Cetrimide. For the PZC estimation, 0.2 g of the PSASA sample was added in each stoppered flask and stirred vigorously for 6 h till equilibrium was attained. After stirring, solutions were further left for 36 h and timed shaking. After 36 h, pH of each solution was then determined. A plot is plotted between change in pH and initial pH and intersection value gave PZC.

2.2.2. Brunnaur- Emmet- Teller (BET) analysis

The PSASA sample was examined with a BET surface area analyser (mean pore diameter, specific surface area, and total pore volume) (BELSORP-max, Japan). The PSASA (0.2 g) was heated at 120 °C under vacuum for 5–6 h. After 6 h, the adsorbent was transferred into a glass sample tube kept in liquid nitrogen for N_2 adsorption and desorption. The surface region and pore measurement were determined utilizing the standard Brunauer–Emmett–Teller (Wager) condition and pore size were determined utilizing Barrett–Joyner–Halenda (BJH) method.

2.2.3. Scanning electron microscopy (SEM) with energy dispersive X-ray spectrometry (EDS) analysis

The PSASA and after adsorption PSASA were fixed in 2.5% glutaraldehyde at 4 °C for a period of 4 h followed by phosphate buffer washing and dehydration using C_2H_5OH (10%, 30%, 50%, 70%, and 95%) for 5 min separately [34]. The final dehydration was done with absolute alcohol for 30 min. After dehydration, samples were further mounted on platinum stub by using carbon tape. SEM coupled with EDS

was done for the SEM image and analysis of composition and distribution of elemental (SEM) (JEOL, Japan; model JSM-6490LV).

2.2.4. Optical profilometry

Optical profilometry data such as surface morphology, surface roughness, and step height of the PSASA were analyzed by using a 3-D optical profilometer (Bruker, USA).

2.2.5. FT-IR analysis

For the FT-IR spectra analysis, the PSASA and after adsorption PSASA were ground with KBr (1:10 ratio) and pelleted. The pellet was further fitted to the socket of FT-IR (Thermo- Scientific Nicole 6700, USA) for functional group analysis. The IR spectrum (4000 - 400 cm^{-1}) was attained with a resolution of 5–7 cm^{-1} and 32 scan numbers for each spectrum.

2.2.6. X-ray diffraction analysis

The crystallographic behaviour of the PSASA and after adsorption PSASA were examined by powder X-ray diffractometer (XRD) (Rigaku-Miniflex II desktop). Samples were scanned with Copper Kα radiation (λ = 1.5405 A°) with a 2°/min scan rate and angle ranging from 20° to 70°. The raw data were examined using Match3 software and Origin pro2016 software.

2.3. Batch adsorption studies

Several experimental batch adsorption methods were attempted to investigate the effects of time and the rate of adsorption utilizing a temperature-controlled magnetic stirrer. . In each batch, solutions of 4-AP with different and specific initial concentrations were taken into 100 ml conical flasks. The 4-AP concentration ranged from 100 to 700 mg/L at the beginning. For every conical flask, 0.1 g of the PSASA was added and the pH was adjusted. These flasks of different initial concentrations were placed at magnetic stirrer at different constant temperatures. Samples were removed from the stirrer at different intervals of time to find out how the removal of 4-AP was impacted by time. A few samples were placed in a magnetic stirrer for 12 h, however, equilibrium was achieved in 4–5 h. The concentration of 4-AP in solution was then measured using a UV–visible spectrophotometer (Carry 100) on samples that were first filtered and centrifuged.

The adsorbed amount of 4-AP at equilibrium is represented by q_e and can be calculated by Eq. (1):

$$q_e = \frac{(C_0 - C_e)V_s}{m} \quad (1)$$

In the sample, Vs (in L) is the volume of the sample, m (in g) is the mass of the PSASA, and Co and Ce are the initial and equilibrium concentration of the 4-AP solution (in mg/L), respectively.

The adsorption capacity of 4-AP at any time (q_t) is calculated by Eq. (2):

$$q_t = \frac{(C_0 - C_t)V_s}{m} \quad (2)$$

where C_t is the concentration of 4-AP solution at any time t.

2.4. Effect of the PSASA dose

The effect of the PSASA dose on adsorption of 4-AP was investigated in this study. It was done by adding 0.1,0.2,0.3,0.4,0.5, and 0.6 g of the PSASA into six different conical flasks each containing 100 mg/L solutions of the 4-AP whereas the pH and temperature were adjusted accordingly at 7.0 and 25 °C, respectively.

2.5. Effect of pH

Change in pH affects the adsorption process and this has been confirmed by several studies [35]. So, the effect of pH on 4-AP adsorption must be researched, as 4-AP's chemistry is influenced by the pH of a solution, and concentrations of $[H^+]$ and $[OH^-]$ directly affect the adsorption process.

The pH of the 4-AP solution was set at a certain value with 0.1 N HCl and 0.1 N NaOH in the research analysis. The pH of the 4-AP solution was adjusted between 5 and 11. The initial 4-AP concentration was fixed at 100 mg/L and temperature at 25 °C with a change in pH values.

2.6. Effect of temperature

4-AP's adsorption to the PSASA was investigated at different temperatures to know the nature of adsorption. Temperature affects adsorbents and adsorbates in various ways, depending on their physical and chemical characteristics and the nature of the bonding between them. Several adsorption studies have been done in which the adsorbent's adsorption capacity was at its maximum at an optimum temperature [36].

The potential of the PSASA for removing 4-AP under varying temperatures was explored in this research. Experiments were performed at different temperatures (25-45 °C) and concentrations of 4-AP (100–700 mg/L) at pH 7.0.

2.7. Effect of KCl and urea addition

It has been proved in several studies that the ionic strength of solution has positive and negative effects on the adsorption process [37]. The presence of urea in the solution also affects the amount of adsorption as it primarily works as a hydrogen bond breaker [37]. Various studies have shown that the addition of these salts and urea affects the amount of adsorption negatively [36,37].

To investigate the effect of KCl and urea on adsorption, a particular amount of different molarities of KCl and urea were introduced to 4-AP containing solution. 0.1–0.6 mol/L concentration of salts and urea were added to 100 mg/L solutions of 4-AP with 0.1 g of the PSASA at pH 7.0 and temperature 25 °C.

2.8. Adsorption isotherm

Adsorption isotherm is a curve representing the amount of adsorbate adsorbed onto per unit mass of adsorbent at a constant temperature. The most commonly used adsorption isotherms for interpretation of adsorption behaviour are Freundlich, Temkin and Langmuir isotherms.

2.8.1. Freundlich isotherm

Heterogeneous surface adsorption is generally explained with Freundlich adsorption isotherm in which no restriction monolayer formation means multilayer adsorption is also possible [38]. This model works on the assumption that active sites for adsorption are distributed at the heterogeneous adsorbent surface exponentially. The Freundlich equation can be stated in non-linear form as follows:

$$q_e = K_F C_e^{1/n} \quad (3)$$

where, K_F: Freundlich constant ($mg^{1-(1/n)}.L^{1/n}.g^{-1}$) and 1/n: Intensity of adsorption. The linear form of the equation is written as:

$$lnq_e = lnK_F + \frac{1}{n} lnC_e \quad (4)$$

the equation proposed by Halsey was used to compute the maximum adsorption capacity [39]:

$$K_F = q_m / C_o^{1/n} \quad (5)$$

where C_o is the initial concentration.

2.8.1.1. Temkin isotherm. The main feature of Temkin isotherm [40] is the assumption of adsorbate-adsorbent interaction which means due to adsorbent-adsorbate interaction, all molecules in the layer exhibit a decrease in heat of adsorption as surface coverage increased. . The non-linear Temkin isotherm form may be written as follows:

$$q_e = \frac{RT}{b} \ln K_T C_e \tag{6}$$

where, K_T and b are Temkin constant (L/g) and heat of adsorption constant (J/mol). The equation can be stated in linear form as:

$$q_e = \frac{RT}{b} lnK_T + \frac{RT}{b} lnC_e \tag{7}$$

2.8.1.2. Langmuir isotherm. Langmuir model hypothesis was based on the fact that the monolayer of the adsorbate is formed at the adsorbent surface during the adsorption and negated the formation of multilayer [41]. This model also denies the interaction among active sites of adsorbent. The Langmuir equation can be written as follows:

$$q_e = \frac{q_m K_L C_e}{1 + K_L C_e} \tag{8}$$

where, K_L (L/mg): Langmuir constant; C_e (mg/L): equilibrium concentration of 4-AP: q_e (mg/g): the amount of 4-AP adsorbed at equilibrium and q_m (mg/g): maximum adsorption. The linear form of the equation is written as:

$$\frac{C_e}{q_e} = \frac{1}{q_m K_L} + \frac{C_e}{q_m} \tag{9}$$

2.9. Kinetic study

The amount of adsorption has been checked at different time intervals to study the reaction kinetics. Different kinetic models were modelled and the model which shows a straight line with the highest value of correlation coefficient (r) and coefficient of determination (R^2) can be used to describe the experimental data. Following kinetic models were applied to investigate the experimental data [42]:

Pseudo-first-order model:

$$\ln(q_e - q_t) = lnq_e - k_1 t \tag{10}$$

Pseudo-second-order model:

$$\frac{t}{q_t} = \frac{1}{k_2 q_e^2} + \frac{t}{q_e} \tag{11}$$

where k_1 and k_2 are pseudo-first and pseudo-second-order rate constant respectively.

2.9.1. Intra particle diffusion model

$$q_t = k_p t^{0.5} + C \tag{12}$$

For kp, which is the particle-related rate constant in units of g/mg. $min^{0.5}$, and C, which is a constant in units of mg/g.

3. Results and discussion

3.1. Characterization of adsorbent

3.1.1. PZC

PZC (Fig. 1a) describes the surface charge of the PSASA [43]. PZC value describes the pH at which surface charge is zero.; pH below the PZC value indicates that surface is positively charged and pH above PZC value indicates that surface is negatively charged. PZC value of the PSASA in the present study was found to be 10.15 which showed that at this pH surface was neutral. At pH below PZC, the PSASA surface tended to be positively charged which may favour the binding of electronegative oxygen or nitrogen of 4-AP through hydrogen bonding.

3.1.2. BET analysis

The physicochemical characteristics viz., specific surface area, surface nature, total pore volume, and particle size distribution of the pea

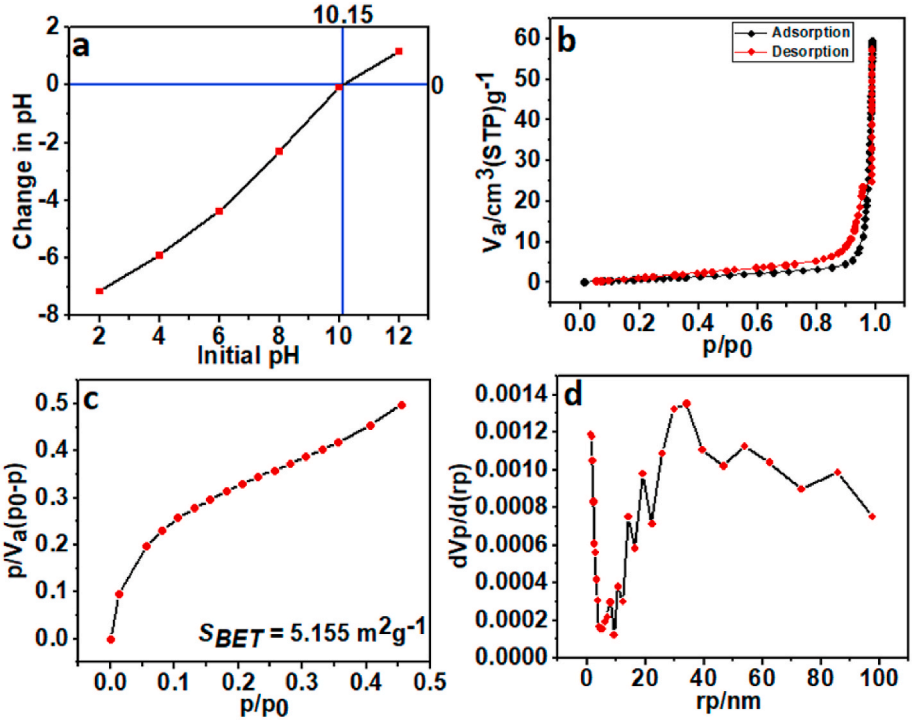

Fig. 1. PZC (a), N_2 adsorption-desorption (b), BET (c) and BJH (d) graphs of the PSASA.

cell adsorbent were analyzed employing Brunauer–Emmett–Teller (BET) analysis (Fig. 1b–d). The pore size distribution of the PSASA was estimated by Barrett–Joyner–Halenda (BJH) model [44]. Results presented that the specific surface area (S_{BET}), mean pore diameter, and total pore volume (p/p_0) of adsorbent were 5.15 m^2/g, 71.309 nm, and 0.990, respectively which confirmed the macroporous nature of the PSASA. In the present study, hysteresis loop (H-3 type) in adsorption-desorption curve reflected lower desorption of some N_2 molecules in the capillaries of the adsorbent which was a clear-cut indication of the porous nature of the PSASA. In addition, the macroporous nature of adsorbent was confirmed by Dabrowski (microporous, <2 nm; mesoporous, 2–50 nm; macroporous, >50 nm) and IUPAC nomenclature [45] through evaluating pore size and adsorption-desorption curve. Similar hysteresis loops have been earlier reported by Singh et al. and Li et al. [37,46].

3.1.3. SEM coupled EDS study

The structural morphology of the PSASA and the after adsorption PSASA were examined using SEM. The SEM image reflects morphological alterations in terms of shape and size (Fig. 2a and b). The SEM image of the PSASA was exhibited variegated shells morphology with round protuberance and porous appearance enhanced the surface roughness. Increased surface roughness of the PSASA signifies the high adsorption potential due to increased adsorption site and surface area [47]. The SEM image of after adsorption PSASA showed organized substantial adsorption of 4-AP over the PSASA surface. SEM coupled EDS data explained the presence of different elements present in the PSASA. EDS data revealed that elemental abundance in terms of % atomic weight. In the case of the PSASA, the maximum elemental composition was observed in the order of O > S > K > Ca > C. The EDS data of the after adsorption PSASA exhibited a high percentage of C and O which reflects the adsorption of 4-AP. A high percentage of C in the adsorbed surface has also been reported by Singh et al. [48].

3.1.4. Optical profilometry

The surface waviness and surface roughness of the PSASA sample has been determined using an optical profilometer (Bruker, USA) in veridical scanning interferometry (VSI) mode (Fig. 2c and d). The areal parameter of the surface was provided by a 3D-optical profilometry (OP) image whereas the 2D-OP image provides topographical parameters. Parameters of surface topography extracted from OP images such as Roughness average (Ra), Maximum profile peak height (Rp), Root mean square (RMS) roughness (Rq), Maximum height of the profile (Rt), and Maximum profile valley depth (Rv) in the PSASA were 12.093 μm, 84.721 μm, 15.698 μm, 155.735 μm, and −71.014 μm, respectively. The present study revealed that a significant difference was observed between Ra and Rt value which clearly showed a greater extent of irregularities in the surface of the PSASA due to strong oxidizing agent H_2SO_4 and high temperature. A very high negative value of Rv shows the formation of capillaries inside the PSASA surface which is a characteristic property of porous materials.

3.1.5. FT-IR analysis

The FT-IR spectrum of the PSASA and after adsorption PSASA is depicted in Fig. 3a and b. The FT-IR spectrum of the PSASA consists of several bands of various functional groups. The band observed at 3430 cm^{-1} may be present due to the O–H stretching of secondary alcohol [49]. The weak band at 2923.5 cm^{-1} corresponds to the C–H stretching of alkane [50]. The band present at 1621 cm^{-1} corresponds to the C═C stretching of the conjugated alkene [50]. The bands present at 1429 and 1108 cm^{-1} correspond to the O–H bending and C–O stretching of the secondary alcohol [49].

The changes observed in the FT-IR spectrum of the after adsorption PSASA confirmed the phenomenon of adsorption of 4-AP over the PSASA surface and gave us an idea about the mechanism of adsorption. Three key variations were identified in the FT-IR spectrum of the after adsorption PSASA. First, a band was observed at 3390.9 cm^{-1} corresponding to the O–H stretching of the hydrogen-bonded alcohol indicating the role of hydrogen bonding between the PSASA surface and 4-AP during the adsorption process. Second, a band was observed at 1506.7 cm^{-1} corresponding to the C═C stretching of the aromatic ring, this band indicates the exchange of π-electrons between the PSASA surface and 4-AP resulting in the weakening of the C═C bond strength of the aromatic ring because the C═C stretching of the pure aromatic ring

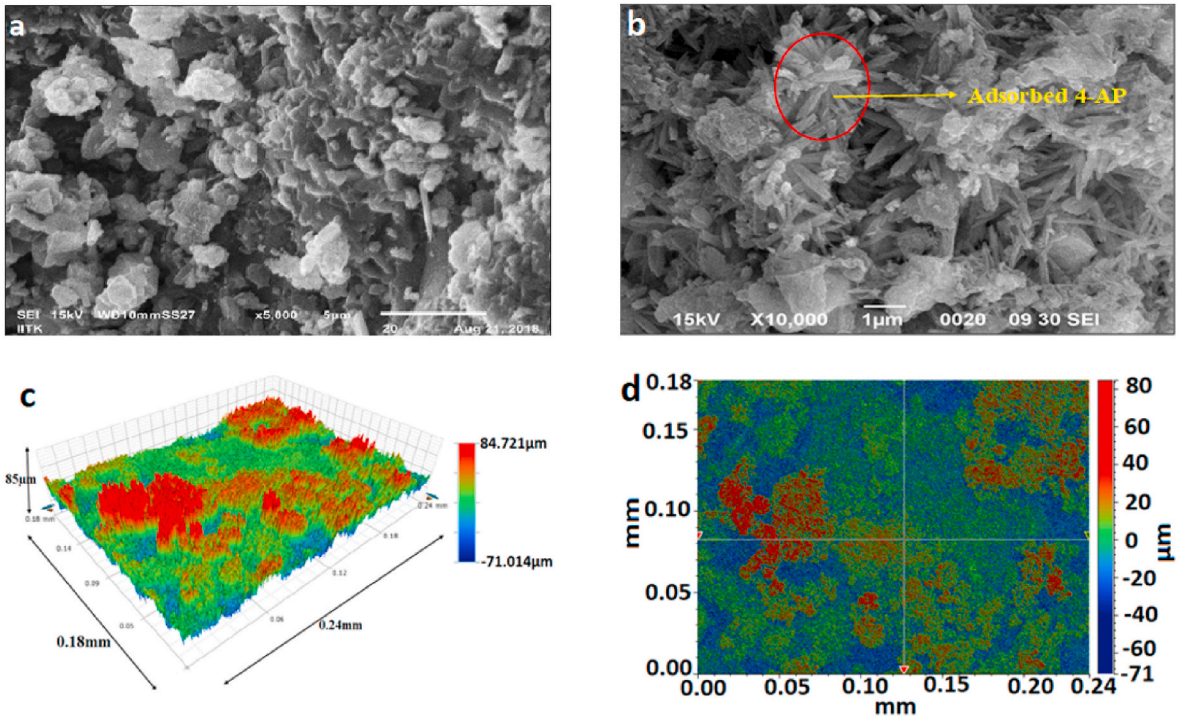

Fig. 2. SEM images of the PSASA (a) and after adsorption PSASA (b), 3D (c) and 2D (d) optical profilometry image of the PSASA.

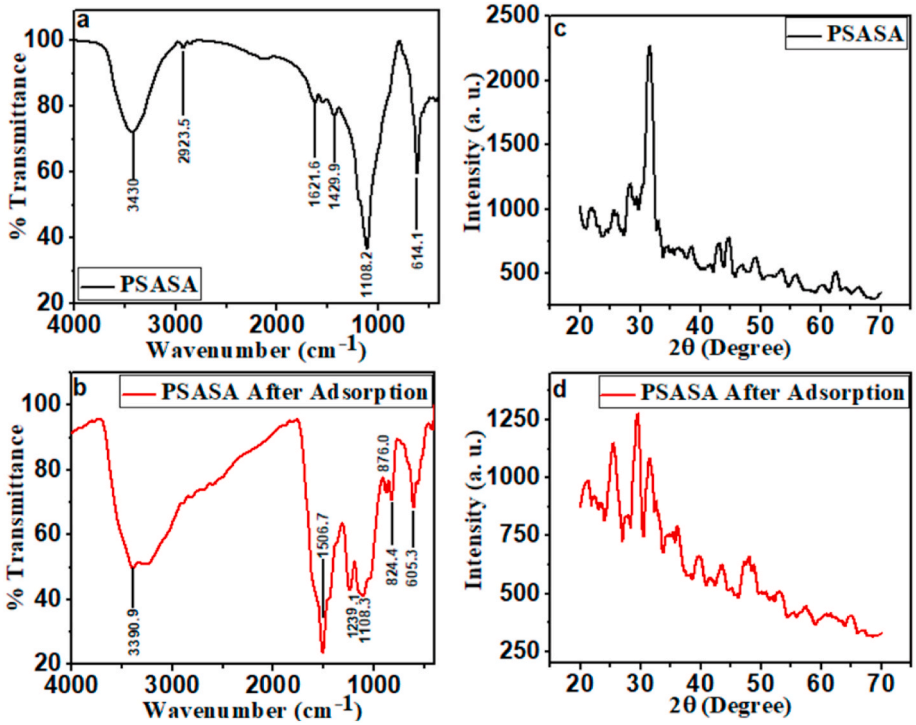

Fig. 3. FTIR spectra of the PSASA (a) and after adsorption PSASA (b) and XRD plot of the PSASA (c) and after adsorption PSASA (d).

of 4-AP is usually observed at relatively higher wavenumber. Third, a band was observed at 1239.1 cm^{-1} corresponds to the C–N stretching of the aromatic amines.

3.1.6. *X-ray diffraction analysis*

Fig. 3c shows the XRD graph of the PSASA. The PSASA XRD spectrum depicts only one sharp peak at a 2θ angle of 33° confirmed the characteristic of the activated carbon [51,52] and indicates an ordered graphitic crystalline structure [53], while other peaks were broad and small in size may be present due to the compounds containing K, S or Ca. The degree of crystallinity study showed that the PSASA had 19.55% crystalline content and 80.45% amorphous content indicating the

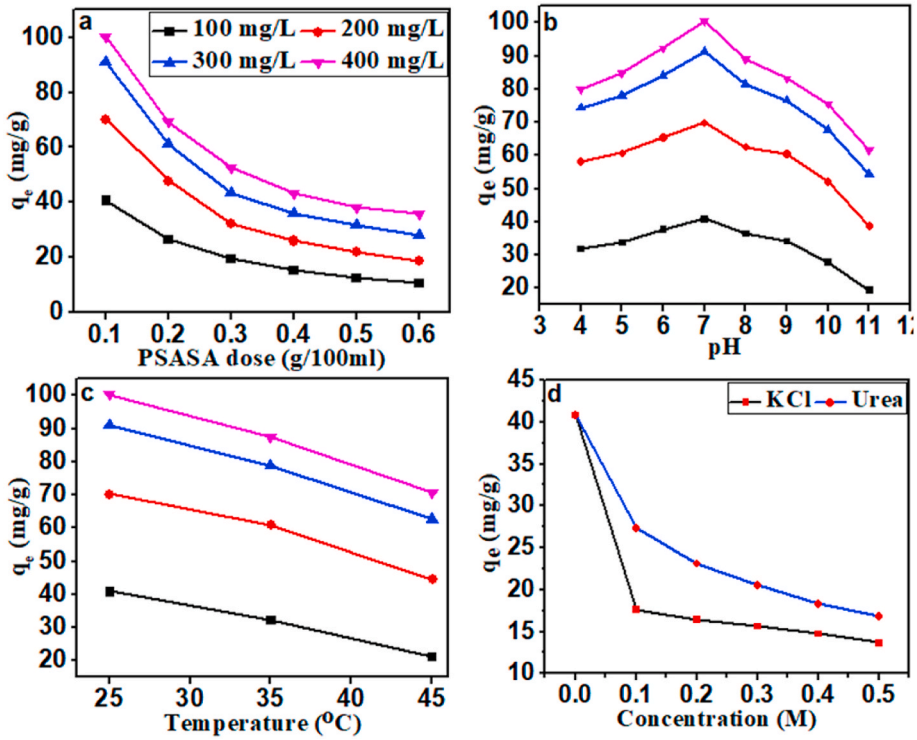

Fig. 4. Effect of the PSASA dose at pH 7.0 & 25 °C (a), effect of pH at 25 °C & 0.1g of the PSASA (b) effect of temperature at pH 7.0 & 0.1 g the PSASA (c), and effect of KCl & urea addition on 100 mg/L concentration at pH 7.0 & 25 °C (d) on uptake of 4-AP.

overall amorphous nature of the PSASA. This fact has been further substantiated by XRD data in which crystalline content of the after adsorption PSASA has reduced to 13.21% and amorphous content has increased to 86.79% which indicated that a sufficient amount of adsorption of 4-AP has taken place. The XRD plot of the after adsorption PSASA has been shown in Fig. 3d.

3.2. Effect of PSASA dose

The effect of the PSASA dose on adsorption of 4-AP is shown in Fig. 4a. The PSASA dose was varied from 0.1 to 0.6 g/100 ml. On increasing the dose of the PSASA from 0.1 g to 0.2 g the adsorption uptake decreased from 40.87 to 26.83 mg/g. The adsorption uptake decreased continuously with the increase in the PSASA dose but at a slower rate. This decrease in adsorption uptake of 4-AP per unit mass of the PSASA was due to the presence of more adsorption sites with the increase in the PSASA dose. The slower rate of adsorption was probably due to a decrease in interaction between 4-AP and the PSASA as initial concentration provides the effective driving force to surpass the resistance of mass transfer from adsorbate to the adsorbent [54]. Maximum removal per unit mass of the PSASA was observed at 0.1 g.

3.3. Effect of pH

The effect of solution pH on adsorption uptake of 4-AP onto PSASA is shown in Fig. 4b. From Fig. 4b, it is apparent that the 4-AP uptake took occurred in two stages. The first stage witnessed an increase in 4-AP uptake from pH 4.0 to 7.0 and in the second stage, it decreased from pH 8.0 to 11.0. The maximum adsorption uptake of 40.87 mg/g was observed at pH 7.0 for 100 mg/L 4-AP concentration. The experiments were repeated for 200–400 mg/L concentration and similar findings were observed. The outcomes of the experiment can be interpreted based on the acidic nature of 4-AP and the PZC of the PSASA. As discussed above, PZC of the PSASA was 10.15 so at pH below this value, the PSASA surface was positively charged. Adsorption uptake of the 4-AP increased from pH 4–7 due to the acidic properties of 4-AP. The pKa value of the 4-AP is 5.48 and so at pH below 5.48, 4-AP was in protonated form resulting in lesser electrostatic interaction between 4-AP and the PSASA surface. When pH was increased to 7.0, 4-AP was in the deprotonated form showing the highest electrostatic interaction between 4-AP and the PSASA surface [55]. The 4-AP uptake gradually decreased in the basic range up to pH 9.0 because the negatively charged [OH^-] was competing with the deprotonated 4-AP for the positively charged PSASA surface. At pH 10.0 the PSASA surface was neutral resulting in a significant decrease in the 4-AP uptake and indicates that the adsorption took place through other mechanisms. At pH 11.0, the PSASA surface was negatively charged and 4-AP was in deprotonated form resulted in a further reduction in 4-AP uptake due to increased electrostatic repulsion.

3.4. Effect of temperature

Fig. 4c depicts the effects of temperature on the adsorption process at 25 °C, 35 °C, and 45 °C. The effect of these temperatures on 4-AP adsorption was evaluated at different concentrations of 4-AP (100–700 mg/L). The lowest 4-AP concentration (100 mg/L) shown the highest reduction in adsorption uptake with an increase in temperature. The 4-AP adsorption uptake fell from 40.87 mg/g to 21.19 mg/g on a 20 °C rise in temperature with an initial concentration of 100 mg/L, which is almost 50% of the initial uptake value. Similar patterns were observed for the higher concentrations of 4-AP but adsorption uptake decreased at a slower rate with an increase in temperature. At initial concentrations of 600 mg/L and 700 mg/L adsorption uptake reduction with increase in temperature was almost 26% and 25% respectively, Which shows that temperature has a greater effect on the lower concentration of 4-AP and lower effect on higher concentrations of 4-AP. The above results confirm the exothermic nature of adsorption.

3.5. Effect of KCl and urea addition

Fig. 4d displays the effect of the addition of KCl and urea at specific concentrations. . It is evident from Fig. 4d that the addition of KCl and urea affected adsorption negatively. When 0.1 M KCl was added to the 4-AP solution the adsorption uptake dropped from 40.87 mg/g to 17.63 mg/g. Further, increasing KCl concentration affected the adsorption uptake to a smaller extent. The decrease in 4-AP uptake after KCl addition is probably because the PSASA surface becomes more positive with dissociation of KCl in water which leads to a competition of negatively charged species for surface sites of the PSASA [56].

To know the role of hydrogen bonding in the adsorption process, urea addition experiments were performed. From the experimental results, it is evident that the addition of different concentrations of urea to the 4-AP solution led to a significant decrease in adsorption uptake as urea is a hydrogen bond breaker. Thus, experimental results confirmed the role of hydrogen bonding in the adsorption process of the studied system.

3.6. Adsorption isotherms

Insight into adsorption behaviour is obtained in adsorption isotherm shape. Giles divided adsorption isotherm shapes into four groups: S, L, H, and C, and these isotherms are further classified into subgroups, depending upon the porous nature of the adsorbent [57]. Graphs plotted between amount adsorbed *versus* equilibrium concentration at different temperatures represented an L type of adsorption isotherm which means there was no competition between solvent and 4-AP molecules to occupy surface sites of the PSASA (Fig. 5a). On increasing the temperature from 25 °C to 45 °C adsorption uptake dropped by 20–25% which represents the exothermic and reversible nature of the adsorption phenomenon. The applicability of three commonly used adsorption isotherm was tested and discussed as follows:

3.6.1. Freundlich isotherm

The linearized Freundlich isotherm was employed to examine experimental data in different conditions, by plotting the graph between $\ln q_e$ *versus* $\ln C_e$. The Freundlich plot is shown in Fig. 5b and the values K_F, n, q_m, r and R^2 are reported in Table 2. The intensity of adsorption (n) at 25 °C, 35 °C, and 45 °C temperatures was found to be 2.48. 2.01 and 1.60 respectively, which represented that the favorability of adsorption gradually declines with rising temperature. It is reported in the literature that the value of n ranging from 2 to 10 represents good adsorption, 1–2 represents moderate adsorption, and less than 1 represents poor adsorption [58]. The R^2 values fall between 0.89 and 0.91. The parameters calculated from the Freundlich equation explained the adsorption experiments well. Nevertheless, Freundlich isotherm showed slight divergence with the adsorption data at higher equilibrium concentrations and temperatures. Thus, Freundlich isotherm is unable to give an accurate explanation of experimental data.

3.6.2. Temkin isotherm

Parameters of the Temkin isotherm equation were determined by linear regression. Temkin isotherm was plotted at a range of temperatures (shown in Fig. 5c) between q_e and lnCe, While the parameters of the Temkin equation are tabulated in Table 2. The assumption of uniform distribution of binding energy seems to be correct as adsorption equilibrium data gives a satisfactory linear fit to the Temkin model. The linear fit value (R^2) was in the range of 0.94–0.97. The R^2 value indicated that the Temkin assumption of linear decrease in heat adsorption with an increase in surface coverage due to adsorbent – adsorbate interaction was correct but diverges at higher equilibrium concentrations of 4-AP.

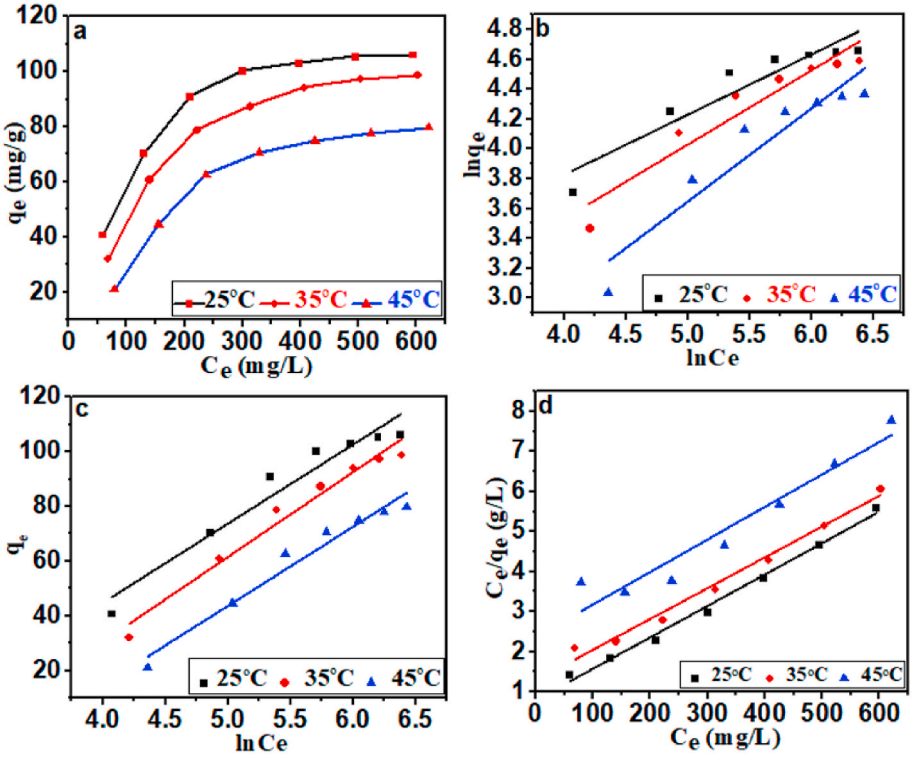

Fig. 5. Variation of 4-AP adsorption with equilibrium concentration at pH 7.0 & 0.1 g of the PSASA (a) and plots of Freundlich isotherm (b), Temkin isotherm (c), and Langmuir isotherm (d).

Table 2
Parameters obtained from different adsorption isotherm models for 4-AP adsorption onto the PSASA.

Parameters	Temperature		
	25 °C	35 °C	45 °C
Langmuir			
K_L (L/mg)	9.9×10^{-3}	6.00×10^{-3}	3.43×10^{-3}
q_m (mg/g)	127.55	125.15	123.15
R_L	0.502	0.625	0.744
r	0.996	0.993	0.964
R^2	0.992	0.986	0.93
Freundlich			
K_F ($mg^{1-(1/n)}$ $L^{1/n}g^{-1}$)	9.12	4.66	1.69
n	2.48	2.01	1.60
q_m (mg/g)	58.41	46.07	29.90
r	0.947	0.954	0.947
R^2	0.896	0.911	0.897
Temkin			
K_T (L/g)	8.5×10^{-2}	4.88×10^{-2}	3.04×10^{-2}
b (J/mol)	85.65	82.55	91.47
r	0.971	0.985	0.982
R^2	0.944	0.971	0.964

3.6.3. Langmuir isotherm

The Langmuir isotherm model was linearized and analyzed by regression analysis. The Langmuir graph was constructed at various temperatures, showing Ce/qe against Ce (Fig. 5d) and Table 2 displays the K_L, qm, r, and R^2 parameters, which were calculated. The degree of adsorption favorability can be represented by a dimensionless constant, R_L [59]: $R_L = 1/(1+ K_L C_0)$, where C_o is the initial concentration of 4-AP and K_L is Langmuir constant. The $R_L = 1$ represents linear adsorption, $R_L > 1$ represents unfavorable adsorption, $R_L = 0$ represents adsorption to be irreversible and $0 < R_L > 1$ represents favourable adsorption. The R_L values (Table 2) at different temperatures were in the range of favourable and reversible adsorption. The R^2 values range between 0.93 and 0.99 giving the best linear fit of the adsorption equilibrium data. The q_m values obtained from the Langmuir equation were more than twice the values of the q_m obtained from the Freundlich equation. Thus, from the above discussion, it is clear that the closest explanation of the equilibrium data is given by Langmuir Isotherm. Mishra et al. observed a similar finding [60].

3.7. Kinetics of adsorption

Fig. 6a illustrates the uptake of 4-AP at various time intervals. The graph was plotted between uptake of 4-AP at various initial concentrations (100–400 mg/L) *versus* time at 25 °C. From the graph, it was observed that with an increase in time, the 4-AP uptake increased irrespective of the initial concentration of 4-AP. The experiments were run for 5 h and it was observed that the graph of 4-AP uptake increased rapidly in the first 60 min, this uptake of 4-AP gradually slowed down and the curve flattens out in the last hours of the experiments. Similar patterns were observed for all the concentrations of 4-AP. It was concluded from the plot that adsorption uptake increased rapidly with an increase in initial concentration of 4-AP, this probably occurred because higher initial concentration creates a higher concentration gradient between 4-AP concentration at the PSASA surface and 4-AP concentration in the bulk of the solution. In the first 60 min of the experiment, the adsorption uptake for 100 mg/L concentration was 25.54 mg/g, the uptake increased to 40.34 mg/g when concentration was doubled to 200 mg/L while the uptake increased to approximately 1.5 times (57.36 mg/g) of the uptake of 100 mg/L concentration when the experiment was carried out at 400 mg/L initial concentration [61].

Using the linearized forms of the rate laws indicated in equations (10)–(12), the kinetic data were evaluated. The values of different parameters of the pseudo-first-order, pseudo-second-order, and intraparticle models were calculated with the help of regression analysis and tabulated in Table 3. The rate laws were plotted for concentrations 100–400 mg/L and shown in Fig. 6a. For the pseudo-first-order kinetics, the graph was plotted between $\ln(q_e - q_t)$ *versus* t, which explained the kinetic results best. The R^2 values for all the concentrations were higher

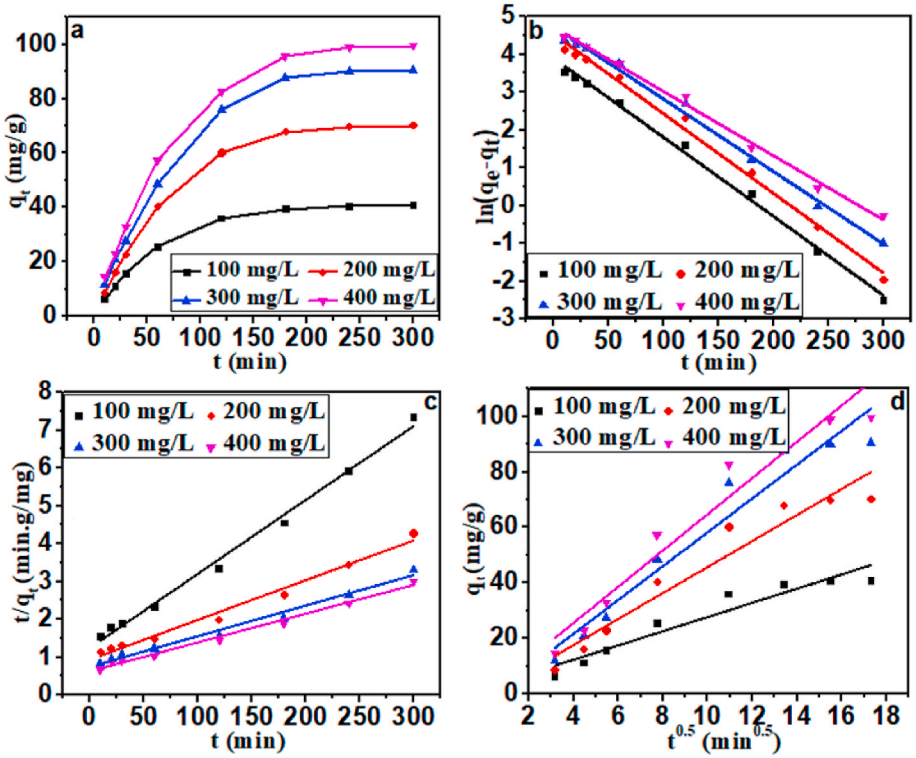

Fig. 6. Variation of 4-AP uptake with time at pH 7.0 & 25 °C (a), pseudo-first-order (b), pseudo-second-order (c) and intra-particle kinetic plot (d).

Table 3
Parameters obtained from different kinetic models for 4-AP adsorption onto the PSASA.

Parameters	Concentration			
	100 mg/L	200 mg/L	300 mg/L	400 mg/L
Pseudo-first-order				
k_1 (min^{-1})	2.09×10^{-2}	2.1×10^{-2}	1.91×10^{-2}	1.69×10^{-2}
q_e (mg/g)	48.97	92.64	112.94	111.06
r	−0.998	−0.997	−0.997	−0.997
R^2	0.996	0.994	0.994	0.995
Pseudo-second-order				
k_2 (g/mg.min)	3.07×10^{-4}	1.19×10^{-4}	8.82×10^{-5}	9.29×10^{-5}
q_e (mg/g)	51.15	95.14	123.76	131.57
r	0.996	0.992	0.993	0.995
R^2	0.993	0.985	0.986	0.990
Intra-particle				
k_p (g/mg. $min^{0.5}$)	2.55	4.67	6.08	6.51
C (mg/g)	2.04	−1.07	−2.69	−0.51
r	0.960	0.966	0.972	0.971
R^2	0.922	0.934	0.944	0.943

than 0.99, which means that the solvent does not affect the adsorption phenomenon [62]. From the graph and calculated values of rate constants, it is evident that the fastest adsorption took place for the initial concentration of 100 mg/L, this increase in adsorption uptake of 4-AP with time would probably be due to saturation of pores of the PSASA with 4-AP molecules.

The r and R^2 values for the plot of the pseudo-second-order and intra-particle model were lower than 0.99 and experimental data was inconsistent with the calculated parameters. The plots of the three kinetic models are shown in Fig. 6b–d.

3.8. Activation energy and thermodynamics of 4-AP adsorption onto PSASA

It is a well-known fact that the reaction temperature directly controls the rate of reaction and rate constant. The activation energy of adsorption is defined as the minimum energy required to complete the adsorption reaction. Using the Arrhenius equation, adsorption activation energy is determined based on the relationship between rate constant and reaction temperature. The Arrhenius equation is given by the following equation.

$$lnk_1 = lnA - \frac{E_a}{RT} \tag{13}$$

where, k_1 = pseudo-first-order rate constant (min^{-1}), A = frequency factor (min^{-1}) and E_a = activation energy (kJ/mol).

It was discussed above that the pseudo-first-order kinetics give the best-fit explanation to the kinetic data and so to calculate the activation energy of adsorption, we first performed the temperature based kinetics (Fig. 7a) and pseudo-first-order kinetic model (Fig. 7b) was modelled and Table 3 includes the k_1 values at different temperatures. . A graph (Fig. 7c) was plotted between lnk_1 *versus* 1/T and Table 4 show the values of Ea and A, respectively, computed from the slope and intercept. In the present study, the activation energy was found to be 7.898 kJ/mol confirming the physical nature of adsorption as this energy lies in the range of 5–40 kJ/mol [63].

The standard state thermodynamic parameters such as change in Gibbs free energy (ΔG^o), change in entropy (ΔS^o), and change in enthalpy (ΔH^o) were calculated with the following Eq.:

$$\Delta G^o = \Delta H^o - T\Delta S^o \tag{14}$$

$$lnK_L^o = \frac{\Delta S^o}{R} - \frac{\Delta H^o}{RT} \tag{15}$$

where $K_L{}^o$ is Langmuir constant in standard state; R is universal gas constant (J/mol.K); and T is absolute temperature (K), respectively.

Following formula was used to determine $K_L{}^o$,

$$\boldsymbol{K_L^o = K_L \times molecular\ weight\ of\ 4-AP \times 1000} \tag{16}$$

Numerous examples are reported in which ΔG^o is calculated from the

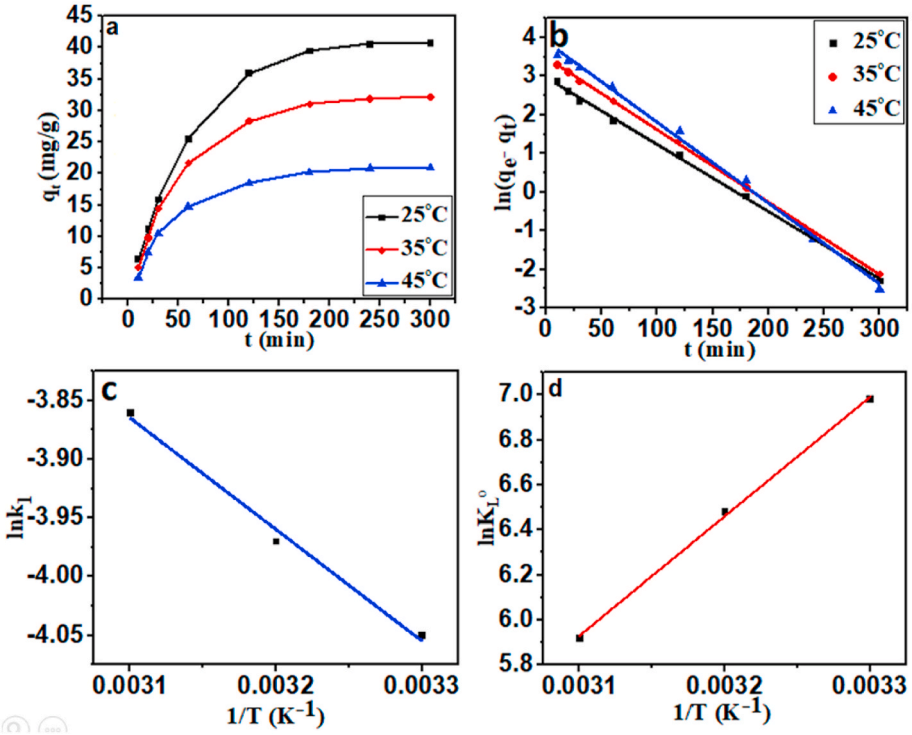

Fig. 7. Temperature based variation of 4-AP uptake with time for 100 mg/L concentration (a), the temperature-based pseudo-first-order kinetic plot for 100 mg/L concentration (b), Arrhenius plot between $\ln k_1$ *versus* 1/T, and thermodynamic plot between ln K_L° versus 1/T (d).

Table 4
Thermodynamic parameters of adsorption.

	25 °C	35 °C	45 °C	
k_1 (min^{-1})	1.73×10^{-2}	1.87×10^{-2}	2.09×10^{-2}	
E_a (kJ/mol)				7.89
A (min^{-1})				0.398
ΔG^o (kJ/mol)	−18.04	−17.17	−16.30	
K_L^o	9.31×10^2	5.64×10^2	3.22×10^2	
ΔH^o (kJ/mol)				−44.06
ΔS^o (J/K.mol)				−87.29

Langmuir constant (L/mg) without making it unitless, which shows a methodological error in thermodynamic data calculation [64]. In this study, we have first converted the Langmuir constant into the standard state, then other parameters were calculated with the help of Eq. (16) [65]. The graph representing the variation of lnK_L^o with 1/T is shown in Fig. 7d and obtained results are tabulated in Table 4. The negative value of ΔS^o indicated the favourable nature of adsorption due to a decrease in the randomness of the system. The exothermic behaviour of adsorption was verified by the negative value of ΔH^o. The ΔG^o calculated at different temperatures were in the range of -40-0 kJ/mol representing adsorption is taking place through physisorption mechanism and negative value confirm the spontaneous nature of adsorption.

4. Conclusions

The present study checked the adsorption potential of the PSASA towards toxic 4-AP removal from an aqueous medium. The PSASA exhibited greater adsorption potential than previously reported adsorbents. The adsorption of 4-AP onto the PSASA was controlled by temperature, pH, adsorbent dose and salt addition. Kinetic and adsorption isotherm was best explained by pseudo-first-order and Langmuir model indicating monolayer adsorption at the PSASA surface. Thermodynamic study confirmed the exothermic and physical nature of adsorption. Thus, It can be reasoned that adsorption is spontaneous, given PSASA's strong adsorption potential, its natural availability, and low cost of chemical activation. The environmental benefits of applying this type of adsorbent are fruitful as their regeneration is not required because it is freely available.

5. Funding information

There were no grants from the public, commercial, or not-for-profit organisations available to sponsor this research.

Conflicts of interest

The manuscript is the original work of authors. All the authors are mutually agreed for submitting this manuscript to 'Journal of the Indian Chemical Society' and have not been published before or submitted to another journal for the consideration of publication. The authors declare that they have no known competing financial interests or personal relationships that could have appeared to influence the work reported in this paper.

Declaration of competing interest

There is no conflict of interest between the authors.

Acknowledgements

PM is grateful to UGC, New Delhi for its financial support (UGC-SRF-133155). The authors also give IIT, Kanpur credit for providing some characterization facilities.

References

[1] P. Singh, A. Borthakur, A review on biodegradation and photocatalytic degradation of organic pollutants: a bibliometric and comparative analysis, J. Clean. Prod. 196 (2018) 1669–1680, https://doi.org/10.1016/J.JCLEPRO.2018.05.289.

[2] S. Zhang, B. Li, X. Wang, G. Zhao, B. Hu, Z. Lu, T. Wen, J. Chen, X. Wang, Recent developments of two-dimensional graphene-based composites in visible-light photocatalysis for eliminating persistent organic pollutants from wastewater, Chem. Eng. J. 390 (2020), 124642, https://doi.org/10.1016/J.CEJ.2020.124642.
[3] W. Raza, J. Lee, N. Raza, Y. Luo, K.H. Kim, J. Yang, Removal of phenolic compounds from industrial waste water based on membrane-based technologies, J. Ind. Eng. Chem. 71 (2019) 1–18, https://doi.org/10.1016/J.JIEC.2018.11.024.
[4] B. Wang, B. Huang, W. Jin, S. Zhao, F. Li, P. Hu, X. Pan, Occurrence, distribution, and sources of six phenolic endocrine disrupting chemicals in the 22 river estuaries around Dianchi Lake in China, Environ. Sci. Pollut. Res. 205 (20) (2012) 3185–3194, https://doi.org/10.1007/S11356-012-1236-Y, 2012.
[5] H.N. Catherine, M.H. Ou, B. Manu, Y. hsin Shih, Adsorption mechanism of emerging and conventional phenolic compounds on graphene oxide nanoflakes in water, Sci. Total Environ. 635 (2018) 629–638, https://doi.org/10.1016/J.SCITOTENV.2018.03.389.
[6] J.S. Park, M.T. Brown, T. Han, Phenol toxicity to the aquatic macrophyte Lemna paucicostata, Aquat. Toxicol. 106–107 (2012) 182–188, https://doi.org/10.1016/J.AQUATOX.2011.10.004.
[7] A. Markiewicz, K. Björklund, E. Eriksson, Y. Kalmykova, A.M. Strömvall, A. Siopi, Emissions of organic pollutants from traffic and roads: priority pollutants selection and substance flow analysis, Sci. Total Environ. 580 (2017) 1162–1174, https://doi.org/10.1016/J.SCITOTENV.2016.12.074.
[8] A. Tolosana-Moranchel, D. Ovejero, B. Barco, A. Bahamonde, E. Díaz, M. Faraldos, An approach on the comparative behavior of chloro/nitro substituted phenols photocatalytic degradation in water, J. Environ. Chem. Eng. 7 (2019), 103051, https://doi.org/10.1016/J.JECE.2019.103051.
[9] Z.L. Hegedus, U. Nayak, Para-aminophenol and structurally related compounds as intermediates in lipofuscin formation and in renal and other tissue toxicities, Arch. Physiol. Biochem. 99 (1991) 99–105, https://doi.org/10.3109/13813459109145911.
[10] P.D. Josephy, T. Eling, R.P. Mason, The horseradish peroxidase-catalyzed oxidation of 3,5,3',5'-tetramethylbenzidine. Free radical and charge-transfer complex intermediates, J. Biol. Chem. 257 (1982) 3669–3675, https://doi.org/10.1016/S0021-9258(18)34832-4.
[11] C. Klos, M. Koob, C. Kramer, W. Dekant, p-Aminophenol nephrotoxicity: biosynthesis of toxic glutathione conjugates, Toxicol. Appl. Pharmacol. 115 (1992) 98–106, https://doi.org/10.1016/0041-008X(92)90372-Y.
[12] G.J. Nohynek, D. Duche, A. Garrigues, P.A. Meunier, H. Toutain, J. Leclaire, Under the skin: biotransformation of para-aminophenol and para-phenylenediamine in reconstructed human epidermis and human hepatocytes, Toxicol. Lett. 158 (2005) 196–212, https://doi.org/10.1016/J.TOXLET.2005.03.014.
[13] J.C. de Souza, B.F. da Silva, D.A. Morales, G.de A. Umbuzeiro, M.V.B. Zanoni, Assessment of the autoxidation mechanism of p-toluenediamine by air and hydrogen peroxide and determination of mutagenic environmental contaminant in beauty salon effluent, Sci. Total Environ. 685 (2019) 911–922, https://doi.org/10.1016/J.SCITOTENV.2019.06.252.
[14] J.C. de Souza, M.V.B. Zanoni, A.M. Oliveira-Brett, Genotoxic permanent hair dye precursors p-aminophenol and p-toluenediamine electrochemical oxidation mechanisms and evaluation in biological fluids, J. Electroanal. Chem. 857 (2020), 113509, https://doi.org/10.1016/J.JELECHEM.2019.113509.
[15] J.C. de Souza, B.F. da Silva, D.A. Morales, G. de A. Umbuzeiro, M.V.B. Zanoni, Assessment of p-aminophenol oxidation by simulating the process of hair dyeing and occurrence in hair salon wastewater and drinking water from treatment plant, J. Hazard Mater. 387 (2020), 122000, https://doi.org/10.1016/J.JHAZMAT.2019.122000.
[16] Y. Park, G.A. Ayoko, R. Kurdi, E. Horváth, J. Kristóf, R.L. Frost, Adsorption of phenolic compounds by organoclays: implications for the removal of organic pollutants from aqueous media, J. Colloid Interface Sci. 406 (2013) 196–208, https://doi.org/10.1016/J.JCIS.2013.05.027.
[17] A. Dabrowski, Adsorption — from theory to practice, Adv. Colloid Interface Sci. 93 (2001) 135–224, https://doi.org/10.1016/S0001-8686(00)00082-8.
[18] J.T. Trimmer, D.C. Miller, J.S. Guest, Resource recovery from sanitation to enhance ecosystem services, 2019, Nat. Sustain. 28 (2) (2019) 681–690, https://doi.org/10.1038/s41893-019-0313-3.
[19] M. Darder, P. Aranda, C. Ruiz-García, F.M. Fernandes, E. Ruiz-Hitzky, The meeting point of carbonaceous materials and clays: toward a new generation of functional composites, Adv. Funct. Mater. 28 (2018), 1704323, https://doi.org/10.1002/ADFM.201704323.
[20] T.A. Saleh, P. Parthasarathy, M. Irfan, Advanced functional polymer nanocomposites and their use in water ultra-purification, Trends Environ. Anal. Chem. 24 (2019), e00067, https://doi.org/10.1016/J.TEAC.2019.E00067.
[21] S.J.T. Pollard, G.D. Fowler, C.J. Sollars, R. Perry, Low-cost adsorbents for waste and wastewater treatment: a review, Sci. Total Environ. 116 (1992) 31–52, https://doi.org/10.1016/0048-9697(92)90363-W.
[22] S. Praveen, R. Gokulan, T.B. Pushpa, J. Jegan, Techno-economic feasibility of biochar as biosorbent for basic dye sequestration, J. Indian Chem. Soc. 98 (2021), 100107, https://doi.org/10.1016/J.JICS.2021.100107.
[23] M. Qiu, B. Hu, Z. Chen, H. Yang, L. Zhuang, X. Wang, Challenges of organic pollutant photocatalysis by biochar-based catalysts, 2021, Biochar 32 (3) (2021) 117–123, https://doi.org/10.1007/S42773-021-00098-Y.
[24] L. Liang, F. Xi, W. Tan, X. Meng, B. Hu, X. Wang, Review of organic and inorganic pollutants removal by biochar and biochar-based composites, 2021 33, Biochar 3 (2021) 255–281, https://doi.org/10.1007/S42773-021-00101-6.
[25] F. Liu, S. Hua, C. Wang, M. Qiu, L. Jin, B. Hu, Adsorption and reduction of Cr(VI) from aqueous solution using cost-effective caffeic acid functionalized corn starch, Chemosphere 279 (2021) 130539, https://doi.org/10.1016/J.CHEMOSPHERE.2021.130539.
[26] K.C. Bedin, A.C. Martins, A.L. Cazetta, O. Pezoti, V.C. Almeida, KOH-activated carbon prepared from sucrose spherical carbon: adsorption equilibrium, kinetic and thermodynamic studies for Methylene Blue removal, Chem. Eng. J. 286 (2016) 476–484, https://doi.org/10.1016/J.CEJ.2015.10.099.
[27] J.Q. Jiang, S.M. Ashekuzzaman, Development of novel inorganic adsorbent for water treatment, Curr. Opin. Chem. Eng. 1 (2012) 191–199, https://doi.org/10.1016/J.COCHE.2012.03.008.
[28] X.R. Zhao, X. Xu, J. Teng, N. Zhou, Z. Zhou, X.Y. Jiang, F.P. Jiao, J.G. Yu, Three-dimensional porous graphene oxide-maize amylopectin composites with controllable pore-sizes and good adsorption-desorption properties: facile fabrication and reutilization, and the adsorption mechanism, Ecotoxicol. Environ. Saf. 176 (2019) 11–19, https://doi.org/10.1016/J.ECOENV.2019.03.069.
[29] R. Shan, Y. He, T. Zi, G. Wang, X. Liu, Z. Han, T. Zhang, Y. Zhu, Immobilization of calcined layered double hydroxide into alginate hydrogel beads for PNP and PAP removal: kinetics, isotherms, thermodynamics, and mechanism, water, Air. Soil Pollut. 229 (2018) 1–18, https://doi.org/10.1007/S11270-018-3976-X/FIGURES/11.
[30] B.B. Tewari, M. Boodhoo, Removal of p-aminophenol and p-nitrophenol from aqueous solution through adsorption on antimony, cadmium, and zirconium ferrocyanides, J. Colloid Interface Sci. 289 (2005) 328–332, https://doi.org/10.1016/J.JCIS.2005.04.032.
[31] X. Li, X. Zhou, J. Mu, L. Lu, D. Han, C. Lu, M. Wang, Thermodynamics and kinetics of p -aminophenol adsorption on poly(aryl ether ketone) containing pendant carboxyl groups, J. Chem. Eng. Data 56 (2011) 4274–4277, https://doi.org/10.1021/JE2009297.
[32] R. Dod, G. Banerjee, S. Saini, Adsorption of methylene blue using green pea peels (pisum sativum): a cost-effective option for dye-based wastewater treatment, Biotechnol. Bioproc. Eng. 17 (2012) 862–874, https://doi.org/10.1007/s12257-011-0614-5.
[33] K. Singh, A. Kumar, S.K. Pandey, S. Awasthi, S.P. Gupta, P. Mishra, Interpretation of adsorption behavior of carboxymethyl cellulose onto functionalized accurel polymeric surface, Ind. Eng. Chem. Res. 59 (2020) 19102–19116, https://doi.org/10.1021/ACS.IECR.0C03894.
[34] D. Prakash, N.N. Nawani, A rapid and improved technique for scanning electron microscopy of actinomycetes, J. Microbiol. Methods 99 (2014) 54–57, https://doi.org/10.1016/J.MIMET.2014.02.005.
[35] A. Abdelhay, A. Al Bsoul, A. Al-Othman, N.M. Al-Ananzeh, I. Jum'h, A.A. Al-Taani, Kinetic and thermodynamic study of phosphate removal from water by adsorption onto (Arundo donax) reeds, Adsorpt. Sci. Technol. 36 (2018) 46–61, https://doi.org/10.1177/0263617416684347.
[36] A. Al Bsoul, M. Hailat, A. Abdelhay, M. Tawalbeh, A. Al-Othman, I.N. Al-kharabsheh, A.A. Al-Taani, Efficient removal of phenol compounds from water environment using Ziziphus leaves adsorbent, Sci. Total Environ. 761 (2021), 143229, https://doi.org/10.1016/J.SCITOTENV.2020.143229.
[37] K. Singh, A. Kumar, S. Awasthi, S.K. Pandey, P. Mishra, Adsorption mechanism of carboxymethyl cellulose onto mesoporous mustard carbon: experimental and theoretical aspects, Colloids Surfaces A Physicochem. Eng. Asp. 581 (2019), 123786, https://doi.org/10.1016/J.COLSURFA.2019.123786.
[38] C. Ng, J.N. Losso, W.E. Marshall, R.M. Rao, Freundlich adsorption isotherms of agricultural by-product-based powdered activated carbons in a geosmin–water system, Bioresour. Technol. 85 (2002) 131–135, https://doi.org/10.1016/S0960-8524(02)00093-7.
[39] G.D. Halsey, The role of surface heterogeneity in adsorption, Adv. Catal. 4 (1952) 259–269, https://doi.org/10.1016/S0360-0564(08)60616-1.
[40] S. Fan, Y. Wang, Z. Wang, J. Tang, J. Tang, X. Li, Removal of methylene blue from aqueous solution by sewage sludge-derived biochar: adsorption kinetics, equilibrium, thermodynamics and mechanism, J. Environ. Chem. Eng. 5 (2017) 601–611, https://doi.org/10.1016/J.JECE.2016.12.019.
[41] I. Langmuir, The constitution and fundamental properties OF solids and liquids. Part I. Solids, J. Am. Chem. Soc. 38 (2002) 2221–2295, https://doi.org/10.1021/JA02268A002.
[42] X. Guo, J. Wang, A general kinetic model for adsorption: theoretical analysis and modeling, J. Mol. Liq. 288 (2019), https://doi.org/10.1016/J.MOLLIQ.2019.111100.
[43] M. Wolthers, L. Charlet, P. Van Cappellen, The surface chemistry of divalent metal carbonate minerals; a critical assessment of surface charge and potential data using the charge distribution multi-site ion complexation model, Am. J. Sci. 308 (2008) 905–941, https://doi.org/10.2475/08.2008.02.
[44] E.P. Barrett, L.G. Joyner, P.P. Halenda, The determination of pore volume and area distributions in porous substances. I. Computations from nitrogen isotherms, J. Am. Chem. Soc. 73 (2002) 373–380, https://doi.org/10.1021/JA01145A126.
[45] A. Dabrowski, Adsorption — from theory to practice, Adv. Colloid Interface Sci. 93 (2001) 135–224, https://doi.org/10.1016/S0001-8686(00)00082-8.
[46] Z. Li, D. Liu, Y. Cai, Y. Wang, J. Teng, Adsorption pore structure and its fractal characteristics of coals by N2 adsorption/desorption and FESEM image analyses, Fuel 257 (2019), 116031, https://doi.org/10.1016/J.FUEL.2019.116031.
[47] H. Zhu, Y. Ju, C. Huang, F. Chen, B. Chen, K. Yu, Microcosmic gas adsorption mechanism on clay-organic nanocomposites in a marine shale, Energy 197 (2020), 117256, https://doi.org/10.1016/J.ENERGY.2020.117256.
[48] K. Singh, A. Kumar, P. Mishra, S.P. Gupta, Binding aspects of carboxymethyl cellulose onto polymeric surface from its aqueous solutions, J. Dispersion Sci. Technol. (2020) 1–14, https://doi.org/10.1080/01932691.2020.1786396.

[49] J.H. van der Maas, E.T.G. Lutz, Structural information from OH stretching frequencies monohydric saturated alcohols, 2005–2019, Spectrochim. Acta Part A Mol. Spectrosc. 30 (1974), https://doi.org/10.1016/0584-8539(74)80047-4.
[50] A.S. Wexler, Infrared determination of structural units in organic compounds by integrated intensity measurements: alkanes, alkenes and monosubstituted alkyl benzenes, Spectrochim. Acta 21 (1965) 1725–1742, https://doi.org/10.1016/0371-1951(65)80085-6.
[51] E. Altintig, M. Onaran, A. Sarı, H. Altundag, M. Tuzen, Preparation, characterization and evaluation of bio-based magnetic activated carbon for effective adsorption of malachite green from aqueous solution, Mater. Chem. Phys. 220 (2018) 313–321, https://doi.org/10.1016/J.MATCHEMPHYS.2018.05.077.
[52] S.B. Lima, S.M.S. Borges, M. do C. Rangel, S.G. Marchetti, Effect of iron content on the catalytic properties of activated carbon-supported magnetite derived from biomass, J. Braz. Chem. Soc. 24 (2013) 344–354, https://doi.org/10.5935/0103-5053.20130044.
[53] G. Feiqiang, L. Xiaolei, J. Xiaochen, Z. Xingmin, G. Chenglong, R. Zhonghao, Characteristics and toxic dye adsorption of magnetic activated carbon prepared from biomass waste by modified one-step synthesis, Colloids Surfaces A Physicochem. Eng. Asp. 555 (2018) 43–54, https://doi.org/10.1016/J.COLSURFA.2018.06.061.
[54] A. Mandal, N. Bar, S.K. Das, Phenol removal from wastewater using low-cost natural bioadsorbent neem (Azadirachta indica) leaves: adsorption study and MLR modeling, Sustain. Chem. Pharm. 17 (2020), 100308, https://doi.org/10.1016/J.SCP.2020.100308.
[55] A. Mandal, S.K. Das, Phenol adsorption from wastewater using clarified sludge from basic oxygen furnace, J. Environ. Chem. Eng. 7 (2019), 103259, https://doi.org/10.1016/J.JECE.2019.103259.
[56] Y. Li, X. Hu, X. Liu, Y. Zhang, Q. Zhao, P. Ning, S. Tian, Adsorption behavior of phenol by reversible surfactant-modified montmorillonite: mechanism, thermodynamics, and regeneration, Chem. Eng. J. 334 (2018) 1214–1221, https://doi.org/10.1016/J.CEJ.2017.09.140.
[57] C.H. Giles, D. Smith, A. Huitson, A general treatment and classification of the solute adsorption isotherm. I. Theoretical, J. Colloid Interface Sci. 47 (1974) 755–765, https://doi.org/10.1016/0021-9797(74)90252-5.
[58] O. Hamdaoui, E. Naffrechoux, Modeling of adsorption isotherms of phenol and chlorophenols onto granular activated carbon: Part I. Two-parameter models and equations allowing determination of thermodynamic parameters, J. Hazard Mater. 147 (2007) 381–394, https://doi.org/10.1016/J.JHAZMAT.2007.01.021.
[59] K.R. Hall, L.C. Eagleton, A. Acrivos, T. Vermeulen, Pore- and solid-diffusion kinetics in fixed-bed adsorption under constant-pattern conditions, Ind. Eng. Chem. Fundam. 5 (2002) 212–223, https://doi.org/10.1021/I160018A011.
[60] P. Mishra, K. Singh, U. Dixit, Adsorption, kinetics and thermodynamics of phenol removal by ultrasound-assisted sulfuric acid-treated pea (Pisum sativum) shells, Sustain. Chem. Pharm. 22 (2021), 100491, https://doi.org/10.1016/J.SCP.2021.100491.
[61] E.C. Lima, F. Sher, A. Guleria, M.R. Saeb, I. Anastopoulos, H.N. Tran, A. Hosseini-Bandegharaei, Is one performing the treatment data of adsorption kinetics correctly? J. Environ. Chem. Eng. 9 (2021), 104813 https://doi.org/10.1016/J.JECE.2020.104813.
[62] D.C.S. Alves, B.B. Coseglio, L.A.A. Pinto, T.R.S. Cadaval, Development of Spirulina/chitosan foam adsorbent for phenol adsorption, J. Mol. Liq. 309 (2020), 113256, https://doi.org/10.1016/J.MOLLIQ.2020.113256.
[63] M. Zulfiqar, S. Sufian, N.E. Rabat, N. Mansor, Photocatalytic degradation and adsorption of phenol by solvent-controlled TiO2 nanosheets assisted with H2O2 and FeCl3: kinetic, isotherm and thermodynamic analysis, J. Mol. Liq. 308 (2020), 112941, https://doi.org/10.1016/J.MOLLIQ.2020.112941.
[64] E.C. Lima, F. Sher, M.R. Saeb, M. Abatal, M.K. Seliem, Comments on "Reasonable calculation of the thermodynamic parameters from adsorption equilibrium constant, J. Mol. Liq. 334 (2021) 116542, J. Mol. Liq. 322 (2021), 114980, https://doi.org/10.1016/J.MOLLIQ.2021.116542.
[65] E.C. Lima, A. Hosseini-Bandegharaei, J.C. Moreno-Piraján, I. Anastopoulos, A critical review of the estimation of the thermodynamic parameters on adsorption equilibria. Wrong use of equilibrium constant in the Van't Hoof equation for calculation of thermodynamic parameters of adsorption, J. Mol. Liq. 273 (2019) 425–434, https://doi.org/10.1016/J.MOLLIQ.2018.10.048.

Sustainable Chemistry and Pharmacy 22 (2021) 100491

Contents lists available at ScienceDirect

Sustainable Chemistry and Pharmacy

journal homepage: www.elsevier.com/locate/scp

Adsorption, kinetics and thermodynamics of phenol removal by ultrasound-assisted sulfuric acid-treated pea (*Pisum sativum*) shells

Prashant Mishra, Kaman Singh *, Utkarsh Dixit

Advance Center of Surface Science, Department of Chemistry, Babasaheb Bhimrao Ambedkar University (A Central University), Lucknow, 226025, India

ARTICLE INFO

Keywords:
Phenol adsorption
Pea shells
Pseudo-second-order
Langmuir isotherm

ABSTRACT

In the present study, waste pea shells were used to synthesize an efficient adsorbent (ultrasound-assisted sulphuric acid-treated pea shells, USAPS) and was applied for phenol removal. The USAPS characterization was done by SEM-EDS, FT-IR, XRD, optical profilometry, BET, and PZC techniques. The use of ultrasound during the chemical activation significantly enhanced the adsorption properties. The adsorption of phenol was probed by varying pH (2–9), temperature (25–45°C), the USAPS dose (0.1–0.6 g/100ml), phenol concentration (50–500 mg/L), and inorganic salt addition (0.1 M KCl and 0.1 M $CaCl_2$). The maximum phenol uptake was found to be 125.77 mg/g for 500 mg/L of phenol concentration at pH 7 and 25°C with 0.1 g/100ml of the USAPS dose. Adsorption was negatively affected by an increase in temperature and the USAPS dose while 0.1 M KCl and 0.1 M $CaCl_2$ addition decreased the maximum phenol uptake from 125.77 mg/g to 103.45 mg/g and 84.11 mg/g, respectively. The time-dependent phenol removal was best explained by the pseudo-second-order kinetic model while equilibrium data were best explained by the Langmuir model. The thermodynamic study revealed the physical nature of adsorption with no structural alteration at the adsorbent-adsorbate interface.

1. Introduction

The continuous growth of the worldwide population leads to a regular augmentation in demand for energy resources and fresh water for their daily needs. To meet the demands of the people, industrial activities increase proportionally which leads to a discharge of toxic wastewater into aquatic systems of the environment (Pham et al., 2020). People are gradually becoming aware of the drawbacks of the preceding activities as these are liable for increased emissions of greenhouse gases and climate change (Alami et al., 2020; Tawalbeh et al., 2019). Phenol and its derivatives are considered critical pollutants for the aquatic environment and are found in wastewater of various industries such as pharmaceutical, steel, plastic, petroleum, rubber plants, and coal tar (Mu'azu et al., 2020; Mukherjee and De, 2014). Phenols have been included in the list of priority pollutants by Environmental Protection Agencies of the United States and European Union (Chakraborty et al., 2019) and these agencies fixed the maximum permissible concentration of phenol to 1 ppm (El-Naas et al., 2010) whereas WHO fixed the maximum concentration to 0.001 ppm in clean and drinkable water (Mandal et al., 2020b). The same concentration is accepted by the Government of India (Dutta et al., 2006). Toxicity caused by phenolic compounds results in various health problems such as vomiting, unconsciousness, dermatitis, bronchial asthma, cerebral pains and infection to the liver and kidneys (Mohammadi et al., 2015; Mukherjee and De, 2014).

The removal of phenol from wastewater effluents has attracted researchers and environmentalists due to its harmful effect on the environment and humans. As phenolic compounds are produced naturally and by anthropogenic activities, so various techniques have been used to bring down the concentration to the permissible extent and such techniques are photo-Fenton (Al Momani et al., 2004), electrocoagulation (Karami et al., 2018), adsorption, membrane processes (Bódalo et al., 2008), ultrasound, biodegradation, steam plasma jet treatment (Ni et al., 2013), and catalytic air oxidation (Sun et al., 2020). The most popular technique for the removal of organic and inorganic pollutants is adsorption whereas activated carbon is the most effective and commonly used adsorbent but despite its high adsorption capacity, it is considered expensive as its high regeneration cost restricts its further utilization (Lin and Juang, 2009; Mukherjee and De, 2014; Tran et al., 2015). Therefore, adsorbents derived from various agricultural wastes have been synthesized as an alternative to the activated carbon and to make the adsorption process feasible and cost-effective (Shokoohi et al.,

* Corresponding author.
E-mail address: singh.kaman@bbau.ac.in (K. Singh).

https://doi.org/10.1016/j.scp.2021.100491
Received 2 June 2021; Received in revised form 15 July 2021; Accepted 17 July 2021

2017).

Several researchers reported the adsorption potential and benefits of using different natural agriculture wastes such as rice husk, eucalyptus leaves, date seeds, banana peels, tea residues, sawdust residues, ziziphus leaves (Abdallah, 2012; Bsoul, 2014; Babel and Kurniawan, 2003; Rengaraj et al., 2002; Mane et al., 2005; Al Bsoul et al., 2021; Jadhav and Vanjara, 2004). Nadavala et al. checked the adsorption potential of pine bark for the removal of phenolic compounds and reported the maximum adsorption capacity of pine bark was 143 mg/g at optimum conditions (Nadavala et al., 2014). In addition to these, some modifications have also been done in the conventional activated carbon such as a composite material prepared from activated carbon modified with chitosan in a 1:1 ratio showing almost 95% of phenol removal at concentrations less than 50 ppm (Carvajal-Bernal et al., 2015). Some adsorbents were also prepared by chemical activation methods like Ashanendu and Sudip reported phenol removal from wastewater by clarified sludge from basic oxygen furnace giving 63% of phenol removal at optimum conditions (Mandal and Das, 2019), Shubham et al. reported phenol removal by corn husk derived magnetized activated carbon (Mishra et al., 2019), Thue et al. synthesized microwave-assisted activated carbon from wood chips for removal of phenol (Thue et al., 2016). Kong et al. reported phenol removal by Toona Sinensis leaves activated with NaOH (Kong et al., 2020). Park et al. reported removal of bisphenol by activated carbon impregnated with nanoparticles of iron oxide (Park et al., 2015), Singh et al. used inexpensive adsorbent from agro-waste (mustard cake) for effective removal of phenol (Singh et al., 2016). The adsorption potential of modified polypropylene for removal of phenolics was studied by Singh et al. (2013).

Pea (***Pisum sativum***) is a cold season plant and grown in various parts of the world from winter to early summers. Pea is grown in a large area in India during winters and its waste i.e. pea shells (PS) is freely available in the market and household.

In the present work, a novel chemically modified adsorbent of PS is reported for effective phenol removal. Its characteristic features make it an efficient adsorbent for phenol removal. The adsorbent is characterized by SEM-EDS, FT-IR, XRD, BET-surface area analysis, optical profilometry and PZC. The mechanism of phenol removal is studied by various experiments such as the effect of pH, adsorbent concentration, temperature, surface charge analysis, inorganic salt addition (KCl and $CaCl_2$). In addition to this, the applicability of different kinetic and adsorption isotherm models were modelled to interpret the adsorption mechanism.

2. Experimental section

2.1. Preparation of ultrasound-assisted sulphuric acid-treated pea shells (USAPS)

Waste pea shells were collected from the local households and washed manifold with deionized water so that water-soluble and insoluble impurities could be removed. The PS was then dried in sunlight for a few days and ground by a mechanical grinder and sieved to particle size less than 75 μm. For chemical activation, the PS was added into 50% v/v H_2SO_4 in a 2:1 ratio. The paste of PS and H_2SO_4 were kept under the ultrasonicator (Sonics Vibra-Cell VCX750) and the power of 25 kHz ultrasound was given for 1 h, after that, the paste was taken out of the sonicator and left for 24 h. After 24 h, this paste was put into the muffle furnace for carbonization at 750°C for 30 min. The sample was then washed, dried and kept in a desiccator for further use.

2.2. Characterization of adsorbent

The surface morphology of the USAPS was probed by scanning electron microscopy (SEM) analysis whereas the elemental composition of the USAPS sample was determined by a micro-analytical method of energy-dispersive x-ray spectroscopy (EDS). Both the analysis was carried out using JEOL, Japan; model JSM-6490LV. The functional group analysis of the USAPS sample was done by FT-IR spectrophotometer (Thermo- Scientific Nicole 6700, USA). The spectrum was recorded in the range of 4000–400 cm^{-1} with 32 scans and a resolution of 5–7 cm^{-1}. Phase analysis of the USAPS was done by powder x-ray diffractometer (RigakuMiniflex II desktop). The USAPS was scanned in a range of 20° to 70° with a scanning rate of 2°/min by copper Kα radiation (λ = 1.5405 A°). Raw data were processed by using origin and match3 software. The topographical parameters and aerial image of the USAPS surface were determined by an optical profilometer (Bruker, USA). The porous character, surface area, and mean pore size of the USAPS were determined by using the N_2 adsorption-desorption curve, BET analysis and Barret-Joyner-Halenda (BJH) method, respectively. The surface area analysis was carried out using a BET surface area analyzer (BELSORP-max, Japan). The PZC measurement was done by using the method of Singh et al. (2020).

2.3. Batch adsorption experiments

Batch adsorption experiments were performed several times to examine the effect of various experimental conditions on the removal of phenol by the USAPS. In each experiment, 100 ml phenol solution at different concentrations was taken into a 100 ml conical flask at different temperatures and pH whereas 0.1 g of the USAPS dose was fixed. The initial concentration of phenol was in the range of 50–500 mg/L. The equilibrium was achieved in 3 h but some samples were left for 6 h and 12 h and the same results were obtained. To know the time dependence of phenol removal, samples were analyzed at particular time intervals using a Systronic double beam spectrophotometer at wavelength 270 nm.

The amount of phenol adsorbed at equilibrium is expressed and calculated by the following equation:-

$$q_e = \frac{(C_0 - C_e)V_s}{m} \quad (1)$$

Where, q_e: the amount of phenol adsorbed at equilibrium, C_o: initial phenol concentration, C_e: phenol concentration at equilibrium, V_s: volume of solution (in L), m: mass of the USAPS added (in g)

The amount of phenol adsorbed at a particular time is expressed and calculated by the following equation:

$$q_t = \frac{(C_0 - C_t)V_s}{m} \quad (2)$$

Where, q_t: the amount of phenol adsorbed at time t (in mg/g), C_t: concentration of phenol at time t (in mg/L).

2.4. Adsorption isotherm

Freundlich, Temkin, and Langmuir adsorption isotherm models were modelled to explain the equilibrium data. The linear form of these isotherms are represented by the following equations:

2.4.1. Freundlich isotherm

$$lnq_e = lnK_F + \frac{1}{n} lnC_e \quad (3)$$

Maximum adsorption capacity (q_m) is calculated by using the equation given by Halsey (1952):

$$K_F = q_m / C_o^{1/n} \quad (4)$$

Where, K_F: Freundlich constant ($mg^{1-(1/n)}$ $L^{1/n}/g$); 1/n: intensity of adsorption; C_o: initial concentration.

2.4.2. Temkin isotherm

$$q_e = \frac{RT}{b} lnK_T + \frac{RT}{b} lnC_e \quad (5)$$

Where, K_T: Temkin constant (L/g) and b: the heat of adsorption constant (J/mol).

2.4.3. Langmuir isotherm

$$\frac{C_e}{q_e} = \frac{1}{q_m K_L} + \frac{C_e}{q_m} \quad (6)$$

Where, K_L: Langmuir constant (L/mg) and q_m (mg/g): maximum adsorption.

2.5. Kinetic study

Kinetic data were analyzed by the pseudo-first-order, pseudo-second-order and Intra-particle diffusion models. These models are represented by the following equations:

2.5.1. Pseudo-first-order model

$$\ln(q_e - q_t) = lnq_e - k_1 \quad (7)$$

2.5.2. Pseudo-second-order model

$$\frac{t}{q_t} = \frac{1}{k_2 q_e^2} + \frac{t}{q_e} \quad (8)$$

Where, k_1: pseudo-first-order (min^{-1}) and k_2: pseudo-second-order rate constant (g/mg.min), respectively.

2.5.3. Intra-particle diffusion model

$$q_t = k_p t^{0.5} + C \quad (9)$$

Where, k_p: particle related rate constant ($g/mg.min^{0.5}$), and C: constant (mg/g).

3. Results and discussion

3.1. Characterization of the USAPS

The surface morphology of the USAPS was obtained by SEM analysis. The SEM image of the USAPS is shown in Fig. 1a. It is apparent from the SEM image that the USAPS has a very irregular surface morphology. A variety of cages and voids are randomly distributed over the USAPS surface. These cages/voids are formed due to the treatment of PS with sulphuric acid and very high temperatures. These cages provide better conditions for the phenol molecules to get trapped into it (Bandosz and Ania, 2018; Giannakoudakis et al., 2019; Christina Kampouraki et al., 2019; Kyzas et al., 2014). The EDS spectrum of the USAPS is shown in Fig. S1, which shows that C, O, S, and Ca are the main elements found in the USAPS. The weight percentage of C, O, S, and Ca are 27.74%, 57.82%, 9.44% and 5.00%, respectively. The SEM image of the ultrasound-assisted sulphuric acid-treated pea shells after adsorption (USAPSAA) is shown in Fig. 1b. From Fig. 1b, it can be seen that the crystals of phenol are deposited over the USAPS surface.

The functional group analysis of the USAPS and the USAPSAA was done by FT-IR spectroscopy and the spectrum is shown in Fig. 1c. The intensive band was observed with three small peaks at 3606.1 cm^{-1}, 3549.3 cm^{-1} and 3407.7 cm^{-1}, these bands may be related to stretching vibrations of the O–H group of pure and hydrogen-bonded alcohol, water or carboxylic acid (Cooke et al., 1986; Zhao et al., 2008). A weak band at 2224.7 cm^{-1} may be related to the –C≡C- triple bond of alkynes (Zhao et al., 2008). The sharp band was observed at 1624.8 cm^{-1} which may be present due to C=C stretching. The band observed at 1146.4 cm^{-1} was probably due to the C–O stretching of a tertiary alcohol. The bands below 700 cm^{-1} may be observed due to C–S, S–O and C–O bending vibrations. In the FT-IR spectrum of the USAPSAA, two major changes were observed. A small band with weak intensity was observed

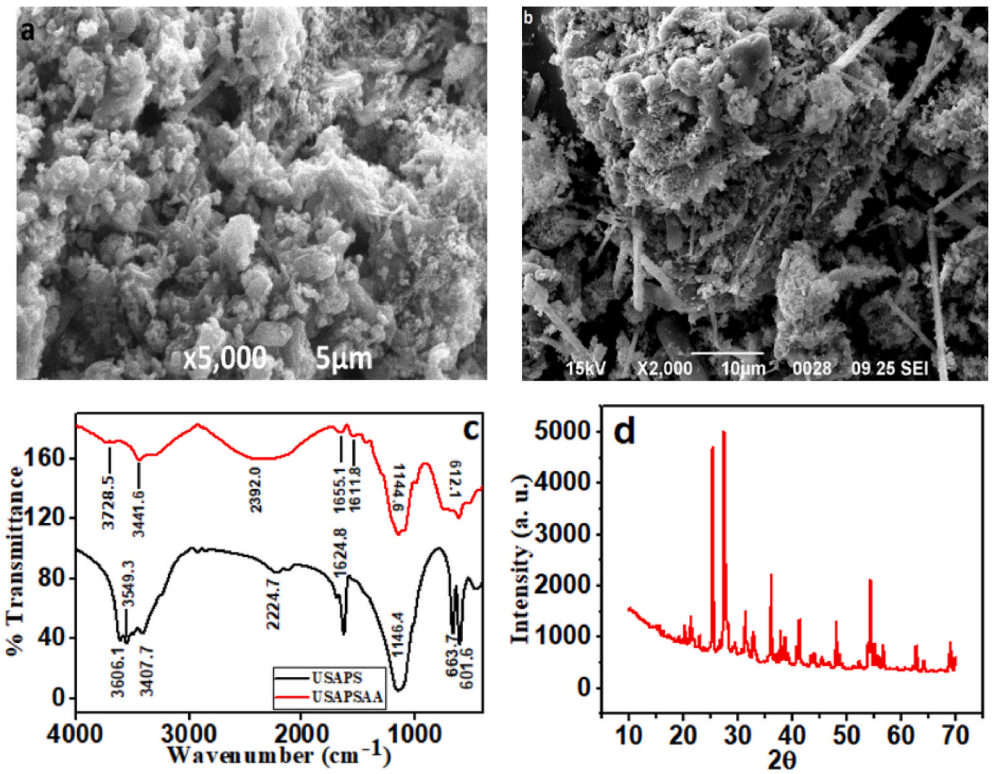

Fig. 1. SEM image of the USAPS (a) and The USAPSAA (b), FT-IR spectrum of the USAPS and the USAPSAA (c) and XRD spectrum (d) of the USAPS.

at 3728.5 cm^{-1} and two bands with weak intensity were observed at 1655.1 cm^{-1} and 1611.8 cm^{-1}. The band at 3728.5 cm^{-1} was attributed to O–H stretching vibration of water molecules confirming the solvent effect during the adsorption process (Liu et al., 2010). The bands observed at 1655.1 cm^{-1} and 1611.8 cm^{-1} were due to a change in bond strength of C═C confirming the electron exchange between the USAPS surface and the aromatic ring of phenol (Kang et al., 2019; Zeng et al., 2019).

XRD spectrum of the USAPS is shown in Fig. 1d. The XRD spectrum was consist of two major peaks in the range of 20° to 30° which is the characteristic feature of activated carbon (Lima et al., 2013). Some smaller peaks were also observed in the range 40° to 70° which were probably due to calcium-containing compounds. The degree of crystallinity study confirmed the amorphous nature of the USAPS as it has 77.76% amorphous content and 24.24% crystalline content.

The surface topography and topographical parameters of the USAPS were determined by an optical profilometer in veridical scanning interferometry (VSI) mode. The topographical image of the USAPS is shown in Fig. 2a, which shows the high unevenness of the USAPS surface with high values of Roughness average (Ra = 14.403 μm), Root mean square roughness (Rq = 18.732 μm), and Maximum profile peak height (Rp = 51.484 μm). From the profilometry image, it is apparent that a high number of valleys are present under the USAPS surface which confirms the porous nature of the USAPS and gives an indication that capillary phenomenon may also take place during the adsorption-desorption cycle. The higher difference between Maximum profile height (Rt = 163.76 μm) and Maximum profile valley depth (Rv = −112.276 μm) confirms the availability of a sufficient number of adsorption sites over the USAPS surface. The comparative assessment without and with ultrasonic treatment revealed that the average roughness of the synthesized adsorbent increased from 11.208 μm to 14.403 μm. The optical profilometry image and topographical parameters of adsorbent without ultrasonic treatment are shown in Fig. S2.

BET surface area analysis was used to determine the physicochemical characteristics of the USAPS surface which are specific surface area, mean pore diameter and total pore volume. The adsorption-desorption curve of N_2 onto the USAPS surface is shown in Fig. 2b Hysteresis loop (H_3 type) was observed in the adsorption-desorption curve which confirmed the lower desorption of N_2. This lower desorption of N_2 is observed when some of the N_2 molecules get adsorbed in the capillaries present on the USAPS surface. In addition, the hysteresis loop in the adsorption-desorption curve confirms the porous nature of the USAPS surface. A similar adsorption-desorption curve was reported by Singh et al. (2019). The BET method (Fig. 2c) was used to determine the specific surface area (S_{BET}) and mean pore diameter of the USAPS and was found to be 7.0735 m^2/g and 63.712 nm respectively. The value of mean pore diameter confirmed the macroporous nature of the USAPS based on the IUPAC nomenclature of porous materials (microporous: <2 nm; mesoporous: 2–50 nm; and macroporous: >50 nm) (Dąbrowski, 2001). The BJH model (Fig. 2d) was used to determine the total pore volume of the USAPS surface and was found to be 0.1139 cm^3/g.

3.2. Point of zero charge (PZC) of the USAPS

The PZC value tells about the pH value at which the charge at the surface of a material is zero. The overall charge of the surface will be positive at the pH value below PZC while an overall charge of the surface will be negative at pH values higher than PZC. In the case of the USAPS, the PZC value lies in the basic range and was found to be 8.38 which means, at pH 8.38, the USAPS surface was neutral whereas at pH below and above 8.38, the net surface charge of the USAPS was positive and negative, respectively. The graph of PZC is depicted in supplementary data (Fig. S3).

3.3. Effect of pH

The variation of phenol uptake with pH is shown in Fig. 3a. While performing the experiments, the pH of the solution was kept in the range of 2–9 whereas other parameters such as phenol concentration (50 mg/L), the USAPS dose (0.1g/100 ml), contact time (180 min) and temperature (25°C) were kept constant. Experiments were repeated for phenol concentrations (100–200 mg/L). The efficiency of adsorption above the initial pH 9 was not checked as the PZC of the USAPS was found to be 8.38. From Fig. 3a, it was found that adsorption of phenol

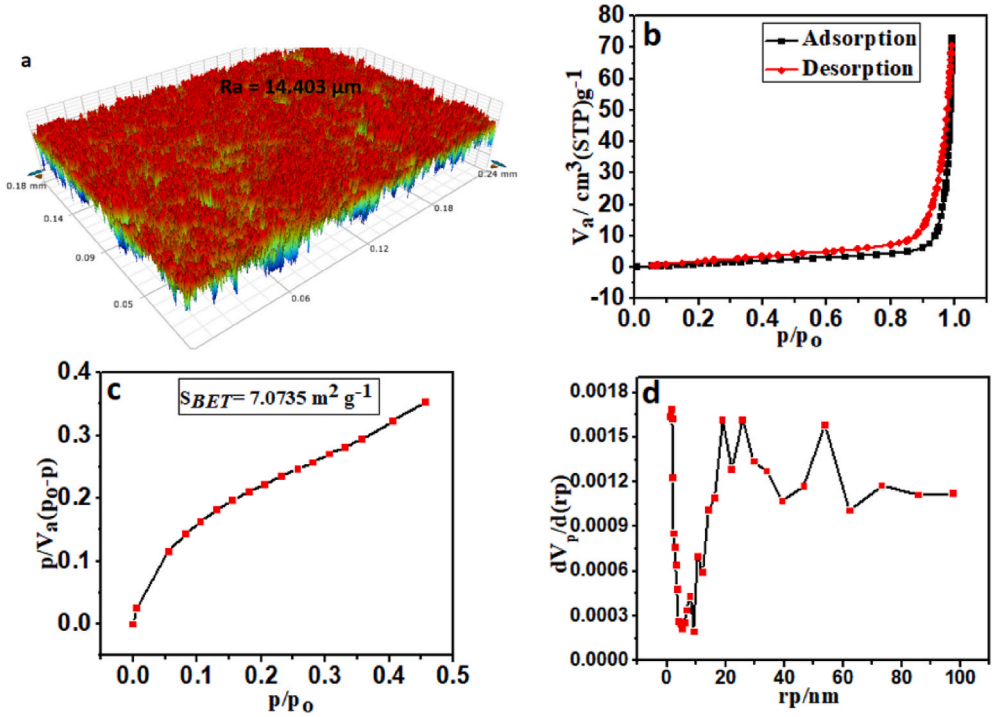

Fig. 2. 3D optical profilometry image (a), N_2 adsorption-desorption (b), BET (c) and BJH (d) graphs of the USAPS.

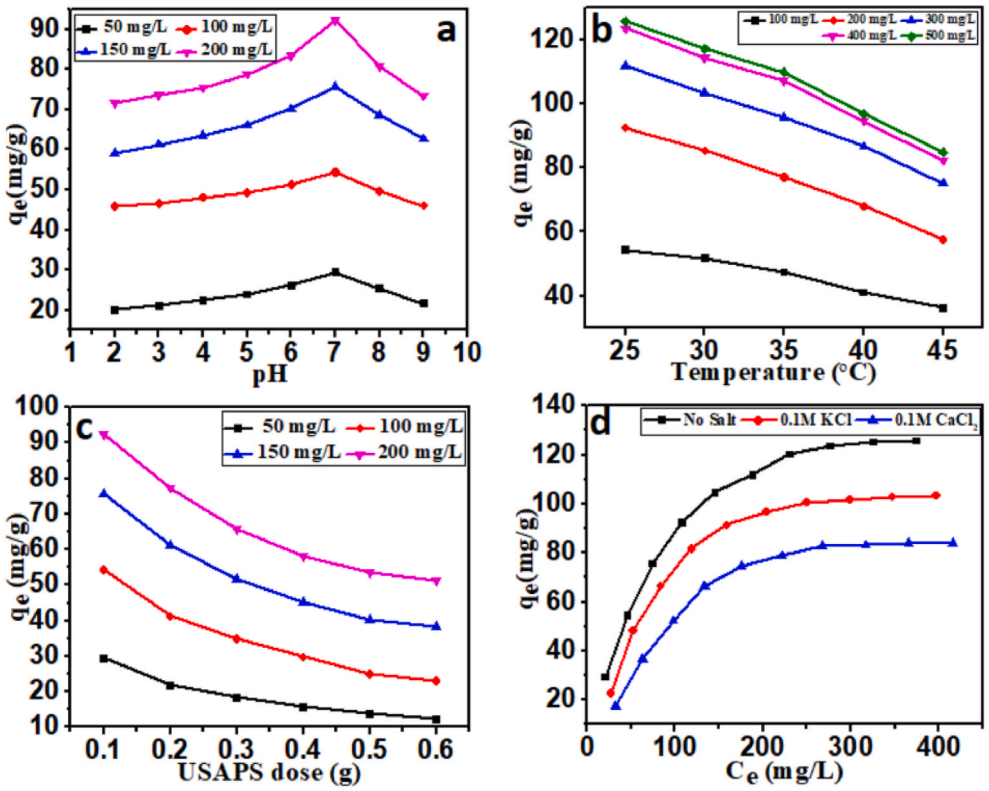

Fig. 3. Effect of pH at 25°C & 0.1 g of the USAPS (a), effect of temperature at pH 7.0 & 0.1 g of the USAPS (b), Effect of the USAPS dose at pH 7.0 & 25°C (c) and effect of salt (KCl & $CaCl_2$) addition at pH 7.0 & 25°C on phenol uptake.

gradually increases from pH 2 to an optimum value of pH 7 and then decreases significantly. Maximum phenol adsorption was observed at pH 7. These results can be explained based on the acidic behaviour of phenol and surface charge of the USAPS. Lower adsorption of phenol was observed between pH 2–6 despite the net positive surface charge of the USAPS, it occurred due to the hindrance created by H^+ ions between phenol molecules and the USAPS adsorption sites. At pH 7, electrostatic interaction was very high between phenol and the USAPS sites as there were no foreign species present to disturb the adsorption process. At pH 8, lower adsorption was observed because, the USAPS surface was positively charged but phenol and OH^- both compete for adsorption sites. At pH 9, adsorption further decreases as the USAPS surface becomes negatively charged and so electrostatic repulsion increases between phenol and the USAPS surface. Similar results were previously reported (Al Bsoul et al., 2021).

3.4. Effect of reaction temperature

The variation of phenol adsorption with temperature is shown in (Fig. 3b). While performing the experiments, the temperature was maintained between 25 and 45°C while other parameters such as phenol concentration (100 mg/L), the USAPS dose (0.1g/100 ml), contact time (180 min) and pH (7) were kept constant. Experiments were repeated for other concentrations as well (200–500 mg/L). From Fig. 3b, it was observed that an increase in temperature resulted in a decrease in phenol adsorption and confirmed the exothermic nature of adsorption. The maximum adsorption uptake was found at 25°C whereas the minimum uptake was found at 45°C. The phenol uptake decreased from 54.37 mg/g to 36.41 mg/g for 100 mg/L concentration. Similar patterns were observed for higher concentrations also. At higher temperatures, the kinetic energy of phenol molecules increases which decreases the probability of interaction with the USAPS surface.

3.5. Effect of the USAPS dose

The change in phenol adsorption with the USAPS dose is shown in Fig. 3c. The USAPS dose changed in the range of 0.1–0.6 g/100ml at a constant concentration (50 mg/L), pH (7), contact time (180 min) and temperature (25°C). Experiments were repeated for the higher concentrations (100, 150 and 200 mg/L). From Fig. 3c, it was observed that phenol uptake dropped from 29.39 to 21.83 mg/g on doubling the USAPS dose (0.1–0.2 g/100ml). Further, phenol uptake continued to decrease with a smaller rate on increasing the USAPS dose. This decrease in phenol uptake with an increase in the USAPS dose is probably due to the formation of a low concentration gradient between liquid phenol concentration and solid phenol concentration as initial concentration act as a driving force for the mass transfer between solid and liquid phase (Mandal et al., 2020).

3.6. Effect of inorganic salt addition

The effect of inorganic salt addition is shown in Fig. 3d. 0.1 M KCl and 0.1 M $CaCl_2$ were separately added to various concentrations of phenol (50–500 mg/L) at constant pH (7), the USAPS dose (0.1 g/100ml), temperature (25°C) and contact time (180 min). From Fig. 3d, it is evident that on the addition of 0.1 M KCl and 0.1 M $CaCl_2$, the amount of adsorption in equilibrium decreased from 125.77 mg/g to 103.45 and 84.11 mg/g, respectively. It was probably due to the blockage of the adsorption sites by inorganic ions so that phenol molecules unable to reach the USAPS surface resulting in the reduction of phenol uptake. It was also observed that cations with low ionic radius, high valency and large hydration sphere affect phenol uptake the most. Similar results were reported by Li et al. (2018).

3.7. Adsorption isotherm

The shape of the adsorption isotherm gives us an idea to interpret the adsorption behaviour. Based on the different adsorption behaviour, Giles has classified adsorption isotherms into four categories which are S, H, L and C (Giles et al., 1974). Adsorption isotherm of phenol removal by the USAPS is shown in Fig. 4a, which depicted that phenol adsorption by the USAPS follows the L type of adsorption isotherm. In the L type of adsorption isotherms, solvent and solute molecules do not compete for the adsorption sites of the adsorbate (Giles et al., 1974). Freundlich, Temkin and Langmuir isotherms were used to analyse the adsorption equilibrium data and its applicability was checked by determining various adsorption parameters, coefficient of determination (R^2) and correlation coefficient (r) by using regression analysis.

The graph of Freundlich isotherm was plotted between $\ln C_e$ *versus* $\ln q_e$ and depicted in Fig. 4b. By using intercept and slope values, adsorption parameters were calculated and are tabulated in Table 1. The n values at different temperatures lie in the range of 1.71–2.04 indicating moderate adsorption. q_m values obtained from Halsey's equation are less than half of the q_m values obtained from the experimental data. The R^2 value lies in the range of 0.93–0.96 showing its incapability of explaining the adsorption phenomenon. Thus, the assumption of adsorption over the heterogeneous surface was discarded for the adsorption of phenol onto the USAPS.

The graph of Temkin isotherm at different temperatures was plotted between q_e *versus* $\ln C_e$ and shown in Fig. 4c. The isotherm parameters are tabulated in Table 1. The R^2 values were in the range of 0.984–0.992 indicating the possibility of uniform binding energy distribution over the USAPS surface. From Fig. 4c, it was observed that Temkin isotherm shows slight divergence at higher concentrations of phenol and so this model was unable to explain the adsorption phenomenon.

The graph of Langmuir isotherm was plotted between C_e/q_e *versus* C_e and shown in Fig. 4d. Adsorption parameters were determined from slope and intercept and are given in Table 1. The values of r and R^2 were greater than 0.99 and the results obtained were in agreement with adsorption experiments. Thus, Langmuir isotherm provides the best linear fit explanation of adsorption experiments and the possibility of monolayer adsorption was assumed to be correct. Similar works were previously reported for phenol removal (Abatal et al., 2020; Thang et al., 2019).

Table 1
Adsorption isotherm parameters of phenol adsorption onto the USAPS.

Parameters	Temperature		
	25°C	35°C	45°C
Langmuir			
K_L (L/mg)	1.26×10^{-2}	8.44×10^{-3}	6.19×10^{-3}
q_m (mg/g)	156.98	149.03	121.95
r	0.998	0.993	0.996
R^2	0.996	0.98	0.993
Freundlich			
K_F ($mg^{1-(1/n)}L^{1/n}/g$)	8.17	4.60	2.87
n	2.04	1.78	1.71
q_m (mg/g)	55.17	41.17	28.33
r	0.967	0.969	0.982
R^2	0.935	0.939	0.965
Temkin			
K_T (L/g)	1.15×10^{-1}	7.52×10^{-2}	4.68×10^{-2}
b (J/mol)	69.90	74.29	103.36
r	0.992	0.991	0.996
R^2	0.984	0983	0.992

3.8. Adsorption kinetics

The variation of phenol uptake (q_t) with time is shown in Fig. 5a. From Fig. 5a, it was observed that the adsorption of phenol onto the USAPS took place in three steps. In the first step (0–45 min), rapid

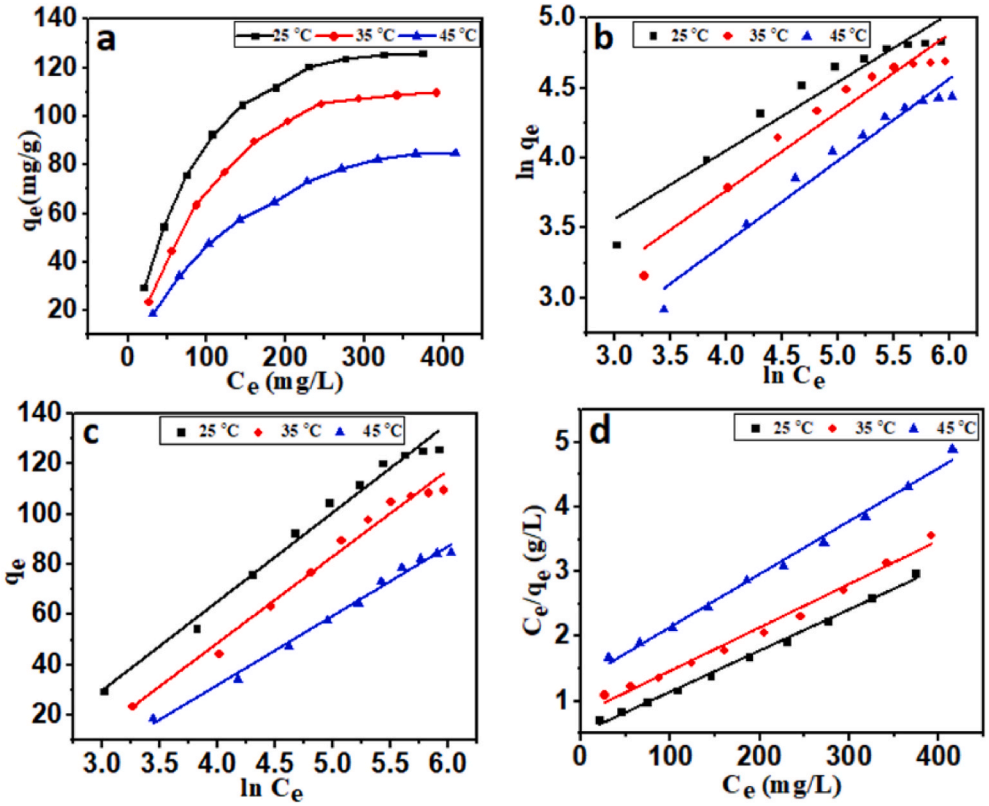

Fig. 4. Amount of phenol adsorbed versus equilibrium concentration at pH 7.0 & 0.1 g of the USAPS (a) and isotherm plots of Freundlich (b) Temkin (c) and Langmuir (d).

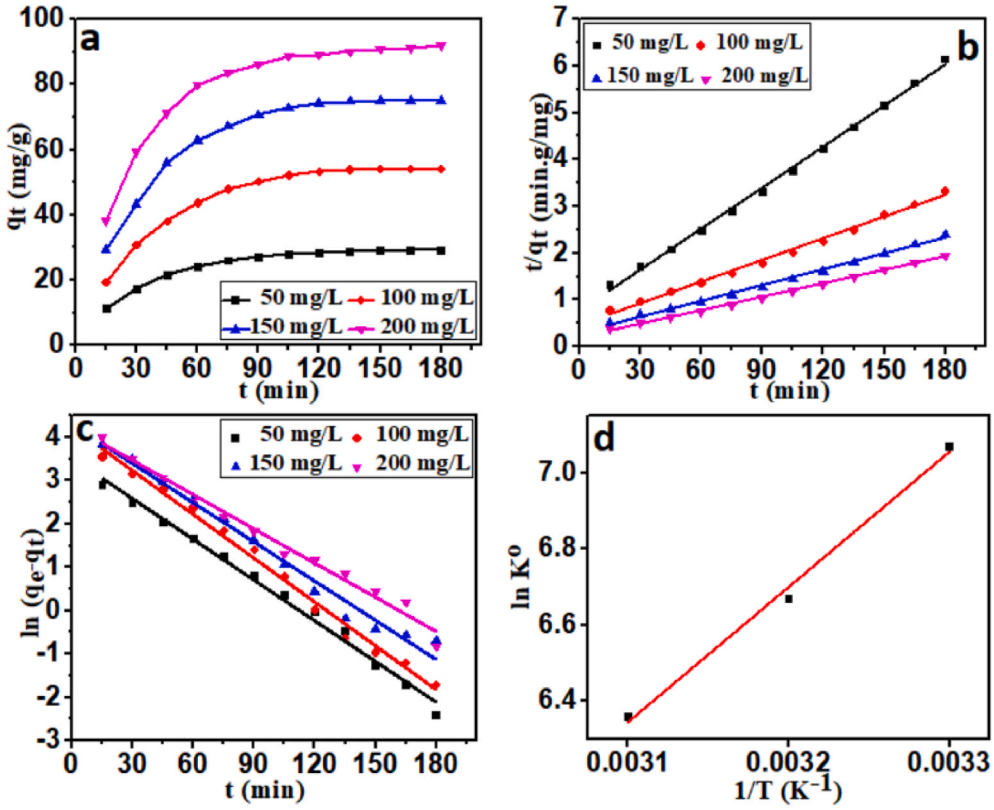

Fig. 5. Variation of adsorption uptake of phenol with time at pH 7.0 & 25°C (a), pseudo-second-order kinetics plot (b), pseudo-first-order kinetics plot (c) and plot of lnK^o *versus* 1/T (d).

phenol uptake was observed, in the second step (45–90 min), moderate phenol uptake was observed while in the third step (90–180 min), negligible phenol uptake was observed. These adsorption steps can be explained based on the availability of a higher number of surface sites in the first step. In the second and third steps adsorption rate slows down as it reaches equilibrium.

Different kinetic models such as pseudo-second-order, pseudo-first-order and intra-particle models were fitted to check the suitability of adsorption experimental data. The graphs of these models are represented in Fig. 5b, c, S4 and parameters obtained from these models are tabulated in Table 2. From Fig. 5b, c and S4, it was observed that pseudo-second-order kinetics give the best-fit explanation of kinetic data as values calculated from this model are in close agreement with values of experimental data. Further, R^2 values greater than 0.99 confirmed the applicability of this model. The results were in agreement with the previously reported work (Abatal et al., 2020; Thang et al., 2019).

The R^2 values for the pseudo-first-order and intra-particle model were in the range of 0.98–0.99 and 0.82–0.87, respectively showing its insignificance for the adsorption phenomenon.

Table 2
Kinetic parameters of different models at various concentrations.

Parameters	Concentration			
	50 mg/L	100 mg/L	150 mg/L	200 mg/L
Pseudo-first-order				
k_1 (min^{-1})	3.12×10^{-2}	3.36×10^{-2}	3.01×10^{-2}	2.62×10^{-2}
q_e (mg/g)	33.60	68.76	72.80	67.63
r	−0.995	−0.995	−0.991	−0.992
R^2	0.991	0.991	0.983	0.985
Pseudo-second-order				
k_2 (g/mg. min)	1.10×10^{-3}	5.18×10^{-4}	4.32×10^{-4}	4.65×10^{-4}
q_e (mg/g)	34.24	64.80	88.57	104.16
r	0.998	0.997	0.997	0.998
R^2	0.997	0.995	0.995	0.997
Intra-particle				
k_p (g/mg.$min^{0.5}$)	1.74	3.46	4.54	4.91
C (mg/g)	8.53	13.33	21.84	33.69
r	0.931	0.934	0.925	0.909
R^2	0.868	0.873	0.857	0.82

3.9. Adsorption thermodynamics

For the thermodynamic study, the temperature based Langmuir constant (K_L) was first made unitless (Lima et al., 2019). Standard state thermodynamic parameters like Gibbs free energy change (ΔG^o), Entropy change (ΔS^o), change in Enthalpy (ΔH^o) were calculated using the following Eq.:

$$lnK^o = \frac{\Delta S^o}{R} - \frac{\Delta H^o}{RT} \quad (10)$$

K^o was calculated using the following formula:

$$\boldsymbol{K^o = K_L \times molecular\ weight\ of\ phenol \times 1000} \quad (11)$$

$\Delta G^o = \Delta H^o - T\Delta S^o$ (12) Where K^o is Standard state Langmuir equilibrium constants; R: universal gas constant (J/mol.K) and T: absolute temperature (K).

The graph plotted between lnK^o *versus* 1/T is shown in Fig. 5d. The values of all the thermodynamic parameters were calculated from the

Table 3
Thermodynamic parameters of adsorption.

	25°C	35°C	45°C	
ΔG^o (kJ/mol)	−17.969	−17.581	−17.193	−29.51
K^o	1185.786	7942.88	582.540	
ΔH^o(kJ/mol)				
ΔS^o (J/K.mol)				−38.74

above equations and are tabulated in Table 3. A negative value of ΔH^o confirmed the exothermic nature of the adsorption phenomenon while negative values of ΔG^oconfirmed the feasibility of adsorption. The increase in ΔG^o value with temperature confirmed that adsorption becomes less feasible with temperature rise. A slight negative value of ΔS^o indicated that adsorption took place with no structural change in the phenol-USAPS interface.

4. Conclusion

The present study concluded that the newly synthesized USAPS was macroporous, amorphous and had a very rough surface with high topographical parameters. Adsorption was negatively affected by an increase in temperature, USAPS dose and salt (KCl and $CaCl_2$) addition. The adsorption data were best explained by Langmuir isotherm and pseudo-second-order kinetics with high determination coefficient values. The thermodynamic study confirmed that adsorption was exothermic and spontaneous with no structural change at the USAPS-phenol interface. So, it can be concluded that the USAPS has a high adsorption potential for the adsorption of phenolic compounds and can be used as an alternative to activated carbon as PS is freely available with low activation cost while regeneration is not needed due to its low cost.

Funding information

This research did not receive any specific grant from funding agencies in the public, commercial, or not-for-profit sectors.

CRediT authorship contribution statement

Prashant Mishra: Conceptualization, Investigation, Validation, Methodology, Writing – original draft. **Kaman Singh:** Conceptualization, Investigation, Validation, Methodology, Supervision, Data curation, Writing – original draft, review & editing. **Utkarsh Dixit:** Conceptualization, Investigation, Validation, Methodology, Writing – original draft.

Declaration of competing interest

The authors declare that they have no known competing financial interests or personal relationships that could have appeared to influence the work reported in this paper.

Acknowledgements

One of the authors (PM is thankful to UGC, New Delhi for financial support (UGC-SRF-133155). IIT, Kanpur is also acknowledged by the authors for providing some characterization facilities.

Appendix A. Supplementary data

Supplementary data to this article can be found online at https://doi.org/10.1016/j.scp.2021.100491.

References

Abatal, M., Anastopoulos, I., Giannakoudakis, D.A., Olguin, M.T., 2020. Carbonaceous material obtained from bark biomass as adsorbent of phenolic compounds from aqueous solutions. J. Environ. Chem. Eng. 8, 103784. https://doi.org/10.1016/J.JECE.2020.103784.

Abdallah, M.A.M., 2012. The potential of different bio adsorbents for removing phenol from its aqueous solution. Environ. Monit. Assess. 185, 6495–6503. https://doi.org/10.1007/S10661-012-3041-Y.

Al Bsoul, A., Hailat, M., Abdelhay, A., Tawalbeh, M., Al-Othman, A., Al-kharabsheh, I.N., Al-Taani, A.A., 2021. Efficient removal of phenol compounds from water environment using Ziziphus leaves adsorbent. Sci. Total Environ. 761, 143229. https://doi.org/10.1016/J.SCITOTENV.2020.143229.

Al Momani, F., Gonzalez, O., Sans, C., Esplugas, S., 2004. Combining photo-Fenton process with biological sequencing batch reactor for 2,4-dichlorophenol degradation. Water Sci. Technol. 49, 293–298. https://doi.org/10.2166/WST.2004.0288.

Alami, A.H., Abu Hawili, A., Tawalbeh, M., Hasan, R., Al Mahmoud, L., Chibib, S., Mahmood, A., Aokal, K., Rattanapanya, P., 2020. Materials and logistics for carbon dioxide capture, storage and utilization. Sci. Total Environ. 717, 137221. https://doi.org/10.1016/J.SCITOTENV.2020.137221.

Babel, S., Kurniawan, T.A., 2003. Low-cost adsorbents for heavy metals uptake from contaminated water: a review. J. Hazard Mater. 97, 219–243. https://doi.org/10.1016/S0304-3894(02)00263-7.

Bandosz, T.J., Ania, C.O., 2018. Origin and perspectives of the photochemical activity of nanoporous carbons. Adv. Sci. 5, 1800293. https://doi.org/10.1002/ADVS.201800293.

Bódalo, A., Gómez, J.L., Gómez, M., León, G., Hidalgo, A.M., Ruíz, M.A., 2008. Phenol removal from water by hybrid processes: study of the membrane process step. Desalination 223, 323–329. https://doi.org/10.1016/J.DESAL.2007.01.219.

Bsoul, A. Al, 2014. The use of eucalyptus leaves as adsorbent for copper ion removal. New pub Balaban 52, 7838–7844. https://doi.org/10.1080/19443994.2013.832637.

Carvajal-Bernal, A.M., Gómez, F., Giraldo, L., Moreno-Piraján, J.C., 2015. Chemical modification of activated carbons and its effect on the adsorption of phenolic compounds. Ing. Y Compet. 17, 109–119.

Chakraborty, P., Sampath, S., Mukhopadhyay, M., Selvaraj, S., Bharat, G.K., Nizzetto, L., 2019. Baseline investigation on plasticizers, bisphenol A, polycyclic aromatic hydrocarbons and heavy metals in the surface soil of the informal electronic waste recycling workshops and nearby open dumpsites in Indian metropolitan cities. Environ. Pollut. 248, 1036–1045. https://doi.org/10.1016/J.ENVPOL.2018.11.010.

Christina Kampouraki, Z., Giannakoudakis, D.A., Triantafyllidis, K.S., Deliyanni, E.A., 2019. Catalytic oxidative desulfurization of a 4,6-DMDBT containing model fuel by metal-free activated carbons: the key role of surface chemistry. Green Chem. 21, 6685–6698. https://doi.org/10.1039/C9GC03234G.

Cooke, N.E., Fuller, O.M., Gaikwad, R.P., 1986. FT-i.r. spectroscopic analysis of coals and coal extracts. Fuel 65, 1254–1260. https://doi.org/10.1016/0016-2361(86)90238-3.

Dąbrowski, A., 2001. Adsorption — from theory to practice. Adv. Colloid Interface Sci. 93, 135–224. https://doi.org/10.1016/S0001-8686(00)00082-8.

Dutta, N.N., Borthakur, S., Patil, G.S., 2006. Phase transfer catalyzed extraction of phenolic substances from aqueous alkaline stream. https://doi.org/10.1080/01496399208019435, 27, 1435, 1448.

El-Naas, M.H., Al-Zuhair, S., Alhaija, M.A., 2010. Removal of phenol from petroleum refinery wastewater through adsorption on date-pit activated carbon. Chem. Eng. J. 162, 997–1005. https://doi.org/10.1016/J.CEJ.2010.07.007.

Giannakoudakis, D.A., Barczak, M., Florent, M., Bandosz, T.J., 2019. Analysis of interactions of mustard gas surrogate vapors with porous carbon textiles. Chem. Eng. J. 362, 758–766. https://doi.org/10.1016/J.CEJ.2019.01.064.

Giles, C.H., Smith, D., Huitson, A., 1974. A general treatment and classification of the solute adsorption isotherm. I. Theoretical. J. Colloid Interface Sci. 47, 755–765. https://doi.org/10.1016/0021-9797(74)90252-5.

Halsey, G.D., 1952. The role of surface heterogeneity in adsorption. Adv. Catal. 4, 259–269. https://doi.org/10.1016/S0360-0564(08)60616-1.

Jadhav, D.N., Vanjara, A.K., 2004. Removal of phenol from wastewater using sawdust, polymerized sawdust and sawdust carbon. Indian J. Chem. Technol. 11, 35–41.

Kang, S., Kim, G., Choe, J.K., Choi, Y., 2019. Effect of using powdered biochar and surfactant on desorption and biodegradability of phenanthrene sorbed to biochar. J. Hazard Mater. 371, 253–260. https://doi.org/10.1016/J.JHAZMAT.2019.02.104.

Karami, T., Elyasi, S., Amani, T., 2018. Modeling and optimizing of electrocoagulation process in treating phenolic wastewater by response surface methodology: precise evaluation of significant variables. Int. J. Environ. Sci. Technol. 15, 2389–2398. https://doi.org/10.1007/S13762-017-1539-0.

Kong, X., Gao, H., Song, X., Deng, Y., Zhang, Y., 2020. Adsorption of phenol on porous carbon from Toona sinensis leaves and its mechanism. Chem. Phys. Lett. 739, 137046. https://doi.org/10.1016/J.CPLETT.2019.137046.

Kyzas, G.Z., Deliyanni, E.A., Matis, K.A., 2014. Graphene oxide and its application as an adsorbent for wastewater treatment. J. Chem. Technol. Biotechnol. 89, 196–205. https://doi.org/10.1002/JCTB.4220.

Li, Y., Hu, X., Liu, X., Zhang, Y., Zhao, Q., Ning, P., Tian, S., 2018. Adsorption behavior of phenol by reversible surfactant-modified montmorillonite: mechanism, thermodynamics, and regeneration. Chem. Eng. J. 334, 1214–1221. https://doi.org/10.1016/J.CEJ.2017.09.140.

Lima, E.C., Hosseini-Bandegharaei, A., Moreno-Piraján, J.C., Anastopoulos, I., 2019. A critical review of the estimation of the thermodynamic parameters on adsorption equilibria. Wrong use of equilibrium constant in the Van't Hoof equation for calculation of thermodynamic parameters of adsorption. J. Mol. Liq. 273, 425–434. https://doi.org/10.1016/J.MOLLIQ.2018.10.048.

Lima, S.B., Borges, S.M.S., Rangel, M. do C., Marchetti, S.G., 2013. Effect of iron content on the catalytic properties of activated carbon-supported magnetite derived from biomass. J. Braz. Chem. Soc. 24, 344–354. https://doi.org/10.5935/0103-5053.20130044.

Lin, S.H., Juang, R.S., 2009. Adsorption of phenol and its derivatives from water using synthetic resins and low-cost natural adsorbents: a review. J. Environ. Manag. 90, 1336–1349. https://doi.org/10.1016/J.JENVMAN.2008.09.003.

Liu, Q.S., Zheng, T., Wang, P., Jiang, J.P., Li, N., 2010. Adsorption isotherm, kinetic and mechanism studies of some substituted phenols on activated carbon fibers. Chem. Eng. J. 157, 348–356. https://doi.org/10.1016/J.CEJ.2009.11.013.

Mandal, A., Bar, N., Das, S.K., 2020a. Phenol removal from wastewater using low-cost natural bioadsorbent neem (Azadirachta indica) leaves: adsorption study and MLR modeling. Sustain. Chem. Pharm. 17, 100308. https://doi.org/10.1016/J.SCP.2020.100308.

Mandal, A., Das, S.K., 2019. Phenol adsorption from wastewater using clarified sludge from basic oxygen furnace. J. Environ. Chem. Eng. 7, 103259. https://doi.org/10.1016/J.JECE.2019.103259.

Mandal, A., Mukhopadhyay, P., Das, S.K., 2020b. Adsorptive removal of phenol from wastewater using guava tree bark. Environ. Sci. Pollut. Res. 2719 27, 23937–23949. https://doi.org/10.1007/S11356-020-08777-2, 2020.

Mane, S.M., Vanjara, A.K., Sawant, M.R., 2005. Removal of phenol from wastewater using date seed carbon. J. Chin. Chem. Soc. 52, 1117–1122. https://doi.org/10.1002/JCCS.200500160.

Mishra, S., Yadav, S.S., Rawat, S., Singh, J., Koduru, J.R., 2019. Corn husk derived magnetized activated carbon for the removal of phenol and para-nitrophenol from aqueous solution: interaction mechanism, insights on adsorbent characteristics, and isothermal, kinetic and thermodynamic properties. J. Environ. Manag. 246, 362–373. https://doi.org/10.1016/J.JENVMAN.2019.06.013.

Mohammadi, S., Kargari, A., Sanaeepur, H., Abbassian, K., Najafi, A., Mofarrah, E., 2015. Phenol removal from industrial wastewaters: a short review. New pub Balaban 53, 2215–2234. https://doi.org/10.1080/19443994.2014.883327.

Mu'azu, N.D., Zubair, M., Jarrah, N., Alagha, O., Al-Harthi, M.A., Essa, M.H., 2020. Sewage sludge $ZnCl_2$-activated carbon intercalated MgFe–LDH nanocomposites: insight of the sorption mechanism of improved removal of phenol from water. Int. J. Mol. Sci. 21, 1563. https://doi.org/10.3390/IJMS21051563.

Mukherjee, R., De, S., 2014. Adsorptive removal of phenolic compounds using cellulose acetate phthalate–alumina nanoparticle mixed matrix membrane. J. Hazard Mater. 265, 8–19. https://doi.org/10.1016/J.JHAZMAT.2013.11.012.

Nadavala, S.K., Che Man, H., Woo, H.-S., 2014. Biosorption of phenolic compounds from aqueous solutions using pine (pinus densiflora sieb) bark powder. BioResources 9, 5155–5174. https://doi.org/10.15376/biores.9.3.5155-5174.

Ni, G., Zhao, G., Jiang, Y., Li, J., Meng, Y., Wang, X., 2013. Steam plasma jet treatment of phenol in aqueous solution at atmospheric pressure. Plasma Process. Polym. 10, 353–363. https://doi.org/10.1002/PPAP.201200155.

Park, H.S., Koduru, J.R., Choo, K.H., Lee, B., 2015. Activated carbons impregnated with iron oxide nanoparticles for enhanced removal of bisphenol A and natural organic matter. J. Hazard Mater. 286, 315–324. https://doi.org/10.1016/J.JHAZMAT.2014.11.012.

Pham, N.M., Huynh, T.L.D., Nasir, M.A., 2020. Environmental consequences of population, affluence and technological progress for European countries: a Malthusian view. J. Environ. Manag. 260, 110143. https://doi.org/10.1016/J.JENVMAN.2020.110143.

Rengaraj, S., Moon, S.H., Sivabalan, R., Arabindoo, B., Murugesan, V., 2002. Agricultural solid waste for the removal of organics: adsorption of phenol from water and wastewater by palm seed coat activated carbon. Waste Manag. 22, 543–548. https://doi.org/10.1016/S0956-053X(01)00016-2.

Shokoohi, R., Movahedian, H., Dargahi, A., Jafari, A.J., Parvaresh, A., 2017. Survey on efficiency of BF/AS integrated biological system in phenol removal of wastewater. Desalin. Water Treat. 82, 315–321. https://doi.org/10.5004/DWT.2017.20957.

Singh, K., Chandra, B., Gautam, M., 2016. Development of inexpensive adsorbent from agro-waste for phenol adsorption. J. Sci. Ind. Res. (India) 75, 444–451.

Singh, K., Kumar, A., Awasthi, S., Pandey, S.K., Mishra, P., 2019. Adsorption mechanism of carboxymethyl cellulose onto mesoporous mustard carbon: experimental and theoretical aspects. Colloids Surfaces A Physicochem. Eng. Asp. 581, 123786. https://doi.org/10.1016/J.COLSURFA.2019.123786.

Singh, K., Kumar, A., Pandey, S.K., Awasthi, S., Gupta, S.P., Mishra, P., 2020. Interpretation of adsorption behavior of carboxymethyl cellulose onto Functionalized accurel polymeric surface. Ind. Eng. Chem. Res. 59, 19102–19116. https://doi.org/10.1021/ACS.IECR.0C03894.

Singh, K., Singh, V.K., Verma, S.K., Bharose, R., Suman, A., 2013. Characterization of modified polypropylene powder (Accurel) and its use for adsorption of phenolics from aqueous solution. Indian J. Chem. Technol. 20, 385–391.

Sun, C., Chen, T., Huang, Q., Zhan, M., Li, X., Yan, J., 2020. Activation of persulfate by CO_2-activated biochar for improved phenolic pollutant degradation: performance and mechanism. Chem. Eng. J. 380, 122519. https://doi.org/10.1016/J.CEJ.2019.122519.

Tawalbeh, M., Tezel, F.H., Al-Ismaily, M., Kruczek, B., 2019. Highly permeable tubular silicalite-1 membranes for CO_2 capture. Sci. Total Environ. 676, 305–320. https://doi.org/10.1016/J.SCITOTENV.2019.04.290.

Thang, P.Q., Jitae, K., Giang, B.L., Viet, N.M., Huong, P.T., 2019. Potential application of chicken manure biochar towards toxic phenol and 2,4-dinitrophenol in wastewaters. J. Environ. Manag. 251, 109556. https://doi.org/10.1016/J.JENVMAN.2019.109556.

Thue, P.S., Adebayo, M.A., Lima, E.C., Sieliechi, J.M., Machado, F.M., Dotto, G.L., Vaghetti, J.C.P., Dias, S.L.P., 2016. Preparation, characterization and application of microwave-assisted activated carbons from wood chips for removal of phenol from aqueous solution. J. Mol. Liq. 223, 1067–1080. https://doi.org/10.1016/J.MOLLIQ.2016.09.032.

Tran, V.S., Ngo, H.H., Guo, W., Zhang, J., Liang, S., Ton-That, C., Zhang, X., 2015. Typical low cost biosorbents for adsorptive removal of specific organic pollutants from water. Bioresour. Technol. 182, 353–363. https://doi.org/10.1016/J.BIORTECH.2015.02.003.

Zeng, T., Rene, E.R., Zhang, S., Lens, P.N.L., 2019. Removal of selenate and cadmium by anaerobic granular sludge: EPS characterization and microbial community analysis. Process Saf. Environ. Protect. 126, 150–159. https://doi.org/10.1016/J.PSEP.2019.03.039.

Zhao, G.-F., Bai, P., Zhu, H.-M., Yan, R.-X., Liu, X.-M., Yan, Z.-F., 2008. The modification of activated carbons and the pore structure effect on enrichment of coal-bed methane. Asia Pac. J. Chem. Eng. 3, 284–291. https://doi.org/10.1002/APJ.147.

ChemistrySelect

Research Article
doi.org/10.1002/slct.202202856

Chemistry Europe
European Chemical Societies Publishing

www.chemistryselect.org

A Comparative Study of Phenol Removal by *Pisum-sativum* Peels Biochars Derived at Different Pyrolysis Temperatures: Isotherm, Kinetic and Thermodynamic Modelling

Prashant Mishra, Kaman Singh,* and Gajanan Pandey[a]

Pea peels were used for the preparation of biochar at different temperatures (250 °C: PP250, 500 °C: PP500 and 750 °C: PP750) using slow pyrolysis for 1 h and used for the phenol removal from an aqueous medium. Biochar samples were characterized by SEM, XRD and FT-IR. The phenol removal was examined as a function of pH, temperature, and here NaCl and urea concentration. The optimum pH and temperature were found to be 6.0 and 25 °C respectively. Presence of NaCl and urea primarily affected the adsorption capacity of PP250 and slightly affected the adsorption potential of PP500 and PP750. The maximum biosorption capacity for the PP250, PP500 and PP750 were found to be 34.63, 46.70, and 60.10 mg/g respectively. The Langmuir isotherm and Pseudo-second order kinetic model best explained the adsorption. Thermodynamic parameters corroborated the physical and exothermic nature of adsorption. PP750 can preferably be used for phenol removal than PP500 and PP250.

Introduction

Phenol is used in a wide range of industries and environments. Because it is water-soluble, it is easily incorporated into wastewater as a result of a variety of industrial activities.[1] The presence of phenolic compounds in water is caused by both natural and human-induced processes.[2] Decomposition of dead plants and animals are natural sources of phenolic chemicals in water pollution (organic debris) which makes it difficult to classify this material as it is extremely detrimental to the environment.[3] They are also produced by microbes and plants in watery environments. Industrial, household, agricultural, and municipal activity are all examples of human-caused phenolic chemical contamination in water[4] resulting in exposure of these compound to human being and disturbs their health due to their toxicity.[5]

Because of their toxicity to humans and aquatic life, phenolic compounds have low permitted limits (0.5–1.0 mg/l) and must be removed from wastewaters in environmentally sound ways.[6] Despite the existence of numerous physicochemical and biological treatment strategies (solvent extraction, resin ion exchange, chemical oxidation by ozone, aerobic or anaerobic biodegradation, and so on),[7–9] the most successful and extensively used approach for phenol elimination is adsorption on activated carbon.[10]

Recent studies are focusing on the exploitation of agricultural wastes for the preparation of activated carbon.[11] Because of its abundant raw ingredients, cheap cost, large surface area, and efficient pore structure, biochar has shown tremendous promise in removing water pollutants.[12] The present study is essentially an extension of our earlier study.[13] Biochar has been employed for a variety of purposes due to its porosity and unique surface functional groups, including pollutant adsorption, catalytic support, soil remediation, and energy storage.[14]

Many scientists are working to understand how biochar removes phenol from water. To remove phenol, Mohammed et al. (2018) utilised biochar of pine fruit shell produced at various temperatures.[15] The maximal adsorption uptake varied from 10.373 to 26.738 mg/g, with a 67–99% removal rate. Thang et al. (2019) synthesised biochar for removing phenol from an aqueous solution using chicken manure; phenol was entirely removed in 90 minutes.[16] For phenol, biochar's highest adsorption capacity was 106.20 mg/g.[16]

To remove phenol, Lawal et al. (2021) employed biochar obtained from oil palm leaves by steam pyrolysis; the adsorption capacity for phenol was 62.89 mg/g.[17] Nitrogen-doped bamboo biochar prepared by pyrolysis for phenol removal and adsorption capacity was observed to be 169.0 mg/g.[18] A biochar composite of pomelo peel was used for phenol removal with q_{max} of 39.32 mg/g.[19] Table 1 represents a comparison of q_{max} of different biochars with present study.

Pisum sativum is a plant that is grown from winter to early summer in many regions of the world. Peas are widely farmed in India throughout the winter, and its waste, pea peels (PP), is widely available in the market and households.

The use of PP biochars for effective phenol removal is described in this paper. Its properties make it an effective adsorbent for the elimination of phenol. SEM-EDS, FT-IR, XRD, and pHzpc are used to characterize the derived biochars. The mechanism of phenol elimination is investigated using a variety of assays, including pH effect, biochar dosage, temperature, and the addition of NaCl and urea. In addition, numerous

[a] *P. Mishra, Prof. K. Singh, Prof. G. Pandey*
Department of Chemistry,
Babasaheb Bhimrao Ambedkar University (A Central University),
Vidya Vihar, Raebareli Road, Lucknow-226025
E-mail: singh.kaman@bbau.ac.in

Supporting information for this article is available on the WWW under https://doi.org/10.1002/slct.202202856

Table 1. Comparison table of q_{max} of various biochars.

Biochar	Pyrolysis temperature (°C)	Phenol concentration range	Conditions		q_{max} (mg/g)	Reference
			pH	T(°C)		
Pine fruit shell (BC350)	350	20–100	6.5	25	10.37	[15]
Pine fruit shell (BC450)	450	20–100	6.5	25	15.97	[15]
Pine fruit shell (BC550)	550	20–100	6.5	25	26.73	[15]
Chicken manure	600	10–200	7.0	22	106.20	[16]
Oil palm frond	500	20–200	6.5	45	62.89	[17]
Nitrogen doped bamboo biochar	700	100–1000	7.0	25	169.00	[18]
Pomelo peel magnetic biochar	600	20–200	5.0	30	39.32	[19]
Food waste	700	10–50	3.0	35	13.49	[34]
Magnetic palm kernel	500	10–70	8.0	30	10.84	[39]
Cow dung	800	20–500	6.0	25	518.89	[40]
Wood apple shell	700	100–400	6.0	30	102.71	[41]
Hizika fusiformis	550	10–100	6.0	25	10.39	[42]
PP250	250	30–300	6.0	25	34.63	Present work
PP500	500	30–300	6.0	25	46.70	Present work
PP750	750	30–300	6.0	25	60.10	Present work

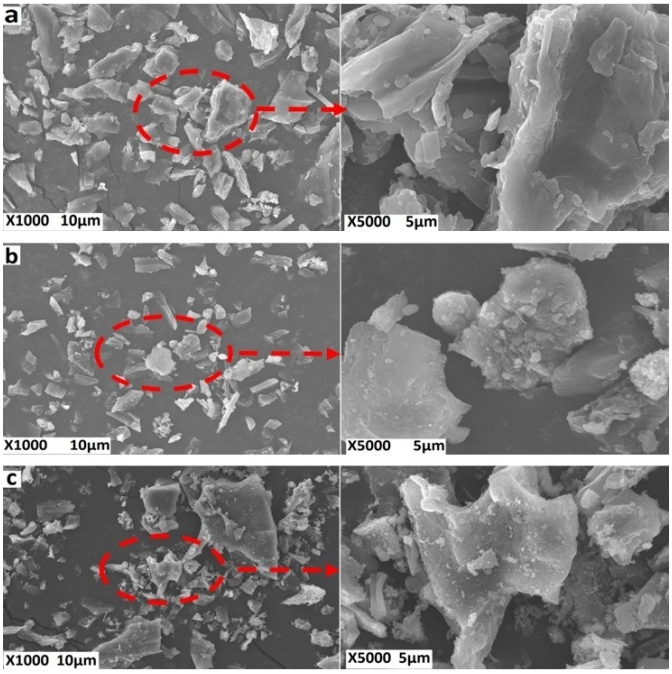

Figure 1. SEM pictures of PP250 (a), PP500 (b) and PP750 (c) at different resolutions.

kinetic and adsorption isotherm models were tested for their relevance in determining the adsorption mechanism.

Results and Discussion

Characterization of biochar

The physicochemical characteristics of biochar PP250, PP500 and PP750 such as biochar yield, ash content, moisture content and pH_{zpc} are tabulated in Table 2. Ash content increased (2.18 - 4.79) and biochar yield decreased (70.24 - 49.34) as the pyrolysis temperature rose from 250 to 750 °C. The decrease in biochar yield with increase in pyrolysis temperature is due to the thermal degradation of lignin and cellulose resulting in the dehydration of hydroxyl groups.[20,21] The rise in ash content is an outcome of increase in mineral content and volatilization of ligno-cellulosic matters.[22,23] The decrease in moisture content (1.47–0.46) with pyrolysis temperature is consistent with the results of the biochar yield and ash content. Similar findings were reported by the other investigators.[24–26] The pH_{ZPC} of PP biochars refer to the pH at which the biochar surface is neutral (i.e. no charge at the surface). At pH below the pH_{ZPC} the biochar surface is positively charged and at pH above the pH_{ZPC} the biochar surface is negatively charged.

The SEM micrograph images of biochar PP250, PP500 and PP750 are shown in Figure 1. From Figure 1, it is apparent that with the increase in a pyrolysis temperature the roughness of the biochar surface increases which increased the porosity and irregularity of the biochar.[27] The increase in pyrolysis temperature results in the dehydration of hydroxyl groups which increases the carbon content of the biochars (Figure S1) with the rise in temperature indicating a high degree of carbon-

Table 2. Physicochemical properties of PP biochars.

Biochar	Yield,[a] % (w/w)	Moisture,[a] % (w/w)	Ash,[a] % (w/w)	pH_{zpc}
PP250	70.24 ± 0.3	1.47 ± 0.04	2.18 ± 0.02	5.1
PP500	55.87 ± 0.2	0.98 ± 0.03	3.85 ± 0.04	6.2
PP750	49.34 ± 0.2	0.46 ± 0.01	4.79 ± 0.01	6.4

[a] Yield, moisture and ash content analysis results are given as mean ± standard deviation for duplicate measurements.

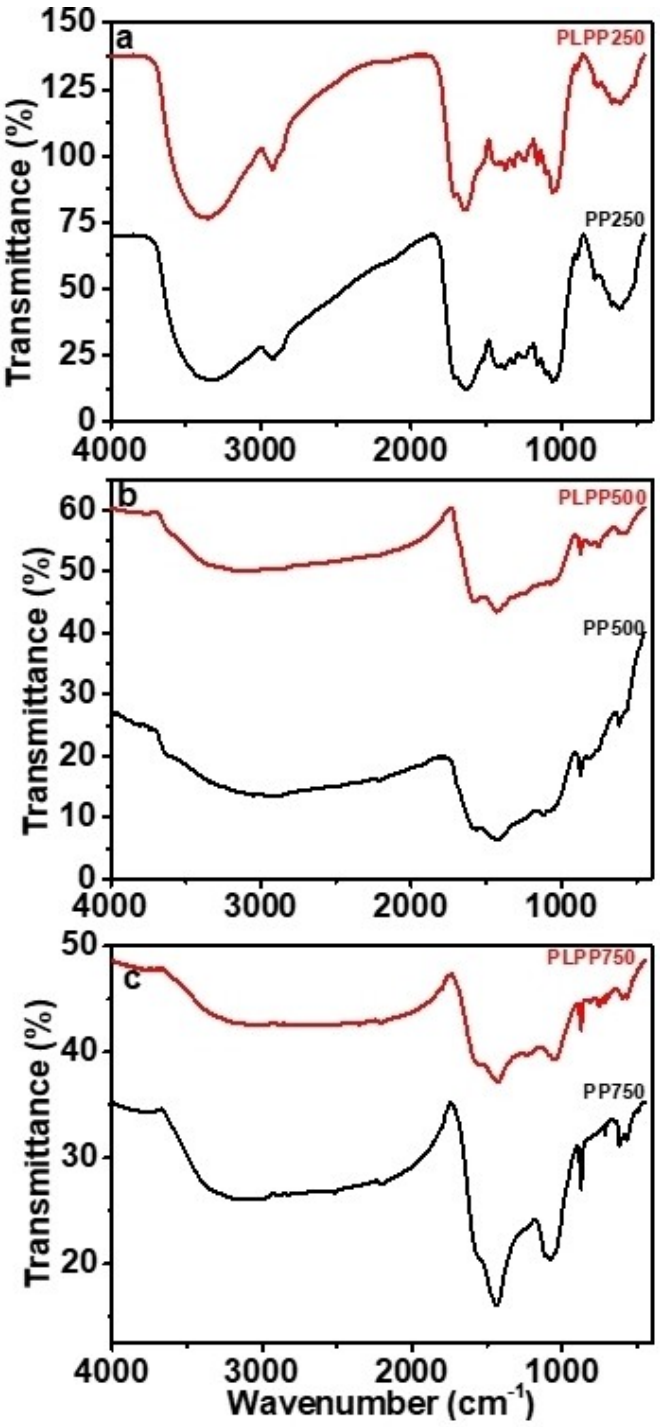

Figure 2. FT-IR spectra of PP250 and PLPP250 (a), PP500 and PLPP500 (b) and PP750 and PLPP750.

ization resulting in greater aromaticity of biochars. Similar behaviour was observed in previous studies.[15–19]

The FT-IR spectra of the PP biochars prepared at different temperatures and phenol loaded biochars (at 25 °C, pH 6.0, biochar dose 2 g/L and 30 mg/L of phenol concentration) are explicated in Figure 2. The changes observed in the functional groups of PP biochar with the increase in pyrolysis temperature are in agreement with the other results of the present study[28] e.g. the polar functional groups (O–H, N–H) are not observed in the FT-IR spectra of PP500 and PP750 indicating increase in carbon content in PP500 and PP750. With the increase in temperature, the polarity of biochar decreases and the degree of aromatization increases resulting in the change in the mechanism of phenol adsorption onto PP biochar.[29] The same has been confirmed by the results of FT-IR.

Figure 2, revealed that PP250 consists of a large number of absorption bands in comparison to PP500 and PP750. The PP250 mainly consists of absorption bands at 3336.97 cm^{-1} (O–H stretching of alcohol), 2922.73 cm^{-1} (C–H stretching of alkanes), 1720 cm^{-1} (C=O stretching of aliphatic ketone), 1632.47 cm^{-1} (C=C stretching of substituted alkene), 1374.48 cm^{-1} (C–H bending of alkane), 1159 and 1059 cm^{-1} (C–O stretching of primary and tertiary alcohols). The PP500 consists of fewer bands than PP250, it mainly had a band at 2910 cm^{-1} (C–H stretching of alkane), 1570 cm^{-1} (C=C stretching alkene), 1415 cm^{-1} (C–H bending of alkene). The PP750 consists of bands similar to the PP500. It mainly consists of a band near 2900 cm^{-1} (C–H stretching of alkene), a shoulder near 1550 cm^{-1} (C=C stretching of alkene) and a peak at 1440 cm^{-1} (due to C–H bending of alkene). The changes perused in the FT-IR spectra of phenol loaded biochars provided a clear picture of the adsorption. In the FT-IR spectrum of Phenol Loaded PP250 (PLPP250), a shift in band position from 3336 cm^{-1} to 3349 cm^{-1} indicates the H-bonding between PP250 and phenol. In PLPP250, A 10–15 cm^{-1} shift in C=O and C=C band was observed indicating the interaction of these functional groups with phenol.[30] In FT-IR spectra of Phenol Loaded PP500 and Phenol Loaded PP750, major changes were observed in the bands of C=C stretching and C–H bending confirming phenol adsorption only through π-π interaction.[15]

The XRD graph of PP250, PP500 and PP750 is mentioned in Figure 3. From Figure 3, it is observed that all the three biochars consist of peaks in the range of 20–30° indicating the presence of systematic graphitic structure.[31] However, peak intensities of PP500 and PP750 indicate that there was no significant change occurred in the degree of graphitization. The peak intensities of biochars between 35–40° have mounted up with rise in pyrolysis temperature resulting in the merger of the small pores into the larger ones.[32]

Factors affecting adsorption

Effect of biochar dose

A plot of phenol uptake against biochar dose is shown Figure 4. 30 mg/L concentration of phenol was taken and the biochar dose was varied between 2–10 g/L. From Figure 4, it was observed that phenol uptake decreases with an increase in biochar dose and after a certain value biochar dose, phenol uptake slightly changes with further increase in biochar dose.[33,34] This experiment was repeated for higher phenol concentration (60 and 90 mg/L) and the same pattern was observed (Figure S2). The decrease in phenol uptake with

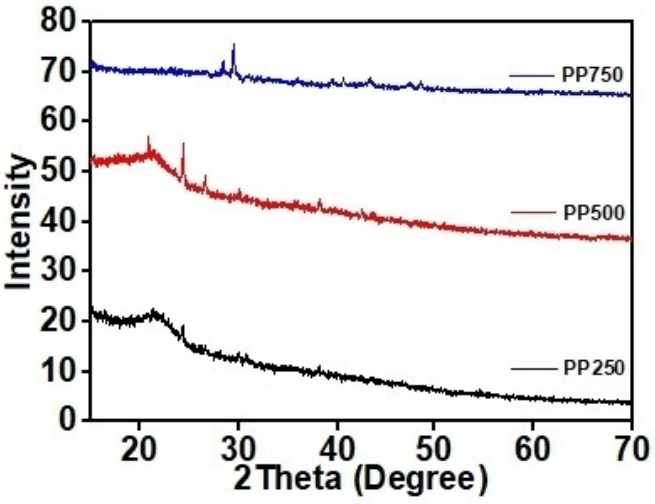

Figure 3. XRD spectra of PP250, PP500 and PP750.

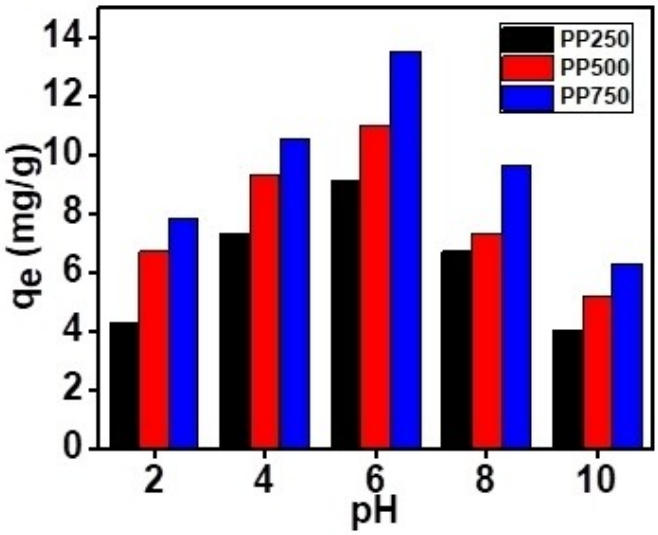

Figure 5. Effect of solution pH on adsorption capacity of PP250, PP500 and PP750 at 25 °C, biochar dose 2 g/L and 30 mg/L of phenol concentration.

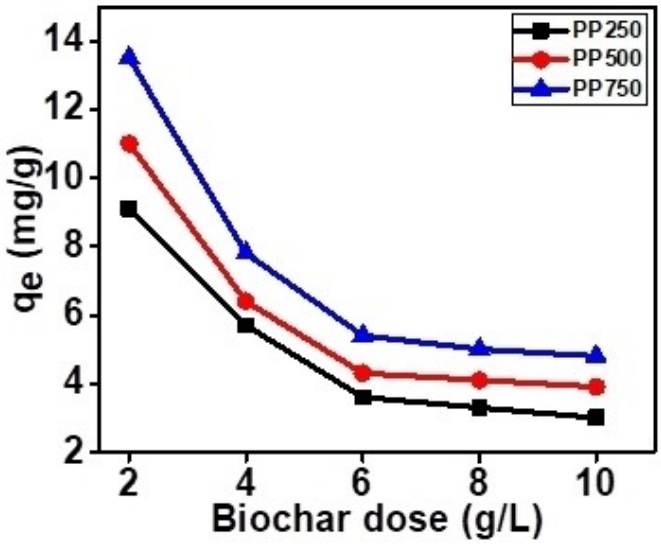

Figure 4. Effect of biochar dose on phenol adsorption at 25 °C, pH 6.0, and 30 mg/L of phenol concentration.

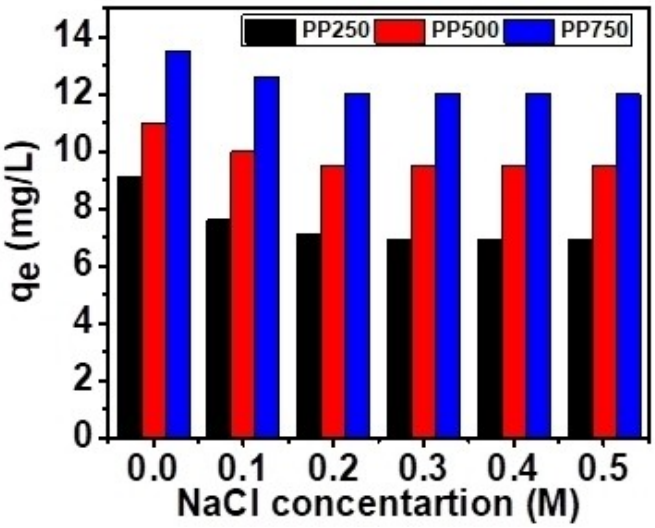

Figure 6. Effect of NaCl addition on phenol adsorption onto PP250, PP500 and PP750 at 25 °C, pH 6.0, biochar dose 2 g/L and 30 mg/L of phenol concentration.

increasing biochar dose is due to the presence of a larger number of adsorption sites and aggregation of biochar resulting in the reduction of adsorption potential of biochar.[35] The maximum phenol uptake for PP250, PP500 and PP750 were 9.1, 11.3 and 13.5 mg/g for the biochar dose of 0.2 g/100 ml (2 g/L).

Effect of pH

The effect of solution pH on phenol uptake by PP250, PP500 and PP750 is depicted in Figure 5. This can be explained based on the fact that the chemistry of phenol is governed by its pH and pH_{zpc} of the adsorbent. The pKa of phenol is 9.92, so when the pH of the solution is below 9.92 phenol exists in the protonated form. From pH 2–5, the phenol uptake for the three biochars increases as the surface of the biochars remains positive. At pH 6, the surface of biochars becomes slightly positive resulting in the interactions between positive and negative poles of the biochar and phenol. So maximum adsorption was observed at pH 6. Above pH 6, the surface becomes negatively charged which leads to the repulsion between the phenol and biochar surface.[13] At pH 10, the biochar surface becomes more negative and phenol exists in deprotonated form resulting in repulsion among phenol molecules and with biochar surface and so phenol uptake decreases at higher pH value.

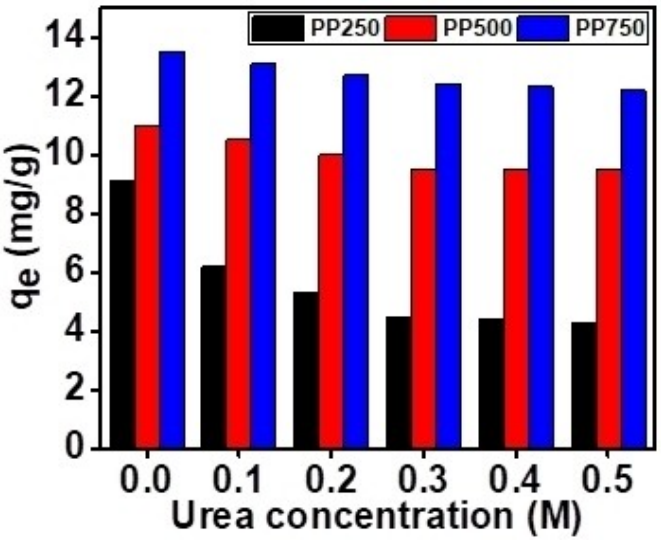

Figure 7. Effect of urea addition on phenol adsorption onto PP250, PP500 and PP750 at 25 °C, pH 6.0, biochar dose 2 g/L and 30 mg/L of phenol concentration.

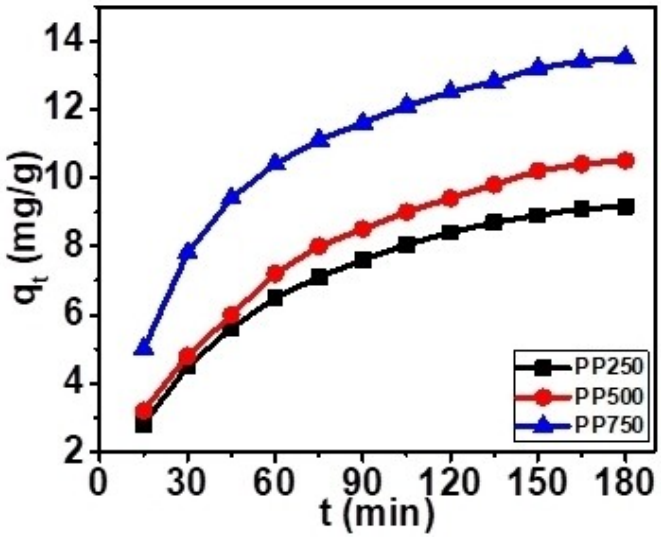

Figure 8. Effect of contact time on phenol adsorption by PP250, PP500 and PP750 at 25 °C, pH 6.0, biochar dose 2 g/L and 30 mg/L of phenol concentration.

Effect of NaCl and urea addition

The impact of NaCl and urea addition on phenol uptake by PP250, PP500 and PP750 is depicted in Figure 6. From Figure 6, it is evident that the phenol uptake by PP250 is affected by the NaCl addition but the phenol uptake by PP500 and PP750 is unaffected by the NaCl addition. This is due to the reason that for PP250, electrostatic interactions play important role in adsorption but in the case of PP500 and PP750 adsorption is due to H-bonding and π-π interactions and so is unaffected by the NaCl addition.

The urea addition negatively affects the phenol uptake by PP250, PP500 and PP750 and is exhibited in Figure 7. It is well known that urea functions as H-bond breaking agent and so confirms the role of H-bonding in the occurrence of adsorption in the present case.[36]

Effect of contact time

A plot of phenol uptake against time is depicted in Figure 8. From Figure 8, it is clear that phenol removal by PP250, PP500 and PP750 is a three-step process. In the first step, fast removal of phenol by three biochars takes place (0–45 min), In the second step, moderate removal of phenol by three biochars takes place (45–90 min). In the third step, slow removal of phenol by three biochars takes place (90–150 min), which later on becomes constant and no phenol removal is observed.[17,37]

Adsorption isotherms

Adsorption isotherm curve illustrates the mechanism of the migration of a substance from liquid to the solid surface.[38] Tests were conducted on the three commonly used adsorption isotherms using equilibrium data of phenol adsorption onto PP250, PP500, and PP750 as depicted in Figure 9. The adsorption parameters obtained from these models at three different temperatures were tabulated in Table 3.

According to Langmuir isotherm, there is no interaction between adsorption sites during monolayer adsorption and constant energy of adsorption for each site. The q_{max} of phenol adsorption onto PP250, PP500, and PP750 were 34.63, 46.70, and 60.10 mg/g respectively. Thus, the phenol adsorption increases with a rise in pyrolysis temperature of PP biochar. The R^2 and χ^2 values were in the range of 0.996–0.997 and 0.137–0.935 respectively confirming the Langmuir model's applicability to the adsorption data.

The Temkin isotherm assumes that as the interactions between adsorbents and adsorbates increase, so does the heat of adsorption of the layer under consideration. The adsorption data is consistent with the assumptions of the Temkin model. The heat of adsorption (b) increases with a rise in temperature resulting in a decrease in adsorbate-adsorbent interactions. The R^2 value increases and the χ^2 value decreases with a rise in temperature indicating the suitability of this model at higher temperatures.

Based on heterogeneous surfaces, Freundlich isotherm describes adsorption. In the present investigation, the Freundlich model does not hold good as the R^2 values are not high (0.90–0.95).

Previous studies reported that the high-temperature biochar has a good adsorption potential than the low-temperature biochar indicating the significance of the present study.[15,16,39–42] Table 1 compares the q_{max} of phenol removal using other biochars to the q_{max} of phenol removal using PP biochars, demonstrating that PP biochars have great adsorption potential for the elimination of hazardous materials.

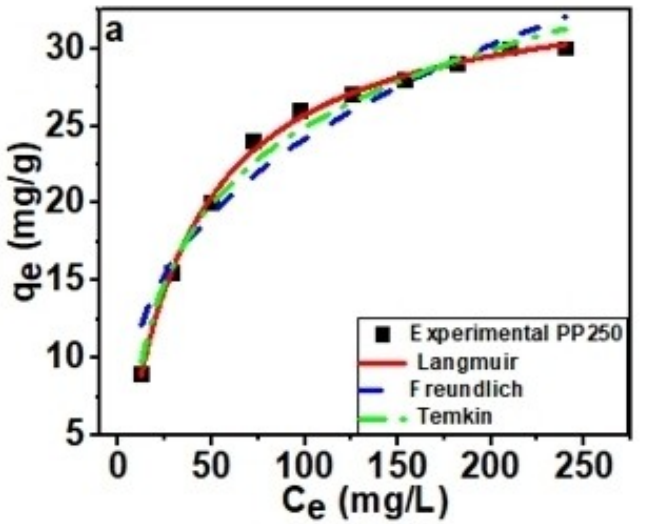

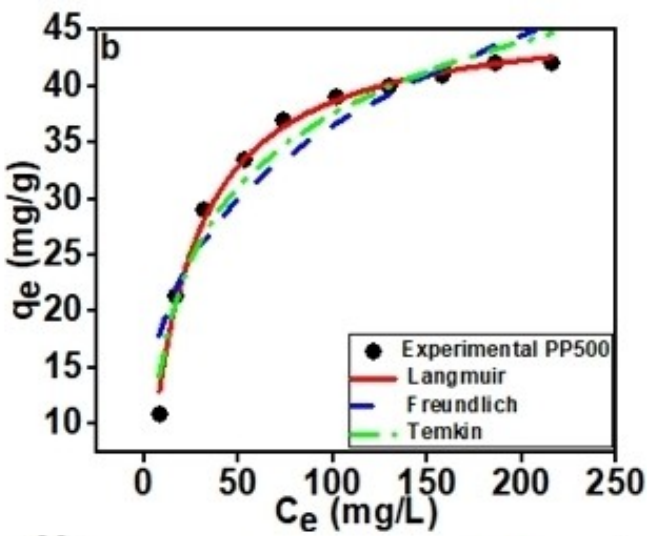

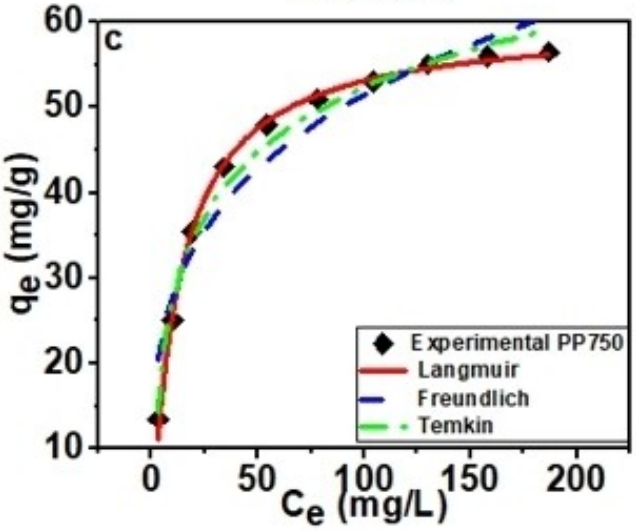

Figure 9. Non-linear fit of Langmuir, Freundlich and Temkin isotherm for phenol adsorption onto PP250 (a), PP500 (b) and PP750 (c).

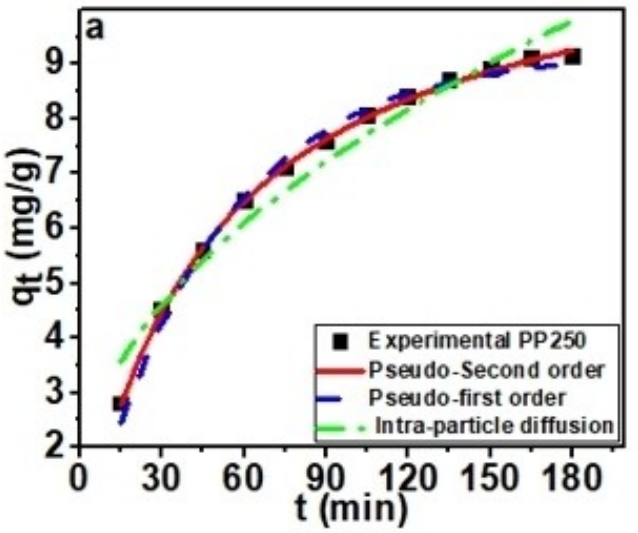

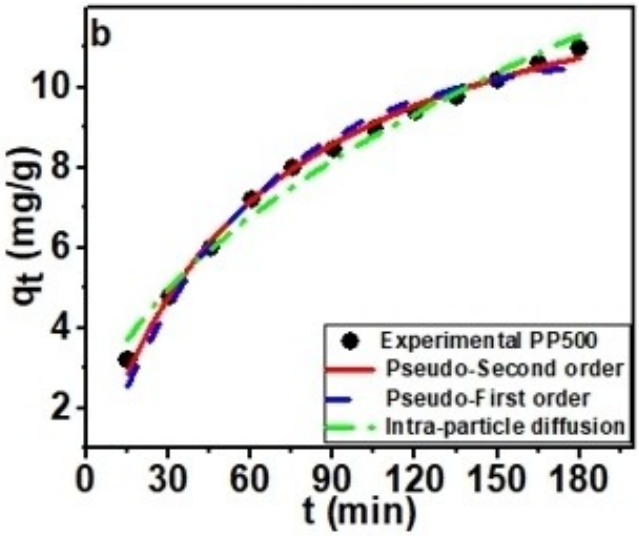

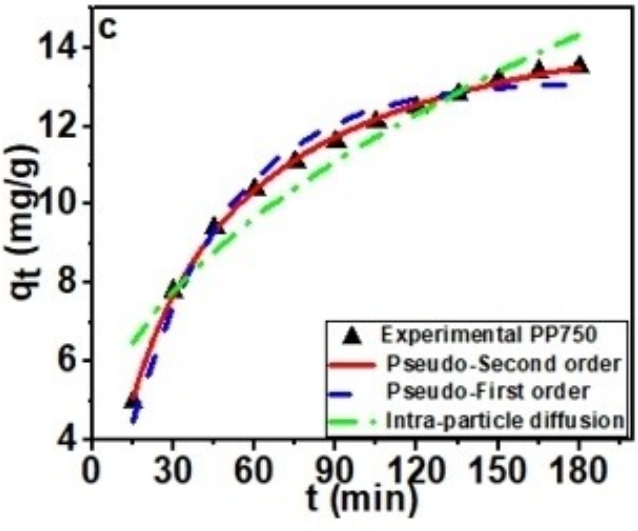

Figure 10. Non-linear fit of PSO, PFO and IPD model for phenol adsorption onto PP250 (a), PP500 (b) and PP750.

Table 3. Adsorption isotherm parameters of phenol adsorption onto PP250, PP500 and PP750 (at pH 6.0, biochar dose 2 g/L and 30–300 mg/L range of phenol concentration).

Adsorbent	PP250			PP500			PP750		
	25 °C	35 °C	45 °C	25 °C	35 °C	45 °C	25 °C	35 °C	45 °C
Langmuir									
q_{max} (mg/g)	34.63	33.36	31.32	46.70	37.37	31.98	60.10	49.00	40.67
K_L (L/mg)	2.87×10^{-2}	2.0×10^{-2}	1.28×10^{-2}	4.77×10^{-2}	3.28×10^{-2}	2.26×10^{-2}	7.60×10^{-2}	4.12×10^{-2}	2.79×10^{-2}
R^2 (COD)	0.997	0.996	0.995	0.994	0.996	0.998	0.996	0.998	0.995
χ^2	0.137	0.157	0.183	0.6788	0.248	0.080	0.935	0.217	0.379
Freundlich									
n	3.09	2.68	2.26	3.53	3.22	2.83	3.77	3.29	2.92
K_F ($mg^{1-(1/n)}\ L^{1/n}g^{-1}$	5.45	3.75	2.17	9.91	6.44	4.097	15.19	9.21	5.83
R^2 (COD)	0.940	0.940	0.955	0.900	0.923	0.948	0.932	0.925	0.941
χ^2	3.253	2.975	1.803	11.861	5.140	2.315	16.175	9.931	4.800
Temkin									
b (J/mol)	343.05	344.73	370.44	267.69	330.67	380.92	228.60	259.44	302.33
K_T (L/g)	0.316	0.186	0.116	0.57	0.360	0.225	1.252	0.489	0.279
R^2 (COD)	0.986	0.988	0.990	0.964	0.978	0.991	0.984	0.981	0.988
χ^2	0.757	0.574	0.379	4.196	1.454	0.387	3.651	2.499	0.903

Table 4. Kinetics parameters.

Biochar	PP250	PP500	PP750
PFO			
$q_{e,cal}$ (mg/g)	9.24	10.97	13.15
k_1 (min^{-1})	2.06×10^{-2}	1.77×10^{-2}	2.76×10^{-2}
R^2 (COD)	0.992	0.984	0.980
χ^2	0.031	0.099	0.141
PSO			
$q_{e,cal}$ (mg/g)	11.74	14.30	15.87
k_2 (mg/g.min)	1.75×10^{-3}	1.17×10^{-3}	1.98×10^{-3}
R^2 (COD)	0.999	0.995	0.998
χ^2	0.002	0.026	0.007
IPD			
k_i	0.652	0.795	0.822
C	1.04	0.63	3.29
R^2 (COD)	0.959	0.983	0.932
χ^2	0.179	0.103	0.490

Table 5. Phenol adsorption on PP250, PP500, and PP750: Thermodynamic parameters.

Biochar	25 °C	35 °C	45 °C	
PP250				
K_L°	2.70×10^3	1.88×10^3	1.20×10^3	
ΔG° ($kJmol^{-1}$)	−20.16	−19.71	−19.25	
ΔH° (kJ/mol)				−33.67
ΔS° (J/K.mol)				−45.33
PP500				
K_L°	4.48×10^3	3.09×10^3	2.12×10^3	
ΔG° ($kJmol^{-1}$)	−21.32	−21.00	−20.69	
ΔH° (kJ/mol)				−30.76
ΔS° (J/K.mol)				−31.67
PP750				
K_L°	7.144×10^3	3.879×10^3	2.622×10^3	
ΔG° ($kJmol^{-1}$)	−22.57	−21.99	−21.35	
ΔH° (kJ/mol)				−41.57
ΔS° (J/K.mol)				−63.74

Adsorption kinetics

The time-dependent phenol removal was tested with PFO, PSO and IPD kinetic models (Figure 10) and the parameters of these models are mentioned in Table 4. 30 mg/L initial phenol concentration was taken. From Figure 10, it is clear that the PSO model provides a better explanation than the PFO model. The R^2 and χ^2 values confirmed the suitability of the PSO model

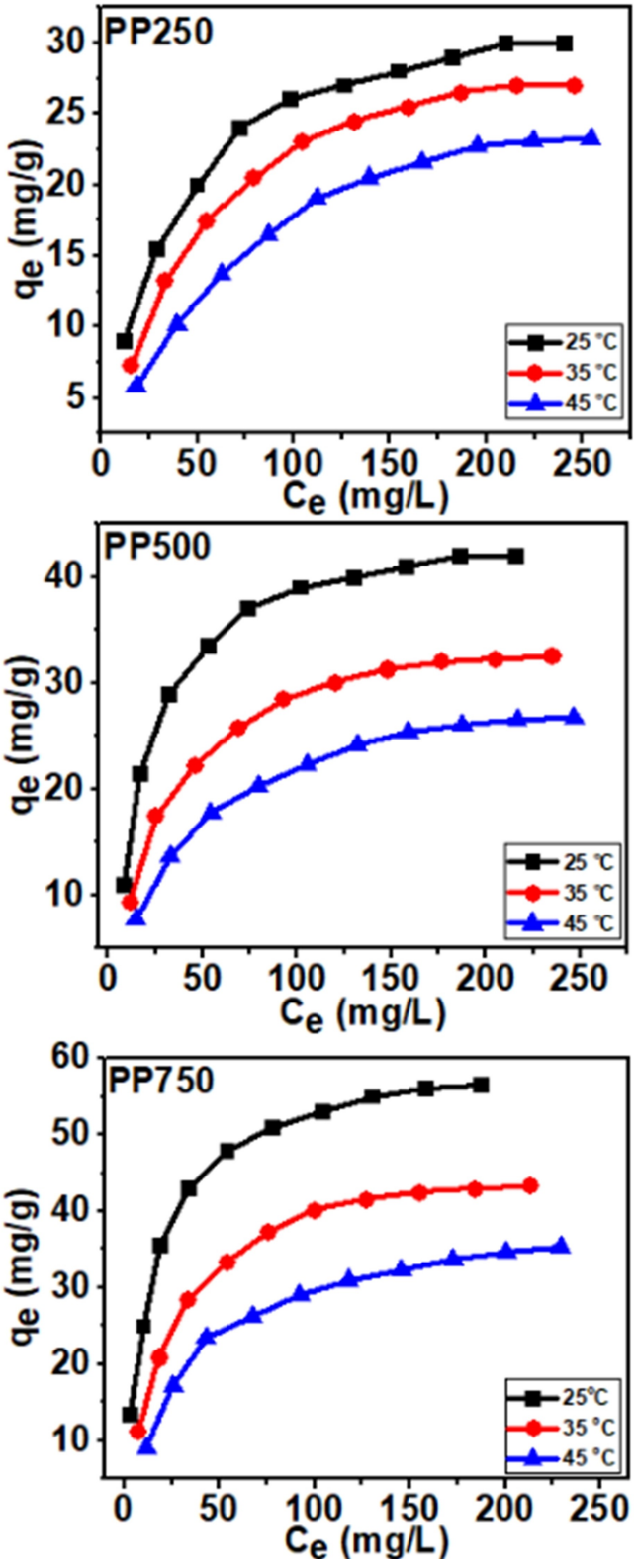

Figure 11. Effect of reaction temperature on phenol adsorption by PP250, PP500 and PP750 at pH 6.0, biochar dose 2 g/L and 30–300 mg/L range of phenol concentration.

for adsorption of phenol onto PP500 and PP750 but for PP250 the PFO and PSO models compete for the best fit. It can be explained based on the fact that for phenol adsorption onto PP250 there is the possibility of electrostatic interactions as well as with H-bonding and π-π interaction between PP250 and phenol but in the case of phenol adsorption onto PP500 and PP750, the possibility of electrostatic interactions was ruled out due to increase in aromatization of biochar and adsorption mainly occurred due to π-π interaction and to some extent with H-bonding.[43] The IPD model does not fit the non-linear regression analysis as its R^2 and χ^2 values did not align with the findings of the kinetic data.

Thermodynamics of adsorption

From the effect of the temperature experiment, it was observed that phenol uptake by PP250, PP500 and PP750 decreased with an increase in temperature (Figure 11). This observation has been concreted by the results of the thermodynamic study. The thermodynamic parameters have been calculated by the following equations and tabulated in Table 5.

$$lnK_L^{\circ} = \frac{\Delta S^{\circ}}{R} - \frac{\Delta H^{\circ}}{RT} \quad (1)$$

$$\Delta G^{\circ} = \Delta H^{\circ} - T\Delta S^{\circ} \quad (2)$$

Where K_L° is the unitless Langmuir Constant calculated by the method given by Lima et al. (2019).[44] ΔG°, ΔH°, and ΔS° are the standard state free energy change, enthalpy change and entropy change respectively.

The plot of lnK_L° *vs* 1/T for PP250, PP500, and PP750 is depicted in Figure 12. Input values for the ΔH°, and ΔS° values were calculated from the slope and intercept, respectively. Free energy change indicates phenol adsorption onto PP250, PP500

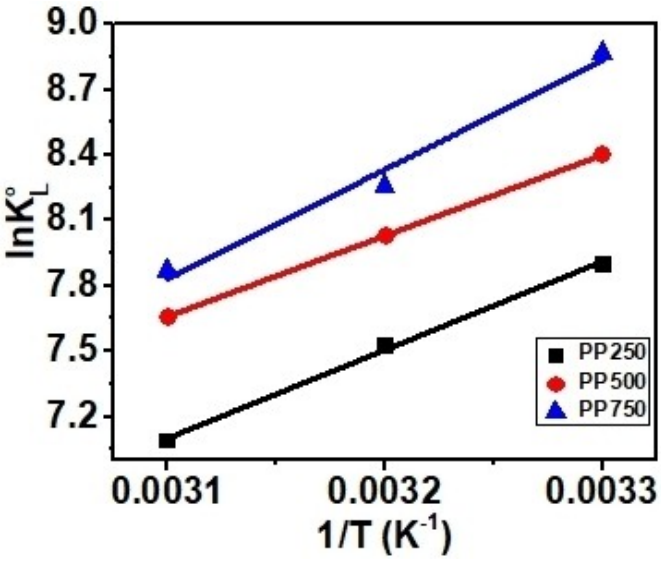

Figure 12. Plot of lnK_L° *vs* 1/T for PP250, PP500 and PP750.

and PP750 are feasible based on their negative value. From 25 °C to 45 °C, there is a decrease in the negative value of free energy change, which speaks to the less use of phenol adsorption onto PP250, PP500 and PP750 at higher temperatures. The highest negative value of free energy change was insinuated by PP750 indicating it to be a suitable adsorbent for phenol removal. The free energy change for PP250, PP500 and PP750 is less than 40 kJ/mol confirming the adsorption mechanism to be governed by the physical adsorption mode.[45]

A negative enthalpy change confirms that phenol adsorption onto PP250, PP500, and PP750 is exothermic. The negative value of entropy change confirmed the reduction in the randomness at the liquid-solid interface.[46]

Conclusions

The present study deals with the preparation of biochar from agriculture waste of PP at three different temperatures (250, 500 and 750 °C) using slow pyrolysis. These biochars were employed for phenol removal from an aqueous medium. The adsorption was controlled by the change in pH, ionic strength and biochar dose. The optimum phenol uptake was observed at pH 6.0, biochar dose 2 g/L and 25 °C. The presence of NaCl in the solution decreased the phenol uptake of PP250 but slightly decreased the uptake of PP500 and PP750 indicating the role of electrostatic interactions during adsorption for PP250. The maximum biosorption capacity for the PP250, PP500 and PP750 were found to be 34.63, 46.70, and 60.10 mg/g respectively. The PSO model provided the best explanation of the phenol removal by PP biochars. The Langmuir model gave the best-fit explanation and confirmed the monolayer type of adsorption. The mechanism of adsorption was governed by hydrogen bonding, electrostatic interactions and π-π interactions for PP250 and for PP500 and PP750, it is governed primarily by π-π interactions with some extent of hydrogen bonding. Adsorption is confirmed to be both physically and exothermically induced. Based on the above results, it is clear that the PP750 exhibited excellent adsorption potential in comparison to PP500 and PP250 biochars. Hence, PP750 can preferably be used for removing contaminants from water/wastewater streams.

Experimental Section

Biochar preparation

The PP was collected from local households and rigorously washed to remove dirt. The dried PP was sun-dried for 48 h and ground with an acoustic grinder to the particle size of 75–300 μm. The ground PP was then placed into the covered crucibles and slowly pyrolysed for 1 h in oxygen-controlled conditions at different temperatures (250, 500 and 750 °C). The pyrolysed PP was then labelled as PP250, PP500, and PP750, respectively. The biochars were then stored in airtight tubes until they could be used again.

Characterization of biochars

Scanning electron microscopy (SEM) analysis was used to examine the surface morphology of the biochars, while EDS was used to evaluate the elemental composition of the biochars. Both analyses were performed using a JEOL JSM-6490LV model from Japan. FT-IR spectrophotometer was used to analyse the functional groups of the biochar sample (Thermo- Scientific Nicole 6700, USA). With 32 scans and a resolution of 5–7 cm^{-1}, the spectra were captured in the range of 4000–400 cm^{-1}. The phase of the biochars was determined using a powder XRD (RigakuMiniflex II desktop). Copper Kα radiation (= 1.5405 Ao) was used to scan the biochars in a range of 2° to 70° at a scanning rate of 2°/min. Using Origin, raw data was processed. El-hanandeh et al. (2016)[47] developed a method for determining characteristics such as pH-zero-point charge, moisture content, ash content, and yield percent (Muffle furnace (UTS AF-777) and weighing balance (WENSAR-62157)). The phenol concentration was checked employing a UV-Vis Spectrophotometer (Carry 100) at 270 nm wavelength.

Biosorption experiments

Biochars were tested for maximum phenol uptake under a variety of adsorption conditions. Every experiment was carried out by placing 100 ml of phenol solution into a conical flask at a different pH and temperature and adding 0.2 g of biochar to the flask. An initial concentration of phenol in the sample ranged between 30–300 mg/L. The equilibrium was reached in 3 h, however, some samples were left for 5 to 8 h with identical results. The test NaCl and urea addition was performed to check the effect of external species on phenol uptake by PP biochars. For this, 0.1–0.5 mol/L of NaCl and urea were separately added to the 30 mg/L phenol solution containing 2 g/L biochar dose at pH 6 and 25 °C. Samples were analysed at fixed time gaps to determine the time dependence of phenol removal.

Equation (3) calculates how much phenol is adsorbed at equilibrium:

$$q_e = \frac{(C_0 - C_e)V_s}{m} \tag{3}$$

There are five factors, the adsorbed amount at equilibrium (q_e) (mg/g), initial concentration (C_o) (mg/L), equilibrium concentration (C_e) (mg/L), solution volume (V) (in L), and mass of biochar added (m) (in g).

Following equation calculates phenol removal at any time 't':

$$q_t = \frac{(C_0 - C_t)V_s}{m} \tag{4}$$

At time t, q_t is the amount adsorbed (in mg/g) and C_t is the concentration (in mg/L).

Isotherm and kinetic analysis

Adsorption isotherm modelling is the best method used to describe the adsorption equilibrium data and provide the actual picture of the adsorption mechanism. The most common isotherm models were modelled to explore the phenol adsorption onto PP biochars are given as follows:

Langmuir model

$$q_e = \frac{q_m K_L C_e}{1 + K_L C_e} \quad (5)$$

Freundlich Model

$$q_e = K_F C_e^{1/n} \quad (6)$$

Temkin Model

$$q_e = \frac{RT}{b} \ln K_T C_e \quad (7)$$

Where, q_m; maximum phenol uptake (mg/g), K_L; Langmuir constant (L/mg), K_F; Freundlich constant ($mg^{1-(1/n)}$ $L^{1/n}$/g), 1/n; intensity of adsorption, K_T; Temkin constant (L/g) and b; heat of adsorption (J/mol).

Pseudo-first-order (PFO)

$$q_t = q_e(1 - e^{-k_1 t}) \quad (8)$$

Pseudo-second-order (PSO)

$$q_t = \frac{k_2 q_e^2 t}{1 + k_2 q_e t} \quad (9)$$

Intra-particle diffusion (IPD)

$$q_t = k_i t^{0.5} + C \quad (10)$$

Where, k_1; PFO (min^{-1}) and k_2; PSO rate constant (g/mg. min), k_i; IPD rate constant ($g/mg.min^{0.5}$), and C: constant (mg/g).

Supporting Information Summary

EDS spectra of PP250, PP500 and PP750 (Figure S1) and the effect of biochar dose at higher concentrations (Figure S2) are provided as supporting information.

Acknowledgements

We humbly welcome the UGC-New-Delhi's financial assistance to P Mishra (UGC-SRF 133155).

Conflict of Interest

The authors declare no conflict of interest.

Data Availability Statement

The data that support the findings of this study are available from the corresponding author upon reasonable request.

Keywords: Biochar · Characterization · Langmuir isotherm · Pea peels · Phenol removal

[1] B. R. Albuquerque, S. A. Heleno, M. B. P. P. Oliveira, L. Barros, I. C. F. R. Ferreira, *Food Funct.* **2021**, *12*, 14–29.
[2] X. Qi, X. Tong, W. Pan, Q. Zeng, S. You, J. Shen, *J. Cleaner Prod.* **2021**, *315*, 128221.
[3] Y. Z. Ren, Z. L. Wu, M. Franke, P. Braeutigam, B. Ondruschka, D. J. Comeskey, P. M. King, *Ultrason. Sonochem.* **2013**, *20*, 715–721.
[4] W. Raza, J. Lee, N. Raza, Y. Luo, K. H. Kim, J. Yang, *J. Ind. Eng. Chem.* **2019**, *71*, 1–18.
[5] N. Arumugam, S. Chelliapan, H. Kamyab, S. Thirugnana, N. Othman, N. S. Nasri, *Int. J. Environ. Res. Public Health* **2018**, *15*, 2851.
[6] W. Duan, F. Meng, H. Cui, Y. Lin, G. Wang, J. Wu, *Ecotoxicol. Environ. Saf.* **2018**, *157*, 441–456.
[7] J. Ali, M. Tuzen, T. G. Kazi, *Food Chem.* **2020**, *306*, 125638.
[8] E. H. Ramos, R. Nomen, J. Sempere, *Ind. Eng. Chem. Res.* **2018**, *57*, 16903–16908.
[9] K. A. Mohamad Said, A. F. Ismail, Z. Abdul Karim, M. S. Abdullah, A. Hafeez, *Process Saf. Environ. Prot.* **2021**, *151*, 257–289.
[10] L. Y. Jun, L. S. Yon, N. M. Mubarak, C. H. Bing, S. Pan, M. K. Danquah, E. C. Abdullah, M. Khalid, *J. Environ. Chem. Eng.* **2019**, *7*, 102961.
[11] K. S. Ukanwa, K. Patchigolla, R. Sakrabani, E. Anthony, S. Mandavgane, *Sustainability* **2019**, *11*, 6204.
[12] L. Liang, F. Xi, W. Tan, X. Meng, B. Hu, X. Wang, *Biochar* **2021**, *3*, 255–281.
[13] P. Mishra, K. Singh, U. Dixit, *Sustainable Chem. Pharm.* **2021**, *22*, 100491.
[14] J. Wang, S. Wang, *J. Cleaner Prod.* **2019**, *227*, 1002–1022.
[15] N. A. S. Mohammed, R. A. Abu-Zurayk, I. Hamadneh, A. H. Al-Dujaili, *J. Environ. Manage.* **2018**, *226*, 377–385.
[16] P. Q. Thang, K. Jitae, B. L. Giang, N. M. Viet, P. T. Huong, *J. Environ. Manage.* **2019**, *251*, 109556.
[17] A. A. Lawal, M. A. Hassan, M. A. Ahmad Farid, T. A. Tengku Yasim-Anuar, M. H. Samsudin, M. Z. Moh Yusoff, M. R. Zakaria, M. N. Mokhtar, Y. Shirai, *Environ. Pollut.* **2021**, *269*, 116197.
[18] Z. Li, B. Xing, Y. Ding, Y. Li, S. Wang, *Chin. J. Chem. Eng.* **2020**, *28*, 2872–2880.
[19] F. X. Dong, L. Yan, X. H. Zhou, S. T. Huang, J. Y. Liang, W. X. Zhang, Z. W. Guo, P. R. Guo, W. Qian, L. J. Kong, W. Chu, Z. H. Diao, *J. Hazard. Mater.* **2021**, *416*, 125930.
[20] J. Zhang, J. Liu, R. Liu, *Bioresour. Technol.* **2015**, *176*, 288–291.
[21] J. Treviño, C. Centeno, R. Caballero, *Anim. Feed Sci. Technol.* **1987**, *16*, 305–309.
[22] W. T. Tsai, S. C. Liu, H. R. Chen, Y. M. Chang, Y. L. Tsai, *Chemosphere* **2012**, *89*, 198–203.
[23] X. Cao, W. Harris, *Bioresour. Technol.* **2010**, *101*, 5222–5228.
[24] L. Liu, G. Deng, X. Shi, *Sci. Rep.* **2020**, *10*, 1–11.
[25] S. M. Yakout, *Proc. Natl. Acad. Sci. India Sect. A* **2017**, *87*, 207–214.
[26] X. Dong, L. Q. Ma, Y. Zhu, Y. Li, B. Gu, *Environ. Sci. Technol.* **2013**, *47*, 12156–12164.
[27] Q. Zhang, D. Zhang, W. Lu, M. U. Khan, H. Xu, W. Yi, H. Lei, E. Huo, M. Qian, Y. Zhao, R. Zou, *Sci. Total Environ.* **2020**, *738*, 139910.
[28] G. Zhang, Q. Zhang, K. Sun, X. Liu, W. Zheng, Y. Zhao, *Environ. Pollut.* **2011**, *159*, 2594–2601.
[29] M. Zolfi Bavariani, A. Ronaghi, R. Ghasemi, *Commun. Soil Sci. Plant Anal.* **2019**, *50*, 402–411.
[30] P. Zhang, Y. Li, Y. Cao, L. Han, *Bioresour. Technol.* **2019**, *285*, 121348.
[31] P. Pariyar, K. Kumari, M. K. Jain, P. S. Jadhao, *Sci. Total Environ.* **2020**, *713*, 136433.
[32] R. Azargohar, S. Nanda, J. A. Kozinski, A. K. Dalai, R. Sutarto, *Fuel* **2014**, *125*, 90–100.
[33] P. Mishra, K. Singh, U. Dixit, A. Agarwal, R. Ahmad Bhat, *J. Indian Chem. Soc.* **2022**, *99*, 100528.
[34] C. G. Lee, S. H. Hong, S. G. Hong, J. W. Choi, S. J. Park, *Water Air Soil Pollut.* **2019**, *230*, 1–13.
[35] K. Singh, A. Kumar, S. Awasthi, S. K. Pandey, P. Mishra, *Colloids Surf. A* **2019**, *581*, 123786.
[36] K. Singh, A. Kumar, S. K. Pandey, S. Awasthi, S. P. Gupta, P. Mishra, *Ind. Eng. Chem. Res.* **2020**, *59*, 19102–19116.
[37] T. Sarchami, N. Batta, L. Rehmann, F. Berruti, *Can. J. Chem. Eng.* **2021**, *99*, 2368–2385.
[38] J. Wang, X. Guo, *Chemosphere* **2020**, *258*, 127279.
[39] M. N. Hairuddin, N. M. Mubarak, M. Khalid, E. C. Abdullah, R. Walvekar, R. R. Karri, *Environ. Sci. Pollut. Res. Int.* **2019**, *26*, 35183–35197.

[40] M. Jain, S. A. Khan, A. Sahoo, P. Dubey, K. K. Pant, Z. M. Ziora, M. A. T. Blaskovich, *Bioresour. Technol.* **2022**, *352*, 127030.
[41] N. S. Kumar, H. M. Shaikh, M. Asif, E. H. Al-Ghurabi, *Sci. Rep.* **2021**, *11*, 1–17.
[42] W. seok Shin, *Environ. Earth Sci.* **2017**, *76*, 1–9.
[43] A. M. Awad, S. M. R. Shaikh, R. Jalab, M. H. Gulied, M. S. Nasser, A. Benamor, S. Adham, *Sep. Purif. Technol.* **2019**, *228*, 115719.
[44] E. C. Lima, A. Hosseini-Bandegharaei, J. C. Moreno-Piraján, I. Anastopoulos, *J. Mol. Liq.* **2019**, *273*, 425–434.
[45] A. Mandal, N. Bar, S. K. Das, *Sustainable Chem. Pharm.* **2020**, *17*, 100308.
[46] X. Kong, H. Gao, X. Song, Y. Deng, Y. Zhang, *Chem. Phys. Lett.* **2020**, *739*, 137046.
[47] A. El Hanandeh, R. A. Abu-Zurayk, I. Hamadneh, A. H. Al-Dujaili, *Water Sci. Technol.* **2016**, *74*, 1899–1910.

Submitted: August 2, 2022
Accepted: September 28, 2022

RESEARCH ARTICLE

Characterization of pea peels biochars using SEM, FT-IR and XRD techniques and their application to remove phenol from aqueous medium. Various aspects of optimization conditions, isotherm, kinetics and thermodynamics has been investigated in the present study.

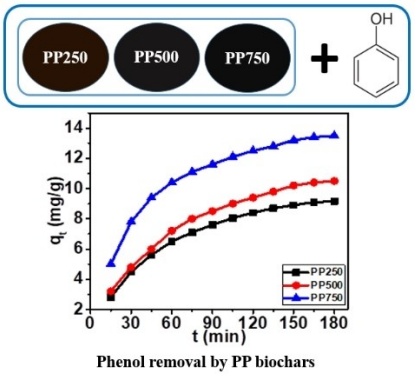

Phenol removal by PP biochars

P. Mishra, Prof. K. Singh, Prof. G. Pandey*

1 – 12

A Comparative Study of Phenol Removal by *Pisum-sativum* Peels Biochars Derived at Different Pyrolysis Temperatures: Isotherm, Kinetic and Thermodynamic Modelling

JOURNAL OF COORDINATION CHEMISTRY
https://doi.org/10.1080/00958972.2022.2083962

Taylor & Francis
Taylor & Francis Group

Antimicrobial studies of the Zn(II) complex of S-benzyl-β-(N-2-methyl-3-phenylallylidene)dithiocarbazate

Rayees A. Bhat[a], Kaman Singh[a], D. Kumar[b], Ashok Kumar[c] and Prashant Mishra[a]

[a]Department of Chemistry, Babasaheb Bhimrao Ambedkar University (A Central University), Lucknow, India; [b]Centre of Research for Chemical Sciences, Govt Model Science College, Jiwaji University, Gwalior, India; [c]Department of Chemistry, Swami Vivekanand Subharti University, Meerut, India

ABSTRACT

Antimicrobial resistance is a global concern with increases in multidrug-resistant bacteria. New coordination compounds could offer a solution. We report S-benzyl-β-(N-2-methyl-3-phenylallylidene)dithiocarbazate (HL) forming bis[S-benzyl-β-(N-2-methyl-3-phenylallylidene)dithiocarbazate]zinc(II), $[Zn(L)_2]$; its bio-efficacy has been examined against the growth of gram-positive *Staphylococcus aureus* and gram-negative *Escherichia coli* to evaluate antimicrobial potential. The inhibition diameter results of *E. coli* and *S. aureus* were compared to standard drug (Erythromycin). Characterization by UV–vis, FT-IR, Raman, ^{1}H NMR, ^{13}C NMR, and mass spectroscopy revealed that $[Zn(L)_2]$ has distorted square planar geometry, coordinated through N_{imine} and $S_{thiolate}$. Density functional calculations of $[Zn(L)_2]$ in gas phase were performed by DFT (RB3LYP) with LanL2DZ basis set and the results are: chemical hardness (η) 0.007915 eV, chemical potential (μ) 0.11643 eV, electron affinity (A) −0.10852 eV, softness (S) 7.855 eV, ionization energy (I) −0.12435 eV, electronegativity (χ) −0.11643 eV, dipole moment (D) 4.0690 Debye and with stabilization energy of −1718.1753 eV. Vibrational energy distribution analysis (VEDA)-4 software was employed for theoretical FT-IR spectrum, which yielded 237 fundamental vibrational modes. Theoretically calculated parameters like UV–vis, FT-IR, ^{1}H NMR, ^{13}C NMR, Raman, HOMO–LUMO energy gap and electrostatic potential were in conformity with experimental observations. The compound was docked with different receptors 1HT0, 1U3T, 1U3V, and 3S7S to find the best ligand–protein interactions.

ARTICLE HISTORY
Received 10 July 2021
Accepted 12 May 2022

KEYWORDS
Dithiocarbazate; Zn-complex; TGA; Schiff base; LanL2DZ; VEDA-4; DFT; PED%

CONTACT Rayees A. Bhat rayeesbinahad@Gmail.com Department of Chemistry, Babasaheb Bhimrao Ambedkar University (A Central University), Lucknow-226025, India

Supplemental data for this article can be accessed online at https://doi.org/10.1080/00958972.2022.2083962.

Asian Sugar Journal, Vol. 1, No. 1, January-April, 2021 : 32-67

Sugar Solutions Colour Measurement : Problems and Prospects

Kaman Singh, K.K. Sharma*, R.K. Singh, Prasant Mishra, Ankita Agarwal, Anita Suman*** and Pankaj Singh**

Department of Chemistry, School of Physical and Decision Science
Babasaheb Bhimrao Ambedkar University
(A Central University)
Vidya Vihar, Raibareli Road Lucknow-226025 U.P. (India)
*Convener, Indian National Committee on ICUMSA, CEO, Dalmia Sugars Pvt. Ltd. Barakhamba Road, New Delhi-110001
**Former Dean, Faculty of Science, University of Lucknow, Lucknow-226007, U.P. (India)
***Department of Chemistry, Faculty of Science, University of Lucknow, Lucknow-226007, U.P. (India)

ABSTRACT

Sugar color in solution has been a topic of intense discussion for the last five decades in the ICUMSA because sugar color is an overall quality parameter in international sugar purchase contract. Sugar is the only product to which Codex Alimentarius Commission (CAC), does not formulate standards but it borrows sugar standards from the ICUMSA. The ICUMSA is the highest organization in the world that sets standard for sugar and standards fixed by ICUMSA are strictly followed by the Codex Alimentarius Commission (WHO and FAO), the EU, the ECC and the US Food Chemicals Codex. It might be surprising to someone to know that the color of white paper (A4 size) is 45 I.U. and polarimeter has been standardized by the ICUMSA and is being followed by all the leading research organization worldwide.

Prior to 70s, color of sugar has been determined by method 4 (without pH adjustment) employing distilled water as a solvent. However, in 1978, ICUMSA came with a proposal that sugar solution should be brought at pH 7.0 by deliberate addition of buffer. Initially HCl/NaOH, Tea buffer and MOPS buffers were tested to set the reference pH 7.0. However, pH 7.0 is just arbitrary and there is no scientific foundation to back up this arbitrary pH 7.0. Therefore, it has been topic of hot discussion during the last 50 years at various ICUMSA sessions. The detailed fact-file of development of arbitrary pH 7.0 has been illustrated at Appendix-'A'. In the present manuscript, an attempt has been made on sugar solution color measurement problem and prospects from physical and chemical point of view and we hope that ICUMSA will take the cognizance of scientist's facts and will take an appropriate action and will make a recommendation for scientifically derived pH 6.4 instead of an arbitrary pH 7.0.

This article is tribute to Mr. K. K. Sharma who had been contributed in various ICUMSA collaborative studies since inception of controversy pH 7.0 in a capacity of convener of the INC on ICUMSA.

Keywords: White sugar, solution, standard, absorbance, filtration, 0.45 µm membrane, MOPS buffer, pH (6.0), primary reference, control, spectrophotometer, ICUMSA.

1.1 Definition of colour: According to Committee[1] on colorimetry of Optical Society of USA "colour consists of that characteristics of light other than spectral and temporal in-homogeneities to which most observers are aware through visual sensation arising from stimulation of retina of eye". Sugar solution colour expressed as ICUMSA units does not fall within this definition, being generally colourless in appearance. The fact has been verified experimentally Fig.1(a) as absorbance maxima (λ_{max}) has not been noticed using sugar solution in the visible range (400-800 nm). The evaluation being carried out currently at best be termed as "absorbance".

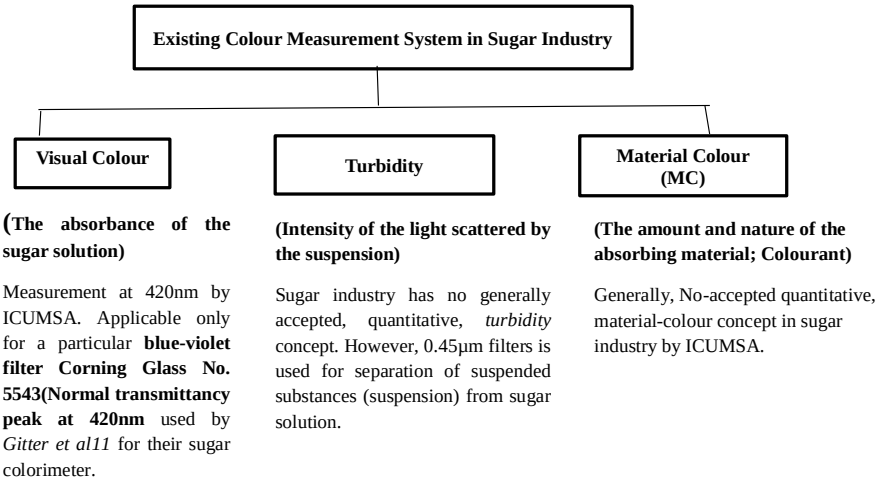

THE INFLUENCE OF DIFFERENT QUALITIES OF MOPS REAGENT ON THE MEASURED SUGAR COLOUR IN SOLUTION

Kaman Singh[1] and Prashant Mishra[2]

ABSTRACT

Colour of the sugar in solution is an important quality parameter and it is measured as per ICUMSA protocol ***(GS9/1/2/3-8).*** *During 31st session of the ICUMSA, it was recommended to study the influence of different qualities of MOPS reagent on the measured sugar colour in solution. Following the above recommendation, we studied the influence of the MOPS reagent of different makes on measured sugar colour in solution. Our study concluded that the MOPS from the different makes has a slight effect on sugar colour solution which seems to be within the experimental error.*

Keywords: MOPS; ICUMSA; Sugar colour.

INTRODUCTION

Colour is especially important in the sugar trade, for control of the operation and maintenance of the quality of the product. Thus, the associated problems have received adequate attention (Singh *et al.,* 2006, 2008, 2009, 2010, 2012, 2013).There is a reference method of determination of colour in solution using MOPS buffer **(GS9/1/2/3-8)**.

Background

ICUMSA during the 31stsession (2018) made the following recommendation:-

"It is recommended to study the influence of different qualities of the MOPS reagent on the measured colour in solution. The study needs support from other referees with regard to sugar samples and MOPS reagents from different suppliers."

In the present study, following the ICUMSA recommendation, authors have investigated the influence of different qualities of MOPS reagent on the measured sugar colour in solution.

EXPERIMENTAL SECTION

Materials

The details of MOPS reagents from different suppliers are shown in Table 1.

[1]Department of Chemistry, E-mail: drkamansingh@yahoo.com/singh.kaman@bbau.ac.in Babasaheb Bhimrao Ambedkar University (A Central University), Lucknow, 226025. [2]E-mail: prashantmishra1128@gmail.com

Kaman Singh, Prashant Mishra, & Ashok Kumar
Proceedings of 77th Annual Convention of STAI: 461 – 480 2019

SELECTION OF pH FOR MEASUREMENT OF SUGAR SOLUTION COLOUR

Kaman Singh[1], Prashant Mishra[2] & Ashok Kumar[3]

ABSTRACT

Sugar color is the most important attribute among various sugar specification which decides the sale value of sugar in the market. Hence, it is very important to keep an eye on the intermediate products of sugar processing as well to achieve desired final sugar color. The determination of sugar solution colour has been the subject of intense discussion in various ICUMSA meetings over the last three decades.From 1954 to 1978, sugar solution colour was determined by Official method No. 4 without pH adjustment using distilled water. In 1978 ICUMSA session, it was recommended that sugar color should be measured at neutral pH i.e. 7.0 it has been well recorded in the ICUMSA proceedings that the choice of pH 7.0 is just arbitrary and there is no scientific background of sugar color measurement at pH 7.0. However, the practice of sugar solution colour measurement continued without pH adjustment until the nineties keeping in view that sugar has no pH by definition, but this fact has been challenged and it was well established that sugar has a pH value of 6.4 by definition which depends on its ionization constant (1.01×10^{-13}). The INC brought this fact to the notice of the ICUMSA and an international collaborative study was recommended in 2008 (Florida session of ICUMSA) to conduct an international collaborative study on the method proposed by INC at pH 6.4 with MOPS buffer along with existing colour method GS9/1/2/3-8 with white sugar, plantation white sugar and other types of sugars with wide colour range." In 2011, an international collaborative study was organized by ICUMSA under the supervision of Dr. Lakenbrink (German and the results of this study were presented in Cambridge Session of ICUMSA

[1]Associate Referee, Subject S3 (Colour, Turbidity and Reflectance Measurement), International Commission for Uniform Methods of Sugar Analysis (ICUMSA), Email: drkamansingh@yahoomail.com/ singh.kaman@bbau.ac.in; Department of Chemistry, Babasaheb Bhimrao Ambedkar University, Lucknow-226025 U.P. (INDIA)

Ouriginal by Turnitin

Document Information

Analyzed document	Thesis Prashant Mishra Without references.pdf (D147899390)
Submitted	10/28/2022 10:52:00 AM
Submitted by	O. P. Saini
Submitter email	gbl.bbau@gmail.com
Similarity	0%
Analysis address	gbl.bbau.bbau@analysis.urkund.com

Sources included in the report

W URL: https://www.researchgate.net/figure/The-effect-of-alginate-concentration-used-in-entrapment-on-the-maximum-degradation-rate_fig1_227182924
Fetched: 12/21/2020 10:54:30 AM — 2

W URL: https://link.springer.com/article/10.1186/2052-336X-11-29
Fetched: 7/24/2020 7:14:42 PM — 3

Entire Document

Chapter-1 Introduction and objectives of the current work
Chapter 1: Introduction and objectives of the current work Prashant Mishra/Ph.D. Thesis/(Enrollment No. 950/17)/DAC/BBAU, Lucknow/2022 1 1.1. Phenol and its derivatives 1.1.1. Properties and application A hydroxyl (-OH) group linked to an aromatic ring distinguishes the family of chemical substances known as phenols or phenolics. The simplest phenolic chemical, phenol is a benzene derivative. A phenyl (-C 6 H 5) group is joined to a hydroxyl (-OH) group to form the molecule. It has the chemical formula C 6 H 5 OH. Despite having the same functional group as alcohols, where the -OH group is joined to an aliphatic carbon, phenols' chemistry is quite dissimilar to that of alcohols. Phenol (C 6 H 5 OH), which is the name of the first member of the family and also serves as a generic word for the entire group, is also referred to as benzenol or carbolic acid [1,2]. When pure, it is a colourless to white solid; however, the commercial product, which includes some water, is a liquid. The crystalline, hygroscopic substance phenol has a distinct unpleasant smell and a strong, burning taste. The phenol odour threshold is 0.04 ppm, and a strong, extremely sweet odour has been noted. A moderate amount of phenol can dissolve in water to form a solution because it evaporates more slowly than water. The term "derivatives of phenol and phenolic compounds" refers to the other members of the family [3]. A colourless, crystalline chemical with a distinctive smell, phenol (hydroxybenzene) is soluble in both water and organic solvents [4]. It is frequently used in the chemical, oil, coal processing, and metallurgical industries for the synthesis of alkylphenols, cresols, xylenols, phenolic resins, aniline, and other chemicals. Additionally, phenol is utilised in the manufacture of textiles, explosives, insecticides, and colours [5–7]. Additionally, it is employed in chemical analysis as a reagent and disinfectant [8,9]. On a large scale, coal tar is used to create phenol [10]. Chemically speaking, phenol